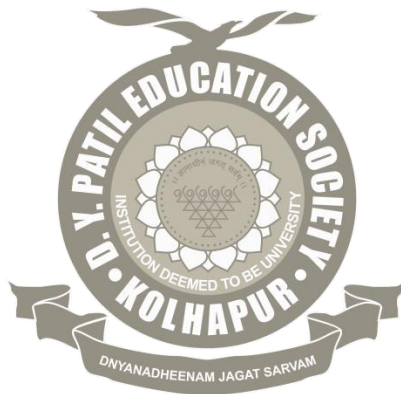


**“SYNTHESIS AND EVALUATION OF A NOVEL
COMBINATION SCAFFOLD AND ITS APPLICATION IN
BONE TISSUE ENGINEERING”**

A THESIS SUBMITTED TO



**D.Y.PATIL EDUCATION SOCIETY (DEEMED TO BE UNIVERSITY),
KOLHAPUR (Declared u/s 3 of the UGC Act 1956)**

FOR THE DEGREE OF
DOCTOR OF PHILOSOPHY

IN
BIOTECHNOLOGY
UNDER THE FACULTY OF INTERDISCIPLINARY STUDIES
BY

Mr. Shivaji Bhikaji Kashte

M.Sc. NET

UNDER THE GUIDENCE OF

Dr. Sachin Kadam

M.Sc., Ph.D.

Chief Technology Officer, Advancells, Noida, India.

Former Associate Professor and Head, Department of Stem Cell and Regenerative Medicine,
Center for Interdisciplinary Research, D.Y. Patil Education Society
(Deemed to be University), Kolhapur- 416006

AND

Prof. (Dr.) R.K. Sharma

MD. Obst & Gynac

Dean, D.Y. Patil Medical College,
D.Y. Patil Education Society (Deemed to be University), Kolhapur- 416006

**CENTER FOR INTERDISCIPLINARY RESEARCH
D.Y. PATIL EDUCATION SOCIETY (DEEMED TO BE UNIVERSITY),
KOLHAPUR- 416 006 (M. S.) INDIA**

May-2019

DECLARATION

I hereby declare that the work presented in this thesis entitled **“Synthesis and Evaluation of a Novel Combination Scaffold and its Application in Bone Tissue Engineering”** is entirely original and was carried out by me independently in the D.Y. Patil Education Society (deemed to be University), Kolhapur under the supervision of Dr. Sachin Kadam, Chief Technology Officer, Advancells, Noida; Former Associate Professor, Department of Stem Cell and Regenerative Medicine, Center for Interdisciplinary Studies, D.Y. Patil Education Society (Deemed to be University), Kolhapur, and Professor (Dr.) R.K. Sharma, Dean, D.Y. Patil Medical College, D.Y. Patil Education Society (Deemed to be University), Kolhapur.

I further declare that present work has not formed the basis for the award of any degree, diploma, fellowship or associateship or similar title of any University or Institution. The extent of information derived from the existing literature has been indicated in the body of thesis at appropriate places giving the references.

Place: Kolhapur

Date: 30-05-2019



Shivaji Bhikaji Kashte

Center for Interdisciplinary Research,
D. Y. Patil Education Society (Deemed to be University),
Kolhapur 416006, India

CERTIFICATE

This is to certify that the work incorporated in this thesis **"Synthesis and Evaluation of a Novel Combination Scaffold and its Application in Bone Tissue Engineering"** submitted herewith for the degree of Doctor of Philosophy in Biotechnology of D.Y. Patil Education Society (Deemed to be University), Kolhapur by Mr. Shivaji Bhikaji Kashte was carried out under our supervision. This thesis or any part of it was not submitted for any Degree/Diploma or any other academic award elsewhere.

Dated: 30-05-2019



Dr. Sachin Kadam
Research Supervisor
Chief Technology Officer
Advancells, Noida, India.
Former Associate Professor and Head,
Dept. of Stem Cell and Regenerative
Medicine, Center for Interdisciplinary
Research, D.Y. Patil Education Society
(Deemed to be University), Kolhapur
416006



Prof. (Dr.) R. K. Sharma
Co-supervisor
Dean, D.Y. Patil Medical College,
D.Y. Patil Education Society
(Deemed to be University),
Kolhapur 416006

Forwarded through



Prof. (Dr.) C. D. Lokhande

Research Director and Dean

Center for Interdisciplinary Research,
D.Y. Patil Education Society (Deemed to
be University), Kolhapur 416006

ACKNOWLEDGEMENTS

This has been a fantastic experience of highs and lows from start to end. Many great peoples have helped me through this work, both in academic and personal terms, and I would like to thank them all here. First of all, I would like to express my deepest gratitude to my Guides Dr. Sachin Kadam and Dr. R.K. Sharma who have supported me for my Ph.D. work unconditionally with invaluable guidance, constant encouragement, inspiring and thought provoking discussions. I am heartily indebted to my supervisors for accepting and training me in my journey to achieve a respectable degree in Biotechnology. I greatly appreciate the freedom my mentors gave me and the opportunity to pursue my research in my own way. Both my guides have been an inextinguishable fire of inspiration to me. You are and will forever remain a constant source of inspiration in my journey of life. I take liberty to dedicate this section of my thesis to them and thank them from the bottom of my heart for all that they have given to me. I will cherish all the moments of enlightenment they have shared with me. Undoubtedly, a free thinker and believer, I will always remember them for their attitude of pushing all limits for their dear students.

This work would not have been possible without the support and motivation of many people namely, Dr. Vikas Dighe, Dr. Rohit Dhumal, Mr. Praveen Solanke, Mr. Sudheer Jadhav, National Centre for Preclinical Reproductive and Genetic Toxicology, National Institute for Research in Reproductive Health (NIRRH), Parel, Mumbai; Dr. Pradip Chaudhary and Mr. Bhabani Shankar Mohanty, Division of Animal Oncology, Advanced Centre for Treatment, research and Education in Cancer (ACTREC), Navi Mumbai; Dr. Manas Kumar Santra and Mrs Neha Gupta, National Centre for Cell Sciences (NCCS), Pune; Dr. Anup Kale and Mrs. Vedashree Sirdeshmukh, College of Engineering (CoEP), Pune; Dr. Sandeep Pai, Amity Institute of Biotechnology, Amity University, Mumbai.

I would like to acknowledge to Prof. (Dr.) Shimpa Sharma, acting Vice-Chancellor, Prof (Dr.) P.B. Behere, former Vice-Chancellor, Dr. V.V. Bhosale, Registrar, Mr. S.P. Kole, Finance Adviser, D.Y. Patil Education Society (Deemed to be University), Kolhapur.

I would like to acknowledge to Prof. (Dr.) C. D. Lokhande, Research Director, Dr. Arvind Gulbake, Dr. Meghnad Joshi, D.Y. Patil Education Society (Deemed to be University), Kolhapur for their support and guidance. And other faculty and staff members who have helped me directly or indirectly during my research work.

I would like to tender my deepest gratitude to Dr. Rohit Teotia, Dr. Hemlata Chhabra, Department of chemical engineering, Indian Institute of Technology Bombay (IIT Bombay), Powai, Mumbai; Dr. Ashutosh Bahulekar, Krishna Institute of Medical Sciences, Karad.

Special thanks to friends and colleagues Mr. Chetan Chavan, Mr. Preetam Bala, Mr. Shreeram Joglekar, Mr. Gajanan Arbade, Mr. Sandesh Raut, Mr. Sachin Kocharekar, Defence Institute of Advanced Technology (DIAT, DU), Girinagar, Pune; Mr. Chetan Aware, Department of Biotechnology, Shivaji University, Kolhapur; Dr. Abhinav Raut, Dr Valmiki Koli, Mr. Nayeem Mulla, Ms. Jagruti Meshram, D.Y. Patil Education Society (Deemed to be University), Kolhapur.

Special thanks to all the group members without their unconditional help and support, this study would not have been successful. To my other co-workers in DIAT, Pune; D.Y. Patil Education Society (Deemed to be University), Kolhapur; NIRRH, Mumbai, NCCS, Pune who are too numerous to name here, I thank all of you for your help, time and input. I am lucky to have had the opportunity to meet all of you.

I acknowledge University Grant Commission (UGC), New Delhi for fellowship assistance.

I take this opportunity to convey my heartily admiration to all my teachers from my school days to post graduation level.

I wish to thank all my friends for being there for me always, especially Sunil Bhapkar, Sumit Totade, Navnath Parve, Subhash Walke, Amar Borade.

My parents Bhikaji Amrutrao Kashte and Saraswati B. Kashte have been a constant source of inspiration for my perseverance during my Ph.D. tenure. I am thankful to my younger brother Vikram to dissolve sweetness in my life and for his constant support.

I sincerely apologize for any omissions and sincerely thanks, all concert.

Shivaji Bhikaji Kashte

May 2019

INDEX

	Page No.
Chapter 1: Introduction	
1.1 Introduction	1
1.2 Aim and Objectives of research	4
Chapter 2: Review of Literature	
2.1 Natural bone	10
2.2 The process of bone formation	11
2.3 Bone defects and bone healing	13
2.4 Available treatments for bone healing or bone regeneration	15
2.5 Bone tissue engineering	18
Chapter 3: Experimental Techniques	
3.1 Introduction	54
3.2 Electrospinning	54
3.3 Surface modification methods	57
3.4 Scanning electron microscopy	58
3.5 Atomic force microscopy	60
3.6 Confocal microscopy	62
3.7 Fourier transform infrared spectroscopy	65
3.8 Thermogravimetric analysis	66
3.9 Mechanical testing	67
3.10 Contact angle measurement	69
3.11 Cell viability assay: MTT assay	70
3.11 Mineralization assay/ Osteoblastic differentiation assay	72
Chapter 4: Synthesis and Characterization of scaffolds	
4.1 Introduction	79

4.2 Materials and Methods	81
4.2.1 Materials	81
4.2.2 Methods	82
4.2.2.1 <i>Cissus quadrangularis</i> callus culture	82
4.2.2.2 Preparation of scaffolds by electrospinning	83
4.2.2.3 Modification of scaffolds by Layer by layer method	84
4.2.2.4 Modification of scaffolds by Paint method	85
4.2.2.5 Characterization of scaffolds	85
4.2.2.6 Isolation and culture of hUCMSCs	88
4.2.2.7 <i>In vitro</i> studies	89
4.3 Statistical analysis	91
Chapter 5: LBL scaffolds	
5.1 Introduction	94
5.2 Results and Discussion	96
5.2.1 CQ callus culture and powder extraction	96
5.2.2 Preparation and Characterization of scaffolds	96
5.2.2.1 Morphological analysis	96
5.2.2.2 Physical analysis	97
5.2.2.3 Wetting properties	100
5.2.2.4 Mechanical properties	103
5.2.3 Isolation and culture of hUCMSCs	103
5.2.4 <i>In vitro</i> studies	104
5.3 Conclusions	111
Chapter 6: Paint scaffolds	
6.1 Introduction	116
6.2 Results and Discussion	118

6.2.1 CQ callus culture and powder extraction	118
6.2.2 Preparation and Characterization of scaffolds	119
6.2.2.1 Morphological analysis	119
6.2.2.2 Physical analysis	119
6.2.2.3 Wetting properties	124
6.2.2.4 Mechanical properties	125
6.2.3 Isolation and culture of hUCMSCs	126
6.2.4 <i>In vitro</i> studies	126
6.3 Conclusions	134
Chapter 7: In vivo Bone tissue engineering	
7.1. Introduction	140
7.2. Materials and Methods	142
7.2.1 Animals and housing	142
7. 2.2 Study design and surgical procedures	142
7.2.3 Blood collection, Haematology and Serum Biochemistry	143
7.2.4 X-ray and micro-CT analysis	144
7.2.5 Histological analysis	145
7.3 Statistical analysis	146
7.4 Results and Discussion	146
7.4.1 Animal weight and organ weight	146
7.4.2 Blood collection, Haematology and Serum Biochemistry	146
7.4.3 X-ray and Micro-CT analysis	153
7.4.4 Histological Analysis	156
7.5 Conclusions	159
Chapter 8: Summary and Conclusions	
8.1 Summary and Conclusions	164

Annexure I: Certificates

Annexure II: Publications

ABBREVIATIONS

AFM: Atomic force microscopy	EDC: 1-Ethyl-3-[3-
ALP: Alkaline phosphatase	dimethylaminopropyl] carbodiimide
ASCs: Adipose tissue derived stem cells	hydrochloride
BAP: 6-Benzylaminopurine	ERK: Extracellular signal-regulated
BDHA: 3D bovine-derived porous HA	kinases
BMD: Bone Mineral Density	ESCs: Embryonic stem cells
BMPs: Bone morphogenic proteins	FESEM: Field emission scanning
BMPs: Bone morphogenic proteins	electron microscopy
BMSCs: Bone marrow mesenchymal	FS: Forsterite
stem cells	FTIR: Fourier Transform Infrared
BSP: Bone sialoprotein	Spectroscopy
BW: Body weight	G: Glycosaminoglycan
CA: Contact angle	GO: Graphene oxide
CLSM: Confocal laser scanning	GP: Graphene
microscope	HA: Hydroxyapatite
CMC: Carboxymethyl cellulose	Hb: Hemoglobin
CNCs: Cellulose nanocrystals	Hf: Hafnium
Co-Cr: Cobalt-Chromium	hFOB: Human fetal osteoblast
Col-mHA: Collagen-HA microsphere	HgCl ₂ : Hypochloride
Col-SF-HA: Collagen-silk fibroin-HA	hUCMSCs: Human umbilical cord
CPCSEA: Committee for the Purpose of	derived mesenchymal stem cells
Control and Supervision of Experimental	IGFs: Insulin-like growth factors
Animals	iPSCs: induced pluripotent stem cells
CQ: <i>Cissus quadrangularis</i>	JNK: c-Jun N-terminal kinase
DAPI: 4, 6- Daimidino-2-2phenylindole,	L: Lymphocytes
dihydrochloride	M: Monocytes
DBM: Demineralized bone matrix	MAPK: Mitogen-activated protein
DMEM: Dulbecco's Modified Eagles	kinase
Medium	MCH: Mean Corpuscular Hemoglobin
E: Eosinophils	MCHC: Mean Corpuscular Hemoglobin
ECM: Extra cellular matrix	Concentration
	mCOB: Mice calvarial osteoblasts

m-CPC: Micro-sized calcium silicate-poly (3-caprolactone) composite	PET: Poly (ethylene terephthalate)
mCT: Micro-computed tomography	PGA: Poly (glycolic acid)
MCV: Mean Corpuscular Volume	PHB: Poly (3-hydroxybutyrate)
MHC: major histocompatibility complex	PHBV: Poly (3-hydroxybutyrate-co-3-hydroxyvalerate)
MSCs: mesenchymal stem cells	PLA: Poly (lactic acid)
MTS: 3-(4, 5-dimethylthiazol-2-yl)-5-(3-carboxymethoxyphenyl)-2-(4-sulfophenyl)-2H-tetrazolium	PLDL: Poly (L/DL-lactide)
MTT: 3-(4, 5-dimethylthiazol-2-yl)-2, 5-diphenyltetrazolium bromide	PLGA: Poly (lactic-co-glycolic acid)
MWCNTs: Multi-walled carbon nanotubes	PLT: Platelets
N: Neutrophils	PSU: Polysulfone
NAA: α -Naphthalene acetic acid	PVA: Poly (vinyl alcohol)
NADPH: Nicotinamide adenine dinucleotide phosphate	RBC: Red Blood Cell
Nb: Niobium	Re: Rhenium
n-CPC: nano-sized calcium silicate-poly (3-caprolactone) composite	Rel weight: Relative weight
NiTi: Nitinol	rGO: Reduced graphene oxide
OBs: Calvarial osteoblasts	RMS: Root mean square roughness
OCN: Osteocalcin	ROI: Region of interest
PAA: Poly (ethyleneimine) (PEI)	Runx2: Runt-related transcription factor2
PBAPCL: Poly-1, 4- butylene adipate-co-polycaprolactam	SF: Silk fibroin from <i>Bombyx mori</i>
PBS: Phosphate buffer saline	SGOT: Serum glutamic oxaloacetic transaminase
PCL: Poly ϵ -caprolactone	SGPT: Serum glutamic pyruvic transaminase
PCV: Packed Cell Volume	SWCNTs: Single-walled carbon nanotubes
PDCs: Periosteum-derived cells	Ta: Tantalum
PDGFs: Platelet-derived growth factors	TCP: Tri-calcium phosphate
PDLLA: Poly-d, l-lactic acid PEDOT:	TGA: Thermal degradation analysis
PSS poly (3,4-ethylene dioxythiophene) poly (4-styrene sulfonate)	TGF- β : Transforming growth factor-beta
	THF: Tetrahydrofuran
	Ti: Titanium
	Ti ₆ Al ₄ V: Titanium-Aluminium (6%)-vanadium (4%) alloy
	TiNbZr: Titanium-Niobium-Zirconium

TNF- α : Transforming growth factor – α

UTM: Universal tensile Machine

VEGFs: Vesicular endothelial growth factors

WBC: White Blood Cell

XTT: 2, 3-bis-(2-methoxy-4-nitro-5-sulfophenyl)-2H-tetrazolium-5-carboxanilide

UTS (σ_u): Ultimate strength or tensile strength

Y (σ_y): Yield strength

CHAPTER 1:

INTRODUCTION



1.1 Introduction

Bone is a complex connective tissue that plays a vital role in providing a structural framework, mechanical support, and flexibility to the body. It is also involved in mineral storage, homeostasis and blood pH regulation^{1,2}. Bone defects and their repair is the most common problem worldwide³; gaining a second most transplanted tissue status followed by blood^{4,5}. In the U.S. alone, more than 6.5 million bone defects⁶ and over 3 million facial injuries⁷ recorded every year. Annually, more than 2.2 million bone graft procedures are performed worldwide. Tumor resection, congenital malformation, trauma, fractures, surgery, or diseases like osteoporosis, arthritis^{8,9} are the major causes of bone defects. Some clinical conditions like skeletal reconstruction of large bone defects or compromised regenerative processes such as avascular necrosis, atrophic non-unions and osteoporosis¹⁰ also require bone related transplants. Though a majority of fractures having sufficient mechanical stabilization are capable of robust repair, 5% - 10% of all fractures result in delayed union or nonunion¹¹. Bone fractures treatment costs a billion dollars and affects societal productivity and individual ability¹². The repair or replacements of such damaged or traumatized bone tissue require urgent attention.

Bone healing is a complex process of biology and biomechanics to restore the form and function of the bone¹³. Though bone regeneration is a substantial medical challenge achieved in initial days through standard approaches like distraction osteogenesis, bone transport⁹ or different bone grafting methods like autografts, allografts, bone graft substitutes or by using growth factors¹⁰. The first commercial bone graft material was introduced in 1993 as Interpore's coral derived Pro-Osteon[®]. Autografts have achieved various degrees of success in treating bone defects. However, the autograft is limited by the donor site morbidity, prolonged rehabilitation, increased risk of deep infection and restricted availability. Although bone allografts resolve transplantable bone samples limitations to some extents, it may induce potential risks of transmissible diseases, viral infection, immunological rejections¹⁴⁻¹⁶, efficacy and cost-effectiveness¹⁰. Because of the avascular and diffusion dependent nature of the bone grafts, the bone defect size and host viability can limit their application¹⁷. Presently, there are no heterologous or synthetic bone substitutes available which are of top-quality or of the same characteristics compared with natural bone. Hence, there is a necessity to develop a novel treatment as an alternative or adjunct to the standard methods used for bone regeneration.

The recent developments in tissue engineering and regenerative medicine to achieve a bone substitute to replace conventional bone grafts have shown a 'ray of hope'¹⁸. Tissue engineering is the art of design and fabrication of new tissues for efficient repair of damaged organs and substitutions of lost parts because of ailment and or trauma. Tissue engineering has shown a full potential of bone repair through the use of osteogenic growth factors like bone morphogenic proteins (BMPs), osteoinductive matrix, gene therapy, use of stem cells etc¹⁹. Limitations of scaffolds to mimic the natural bone tissue eliminate most of these materials during animal trials, with very few exceptions that have reached human trials. Truly, the choice of appropriate scaffold material with the desired characteristics is the need of the hour.

Number of materials including metals [stainless steel, Cobalt-Chromium (Co-Cr) alloys and Titanium (Ti) alloys, etc.]²⁰, ceramics, Hydroxyapatite (HA), tri-calcium phosphate (TCP), etc.)²¹, natural polymers (collagen, chitosan, etc.)²² and synthetic polymers (poly (lactic acid) (PLA), poly (glycolic acid) (PGA), etc.) and their combinations have been explored for replacement and repair of damage or traumatized bone tissues. However, due to their limitations and complexity, ideal scaffolds or their supreme combinations still remain a need of time for better bone regeneration.

The poly ϵ -caprolactone (PCL) is the FDA approved biocompatible and biodegradable polymer largely used in tissue engineering applications. In various studies, PCL in combination with Hydroxyapatite (HA)²³, or gelatin hybrid nano-fibrous membranes²⁴, or (Poly-1,4- butylene adipate-co-polycaprolactam (PBAPCL)- HA composite²⁵, has shown its potential in bone tissue engineering applications. Though PCL is a good scaffolding material, alone it lacks the osteoinductive and osteoconductive properties. In the present study, along with PCL, we used graphene oxide (GO), graphene (GP) and *Cissus quadrangularis* (CQ) callus culture extract as physical, chemical, and biological property enhancers in the preparation of scaffolds for bone tissue engineering.

GP has gained attraction in bone tissue engineering because of its large surface area, low biological toxicity and osteoinductive nature²⁶. GP-chitosan films²⁷, GP coated cobalt- chromium-molybdenum-based alloy²⁸, GP nanosheets coated titanium alloys²⁹ showed biocompatibility and its potential in tissue engineering. On the other hand, GO has more hydrophilic groups and easy dispersion ability than GP³⁰. GO along with HA

and chitosan functionalized graphene nanoplatelets reinforced with polyvinyl alcohol,³¹ GO with Polylactic acid and HA³², GO doped poly (lactic-co-glycolic acid) (PLGA) scaffolds³⁰, GO-poly-L-lysine composites³³ have successfully been used for bone tissue engineering. GP and GO are most fascinating materials of today and their interaction with stem cells revealed cellular compatibility and ability to differentiate stem cells into osteoblasts, chondroblasts, and neuronal lineages^{28,29,34}.

Cissus quadrangularis, also known as Vajravalli, Hadjod, or Kandvelis widely used in Ayurveda as Asthiyuk (bone strengthener)³⁵. The stem extract of this plant is rich in calcium ions (4% weight) and phosphorous³⁶ and ethanolic extract contains triterpenes, β -sitosterol, α and β -amyrins, ketosteroids, phenols, tannins, carotene and vitamin C³⁵. This extract is proved to be useful in the healing of fractured bone. The active constituents of CQ may promote proliferation and osteoblastic differentiation of mesenchymal stem cells (MSCs)³⁷ and bone formation via wnt-LRp5- β -catenin or MAPK dependent pathway. The isolated phytogenic steroid is believed to be the main constituent in CQ³⁸. Methanolic extract of CQ³⁹ and its use in PCL-CQ-HA nano-fibrous scaffolds found to be a potential biocompatible material for bone tissue engineering⁴⁰. The callus culture of CQ contains a pure and larger quantity of metabolites like phytosterols than crude stem extract of the plant. Hence, we have used CQ callus culture extract as an active natural ingredient in our prepared bone regenerating scaffold.

The interaction between tissue and foreign surface largely depends upon the surface properties of materials such as wettability, roughness or topography, surface charge and chemistry⁴¹. Rough surfaces with porosity are significant in cell behavior. For better cell attachment, scaffolds should possess adequate surface structure and chemistry⁴². The surface modification also helps in the improvement of the biological properties of scaffolds like cell attachment and proliferation.

In this study, porous PCL electrospun sheets are modified with GO or GP and CQ solution/ ink using layer by layer method and paint method. The layer by layer method offers advantages of both these approaches as a surface modification technique for polymers. It is a simple, relatively fast, environmentally benign, and potentially economic process to prepare uniform multilayer films on substrates from solution⁴³. The paint method is very similar to ordinary painting and easy to apply for a modification of

scaffolds as compared to plasma treatment, spin coating, etc. These composite scaffolds are characterized and studied for bone tissue engineering.

1.2 Aim and Objectives of research:

Aim of the present study is to prepare simple yet effective composite bone regenerating scaffold and its *in vitro* and *in vivo* evaluation in bone tissue engineering.

The main objectives of the thesis are:

a) Preparation and characterization of scaffolds:

Prepare the scaffolds using simple method to improve morphological, mechanical and biological properties along with stimulating osteoconductive, osteogenic and osteoinductive properties. The scaffold of polycaprolactone (PCL) is prepared by electrospinning as previously described by Jaiswal *et al*⁴⁴. Scaffolds then modified using layer by layer method and paint method with graphene (GP), graphene oxide (GO), and *Cissus quadrangularis* plant callus culture extract (CQ). These scaffolds are characterized for morphological, mechanical and biological properties.

b) Isolation, and expansion of human umbilical cord mesenchymal stem cells (hUCMSCs):

Isolation of mesenchymal stem cells from Wharton's jelly part of human umbilical cord is performed by the method described by Kadam *et al*⁴⁵. These isolated hUCMSCs are used for further studies.

c) *In vitro* bone tissue engineering:

The novel combination scaffolds are used to spontaneously differentiate hUCMSCs into osteoblasts devoid of any osteoinductive medium or growth factors. The cell viability, cell attachment and the osteogenic differentiation of hUCMSCs, the extent of mineralization are observed.

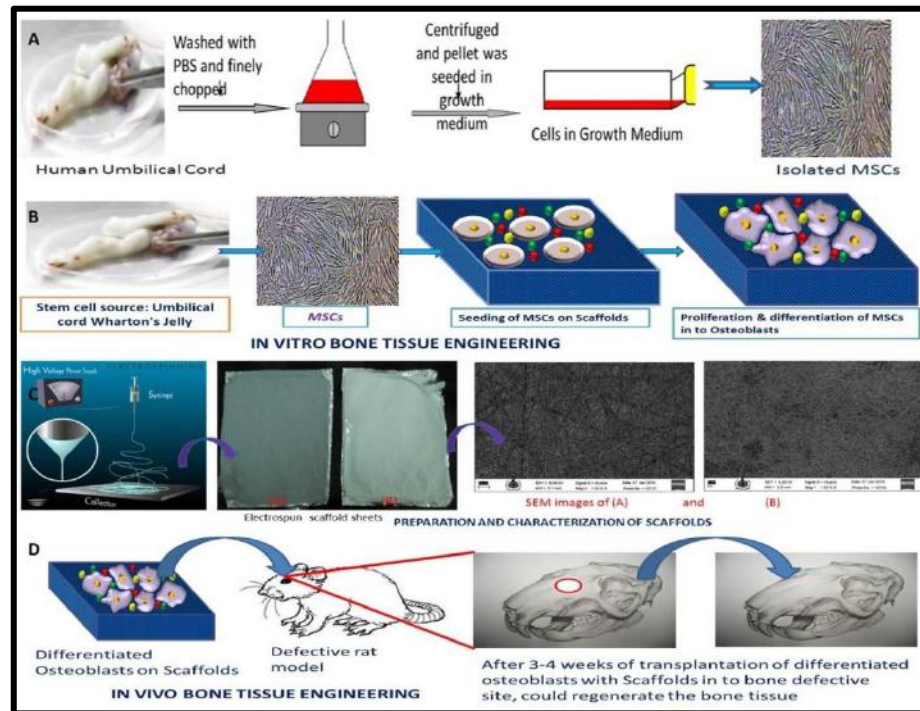


Figure -1.1: Overview of Bone tissue engineering. A. Isolation, and expansion of human umbilical cord mesenchymal stem cells (hUCMSCs); B. Preparation and Characterization of scaffolds; C. *In vitro* Bone tissue engineering; D. *In vivo* Bone tissue engineering

d) *In vivo* Bone tissue engineering:

The potential of these novel combination scaffolds is studied in presence of hUCMSCs for bone fracture healing in animal model. The rats with critical size bone defects are used for the *in vivo* bone regeneration. The amalgamation of hUCMSCs and different blend of scaffolds are transplanted into these rat models through surgical methods. After 6 and 12 weeks, animal models are analyzed for *in vivo* bone regeneration.

References:

- 1 D. Marolt, M. Knezevic and G. V. Novakovic, *Stem Cell Res. Ther.*, 2010, **1**, 1–10.
- 2 J. A. Sowjanya, J. Singh, T. Mohita, S. Sarvanan, A. Moorthi, N. Srinivasan and N. Selvamurugan, *Colloids Surf. B. Biointerfaces*, 2013, **109**, 294–300.
- 3 J. Venkatesan, I. Bhatnagar and S.-K. Kim, *Mar. Drugs*, 2014, **12**, 300–316.
- 4 M. Fröhlich, W. L. Grayson, D. Marolt, J. M. Gimble, N. Kregar-Velikonja and G. Vunjak-Novakovic, *Tissue Eng. Part A*, 2010, **16**, 179–189.
- 5 A. Oryan, S. Alidadi, A. Moshiri and N. Maffulli, *J. Orthop. Surg. Res.*, 2014, **9**, 1–27.
- 6 M. Deng, R. James, C. T. Laurencin and S. G. Kumbar, *IEEE Trans. Nanobioscience*, 2012, **11**, 3–14.
- 7 T. P. Arthur K Adamo, Haitham Al Shetawi, *Medscape Ref.*, 2012, **4**, 1–10.
- 8 E. Jimi, S. Hirata, K. Osawa, M. Terashita, C. Kitamura and H. Fukushima, *Int. J. Dent.*, 2012, **2012**, 1–7.
- 9 D. Smrke, P. Rožman, M. Veselko and B. Gubina, in *Regenerative Medicine and Tissue Engineering. IntechOpen*, 2013, pp. 325–340.
- 10 R. Dimitriou, E. Jones, D. McGonagle and P. V Giannoudis, *BMC Med.*, 2011, **9**, 66–76.
- 11 S. Stewart, S. J. Bryant, J. Ahn and K. D. Hankenson, in *Translational Regenerative Medicine.*, Elsevier Inc., 2015, pp. 313–333.
- 12 M. S. Ghiasi, J. Chen, A. Vaziri, E. K. Rodriguez and A. Nazarian, *Bone Reports*, 2017, **6**, 87–100.
- 13 A. R. Shrivats, P. Alvarez, L. Schutte and J. O. Hollinger, in *Principles of Tissue Engineering.*, Elsevier, 4th edn., 2013, pp. 1201–1221.
- 14 Z. Xia, X. Yu, X. Jiang, H. D. Brody, D. W. Rowe and M. Wei, *Acta Biomater.*,

- 2013, **9**, 7308–7319.
- 15 L. Chen, J. Hu, J. Ran, X. Shen and H. Tong, *Int. J. Biol. Macromol.*, 2014, **65**, 1–7.
- 16 C. Zhao, A. Tan, G. Pastorin and H. K. Ho, *Biotechnol. Adv.*, 2013, **31**, 654–668.
- 17 K. J. . Burg, S. Porter and J. F. Kellam, *Biomaterials*, 2000, **21**, 2347–2359.
- 18 A. I. Rodrigues, M. E. Gomes, I. B. Leonor and R. L. Reis, *Acta Biomater.*, 2012, **8**, 3765–3776.
- 19 B. Garg and R. Malhotra, *JIMSA*, 2011, **24**, 27–28.
- 20 J. E. L. Buddy D. Ratner, Allan S. Hoffman, Frederick J. Schoen, in *Biomaterials science: an introduction to materials in medicine.*, Elsevier Inc, 1996, pp. 415–455.
- 21 F. J. O’Brien, *Mater. Today*, 2011, **14**, 88–95.
- 22 C.-K. C. Yang, Shoufeng, Kah-Fai Leong, Zhaohui Du, *Tissue Eng.*, 2001, **7**, 679–689.
- 23 B. Chuenjitkuntaworn, T. Osathanon, N. Nowwarote, P. Supaphol and P. Pavasant, *J Biomed Mater Res Part A*, 2015, **104**, 264–271.
- 24 K. Ren, Y. Wang, T. Sun, W. Yue and H. Zhang, *Mater. Sci. Eng. C*, 2017, **78**, 324–332.
- 25 V. Y. Chakrapani, T. S. S. Kumar, D. K. Raj and T. V Kumary, *J. Nanosci. Nanotechnol.*, 2017, **17**, 2320–2328.
- 26 P. Yu, R. Y. Bao, X. J. Shi, W. Yang and M. B. Yang, *Carbohydr. Polym.*, 2017, **155**, 507–515.
- 27 H. Fan, L. Wang, K. Zhao, N. Li, Z. Shi, Z. Ge and Z. Jin, *Biomacromolecules*, 2010, **11**, 2345–2351.
- 28 Q. Zhang, K. Li, J. Yan, Z. Wang, Q. Wu, L. Bi, M. Yang, K. Li, J. Yan, Z. Wang,

- Q. Wu, L. Bi, M. Yang and Y. Han, *Biochem. Biophys. Res. Commun.*, 2018, **497**, 1011–1017.
- 29 J. Qiu, J. Guo, H. Geng, W. Qian and X. Liu, *Carbon N. Y.*, 2017, **125**, 227–235.
- 30 Y. Luo, H. Shen, Y. Fang, Y. Cao, J. Huang, M. Zhang, J. Dai, X. Shi and Z. Zhang, *ACS Appl. Mater. Interfaces*, 2015, **7**, 6331–6339.
- 31 T. Kaur, A. Thirugnanam and K. Pramanik, *Mater. Today Commun.*, 2017, **12**, 34–42.
- 32 H. Ma, W. Su, Z. Tai, D. Sun, X. Yan, B. Liu and Q. Xue, *Chinese Sci. Bull.*, 2012, **57**, 3051–3058.
- 33 W. Qi, W. Yuan, J. Yan and H. Wang, *J. Mater. Chem. B*, 2014, **2**, 5461–5467.
- 34 L. R. Jaidev, S. Kumar and K. Chatterjee, *Colloids Surfaces B Biointerfaces*, 2017, **159**, 293–302.
- 35 A. Siddiqua and S. Mittapally, *Int. Res. J. Pharm. Biosci.*, 2017, **4**, 9–29.
- 36 M. S. Rao, P. Bhagath Kumar, V. B. Narayana Swamy and N. Gopalan Kutty, *Pharmacologyonline*, 2007, **3**, 190–202.
- 37 B. K. Potu, M. S. Rao, N. G. Kutty, K. M. R. Bhat, M. R. Chamallamudi and S. R. Nayak, *Clinics (Sao Paulo).*, 2008, **63**, 815–820.
- 38 N. Singh, V. Singh, R. Singh, A. Pant, U. Pal, L. Malkunje and G. Mehta, *Natl. J. Maxillofac. Surg.*, 2013, **4**, 52–56.
- 39 D. K. Deka, L. C. Lahon, A. Saikia and Mukit, *Indian J Pharmacol*, 1994, **26**, 44–45.
- 40 S. Suganya, J. Venugopal, S. Ramakrishna, B. S. Lakshmi and V. R. Giri Dev, *J. Appl. Polym. Sci.*, 2014, **131**, 1–11.
- 41 W. M. Gallagher, I. Lynch, L. T. Allen, I. Miller, S. C. Penney, D. P. O'Connor, S. Pennington, A. K. Keenan and K. A. Dawson, *Biomaterials*, 2006, **27**, 5871–5882.

- 42 S. Yang, K. F. Leong, Z. Du and C. K. Chua, *Tissue Eng.*, 2001, **7**, 679–689.
- 43 W. Chen and T. J. McCarthy, *Macromolecules*, 1997, **9297**, 78–86.
- 44 A. K. Jaiswal, S. S. Kadam, V. P. Soni and J. R. Bellare, *Appl. Surf. Sci.*, 2013, **268**, 477–488.
- 45 S. Kadam and R. Bhonde, *Islets*, 2010, **2**, 112–120.

CHAPTER 2:

REVIEW OF LITERATURE

2.1 Natural Bone:

Bone is a type of connective tissue that supports the entire body structure in vertebrates. Typical bone structure (Figure.2.1)¹ comprises of 10-30% of compact porous hard outer layer known as ‘cortical bone’ and a spongy 30-90% of porous interior part called ‘cancellous bone’². These two types of bone structures are differentiated on the basis of their porosity and density. As compared to cortical bone, the cancellous bone is younger, metabolically more active and remodelled¹. The microstructure of cortical bone shows cylindrical shape lamellae (3-7 μm), while cancellous bone has spiral shaped lamellae. Lamellae are formed by mineralized collagen fibres and the sheets of lamellae (3-8 lamellae per sheet) envelope the central canal to form the Osteon or Haversian system, a functional unit of cortical bone¹. In the cortical bone, there is a compact arrangement of osteons while in the cancellous bone it forms a trabecular network of microporous bone³⁻⁵.

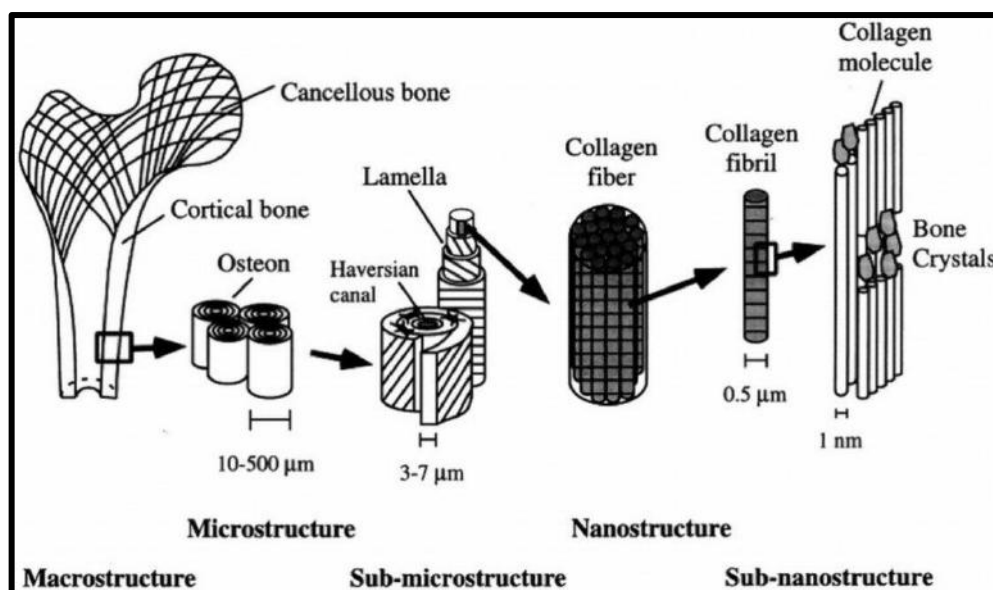


Figure 2.1: Hierarchical structural organization of bone, adapted from¹ with copyright permission from Elsevier (License No. 4578741170592).

Natural bone comprise (Figure 2.2) of a 65% mineral, 25% organic and 10% water by weight and 33-43% apatite minerals, 32-44% organic and 10-15% water by volume³. This unique organic and inorganic material composition gives mechanical properties to

the bone. The organic bone phase mostly contains >90% of the collagen⁶ and the rest is of mucopolysaccharides, peptides, enzymes⁷, lipids and ions like sodium, magnesium, fluoride and citrate. The inorganic or minerals consist of mostly calcium and phosphorus (2:1 ratio in bone) in the form of tricalcium phosphate and hydroxyapatite⁸. The 70% mineral phase of bone mostly contains nanoscale HA crystals^{4,8}.

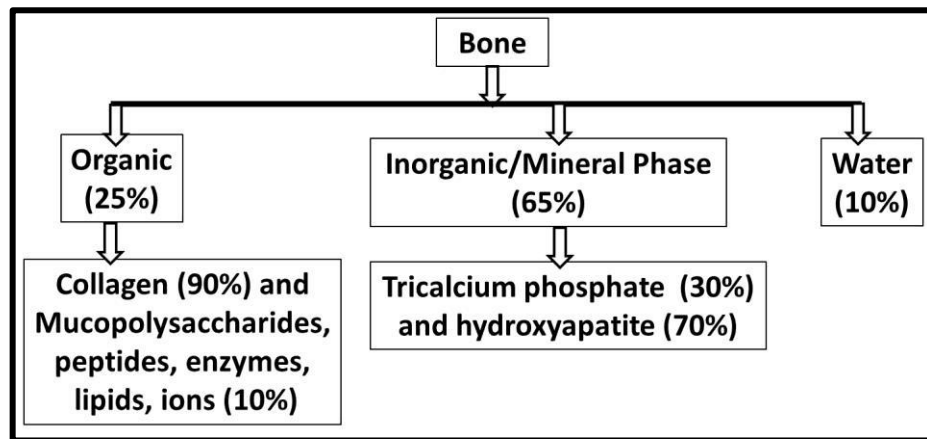


Figure 2.2: Flowchart explaining natural bone composition

2.2 The process of bone formation:

The process of bone formation (ossification or osteogenesis) is of two types: Endochondral ossification (primary bone formation) and Intramembranous ossification (secondary bone formation)⁹. Intramembranous ossification is the direct method of bone formation in which mesenchymal cells directly differentiate into osteoblasts and replaces connective tissue sheets with bony tissue. The endothelial cells change into polymorphic cells and then transform to the osteoblastic phenotype. There is the absence of cartilaginous phase. There is the formation of hard callus mediated through osteoprogenitor cells and undifferentiated mesenchymal cells e.g. flat bones like skull, face, clavicle and mandible^{4,9}.

Endochondral ossification is two-step process of bone formation; hyaline cartilage which is formed first and then replaced by bony tissue formation. Here, mesenchymal cells at first differentiate into chondrocytes and secrete cartilaginous matrix. The woven bone is formed with cartilage, followed by calcification and replacement of bone. The

stages of endochondral bone formation include hematoma formation, inflammation, angiogenesis, cartilage formation, cartilage calcification, cartilage removal, bone formation and finally bone remodelling. In the bone remodelling, young woven bone is gradually replaced by a lamellar bone to restore the mechanical integrity of the healing site E.g. long, short and irregular bones like the femur, tibia, humerus and radius^{4,9,10}. The bone homeostasis is maintained by osteoblasts, osteocytes and osteoclasts.

Osteoblasts, bone forming cells originated from mesenchymal stem cells. Osteoblast resides on bony surfaces. They have unique ability to secrete Type I collagen-rich extracellular matrix (ECM) that eventually mineralized in the process of bone formation. There are different maturation phases of osteoblasts, as pre-osteoblasts, mature osteoblasts, osteoid osteocytes, early osteocyte and mature osteocytes. The niche for osteoprogenitors in bone is the periosteum, the endosteum and the marrow stroma. The mesenchymal progenitor cells serve as a stem cell reservoir to be recruited to the injury site on the insight of bone trauma or fracture. A master control gene Runx2 (Runt-related transcription factor-2) is responsible for the differentiation of progenitor cells to osteoblasts. The mature and active osteoblasts are cuboidal or polygonal in shape. They secrete bone matrix or osteoid. These cells contain abundant endoplasmic reticula and enlarged Golgi apparatus. The major protein secreted is Type I collagen, a fibrillar extracellular matrix protein. Also, they secrete non-collagenous proteins like osteocalcin to form the unmineralized matrix in the osteoid seam. Other cells derived from the osteoblastic lineage are bone lining cells. Though their origin thought to be controversial, are considered to be resting osteoblasts, pre-osteoblasts or post-osteoblasts. Bone lining cells cover almost all surfaces in the adult bone to build a connective tissue barrier. They contribute in bone remodelling. They are involved in the homeostatic processes as they are in communication with the osteocyte network and also an element of the strain sensing network^{11,12}.

Osteocytes are advanced osteoblasts and embedded in the innate bone matrix. They have developed long slender-like cell processes and have loosed many of their cytoplasmic organelles, with the stellar shape. They have a unique location in bone, within lacunae inside the bone matrix. These cells form a connective network by sending

their dendritic processes through canaliculi connecting and spanning throughout the whole bone volume. Osteocytes are multifunctional. Osteocytes trigger the response to physical forces upon bone and respond to formation or resorption of bone. Osteocyticosteolysis breaks down the bone matrix to release the calcium for calcium homeostasis. They also control phosphate homeostasis. Osteocyte lacunocanalicular complex can act as an endocrine system, affecting remote organs such as the kidney. They act as orchestrators of both bone formation and bone resorption. It can produce sclerostin which inhibits osteoblastic bone formation. Osteocytes can support osteoclast formation, especially in apoptotic phase. Osteocytes derived from osteoblast make up 90% of cells of the mature skeleton. They are the most abundant cell type found in bone¹¹⁻¹³.

Osteoclasts, the bone resorbing cells are of hematopoietic origin that resorbs extracellular matrix in the process of bone resorption. The osteoclast precursor cells are employed to the bone exterior where they blend to develop multinucleated cells. Osteoclasts are very rare in bone, only two to three cells per μm^3 bone. These active, multinucleated giant cells found in specialized cavities on the bone surface, called Howship's lacunae. The osteoclasts seal the cavity around its ruffled border and then secrete protons and a variety of proteolytic enzymes, like collagenases, gelatinases, into the cavity; the pH is reduced to approximately 2-3, to carry out the organic breakdown of the ECM. Chondrocytes with mesenchymal origin reside in cartilage and also involved in endochondral ossification^{11,12}.

2.3 Bone defects and bone healing:

Bone is prone to injury due to trauma, infection, tumours and compromised blood supply. Though a majority of fractures having sufficient mechanical stabilization are capable of robust repair, 5%-10% of all fractures result in delayed union or nonunion¹⁴. Bone healing is the complex process involving mechanobiological processes. It is like the recapitulation of the ontological events taking place during the embryonic development of the skeleton. It restores the composition, structure and function of the damaged organ to its pre-injury status. Bones healing depending upon type of fractures are classified as primary bone healing and secondary bone healing.

2.3.1 Primary bone healing:

The fracture of less than 0.1 mm gap with rigidly stabilized fracture site healed by primary or direct bone healing by intramembranous ossification process. It is believed that bone gap is filled directly by continuous ossification and subsequent Haversian remodelling. However, this process of direct continuous bone formation is controversial due to the lack of neither histological evidence and clinical cases¹⁵⁻¹⁸.

2.3.2 Secondary bone healing:

When the edges of the fracture site are less than twice the diameter of the injured bone, then the secondary or indirect bone healing is most common. It is a multi-event process involving blood clotting, inflammatory process, fibro-cartilage callus formation, intramembranous and endochondral ossification and bone remodelling.

The bone fracture healing is initiated with major metabolic activity, an anabolic phase, where inflammation results in an increase of local tissue volume. After the bone splintering, the hematoma is developed at the splinter site. It shams as a provisional scaffold for stem cell differentiation into fibrous tissue, cartilage and bone. In the inflammatory phase, several biological factors including transforming growth factor – alpha (TNF- α), transforming growth factor-beta (TGF- β), bone morphogenic proteins (BMPs), Interleukins (IL-1 β , IL-6, IL-17Fand IL-23) and cytokines are released. The mechanical strain or hydrostatic pressure also plays a role in fracture healing. These factors associated micro-environment regulate activities of endothelial cells, fibroblasts, MSCs, chondrocytes and osteoblasts. The anabolic activities continue in a prolonged phase, which is dominated by catabolic activities. The growth in healing shapes the cartilaginous callus or soft callus via the actions of skeletal and endothelial cells. It ties the rift amongst the bone fragments. After that soft callus is an advance to form hard callus. The reduction of callus tissue volume is the symbol of this activity. The catabolic phase reaches its final stage on increasing vascular bed and normalcy of vascular flow rate. Once hard callus has fully formed composed of woven bone, the final stage of healing is remodelling. The woven bone is remodelled to form mature bone. During this

phase, Haversian remodelling of the callus and lamellar bone transformation continues long after the fracture has clinically healed¹⁴⁻¹⁹.

2.3.3 Distraction Osteogenesis:

Distraction Osteogenesis is a process of bone regeneration in which a corticotomy is performed followed by gradual distraction, resulting in the formation of new bone. Three stages as latency, distraction and consolidation are involved in the distraction osteogenesis¹⁶. The latency involves the inflammatory stage and endochondral ossification. The distraction involves the similar process to intramembranous ossification, there is no cartilage callus. The consolidation is similar to the final stage of endochondral ossification¹⁶.

2.3.4 Critical-sized bone defects:

The Critical sized bone defects or large segmental bone defect is an extreme condition in bone healing. It can be caused by high energy trauma, diseases, developmental deformities, revision surgery and tumour resection or osteomyelitis. The large bone damage in this defect has been displayed to direct revascularization and tissue differentiation and ultimately advances to impulsive bone fracture which may lead to non-union without interventions. A critical-sized segmental bone defect is defined as the smallest osseous defect in a particular bone and species of animal that will not heal spontaneously during the lifetime of the animal or shows less than 10% bony regeneration during the lifetime of the animal. The length of defect exceeding 2-2.5 times the diameter of the affected bone, the minimum size in most species is considered as a critical bone defect. These critical size defects are particularly problematic for severe trauma. It affects the quality of life of patients. It entails long and postoperative therapies expense and also cause large surgical, socio-economic problems. The patients with diabetes or smoking or ageing have low bone healing potential^{14,15}.

2.4 Available treatments for Bone healing or bone regeneration:

Bone regeneration is a marvellous *pas de deux* of biology and biomechanics to restore the form and function of the bone²⁰. This is achieved in the initial days through the

natural grafts such as autografts, allografts, xenografts and synthetic grafts. In general, the grafts contain the cells while implants do not, with exceptions of few acellular allografts. These substitutes serve as combined functions of mechanical support and osteo-regeneration

2.4.1 Autografts:

An osseous graft harvested from an anatomic site and transplanted to another site within the same individuals is called autologous bone graft. The autografts are intrinsically vascularized and maybe co-harvested with a vascular pedicle. It possesses all osteogenesis, osteoinduction and/or osteoconduction properties with low risk of immunological reactions. Therefore, it can integrate into the host bone more rapidly and completely. Autologous bone graft is a benchmark for evaluating other bone substitutes and is considered as the gold standard in treating bone defects. The healing rate of autografts ranges from 60% to 100% and failure is usually associated with the harvesting, handling and implantation method used. However, the limitations of autografts have been extensively reported like perioperative and postoperative morbidity, shape restrictions often require extensive intra-operative modifications, the potential for increased surgical site infection, donor site complication and pain, inflammation, blood loss, increased operative time and the finite availability of graft material^{14,15,20}.

Cancellous autografts, most commonly used, has osteogenic potential and ability to regenerate bone due to few osteoblasts and osteocytes and mesenchymal stem cells (MSCs). Also, there is the presence of osteoinductive graft-derived proteins. Cortical autografts have limited number of osteoprogenitor cells and are mechanically supportive of structural integrity and have increased osteoinductive capacity^{14,15}.

2.4.2 Allografts:

An osseous graft harvested from one individual and transplanted to a genetically different individual of the same species is called an allograft. It is obtained from multiple sources including cadavers and organ donors. These are alternative to autografts. Allografts are used extensively for patients with poor healing potential, extensive comminution after fractures and established non-union. However, they are immunogenic

due to activation of major histocompatibility complex (MHC) antigen and have a higher failure rate compared with autografts. The immunological rejection of the graft can occur at a rate of up to 50%. There is a risk of spreading viral infection. The application of fresh allografts is always limited. Allografts undergoes processing like freeze drying, washing, demineralization and gamma-irradiation or ethylene oxide sterilization to reduce the risk of disease transmission and immunological responses but they reduce osteogenic function due to an absence of viable cells^{14,15,20}.

Cancellous allografts supplied in the form of cuboid blocks. They are mainly used in spinal fusion augmentation and filler material for cavitary skeletal defects. Cortical allografts are also used in spinal fusion augmentation for filling large skeletal defects. They are with rigid mechanical properties. Demineralized bone matrix (DBM) is well treated allografts with as a minimum 40% of the mineral content of the bone matrix separated by mild acid, while collagens, non-collagenous proteins and growth factors persist. It used as bone filling material^{14,15,20}.

2.4.3 Xenografts:

When the graft material is harvested from one species and used in an individual of a different species, it is called xenograft. They are substitute toward autografts and allografts. They are processed to ensure sterility and biocompatibility. It is widely used as bone void filler. Examples comprise an inorganic matrix from cows known as BioOss and porcine organic bone matrix known as XCM™ (Synthes). However, the risk of disease transmission and ethical issues limited their uses^{14,20}.

2.4.4 Synthetic bone grafts substitutes:

The severe scarcity of natural bone grafts and the minute possibility of resource meeting the needs in elderly residents have caused the bloom of bone grafts and substitutes arcade. Calcium sulphate, calcium phosphate, ceramics, bioactive glass or combinations are most commonly used¹⁵.

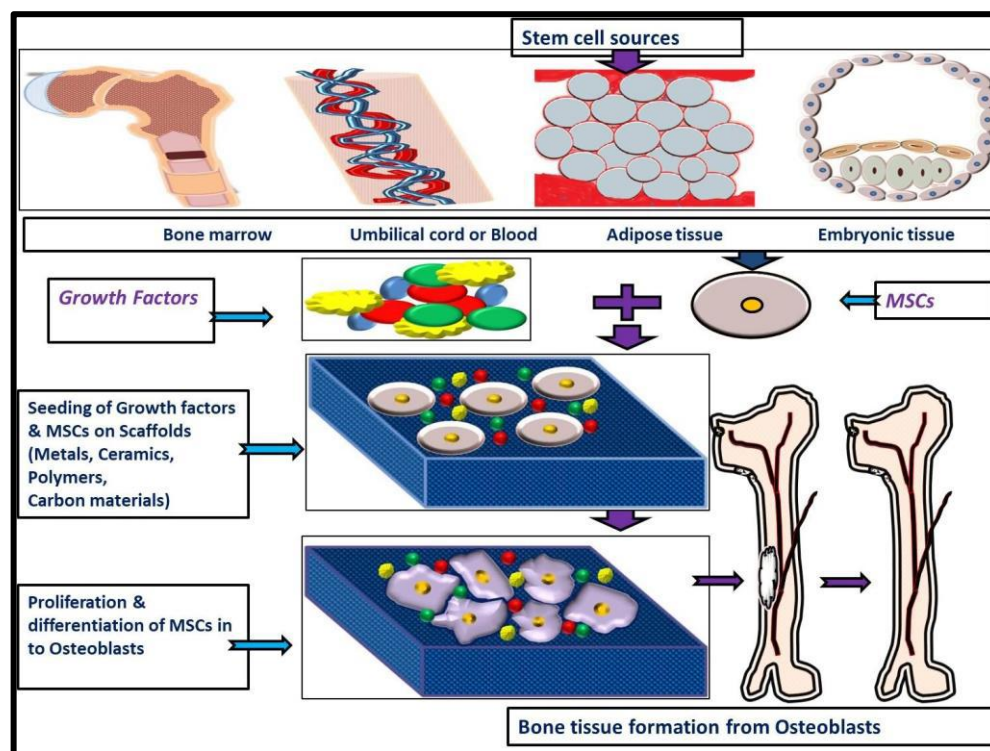


Figure 2.3: Outline of bone tissue engineering: Mesenchymal stem cells from different sources along with growth factors can be seeded on biomaterials for bone healing, adapted from²¹ with copyright permission from Springer Nature (License No. 4578750332409).

2.5 Bone Tissue engineering:

The well-known limitations of autografts and allografts continue to drive the effort to develop bone graft substitutes, using the principles of biomaterials and tissue engineering. A rational approach to regenerate bone tissue engineered products must be based on fundamental osteobiology. Tissue engineered products are bioactive and resorbable, gradually degradable and replaced by host tissues, thereby, facilitating repair in situ. The general outline for bone tissue engineering explained in Figure 2.3, adapted from²¹.

2.5.1 Bone tissue engineering using a cellular aspect:

In tissue engineering cell source can be of autologous or allogenic origin. However autologous cells are usually the better choice, as the allogeneic cells could incite immune

rejection by the recipient. Although pre-differentiated cells are widely been used in (bone)tissue engineering, the stem cells are known key element to achieving the best possible results²².

Embryonic stem cells (ESCs) are widely studied for bone tissue engineering including differentiation into the osteoblasts²³. ESCs when co-cultured with foetal fibroblasts enhanced the formation of bone nodules²⁴. Although ESCs shows *in vitro* and *in vivo* mineralization when differentiated into osteoblasts²⁵ formation of teratomas limits its clinical applications²⁶.

Mesenchymal stem cells (MSCs) are known to differentiate into matured cells like osteoblasts, chondroblasts and chondrocytes on external stimuli (like the addition of ascorbic acid, β -glycerophosphate and dexamethasone)²⁷. Bone marrow and peripheral blood are traditional sources for MSCs. MSCs isolated from peripheral blood of rabbit have been differentiated into osteoblasts, chondrocytes and healed critical-sized bone defects in rabbit models with the use of porous calcium phosphate resorbable substitute²⁸. The adequate availability and supply of adipose tissue make it as an alternative source for MSCs²⁹. However, invasive tissue extraction procedure and an age of donor³⁰ are some of the disadvantages associated with these tissue source.

The induced pluripotent stem cells (iPSCs) have recently emerged as an alternative to MSCs or ESCs. There are reports available of differentiation of human iPSCs into osteoblasts *in vitro*³⁰ and *in vivo* with no teratoma formation²⁶. The study of murine iPSCs with TGF β 1, TGF β 3 and retinoic acid showed *in vitro* differentiation into osteoblasts and *in vivo* bone formation³¹.

2.5.2 Bone tissue engineering using Growth factors:

Many growth factors viz. Bone morphogenetic proteins (BMPs), Fibroblast growth factors (FGFs), Platelet-derived growth factors (PDGFs), Transforming growth factors (TGF- β), Vesicular endothelial growth factors (VEGFs), Insulin-like growth factors (IGFs) are known to play important role in the regulation of bone formation at the different level (Ref). BMP is involved in skeletal development, adult bone homeostasis and fracture healing along with³² differentiation of MSCs into the cartilage, bone,

Table 2.1: Cells for bone tissue engineering, adapted from²¹ with copyright permission from Springer Nature (License No. 4578750332409).

Cells for Bone		
Tissue Engineering	Tissue repair	References
ESCs	Osteoblast differentiation but Teratoma formation in SCID mice	[24,25]
BMSCs	Osteoblast differentiation; osteoinduction; osteogenesis; mineralization; <i>in vitro</i> & <i>in vivo</i> bone regeneration	[22,29,63,109,138,147,149, 153]
ADSCs	Osteoblast differentiation	[29, 35, 137]
DPSCs	mineralization; <i>in vivo</i> bone regeneration	[40-43]
AFSCs	Osteoblast differentiation; <i>in vivo</i> bone regeneration	[39-41]
UCMSCs	Osteoblast differentiation; mineralization;	[35,36,38]
iPSCs	Osteoblast differentiation; mineralization; <i>in vitro</i> & <i>in vivo</i> bone regeneration	[26,30,31]
MG63 cells	Osteoblast differentiation;	[53]
MC3T3-E1	Osteoblast differentiation;	[88]
Osteoblast cells	Biocompatibility; mineralization; <i>in vivo</i> bone regeneration	[87,94,123,124,136]

tendon/ligament. BMP2, BMP6, BMP7, BMP9 are found to have the highest *in vitro* and *in vivo* osteogenic potential³³. The high doses requirement of BMPs limits its direct use in regenerative medicine³², but BMPs with different combinations of growth factors have been used in the regeneration of bone. Adenovirus-based expression vectors AdCMVBMP2, AdCMVCbfa1 and AdCMVRunx2 were used to express BMP2 and Runx2 respectively in the pluripotent C3H10T1/2 cell line³⁴. The combined effect of AdCMVBMP2 and AdCMVRunx2 had increased 10 fold osteoblastic differentiation than

any factor alone³⁴. AdCMVBMP2 plus AdCMVCbfa1 showed higher bone formation *in vivo* in immune-deficient mice³⁴.

The stimulation of FGF2 showed a positive effect on osteoblasts differentiation and bone formation via regulation of Wnt/catenin pathway³⁵. Bone marrow mesenchymal stem cells (BMSCs) were co-transduced to express recombinant basic fibroblast growth factor (bFGF) and sonic hedgehog (Shh). These transgenic BMSCs with β -tricalcium phosphate transplanted into the critical-sized calvarial defect site in rats showed increased bone regeneration³⁶. The bFGF with gelatin hydrogels showed improved bone regeneration in skull defects of rabbits³⁷ and monkeys³⁸. The PDGF stimulate VEGF secretion by pericytes through their recruitment at the site of bone injury. This recruits MSCs and BMP, Wnt signalling differentiates them into the osteoprogenitor cells and then osteoblasts. PDGF contributes to the osteogenic lineage and helps to the formation of new bone³⁹. PDGF-BB with chitosan-tricalcium phosphate enhanced the bone regeneration in rat calvarial defects⁴⁰. TGF- β plays an inhibitory role in bone regeneration³². *In vitro* and *in vivo* experiments revealed the negative effect of TGF-1 via suppression of IGF-1 and down regulation of P13K/Akt pathway on osteoblast differentiation and bone formation⁴¹.

The study with gene activated matrix formed of plasmid encoding human VEGF165 coated on collagen showed vascularization and bone regeneration in critical-sized bone defect rabbit models⁴². Though VEGF alone did not improve bone regeneration the synergistic effect of VEGF and BMP-4 recruited MSCs and contributed to endochondral bone formation⁴³. When synergistically BMP-2 and VEGF transfected periosteum-derived cells were implanted in nude mice, there was increased bone formation⁴⁴. The combined use of BMP-4 and VEGF with PLGA scaffolds and human BMSCs gave rise to higher bone regeneration than any growth factor alone⁴⁵. VEGF has a positive effect on the formation of hard bony callus. VEGF inhibition affected the healing of a tibial cortical bone defect in rabbit models⁴⁶.

IGF-1 is secreted by mature osteoblasts and stimulates *in vitro* and *in vivo* proliferation and differentiation of osteoblasts⁴¹. Human periodontal ligament stem cells treated with exogenous IGF-1 showed the *in vitro* osteogenic differentiation via up

regulation of Extracellular signal-regulated kinases (ERK) and c-Jun N-terminal kinase (JNK)-Mitogen-activated protein kinase (MAPK) pathways and *in vivo* mineralization in the tissues⁴⁷. The MSC IGF transplanted in the mice models improved the bone fractures through the callus mineralization and autocrine osteogenic effects via IRS-1 signalling⁴⁸. IL-3 is an inhibitor of osteoclastogenesis and bone resorption, thus enhancing the differentiation of MSCs into the osteoblasts and bone regeneration both *in vitro* and *in vivo* through induction of BMP2 and activation of Smad1/5/8⁴⁹.

Table 2.2: Growth factors used for bone tissue engineering adapted from²¹ with copyright permission from Springer Nature (License No. 4578750332409).

Growth Factors	Tissue repair	References
BMPs	Osteoblastic differentiation; <i>in vivo</i> bone formation	[32,33,34]
FGFs	Mineralization; <i>in vivo</i> bone regeneration	[36-38]
PDGFs	Stimulate VEGF secretion; osteogenic lineage differentiation; <i>in vivo</i> bone regeneration	[49, 40]
VEGFs	Osteogenic and angiogenic potential; bone formation	[42-46]
IGFs	Osteogenic differentiation; mineralization	[47-49]

2.5.3 Bone tissue engineering with Scaffolds:

Scaffolds are porous 3D matrices that act as temporary templates for cell adhesion and proliferation while providing mechanical support until the formation of new tissue at the affected area⁵⁰. Scaffolds can also mimic the natural extracellular matrix (ECM)^{51,52} without activating host immune response or secretion of toxic metabolites⁵³. A variety of materials such as metals [stainless steel, Cobalt-Chromium (Co-Cr) alloys and Titanium (Ti) alloys, etc.]⁵⁴, ceramics [Hydroxyapatite (HA), tri-calcium phosphate (TCP), etc.]⁵⁵, natural polymers (collagen, chitosan, etc.)⁵⁶ and synthetic polymers (poly (lactic acid) (PLA), poly (glycolic acid) (PGA), etc.) and their combinations have been explored for

replacement and repair of damaged or traumatized bone tissues. Biomaterials for orthopaedic implants have a great financial impact all over the world. In the U.S. alone it was predicted that the biomaterials for orthopaedic implants will cost as much as \$3.5 billion by the end of 2017⁵⁷.

2.5.3.1 Properties of Scaffolds:

The degree of success of bone tissue engineering greatly depends on the properties of the material to be used for the preparation of scaffolds to obtain bone regeneration and the ideal properties to be possessed by scaffolds are:

2.5.3.1.1 Biocompatibility:

The ability of a material to perform with an appropriate host response in a specific situation is called biocompatibility⁵⁸. It is the ability to support normal cellular activity including molecular signalling systems without any local and systemic toxic effects to the host tissue⁵⁹. Biocompatibility involves many terms like toxicity of the material, tissue compatibility and hemocompatibility of the material⁶⁰. The scaffolds should not evoke cytotoxic effects and inflammatory response⁶¹ and should be bioactive promoting the aimed biological process. The bioactive materials form tissue–biomaterial interface through the apatite layer which makes connections with living bone⁶² Also, scaffolds should show angiogenic properties for better nutrient, oxygen and waste transport, within a few weeks of transplantation³.

The molecular weight (MW) of the material may affect the Biocompatibility as revealed lower protein adsorption and platelet adhesion on low MW polymers as compared to higher MW polymers. Also, surface porosity affects Biocompatibility of the materials⁶⁰.

2.5.3.1.2 Biodegradability:

Biodegradation, as name suggest is a degradation of the material mediated by biological system⁵⁸. Degradation of scaffolds/materials is important as it is replaced by natural tissues. The scaffold degradation rate depends upon the physical and chemical

properties of scaffolds. Degradation of the scaffolds produces variety of by-products that may cause adverse effects on the tissues like inflammation, etc⁶³. The local tissue response is reliance on biocompatibility and biodegradability of scaffolds⁶⁴. The rate of degradation depends upon the application of scaffolds and it varies from few weeks to months or even a year depending upon the physicochemical properties of scaffold and site of implant².

2.5.3.1.3 Osteoinductivity:

Osteoinduction is the recruitment and differentiation of immature or undifferentiated cells into osteoblasts and promotes osteogenesis⁶⁵. The osteoinductive material promotes the repair of tissues in the areas that if left untreated, cannot heal their self⁶⁴.

2.5.3.1.4 Osteoconductivity:

Osteoconductive biomaterial favours the growth of osteoblasts and guides the bone formation on the surfaces of biomaterials⁶⁵. Osteoconductive material promotes the repair of tissues in the areas that if left untreated, heal their self naturally⁶⁴.

2.5.3.1.5 Mechanical properties:

The scaffolds with higher mechanical strength support cell-based bone regeneration via an endochondral ossification⁶⁶. The scaffolds should be mechanically stable so that will retain its structure after *in vivo* implantation in load-bearing tissues such as bones^{56,67}. The mechanical properties of implanted scaffolds should be comparable with the native tissue^{68,69}. The mechanical properties of cortical and cancellous bone are different from each other. The mechanical properties of cortical and cancellous bone such as compressive strength are 130-180 MPa and 0.1-16 MPa, stiffness 7-30 GPa and 0.05-0.5 GPa, density 1.7-2.0 g/cm³ and 0.03-0.12 g/cm³, microhardness 0.62-0.74 GPa and 0.63±0.11 GPa respectively and fracture toughness of cortical bone are 2-12 MPam^{1/270}. Young's modulus of cortical and cancellous bone is 15-20 GPa and 0.1-2.0 GPa respectively. Therefore, it is quite difficult to make an ideal scaffold of mechanical

properties. The mechanical properties is also affected by the grain size, the grain size is inversely proportional to the mechanical properties⁷⁰.

2.5.3.1.6 Scaffold porosity and pore size:

Scaffold porosity provides an exchange of nutrients and metabolites^{56,63}. Mainly the interconnected and diffuse porosity required for the nutrient supply, tissue growth⁶⁸ and *in vivo* neovascularization⁷¹. It allows cell attachment, proliferation, differentiation and thus promoting bone formation, repair and regeneration⁷².

Porosity parameter varies according to *in vitro* and *in vivo* conditions. Lower porosity favours osteogenesis *in vitro* while for better bone ingrowth higher porosity and pore size is needed⁷³. Still, there are controversies about the ideal pore size of the scaffolds used for bone regeneration. It may range from 100-350 μm or 300-500 μm ^{74,75}. The optimum pore size for the growth of osteoblasts type cells is 380-405 μm ⁷⁶. For the regeneration of bone, pore size should be $>300 \mu\text{m}$. The pore size of $<50 \mu\text{m}$ slows down cell migration and long-term vascular ingrowth while pore size $>1000 \mu\text{m}$ provides an insufficient surface area for cell attachment^{77,78}. Well vascularized large pores stimulate direct osteogenesis, however small pores stimulates osteochondral formation prior to osteogenesis⁷⁴. The response of the cells to the scaffolds is largely depended upon the pore size and pore shape of the scaffolds. Small pores give the large surface area that facilitates cell adhesion while larger pores facilitate cell permeability sacrificing mechanical properties of the scaffolds⁷⁹. Mechanical interlocking between the scaffold and the surrounding host tissue can be improved by appropriate porosity⁷¹. The natural bone has inconsistent porosity distribution, higher porosity in the core region with strong and dense outer shell⁸⁰. Therefore it is not necessary to construct scaffolds of uniform distribution but of gradient distribution from centre to periphery.

2.5.3.1.7 Surface Chemistry:

The interaction between tissue and foreign surface largely depends upon the surface properties of materials such as wettability, roughness or topography, surface charge and chemistry⁸¹. For better cell attachment scaffolds should possess adequate surface structure and chemistry. It has been observed that a concave surface favours better cell adhesion

and proliferation than a convex surface. A concave surface is involved in the initiation of the bone formation⁸². The cube or disc-shaped scaffold is more suitable for bone tissue engineering⁶³.

The optimum wettability of the scaffolds for stem cells observed to be 70 measured via water contact angle⁸³. Wettability increases the cell adhesion of hydrophilic scaffolds. Surface wettability regulates cytoskeletal organization and cell morphology⁸⁴. Along with wettability, a water holding capacity that promotes the expansion of culture medium inside the scaffold is required for uniform distribution of cells⁸⁵. The hydrophilic surface provides better cell attachment, spreading and proliferation of cells than hydrophobic surfaces⁸⁶. The hydrophilic surface allows absorption of fibronectin which is important in osteoblast adhesion *in vitro*⁸⁷. Surface roughness affects the adsorption of fibronectin and albumin *in vitro*⁸⁸ and promotes cell attachment and adhesion on the surfaces of composites and osteoblast proliferation, differentiation and matrix synthesis and local factor production⁸⁷. Surface roughness has a positive effect on bioactivity, water uptake and cytocompatibility of the composites⁸⁹.

The surface modification also helps in the improvement of the biological properties of scaffolds. The hydrophilic surfaces with positively charged amines negatively charged clean glass, surfaces with methyl silica gradients showed better cell attachment⁹⁰.

Surface properties like morphology, hydrophilicity, zeta-potential and surface energy promote cell adhesion, migration, phenotype maintenance and intracellular signalling *in vitro* and recruitment of cells at the tissue-scaffold interface *in vivo*⁷¹. The scaffolds should be biocompatible, biodegradable, nonimmunogenic and nontoxic and should promote cell growth, attachment, differentiation, migration⁹¹. They should be easy to manufacture, sterilizable and microsurgically implantable⁶³. They should have adequate porosity, structural strength, large surface area^{71,92}.

2.5.3.2 Types of scaffolds used for bone tissue engineering:

2.5.3.2.1 Metals:

The metallic materials such as Stainless steel, Co-Cr alloys and Ti alloys⁵⁴ are in used over 100 years ago for the bone replacements because of its mechanical properties⁹³. However, these materials are corrosive and release cytotoxic ions^{93,94} and often suffer from the wear and stress-shielding effect on transplantation into the human body⁹⁵. Stainless steel is the most common bone implant material because of the combination of properties like mechanical properties, biocompatibility, corrosion resistance and cost effectiveness⁹⁶. Recently nickel-free stainless steel implants are in focus to avoid nickel sensitivity (nickel as an allergen)⁹⁶. Lotus type porous nickel-free stainless steel when implanted into rats showed osteocompatibility and bone in growth⁹⁷.

Biocompatibility and osteogenesis were observed with corrosive resistant implants made from Tantalum (Ta), Hafnium (Hf) Niobium (Nb), Titanium (Ti), Rhenium (Re)⁹⁸. The properties of pure metals can be enhanced by allowing the different types of metals⁹⁴. Co-Cr alloys are worn resistant⁹⁴ but possess corrosion properties⁹⁹. The coiled wire and particle form of Co-Cr alloy and Ti implants are found to be diploid of inflammatory response upon transplantation¹⁰⁰.

Ti and Ti alloys like Titanium-Aluminium (6%)-vanadium (4%) alloy (Ti₆Al₄V) have excellent tensile strength, resistance to corrosion⁹⁴, lower modulus and superior biocompatibility as compared to stainless steel, Co-based alloys¹⁰¹. They can link to living bone in the host via the development of apatite layer by TiO₂¹⁰². The macropores and micropores Ti foams, when immersed in the simulated body fluid, showed bone-like apatite formation¹⁰². Titanium-Niobium-Zirconium (TiNbZr) alloy, calcium phosphate coated TiNbZr alloy¹⁰³ and Porous Titanium- Tantalum (6%)-Tin (4%) (Ti₆Ta₄Sn) alloy¹⁰⁴ showed adhesion and proliferation of human SaOS2 osteoblast-like cells. Ti₆Al₄V mesh scaffolds also showed vitality and proliferation with human osteoblast cells¹⁰⁵. Nickel-titanium alloy called Nitinol (NiTi) possesses a shape memory effect, biocompatibility, superplasticity, damping properties^{94,106,107}. NiTi, stainless steel and Ti₆Al₄V were implanted in the rats for 8 weeks and found that biocompatibility, bone

mineral density and growth of new bone were higher in NiTi as compared to stainless steel and Ti6Al4V¹⁰⁷. The porous NiTi scaffolds when implanted in the femur of rabbits, showed better bone-implant contact with osteoconductivity and osteointegration¹⁰⁸.

2.5.3.2.2 Ceramics:

Ceramics such as HA, bioactive glasses, calcium phosphate ceramics are widely used for bone repair^{55,109}. These are similar to the inorganic component of natural bone and possess good osteoconductivity and osteoinductivity¹¹⁰. Ceramic scaffolds have a high mechanical stiffness (Young's modulus), low elasticity, hard, brittle surface and have chemical and structural similarity to the native bone¹⁰⁹. Metals and ceramics lack degradability in a biological environment and their limited processability^{2,111–113} can become a hurdle in tissue engineering. The first generation of bioceramics is focused on inert materials like alumina, zirconia while second-generation focuses on bioactive biomaterials like bioactive glasses, highly porous HA, microporous BCP (Biphasic calcium phosphate). In third generation of bioceramics BCP takes center stage^{54,65,114}. The 1st generation inert ceramics were developed to substitute natural bone while 2nd generation was developed to mimic some biomineralization functions. The focus of 3rd generation bioceramics is on osteoregeneration rather than osteointegration aiming to only help bone cells to do their work¹¹⁵. Bioinert materials are biologically inactive and cannot form a direct bond with host tissue, unlike bioactive materials which also promote bone formation by chemical reactivity with its surrounding environment. Because of these properties, scientists are now concentrating more on bioactive glasses or ceramics which are capable of forming bone-like apatite on the surface *in vitro* and *in vivo*¹¹⁶.

HA is a biocompatible and biodegradable material that gets integrated well into the host tissue and does not elicit an immune response. Being a natural component of bone, HA has been widely used in different types of scaffolds as a major or partial component. The 3D bovine-derived porous HA (BDHA) scaffolds seeded with human BMSCs exhibited cell attachment, proliferation and osteogenic differentiation potential¹¹⁷. Through the *in situ* co-precipitation synthesis and electrospinning process, biomimetic nanocomposite nanofibers of HA-chitosan prepared¹¹⁸. These composite scaffolds on culturing with human fetal osteoblast (hFOB) revealed significant bone formation as

compared to only chitosan scaffolds¹¹⁸. Nanocomposite membranes of nano-HA (nHA), silk fibroin from *Bombyxmori* (SF) and polyhydroxybutyrate co-(-3-hydroxyvalerate) with 2% valerate fraction (PHBV) prepared has slow biodegradation, high biocompatibility and bioactive properties¹¹⁹. These nHA-SF-PHBV nanocomposite membranes also support bone-like apatite crystal growth with osteoblast cells infiltration, attachment and proliferation¹¹⁹. Bone sialoprotein (BSP)-derived collagen binding (CB) peptide has been shown to be osteogenic. The CB-HA scaffolds showed higher bone formation as compared to control HA scaffolds alone *in vivo*¹²⁰. The composites of HA-alumina and silicon carbide showed interconnected and uniform pore morphologies with osteoblast attachment and growth but no uniform distribution of cells was observed¹²¹.

With comparable properties to that of HA forsterite (FS) ceramic revealed optimum bending strength and fracture toughness including cellular properties¹²². Shahini *et al* prepared 3D electrically conductive scaffolds in the nanocomposites of gelatin and bioactive glass by using poly (3,4-ethylene dioxythiophene) poly (4-styrene sulfonate) (PEDOT: PSS)¹²³. These composite scaffolds had a microstructure with improved electrical signalling and enhanced mechanical and structural properties similar to that of bone. These scaffolds were biocompatible and supported MSCs growth and showed appropriate degradation rate¹²³.

Calcium phosphate ceramics are biocompatible, safe, cost-effective, easily available and show lower morbidity hence widely used as bone substitutes, coatings, types of cement, drug delivery systems and tissue engineering scaffolds⁶⁵. Biomimetic composites of calcium phosphate and mixtures of chitosan, a hyaluronic acid found to have biodegradability and good biocompatibility with osteoblasts cells¹²⁴. The nano-sized calcium silicate-poly (3-caprolactone) composite (n-CPC) are preferred over micro-sized calcium silicate-poly (3-caprolactone) composite (m-CPC) because of better mechanical properties, hydrophilicity and cellular activities⁸⁶.

BCP, which is made up of varying concentration of HA and β -tricalcium phosphate, possesses controllable biological and chemical properties and has become the preferred choice for promoting bone ingrowth over other calcium phosphate ceramics^{65,125–127}. However small pore interconnection size limits BCP applications in bone tissue

engineering¹²⁸. Bio-inspired 3D sandwich scaffolds of mesoporous silica fibres and gelatin showed cell infiltration and tissue in growth. These 3D scaffolds revealed the proliferation and differentiation of MG63 cells¹²⁹.

Another ceramic material proved to be potential as a scaffold for bone tissue engineering is Bioglass. Bioglass 45S5 showed good osteogenic cellular activities such as alkaline phosphatase (ALP) activity, osteocalcin synthesis and calcified extracellular matrix production along with the formation of calcified bone nodule^{130,131} hence proposed for bone tissue engineering¹³².

2.5.3.2.3 Polymers:

Polymers, be it natural or synthetic are widely used in biomaterial applications worldwide. For bone tissue engineering natural polymers such as collagens, glycosaminoglycans, starch, chitin and chitosan are used¹⁰⁹ which possess good biocompatibility but have poor mechanical strength^{55,110}. Natural polymers possess the advantage of biological recognition which may help for cell adhesion. Despite this, in some cases, they may exhibit immunogenicity and contain pathogenic impurities. Other disadvantages include less control over their mechanical properties, biodegradability and batch-to-batch consistency. A limited supply of many of these polymers can affect the cost efficacy¹¹¹.

The composites based on the natural polymers like collagen, chitosan, starch, cellulose and gelatin have been widely studied for regeneration of bone or repairing bone defects. Collagen is the most accepted scaffold among all due to its biocompatibility and availability. Type I collagen constitutes >90% of the organic mass of the bone¹³³. RGD (Arg-Gly-Asp) and non-RGD domains of type I collagenase play important role in the cell attachment, proliferation and differentiation. Type I collagen promotes proliferation and differentiation of human MSCs into the osteoblasts *in vitro*^{134,135} and osteogenesis *in vivo*⁵⁵. The composite scaffolds of collagen-apatite with adjustable composition and pore size in combination with mice calvarial osteoblasts (mCOB) cells, when transplanted in mice with a calvarial defect, supported bone repair.¹³⁶ Similar results were obtained by BSP-collagen composite scaffolds¹³⁷. Collagen and ceramics together are used to prepare

composites like collagen-HA microsphere (Col-mHA) scaffolds and collagen-silk fibroin-HA (Col-SF-HA) nanocomposites. These nanocomposites showed good biocompatibility and bone regeneration properties¹¹⁰. Among these nanocomposites, silk fibroin enhanced the elastic modulus of the scaffolds as compared to the Col-HA scaffolds¹³⁸. The collagen-glycosaminoglycan (GAG) (CG) scaffolds with optimized composition, pore size and cross-linking density showed osteoblasts attachment and migration into a deep section of scaffolds and *in vivo* calvarial bone defect healing⁵⁵.

A natural polymer chitosan is a partially deacetylated form (poly-b (1, 4)-2-amino-2-deoxy-D-glucose) of chitin having biocompatibility, biodegradability, hydrophilicity and good cell adhesion¹³⁹. Chitosan has been shown to stimulate the differentiation of osteoprogenitor cells¹⁴⁰. The biocomposite scaffolds of chitosan, alginate (Alg) and nano silica (nSiO₂) (chitosan -Alg- nSiO₂) were biodegradable and showed apatite deposition. On seeding with osteogenic lineage cells, these scaffolds were found to be biocompatible¹⁴¹. The chitosan-gelatin-nSiO₂ nanocomposite scaffolds revealed osteoblastic differentiation of MG63 cells with no toxic effects. As compared to control chitosan and chitosan-gelatin scaffold, chitosan-gelatin-nSiO₂ nanocomposite scaffolds showed improved bioactivity and cellular behaviour¹⁴². The water uptake ability, protein adsorption, biodegradability and mineralization and ALP activity with MG-63 cells were higher on chitosan-Alg-fucoidan composite than chitosan-Alg. These scaffolds were revealed to be biocompatible and non-cytotoxic¹⁴³. Porous chitosan-HA scaffolds with silver nanoparticles showed increased osteoconductivity and nanosilver layer improved antibacterial activity¹⁴⁴. The composite scaffolds of chitosan matrix reinforced with forsterite (FS) nanopowder prepared with high interconnected porosity and high mechanical strength than chitosan scaffolds alone. The composite Chitosan-FS scaffolds showed biocompatibility with MG63 cells without any toxic effects¹¹³. Chitosan-collagen- β - glycerophosphate (GP) hydrogel composite showed good spreading and growth of bone marrow precursor cells as well as the formation of mineral nodules, differentiation into osteogenic lineage without the use of any external factors¹⁴⁵.

Combinations of natural and synthetic polymers are widely used in the preparation of composite scaffolds for bone tissue engineering, for example, corn starch with

polycaprolactone scaffolds functionalized with Si-OH groups¹⁴⁶. Starch-polycaprolactone (SPCL) scaffolds with BMSCs on subcutaneous transplantation in rats showed osteogenic differentiation with *in vivo* bone formation¹⁴⁷. The SPCL (30/70 weight %) and SPLA (starch with polylactic acid, 30/70 weight %) fibre meshes showed adequate mechanical properties for growth and adhesion of cells on to the fibre with highly interconnected pores and porosity¹⁴⁶. The SPCL showed higher water uptake ability than SPLA fibres. Also, both fibres are degradable with enzymes like α -amylases and lipases¹⁴⁶.

Bacterial cellulose (BC) from strain ATCC 53582 of *Acetobacter xylinum* has good biocompatibility, biodegradability, high tensile strength and elastic modulus¹⁴⁸ and can be used as a biomaterial for medical applications. The human adipose-derived stem cells (ASCs) seeded on the BC with 3D nanonetwork showed good adhesion, proliferation and differentiation into osteogenic lineage¹⁴⁹. Modified cellulose- poly (vinyl alcohol) (PVA) prepared by electrospinning is a very promising scaffold for bone tissue regeneration¹²⁸. Carboxymethyl cellulose (CMC) incorporated nHA- chitosan (nHA-chitosan-CMC) composite scaffolds showed high interconnected pore structure, high compressive strength, good structural stability and degradation¹⁵⁰. Study of these scaffolds with MSCs and MG-63 cells revealed their growth and attachment without any adverse effect¹⁵⁰. Researchers have also prepared nontoxic composite scaffolds from ovalbumin (Ova) from the chicken egg and cellulose nanocrystals (CNCs) from wood pulp. The pore size, hydrophilic nature and surface roughness of the composites increased with the composition of CNCs. The wettability of the Ova-CNCs composites was higher than unmodified Ova scaffolds¹⁵¹.

1-Ethyl-3-[3-dimethylaminopropyl] carbodiimide hydrochloride (EDC) treated gelatin scaffolds have high stiffness and high elastic modulus. These scaffolds, when transplanted in mice subcutaneously with primary mouse BMSCs transduced with BMP, developed ossicles⁶⁶ with higher bone mineral content and bone volume as that of control⁶⁶.

When compared to natural polymers, synthetic polymers have an advantage of reproducible large-scale production with controlled properties of strength, degradation rate and microstructure. Poly (α -hydroxy acids), including PGA, PLA and their

copolymer PLGA, are the most popular and widely used synthetic polymeric materials in bone tissue engineering. On degradation, PGA, PLA and PLGA secretions are nontoxic, natural metabolites. They are ultimately removed from the body in terms of carbon dioxide and water¹¹¹. The composite fibres like PCL-CaCO₃¹⁵², HA-gelatin¹⁵³, silk-HA¹⁵⁴, PLA-HA¹⁵⁵ and triphasic HA-collagen-PCL¹⁵⁶ have been used for bone regeneration applications.

A wide range of PLLA based composites like PLLA-HA, PLLA-gel, PLLA-gel-HA, PLLA-apatite has been studied by various groups worldwide. Composite polymers prepared using a combination of PLLA with various other materials increased its suitability for bone regeneration. For example, the osteoblast survival and growth were significantly enhanced in PLLA-HA composites compared to the plain PLLA scaffolds¹¹¹. The nanocomposites of PLLA-HA when transplanted into the median sternotomy rabbit model, showed complete repair of bone in the scaffold treated area with the formation of new bone trabeculae¹⁵⁷. PLLA and PLLA-Gel nanofibrous scaffolds fabricated via electrospinning followed by mineralization with an alternate soaking process for HA deposition proved to be cytocompatible and evoked minimum complement activation with osteostimulation as compared to PLLA and PLLA-HA¹⁵⁸. The mono-phasic scaffolds of larger pores and bi-phasic scaffolds of smaller pores containing HA nanocrystals, PCL and PLLA showed colonization and proliferation of MSCs and were biocompatible in nature⁷².

Highly porous biodegradable PLLA-HA and PLGA-HA composite foams demonstrated higher density, compressive modulus and compressive yield strength than PLLA-HA foams¹⁵⁹. PLGA sintered cylinder scaffolds, PLGA sintered tubular scaffolds, integrated scaffolds with PCL spiral insert without fibre coating and integrated scaffolds with PCL spiral insert with fibre coating showed higher cell penetration, proliferation and differentiation of human osteoblasts and calcium accumulation than rest of the scaffolds⁶⁹.

The biomorphic scaffolds are produced by complex living and non-living biological products from raw materials such as living tissues, molecules, extracellular matrices and biomaterials. The classical examples of biomorphic scaffolds are demineralized bone

matrixes, calcined animal bone and decellularized ECM derived from various tissues¹⁶⁰. Cheng *et al* reviewed that decellularized bone matrix scaffolds promoted differentiation of ASCs, MSCs, ESCs, iPSCs into the osteoblasts and supported bone regeneration¹⁶¹. The biomorphic poly (DL-lactic-co-glycolic acid)-nano hydroxyapatite (PLGA-nHA) composite scaffolds prepared using a cane as a template. These scaffolds with MC3T3-E1 cells showed cell attachment, proliferation and osteogenic differentiation¹⁶⁰.

The transplantation of bone marrow-derived rat MSCs on electrospun nanofiber scaffolds poly ϵ -caprolactone (PCL) fibres showed bone formation in the rat model²⁷. The mechanical properties of nanofibrous PCL scaffolds such as ultimate tensile strength, elastic modulus, elongation at breaking point was higher than its composite PCL-nHA and PCL-TCP scaffolds. All these scaffolds showed good cell adhesion and spreading of hMSCs with increased activity of ALP, Runx-2, BSP in absence of osteogenic supplements¹⁶². The composites with different compositions of PCL, PLGA and HA such as 10% PCL-90% PLGA +10% HA showed 80% porosity with higher Young's modulus, tensile strength and cellular activities¹⁶³.

The poly-D, L-lactic acid (PDLLA) scaffolds enriched with ulvan particles extracted from green algae demonstrated good cytocompatibility as compared to PDLLA alone¹⁶⁴. In the PDLLA-TiO₂ composite scaffolds, surface roughness and fracture surface area increased with the amount of TiO₂ nanoparticles. TiO₂ nanoparticles at the physiological range had no significant effect on MG-63 cells but at high concentrations (>5000/ml) affected the viability of cells¹⁶⁵. PDLLA-nHA composites with high porosity, interconnected macroporous structure improve hydrophilicity, biocompatibility, bioavailability and compressive strength as compared to PDLLA scaffolds¹⁶⁶. The polypyrrole centred conducting scaffold was prepared by integration of polypyrrole-alginate (PPy-Alg) amalgam with chitosan. PPy-Alg composite scaffold seeded with MG63 cells showed biocompatibility and cell attachment. There were extensive distribution and density of MG63 cells on PPy-Alg composite scaffolds and showed *in vitro* mineralization¹⁶⁷. The composite membrane fabricated by using poly (L/DL-lactide) (PLDL) and nHA showed *in vitro* mineralization with human primary NHOst cells compatibility, attachment, proliferation and osteogenic differentiation⁹². Similar results

were obtained by composites of polysulfone (PSU)- MWCNTs¹⁶⁸. The poly (3-hydroxybutyrate)-nano sized bioactive glass (P (3HB)-nBG) composites formed HA on metal surfaces *in vitro*. The nBG content was found to increase the weight loss and water uptake capacity. There was cell attachment, proliferation and differentiation of MG63 cells on (P (3HB)-nBG composites¹⁶⁹. Among PLA, PLA-HA and PLA-HA-GO scaffold PLA scaffolds have a smooth surface, while PLA-HA or PLA-HA-GO showed better cell attachment, penetration and attachment on its surface with osteoblast growth and proliferation on PLA-HA-GO scaffolds than other scaffolds¹⁷⁰. The 4 types of poly (3-hydroxybutyrate) (PHB) based nanofibrous scaffolds namely PHB, PHB-gelatin, PHB-gelatin-nHA and PHB-gelatin with electrosprayed nHA were comparatively studied. The human mesenchymal stromal cells seeded on to these scaffolds revealed gelatin containing scaffolds are better for cell adhesion and proliferation. The electrosprayed nHA composites showed a higher level of ALP activity and matrix biomineralization after seeding of human mesenchymal stromal cells for 21 days than these scaffolds¹⁷¹.

2.5.3.2.4 Carbon materials:

Due to the similar dimensions, carbon nanomaterials are considered to be a physical analogue of ECM components like collagen fibres¹⁷². Nowadays the use of carbon-based materials has increased in the field of tissue engineering for different purposes. Various forms of carbon materials or their composites like Single-walled carbon nanotubes (SWCNTs), Multi-walled carbon nanotubes (MWCNTs) and graphene oxide (GO) have been investigated for their efficacy in tissue engineering in the last couple of years.

SWCNTs thin films showed a proliferation of Saos-2 cells in low concentrations of serum¹⁷³. The nHA-SWCNT scaffold in chitosan enhanced the mechanical properties suitable for bone tissue engineering. These scaffolds showed osteoblast adhesion and proliferation¹⁷⁴. MWCNTs scaffolds showed biocompatible and nontoxic nature along with cellular compatibility when seeded with hADSCs and MC3T3 cells¹⁷⁵. The composites of polysulfone (PSU)-single-walled carbon nanohorns (SWCNHs) and PSU-MWCNTs revealed increased tensile strength, Young's modulus, rough surface and water contact angle of more than 85. SWCNHs or MWCNTs based composites showed

Table 2.3: Types of Scaffolds used for Bone tissue engineering, adapted from²¹ with copyright permission from Springer Nature (License No. 4578750332409).

Sl. No	Type of Scaffolds	Type of study	References
Metals			
1	Lotus type porous nickel free stainless steel	<i>In vivo</i>	[97]
2	Cobalt-Chromium (Co-Cr) alloys	<i>In vivo</i>	[54,94,180]
3	Titanium-Niobium-Zirconium (TiNbZr) alloy	<i>In vitro</i>	[103]
4	Ti6Ta4Sn alloy	<i>In vitro</i>	[104]
5	Nitinol (NiTi) alloy	<i>In vitro & In vivo</i>	[94,106-108]
Ceramics			
1	BDHA scaffolds	<i>In vitro</i>	[117]
2	HA-chitosan	<i>In vivo</i>	[118]
3	nHA-SF-PHBV nanocomposite	<i>In vitro</i>	[119]
4	CB-HA scaffolds	<i>In vivo</i>	[120]
5	HA-FS composite	<i>In vivo</i>	[122]
6	CPC composite	<i>In vitro</i>	[86]
7	Bioglass 45S5	<i>In vitro</i>	[130-132, 182]
Polymers			
1	Col-SF-HA nanocomposites	<i>In vitro</i>	[110]
2	Col- GAG scaffolds	<i>In vitro & In vivo</i>	[55]
3	Chitosan-gelatin-nSiO ₂ nanocomposite	<i>In vitro</i>	[142]
4	Chitosan-Alg-fucoidan composite	<i>In vitro</i>	[143]
5	Chitosan-forsterite composite	<i>In vitro</i>	[113]
6	Chitosan-collagen-β- glycerophosphate	<i>In vitro</i>	[145]
7	SPCL, SPLA scaffolds	<i>In vivo</i>	[146,147]
8	EDC treated Gelatin scaffolds	<i>In vivo</i>	[66]
9	PLLA-HA nanocomposites	<i>In vivo</i>	[111,157,158]
10	PLGA, PLGA-PCL scaffolds	<i>In vivo</i>	[69]
11	PLGA-nHA composite	<i>In vitro</i>	[160]

Sl. No	Type of Scaffolds	Type of study	References
12	PDLLA-TiO ₂ scaffolds	<i>In vitro</i>	[165]
13	PPy-Alg composite	<i>In vitro</i>	[167]
Carbon materials			
1	SWCNTs scaffold	<i>In vitro</i>	[173]
2	nHA + SWCNT scaffold	<i>In vitro</i>	[174]
3	PSU- SWCNHs, PSU-MWCNTs	<i>In vitro</i>	[168]
4	Au-HA- Few layer graphene	<i>In vitro</i>	[176]
5	SWCNT networks, rGO	<i>In vitro</i>	[177]
6	HA-GN composites	<i>In vitro</i>	[178]

adhesion, spreading and metabolic activity with the increased β -actin cytoskeleton of seeded MG 63 cells¹⁶⁸. Au-HA composite layered with graphene when seeded with murine calvaria derived MC3T3-E1 osteoblast-like cells showed minimal cellular toxicity¹⁷⁶. The SWCNT networks and reduced graphene oxide (rGO) were studied with the neuroendocrine PC12 cells, oligodendroglia cells and osteoblasts. The SWCNT networks and rGO were chemically similar in nature but they differed by topographical features. The SWCNT networks were 10.9 nm in surface roughness while rGO has the surface roughness of 1.6nm. The SWCNT networks were inhibitory to the PC12 cells and osteoblasts while rGO found to be biocompatible to all these cells¹⁷⁷. The rough, porous HA-graphene nanosheet (GN) composites enhanced the fracture properties of HA-based scaffolds. These scaffolds showed attachment of filopodia of osteoblasts cells via fibronectin to GN *in vitro* and post-mineralization apatite formation¹⁷⁸.

2.5.3.3 Surface modification of scaffolds:

Altering the physicochemical surface properties can change biocompatibility, influence cell adhesion and growth; can improve wear resistance and corrosion resistance properties of materials to be used as biomaterial. The surface modification can be achieved by various methods such as coating by self-assembled film/electrolyte

multilayers, surface gradient, surface activation and surface chemical reaction. Stainless steel screws, when coated with a bisphosphonate, increased new bone formation around implants¹⁷⁹. Similarly Co-Cr alloy coated with HA showed superior osteogenesis and integration than uncoated alloy¹⁸⁰.

Osteoblasts were able to adhere and proliferate on composites of β -TCP-HA scaffolds coated with alginate⁵³. The uniform Ca-P-polydopamine composite nanolayer was prepared on the surface of β -TCP bioceramics. This nanolayer improved the surface roughness and hydrophilicity of β -TCP bioceramics. These composites, when seeded with hBMSCs, showed cell attachment, proliferation and alkaline phosphatase activity and expression of bone-related genes (ALP, OCN, COL1 and Runx2)¹⁸¹. The interconnected porous β -TCP scaffolds improved by ZnO showed good mechanical properties like compressive strength, stiffness, fracture toughness and microhardness. These scaffolds showed bioactivity, biodegradability *in vitro* and cell attachment, the proliferation of MG-63 cells⁷⁰. Porous 45S5 Bioglass® based scaffolds fabricated and coated with poly (3-hydroxybutyrate-co-3-hydroxyvalerate) (PHBV) revealed higher porosity with increased interconnected pore structure and high mechanical properties¹⁸² hence ideal candidate for bone tissue engineering.

The corn starch-ethylene-vinyl alcohol (50/50 wt %) based scaffolds when coated with Ca-P showed compressive modulus of 224.6 and compressive strength of 24 without affecting normal cellular activity but an expression of osteopontin, collagen type I and alkaline phosphatase activity (ALP)⁸. PDLLA foams and PDLLA foams coated with Bioglass® particles showed complete covering with HA in 28 days of incubation in SBF. Osteoblasts were attached and spread on both PDLLA uncoated and coated foams¹¹⁴. While in another *in vitro* study with SBF, the HA formation was slower in uncoated composites than coated composites of PDLLA¹⁸³. Dextran-coated polyvinyl formal (PVF) sponges with water holding capacity showed more adhesion, proliferation and differentiation of BMSCs *in vitro* along with increased DNA content, ALP activity, osteocalcin content and calcium deposition⁸⁵.

2.5.3.4 Future perspectives:

Table 2.4: Limitations and challenges of Bone tissue engineering.

Sl. No.	Limitations	Challenges
	Physico-mechanical stability of biomaterials	Utile combinations of cell, growth factor and biomaterial
	Donor Vs. host immune reactions	Vascularization
	Inflammatory response	Host integration
	Fibrous tissue formation	Regeneration of quality bone
	Appropriate animal models	FDA approval
	Prolonged regulatory processes	Cost of therapy
	Donor Vs. host immune reactions	Patient safety

From the first attempt of bone regeneration by Urist, the field of bone tissue engineering flooded with the research of developing methods, use of different biomaterials and various factors that can be used for regeneration of bone. Different kind of *in vitro* and *in vivo* studies explains the potential of cells to differentiate into osteoblasts and the supporting role of growth factors and or biomaterials.

There are certain limitation and challenges (Table 2.4). Most of these studies had revealed the biocompatibility, biodegradability, osteoinductivity, osteoconductivity, osteogenicity and or physic-mechanical properties. Some *in vivo* studies showed repair of bone defects or bone regeneration. These tissue engineering studies revealed a great potential for repair or regeneration of bone. But still, there were neither ideal combination of stem cells or growth factors or biomaterials that successfully came forward for bone regeneration nor sufficient attempts have been made to bring clinical trials in humans. Therefore there is only hope and continuous efforts to develop biomimicking scaffold which can replace defective bone in reality that further attempts of tissue engineering will bring fruitful treatments in curing bone defects and diseases via bone regeneration.

References:

- 1 J. Y. Rho, L. Kuhn-Spearing and P. Zioupos, *Med. Eng. Phys.*, 1998, **20**, 92–102.
- 2 S. Bose, M. Roy and A. Bandyopadhyay, *Trends Biotechnol.*, 2012, **30**, 546–554.
- 3 M. J. Olszta, X. Cheng, S. S. Jee, R. Kumar, Y.-Y. Kim, M. J. Kaufman, E. P. Douglas and L. B. Gower, *Mater. Sci. Eng. R Reports*, 2007, **58**, 77–116.
- 4 A. Oryan, S. Monazzah and A. Bigham-sadegh, *Biomed. Environ. Sci.*, 2015, **28**, 57–71.
- 5 S. H. Ralston, *Med. (United Kingdom)*, 2017, **45**, 560–564.
- 6 K. Gelse, E. Pöschl and T. Aigner, *Adv. Drug Deliv. Rev.*, 2003, **55**, 1531–1546.
- 7 M. J. Glimcher, *Rev. Mod. Phys.*, 1959, **31**, 359–393.
- 8 A. J. Salgado, J. E. Figueiredo, O. P. Coutinho and R. L. Reis, *J. Mater. Sci. Mater. Med.*, 2005, **16**, 267–275.
- 9 J. Street, M. Bao, L. DeGuzman, S. Bunting, F. V. J. Peale, N. Ferrara, N. Steinmetz, J. Hoeffel, J. L. Cleland, A. Daugherty, N. van Bruggen, H. P. Redmond, R. A. Carano and E. H. Filvaroff, *Proc Natl Acad Sci USA*, 2002, **99**, 9656–9659.
- 10 F. Ronci, P. Reale, B. Scrosati, S. Panero, V. Rossi Albertini, P. Perfetti, M. di Michiel and J. M. Merino, *J. Phys. Chem. B*, 2002, **106**, 3082–3086.
- 11 N. Rucci and A. Teti, in *Reference Module in Biomedical Sciences*, Elsevier Inc., 2nd edn., 2018, vol. 5, pp. 1–9.
- 12 L. F. Bonewald and K. Ja, in *In Pediatric Bone*, Academic Press., 2012, pp. 1–8.
- 13 R. R. Buckwalter, J. A.; Glimcher, M. J.; Becker, *J. Bone Jt. Surg. (Instructional Course Lect.*, 1995, **77**, 1256–1275.

- 14 S. Stewart, S. J. Bryant, J. Ahn and K. D. Hankenson, in *Translational Regenerative Medicine.*, Elsevier Inc., 2015, pp. 313–333.
- 15 W. Wang and K. W. K. Yeung, *Bioact. Mater.*, 2017, **2**, 224–247.
- 16 V. Sathyendra and M. Darowish, *Hand Clin.*, 2013, **29**, 473–481.
- 17 A. Malhotra, C. van Blitterswijk and P. Habibovic, in *Biology and Engineering of Stem Cell Niches*, Elsevier Inc., 2017, pp. 499–516.
- 18 R. Marsell and T. A. Einhorn, *Injury*, 2011, **42**, 551–555.
- 19 M. S. Ghiasi, J. Chen, A. Vaziri, E. K. Rodriguez and A. Nazarian, *Bone Reports*, 2017, **6**, 87–100.
- 20 A. R. Shrivats, P. Alvarez, L. Schutte and J. O. Hollinger, in *Principles of Tissue Engineering*., Elsevier, 4th edn., 2013, pp. 1201–1221.
- 21 S. Kashte, A. K. Jaiswal and S. Kadam, *Tissue Eng. Regen. Med.*, 2017, **14**, 1–14.
- 22 S. Kashte and S. Kadam, *Br. Biomed. Bull.*, 2014, **2**, 677–694.
- 23 V. Sottile, A. Thomson and J. McWhir, *Cloning Stem Cells*, 2003, **5**, 149–155.
- 24 L. D. Buttery, S. Bourne, J. D. Xynos, H. Wood, F. J. Hughes, S. P. Hughes, V. Episkopou and J. M. Polak, *Tissue Eng.*, 2001, **7**, 89–99.
- 25 R. C. Bielby, A. R. Boccaccini, J. M. Polak and L. D. K. Buttery, *Tissue Eng.*, 2004, **10**, 1518–1525.
- 26 B. Levi, J. S. Hyun, D. T. Montoro, D. D. Lo, C. K. F. Chan, S. Hu, N. Sun, M. Lee, M. Grova, A. J. Connolly, J. C. Wu, G. C. Gurtner, I. L. Weissman, D. C. Wan and M. T. Longaker, *Proc. Natl. Acad. Sci. U. S. A.*, 2012, **109**, 20379–20384.
- 27 M. Shin, H. Yoshimoto and J. Vacanti, *Tissue Eng.*, 2004, **10**, 33–41.
- 28 C. Wan, Q. He and G. Li, *J. Orthop. Res.*, 2006, **24**, 610–618.

-
- 29 W. Lu, K. Ji, J. Kirkham, Y. Yan, A. R. Boccaccini, M. Kellett, Y. Jin and X. B. Yang, *Cell Tissue Res.*, 2014, **356**, 97–107.
- 30 A. Ardeshirylajimi, S. Hosseinkhani, K. Parivar, P. Yaghmaie and M. Soleimani, *Mol. Biol. Rep.*, 2013, **40**, 4287–4294.
- 31 F. Li and C. Niyibizi, *BMC Cell Biol.*, 2012, **13**, 35–45.
- 32 D. J. J. De Gorter, M. Van Dinther, O. Korchynskyi and P. Ten Dijke, *J. Bone Miner. Res.*, 2011, **26**, 1178–1187.
- 33 H. H. Luu, W.-X. Song, X. Luo, D. Manning, J. Luo, Z.-L. Deng, K. A. Sharff, A. G. Montag, R. C. Haydon and T.-C. He, *J. Orthop. Res.*, 2007, **25**, 665–677.
- 34 S. Yang, D. Wei, D. Wang, M. Phimphilai, P. H. Krebsbach and R. T. Franceschi, *J. Bone Miner. Res.*, 2003, **18**, 705–715.
- 35 Y. Fei, L. Xiao, T. Doetschman, D. J. Coffin and M. M. Hurley, *J. Biol. Chem.*, 2011, **286**, 40575–40583.
- 36 K. Song, N.-J. Rao, M.-L. Chen, Z.-J. Huang and Y.-G. Cao, *Injury*, 2011, **42**, 796–802.
- 37 Y. Tabata, K. Yamada, S. Miyamoto, I. Nagata, H. Kikuchi, I. Aoyama, M. Tamura and Y. Ikada, *Biomaterials*, 1998, **19**, 807–815.
- 38 Y. Tabata, K. Yamada, L. Hong, S. Miyamoto, N. Hashimoto and Y. Ikada, *J. Neurosurg.*, 1999, **91**, 851–566.
- 39 A. I. Caplan and D. Correa, *J. Orthop. Res.*, 2011, **29**, 1795–1803.
- 40 Y. M. Lee, Y. J. Park, S. J. Lee, Y. Ku, S. B. Han, P. R. Klokkevold and C. P. Chung, *J. Periodontol.*, 2000, **71**, 418–424.
- 41 H. Ochiai, S. Okada, A. Saito, K. Hoshi, H. Yamashita, T. Takato and T. Azuma, *J. Biol. Chem.*, 2012, **287**, 22654–22661.
-

-
- 42 F. Geiger, H. Bertram, I. Berger, H. Lorenz, O. Wall, C. Eckhardt, H.-G. Simank and W. Richter, *J. Bone Miner. Res.*, 2005, **20**, 2028–2035.
- 43 H. Peng, V. Wright, A. Usas, B. Gearhart, H. C. Shen, J. Cummins and J. Huard, *J. Clin. Invest.*, 2002, **110**, 751–759.
- 44 M. Samee, S. Kasugai, H. Kondo, K. Ohya, H. Shimokawa and S. Kuroda, *J. Pharmacol. Sci.*, 2008, **108**, 18–31.
- 45 Y.-C. Huang, D. Kaigler, K. G. Rice, P. H. Krebsbach and D. J. Mooney, *J. Bone Miner. Res.*, 2005, **20**, 848–857.
- 46 J. Street, M. Bao, L. DeGuzman, S. Bunting, F. V Peale, N. Ferrara, H. Steinmetz, J. Hoeffel, J. L. Cleland, A. Daugherty, N. van Bruggen, H. P. Redmond, R. A. D. Carano and E. H. Filvaroff, *Proc. Natl. Acad. Sci. U. S. A.*, 2002, **99**, 9656–9659.
- 47 Y. Yu, J. Mu, Z. Fan, G. Lei, M. Yan, S. Wang, C. Tang, Z. Wang, J. Yu and G. Zhang, *Histochem. Cell Biol.*, 2012, **137**, 513–525.
- 48 F. Granero-Moltó, T. J. Myers, J. A. Weis, L. Longobardi, T. Li, Y. Yan, N. Case, J. Rubin and A. Spagnoli, *Stem Cells*, 2011, **29**, 1537–1548.
- 49 A. P. Barhanpurkar, N. Gupta, R. K. Srivastava, G. B. Tomar, S. P. Naik, S. R. Joshi, S. T. Pote, G. C. Mishra and M. R. Wani, *Biochem. Biophys. Res. Commun.*, 2012, **418**, 669–675.
- 50 D. S. Kohane and R. Langer, *Pediatr. Res.*, 2008, **63**, 487–491.
- 51 M. E. Furth, A. Atala and M. E. Van Dyke, *Biomaterials*, 2007, **28**, 5068–5073.
- 52 W. Li, P. Noeaid, J. A. Roether, D. W. Schubert and A. R. Boccaccini, *J. Eur. Ceram. Soc.*, 2014, **34**, 505–514.
- 53 L. Torres, V. M. Gaspar, I. R. Serra, G. S. Diogo, R. Fradique, P. Silva and I. J. Correia, *Mater. Sci. Eng. C. Mater. Biol. Appl.*, 2013, **33**, 4460–4469.
-

- 54 J. E. L. Buddy D. Ratner, Allan S. Hoffman, Frederick J. Schoen, in *Biomaterials science: an introduction to materials in medicine.*, Elsevier Inc, 1996, pp. 415–455.
- 55 F. J. O'Brien, *Mater. Today*, 2011, **14**, 88–95.
- 56 S. Yang, K. F. Leong, Z. Du and C. K. Chua, *Tissue Eng.*, 2001, **7**, 679–689.
- 57 Report #A322, "U.S. Markets for Orthopedic Biomaterials for Viscosupplementation and Cartilage, Ligament, and Tendon Repair and Regeneration, <http://www.medtechinsight.com/ReportA321.html#orderinfoA420>, (accessed 21 November 2015).
- 58 A. S. Greenwald, *J. Bone Jt. Surgery-American Vol.*, 2001, **83**, 970.
- 59 D. F. Williams, *Biomaterials*, 2008, **29**, 2941–2953.
- 60 X. Wang, Y. L. Robertson, J. B. Spillman, W and O. Claus, R, *Pharm. Res.*, 2004, **21**, 1362–1373.
- 61 D. W. Hutmacher, *Biomaterials*, 2000, **21**, 2529–2543.
- 62 C. J. Kirkpatrick, F. Bittinger, M. Wagner, H. Köhler, T. G. van Kooten, C. L. Klein and M. Otto, *Proc. Inst. Mech. Eng. Part H J. Eng. Med.*, 1998, **212**, 75–84.
- 63 M. Patel and J. P. Fisher, *Pediatr. Res.*, 2008, **63**, 497–501.
- 64 H. Shen, L. Zhang, M. Liu and Z. Zhang, *Theranostics*, 2012, **2**, 283–294.
- 65 S. E. Lobo and T. L. Arinzeh, *Materials (Basel).*, 2010, **3**, 815–826.
- 66 H. Sun, F. Zhu, Q. Hu and P. H. Krebsbach, *Biomaterials*, 2014, **35**, 1176–1184.
- 67 C. Y. Lin, N. Kikuchi and S. J. Hollister, *J. Biomech.*, 2004, **37**, 623–636.
- 68 M. Tarik Arafat, I. Gibson and X. Li, *Rapid Prototyp. J.*, 2014, **20**, 13–26.
- 69 J. Wang and X. Yu, *Acta Biomater.*, 2010, **6**, 3004–3012.

-
- 70 P. Feng, P. Wei, C. Shuai and S. Peng, *PLoS One*, 2014, **9**, 87755–87765.
- 71 R. A. A. Muzzarelli, *Carbohydr. Polym.*, 2011, **83**, 1433–1445.
- 72 I. G. Lesci, L. Ciocca, B. Dozza, E. Lucarelli, S. Squarzoni, D. Donati and N. Roveri, *Key Eng. Mater.*, 2013, **583**, 56–63.
- 73 J. Baldwin, J. Henkel and D. W. Hutmacher, *Compr. Biomater. II*, 2017, **6**, 54–74.
- 74 V. Karageorgiou and D. Kaplan, *Biomaterials*, 2005, **26**, 5474–5491.
- 75 K. Whang, K. E. Healy, D. R. Elenz, E. K. Nam, D. C. Tsai, C. H. Thomas, G. W. Nuber, F. H. Glorieux, R. Travers and S. M. Sprague, *Tissue Eng.*, 1999, **5**, 35–51.
- 76 S. H. Oh, I. K. Park, J. M. Kim and J. H. Lee, *Biomaterials*, 2007, **28**, 1664–1671.
- 77 B. Feng, Z. Jinkang, W. Zhen, L. Jianxi, C. Jiang, L. Jian, M. Guolin and D. Xin, *Biomed. Mater.*, 2011, **6**, 15007–15017.
- 78 F. M. Klenke, Y. Liu, H. Yuan, E. B. Hunziker, K. A. Siebenrock and W. Hofstetter, *J. Biomed. Mater. Res. Part A*, 2008, **85A**, 777–786.
- 79 F. J. O’Brien, B. A. Harley, I. V. Yannas and L. J. Gibson, *Biomaterials*, 2005, **26**, 433–441.
- 80 S. Bose and M. Roy, *Trends Biotechnol.*, 2013, **30**, 546–554.
- 81 W. M. Gallagher, I. Lynch, L. T. Allen, I. Miller, S. C. Penney, D. P. O’Connor, S. Pennington, A. K. Keenan and K. A. Dawson, *Biomaterials*, 2006, **27**, 5871–5882.
- 82 A. Graziano, R. D’Aquino, M. G. C.-D. Angelis, F. De Francesco, A. Giordano, G. Laino, A. Piattelli, T. Traini, A. De Rosa and G. Papaccio, *J. Cell. Physiol.*, 2008, **214**, 166–172.
- 83 Y. Mei, K. Saha, S. R. Bogatyrev, J. Yang, A. L. Hook, Z. I. Kalcioglu, S.-W. Cho, M. Mitalipova, N. Pyzocha, F. Rojas, K. J. Van Vliet, M. C. Davies, M. R. Alexander, R. Langer, R. Jaenisch and D. G. Anderson, *Nat. Mater.*, 2010, **9**, 768–
-

- 778.
- 84 K. Webb, V. Hlady and P. A. Tresco, *J Biomed Mater Res*, 2012, **49**, 362–368.
- 85 W. Togami, A. Sei, T. Okada, T. Taniwaki, T. Fujimoto, T. Nakamura, S. Tahata, Y. Nakanishi and H. Mizuta, *J. Biomed. Mater. Res. A*, 2013, **102A**, 247–253.
- 86 J. Wei, S. J. Heo, D. H. Kim, S. E. Kim, Y. T. Hyun and J.-W. Shin, *J. R. Soc. Interface*, 2008, **5**, 617–630.
- 87 M. Yang, S. Zhu, Y. Chen, Z. Chang, G. Chen, Y. Gong, N. Zhao and X. Zhang, *Biomaterials*, 2004, **25**, 1365–1373.
- 88 D. Deligianni, N. Katsala, S. Ladas, D. Sotiropoulou, J. Amedee and Y. Missirlis, *Biomaterials*, 2001, **22**, 1241–1251.
- 89 S. K. Misra, T. Ansari, D. Mohn, S. P. Valappil, T. J. Brunner, W. J. Stark, I. Roy, J. C. Knowles, P. D. Sibbons, E. V. Jones, A. R. Boccaccini and V. Salih, *J. R. Soc. Interface*, 2010, **7**, 453–465.
- 90 K. Webb, V. Hlady and P. A. Tresco, *J. Biomed. Mater. Res.*, 1998, **41**, 422–430.
- 91 J. A. Roether, J. E. Gough, A. R. Boccaccini, L. L. Hench, V. Maquet and R. Jérôme, *J. Mater. Sci. Mater. Med.*, 2002, **13**, 1207–1214.
- 92 I. Rajzer, E. Menaszek, R. Kwiatkowski and W. Chrzanowski, *J. Mater. Sci. Mater. Med.*, 2014, **25**, 1239–1247.
- 93 B. Vagaská, L. Bačáková, E. Filová and K. Balík, *Physiol. Res.*, 2010, **59**, 309–322.
- 94 H. Hermawan, D. Ramdan and J. R. P. Djuansjah, in *Biomedical Engineering - From Theory to Applications*, 2009.
- 95 C. Z. Liao, K. Li, H. M. Wong, W. Y. Tong, K. W. K. Yeung and S. C. Tjong, *Mater. Sci. Eng. C*, 2013, **33**, 1380–1388.

-
- 96 J. A. Disegi and L. Eschbach, *Injury*, 2000, **31**, 2–6.
- 97 K. Alvarez, S.-K. Hyun, T. Nakano, Y. Umakoshi and H. Nakajima, *Mater. Sci. Eng. C*, 2009, **29**, 1182–1190.
- 98 H. Matsuno, A. Yokoyama, F. Watari, M. Uo and T. Kawasaki, *Biomaterials*, 2001, **22**, 1253–1262.
- 99 R. Michel, M. Nolte, M. Reich and F. Löer, *Arch. Orthop. Trauma Surg.*, 1991, **110**, 61–74.
- 100 S. B. Goodman, V. L. Fornasier, J. Lee and J. Kei, *J. Biomed. Mater. Res.*, 1990, **24**, 1539–1549.
- 101 M. Long and H. J. Rack, *Biomaterials*, 1998, **19**, 1621–1639.
- 102 M. M. Wen, C. E., Y. Yamada, K. Shimojima, Y. Chino, H. Hosokawa, *J. Mater. Res.*, 2002, **17**, 2633–2639.
- 103 C. W. Wang, Xiaojian, Yuncang Li, Peter D. Hodgson, *Tissue Eng. Part A*, 2009, **16**, 309–316.
- 104 C. W. Li, Yuncang, Jianyu Xiong, Cynthia S. Wong, Peter D. Hodgson, *Tissue Eng. part A*, 2009, **15**, 3151–3159.
- 105 D. Marolt, M. Knezevic and G. V. Novakovic, *Stem Cell Res. Ther.*, 2010, **1**, 1–10.
- 106 K. Alvarez and H. Nakajima, *Materials (Basel)*, 2009, **2**, 790–832.
- 107 A. Kapanen, J. Ryha, A. Danilov and J. Tuukkanen, *Biomaterials*, 2001, **22**, 2475–2480.
- 108 S. L. Zhu, X. J. Yang, M. F. Chen, C. Y. Li and Z. D. Cui, *Mater. Sci. Eng. C*, 2008, **28**, 1271–1275.
- 109 C.-K. C. Yang, Shoufeng, Kah-Fai Leong, Zhaohui Du, *Tissue Eng.*, 2001, **7**, 679–689.
-

-
- 110 K. P. Sanosh, F. Gervaso, A. Sannino and A. Licciulli, *Key Eng. Mater.*, 2013, **587**, 239–244.
- 111 X. Liu and P. Ma, *Ann. Biomed. Eng.*, 2004, **32**, 477–486.
- 112 V. Maquet and R. Jerome, *Mater. Sci. Forum*, 1997, **250**, 15–42.
- 113 F. Scalera, F. Gervaso, K. P. Sanosh, I. E. Palamà, S. Dimida and A. Sannino, *Key Eng. Mater.*, 2014, **587**, 249–254.
- 114 J. A. Roether, J. E. Gough, A. R. Boccaccini and L. L. Hench, *J. Mater. Sci. Mater. Med.*, 2002, **3**, 1207–1214.
- 115 D. Arcos, I. Izquierdo-Barba and M. Vallet-Regí, *J. Mater. Sci. Mater. Med.*, 2009, **20**, 447–455.
- 116 L. L. Hench and J. M. Polak, *Science*, 2002, **295**, 1014–1017.
- 117 G. Krishnamurithy, M. R. Murali, M. Hamdi, A. A. Abbas, H. B. Raghavendran and T. Kamarul, *Ceram. Int.*, 2014, **40**, 771–777.
- 118 Y. Zhang, J. R. Venugopal, A. El-Turki, S. Ramakrishna, B. Su and C. T. Lim, *Biomaterials*, 2008, **29**, 4314–4322.
- 119 E. I. Paşcu, J. Stokes and G. B. McGuinness, *Mater. Sci. Eng. C*, 2013, **33**, 4905–4916.
- 120 Y. J. Choi, J. Y. Lee, C.-P. Chung and Y. J. Park, *J. Biomed. Mater. Res. A*, 2013, **101**, 547–554.
- 121 M. Saki, M. K. Narbat, a Samadikuchaksaraei, H. B. Ghafouri and F. Gorjipour, *Yakhteh*, 2009, **11**, 55–60.
- 122 S. Ni, L. Chou and J. Chang, *Ceram. Int.*, 2007, **33**, 83–88.
- 123 K. J. Walker, M. A. Eastman, B. J. Smith and J. L. Ricci, 2014, 167–181.
-

-
- 124 F. D. Ivan, A. Marian, C. E. Tanase, M. Butnaru and L. Vereștiuc, *Key Eng. Mater.*, 2013, **587**, 191–196.
- 125 D. Le Nihouannen, L. Duval, A. Lecomte, M. Julien, J. Guicheux, G. Daculsi and P. Layrolle, *J. Mater. Sci. Mater. Med.*, 2007, **18**, 1983–1990.
- 126 C. Schwartz, P. Liss, B. Jacquemaire, P. Lecestre and P. Frayssinet, *J. Mater. Sci. Mater. Med.*, 1999, **10**, 821–825.
- 127 T. Albrektsson and C. Johansson, *Eur. Spine J.*, 2001, **10**, 96–101.
- 128 S. Chahala, F. S. J. Hussain and M. M. Yusoff, *Procedia Eng.*, 2013, **53**, 683–688.
- 129 R. Ravichandran, D. Sundaramurthi, S. Gandhi, S. Sethuraman and U. M. Krishnan, *Microporous Mesoporous Mater.*, 2014, **187**, 53–62.
- 130 I. D. Xynos, M. V. J. Hukkanen, J. J. Batten, L. D. Buttery, L. L. Hench and J. M. Polak, *Calcif. Tissue Int.*, 2000, **67**, 321–329.
- 131 J. P. Fan, P. Kalia, L. Di Silvio and J. Huang, *Mater. Sci. Eng. C*, 2014, **36**, 206–214.
- 132 S. Izadi, S. Hesarakı and M. Hafezi-Ardakani, *Adv. Mater. Res.*, 2013, **829**, 289–293.
- 133 K. Gelse, *Adv. Drug Deliv. Rev.*, 2003, **55**, 1531–1546.
- 134 S. H. Tsai, Kuo-Shu, Shou-Yen Kao, Chien-Yuan Wang, Yng-Jiin Wang, Jung-Pan Wang, *J. Biomed. Mater. Res. Part A*, 2010, **94**, 673–682.
- 135 T. E. Kruger, A. H. Miller and J. Wang, *ScientificWorldJournal.*, 2013, **2013**, 1–6.
- 136 Z. Xia, X. Yu, X. Jiang, H. D. Brody, D. W. Rowe and M. Wei, *Acta Biomater.*, 2013, **9**, 7308–7319.
- 137 J. Wang, H. Y. Zhou, E. Salih, L. Xu, L. Wunderlich, X. Gu, J. G. Hofstaetter, M. Torres and M. J. Glimcher, *Calcif. Tissue Int.*, 2006, **79**, 179–189.
-

-
- 138 L. Chen, J. Hu, J. Ran, X. Shen and H. Tong, *Int. J. Biol. Macromol.*, 2014, **65**, 1–7.
- 139 A. R. C. Duarte, J. F. Mano and R. L. Reis, *J. Supercrit. Fluids*, 2010, **54**, 282–289.
- 140 R. a Muzzarelli, C. Zucchini, P. Ilari, a Pagnaloni, M. Mattioli Belmonte, G. Biagini and C. Castaldini, *Biomaterials*, 1993, **14**, 925–929.
- 141 J. A. Sowjanya, J. Singh, T. Mohita, S. Sarvanan, A. Moorthi, N. Srinivasan and N. Selvamurugan, *Colloids Surf. B. Biointerfaces*, 2013, **109**, 294–300.
- 142 K. C. Kavya, R. Jayakumar, S. Nair and K. P. Chennazhi, *Int. J. Biol. Macromol.*, 2013, **59**, 255–263.
- 143 J. Venkatesan, I. Bhatnagar and S.-K. Kim, *Mar. Drugs*, 2014, **12**, 300–316.
- 144 M. Tylman and M. Mucha, *Mater. Sci. Technol.*, 2014, **30**, 582–586.
- 145 B. Sun, W. Ma, F. Su, Y. Wang, J. Liu, D. Wang and H. Liu, *J. Mater. Sci. Mater. Med.*, 2011, **22**, 2111–2118.
- 146 A. I. Rodrigues, M. E. Gomes, I. B. Leonor and R. L. Reis, *Acta Biomater.*, 2012, **8**, 3765–3776.
- 147 S. I. Correia, H. Pereira, C. N. Van Dijk, J. M. Oliveira and R. L. Reis, *J. R. Soc. Interface*, 2014, **11**, 20130784.
- 148 W. K. Czaja, D. J. Young, M. Kawecki and R. M. Brown, *Biomacromolecules*, 2007, **8**, 1–12.
- 149 S. Zang, Q. Zhuo, X. Chang, G. Qiu, Z. Wu and G. Yang, *Carbohydr. Polym.*, 2014, **104**, 158–165.
- 150 J. Liuyun, L. Yubao and X. Chengdong, *J. Biomed. Sci.*, 2009, **16**, 65–75.
- 151 B. P. Glaesemann, Virginia Polytechnic Institute and State University, 2011.
-

-
- 152 K. Fujihara, M. Kotaki and S. Ramakrishna, *Biomaterials*, 2005, **26**, 4139–4147.
- 153 B. H. Kim, J. Song and H. Kim, *Adv. Funct. Mater.*, 2005, **15**, 1988–1994.
- 154 C. Li, C. Vepari, H.-J. Jin, H. J. Kim and D. L. Kaplan, *Biomaterials*, 2006, **27**, 3115–3124.
- 155 G. Sui, X. Yang, F. Mei, X. Hu, G. Chen, X. Deng and S. Ryu, *Jounal Biomed. Mater. Res. Part A*, 2007, **82A**, 445–454.
- 156 S. A. Catledge, W. C. Clem, N. Shrikishen, S. Chowdhury, A. V Stanishevsky, M. Koopman and Y. K. Vohra, *Biomed. Mater.*, 2007, **2**, 142–150.
- 157 A. Rainer, C. Spadaccio, P. Sedati, F. De Marco, S. Carotti, M. Lusini, G. Vadalà, A. Di Martino, S. Morini, M. Chello, E. Covino, V. Denaro and M. Trombetta, *Ann. Biomed. Eng.*, 2011, **39**, 1882–1890.
- 158 A. K. Jaiswal, S. S. Kadam, V. P. Soni and J. R. Bellare, *Appl. Surf. Sci.*, 2013, **268**, 477–488.
- 159 R. Y. Zhang and P. X. Ma, *J. Biomed. Mater. Res.*, 1999, **44**, 446–455.
- 160 J. Qian, W. Xu, X. Yong, X. Jin and W. Zhang, *Mater. Sci. Eng. C. Mater. Biol. Appl.*, 2014, **36**, 95–101.
- 161 C. W. Cheng, L. D. Solorio and E. Alsberg, *Biotechnol. Adv.*, 2014, **32**, 462–484.
- 162 A. Polini, D. Pisignano, M. Parodi, R. Quarto and S. Scaglione, *PLoS One*, 2011, **6**, 1–8.
- 163 K. G. Marra, J. W. Szem, P. N. Kumta, P. A. DiMilla and L. E. Weiss, *J. Biomed. Mater. Res.*, 1999, **47**, 324–335.
- 164 A. Alves, A. R. C. Duarte, J. F. Mano, R. A. Sousa and R. L. Reis, *J. Supercrit. Fluids*, 2012, **65**, 32–38.
- 165 L. C. Gerhardt, G. M. R. Jell and a. R. Boccaccini, *J. Mater. Sci. Mater. Med.*,
-

- 2007, **18**, 1287–1298.
- 166 J. Ren, P. Zhao, T. Ren, S. Gu and K. Pan, *J. Mater. Sci. Mater. Med.*, 2008, **19**, 1075–1082.
- 167 K. M. Sajesh, R. Jayakumar, S. V Nair and K. P. Chennazhi, *Int. J. Biol. Macromol.*, 2013, **62**, 465–471.
- 168 L. Stankova, A. Fraczek-Szczypta, M. Blazewicz, E. Filova, S. Blazewicz, V. Lisa and L. Bacakova, *Carbon N. Y.*, 2014, **67**, 578–591.
- 169 S. K. Misra, T. Ansari, D. Mohn, S. P. Valappil, T. J. Brunner, W. J. Stark, I. Roy, J. C. Knowles, P. D. Sibbons, E. V. Jones, a. R. Boccaccini and V. Salih, *J. R. Soc. Interface*, 2009, **7**, 453–465.
- 170 H. Ma, W. Su, Z. Tai, D. Sun, X. Yan, B. Liu and Q. Xue, *Chinese Sci. Bull.*, 2012, **57**, 3051–3058.
- 171 J. Ramier, D. Grande, T. Boudierlique, O. Stoilova, N. Manolova, I. Rashkov, V. Langlois, P. Albanese and E. Renard, *J. Mater. Sci. Mater. Med.*, 2014, **25**, 1563–1575.
- 172 S. H. Ku, M. Lee and C. B. Park, *Adv. Healthc. Mater.*, 2013, **2**, 244–260.
- 173 T. Akasaka, A. Yokoyama, M. Matsuoka, T. Hashimoto and F. Watari, *Mater. Sci. Eng. C*, 2010, **30**, 391–399.
- 174 O. Im, J. Li, M. Wang, L. G. Zhang and M. Keidar, *Int. J. Nanomedicine*, 2012, **7**, 2087–2099.
- 175 B. S. Lalwani, Gaurav, Yahfi Talukdar, *Micro Nanotechnologies Eng. Stem Cells Tissues*, 2013, **101**, 220–235.
- 176 A. R. Biris, M. Mahmood, M. D. Lazar, E. Dervishi, F. Watanabe, T. Mustafa, G. Baciut, M. Baciut, S. Bran, S. Ali and A. S. Biris, *J. Phys. Chem. C*, 2011, **115**, 18967–18976.

- 177 S. Agarwal, X. Zhou, F. Ye, Q. He, G. C. K. Chen, J. Soo, F. Boey, H. Zhang and P. Chen, *Langmuir*, 2010, **26**, 2244–2247.
- 178 Y. Liu, Z. Dang, Y. Wang, J. Huang and H. Li, *Carbon N. Y.*, 2014, **67**, 250–259.
- 179 K. Wermelin, F. Suska, P. Tengvall, P. Thomsen and P. Aspenberg, *Bone*, 2008, **42**, 365–371.
- 180 J. A. Hunt, J. T. Callaghan, C. J. Sutcliffe, R. H. Morgan, B. Halford and R. A. Black, *Biomaterials*, 2005, **26**, 5890–5897.
- 181 C. Wu, P. Han, X. Liu, M. Xu, T. Tian, J. Chang and Y. Xiao, *Acta Biomater.*, 2014, **10**, 428–438.
- 182 W. Li, P. Nooeaid, J. A. Roether, D. W. Schubert and A. R. Boccaccini, *J. Eur. Ceram. Soc.*, 2014, **34**, 505–514.
- 183 A. R. Boccaccini, I. Notingher, V. Maquet and R. Je, *J. Mater. Sci. Mater. Med.*, 2003, **4**, 443–450.

CHAPTER 3:

EXPERIMENTAL

TECHNIQUES

3.1 Introduction:

Design and development of suitable scaffold for bone tissue engineering is one of the major challenges. Biocompatibility, biodegradability, pore size, pore connectivity, mechanical strength etc. are major primary concerns in development of bone scaffolds. Synthesis and characterization of scaffolds can be performed with the various experimental techniques. In this aforementioned study the scaffolds were fabricated using electrospinning technique. The surface of the scaffolds was further modified with layer by layer method and paint method to increase the suitability for bone tissue engineering. These scaffolds were then characterized for morphological properties using field emission scanning electron microscopy (FESEM), atomic force microscopy (AFM); Physicochemical properties using Fourier Transform Infra-Red spectroscopy (FTIR), Thermal degradation analysis (TGA) by thermogravimetric analyser, Contact angle measurement by sessile drop method with contact angle goniometer, tensile properties by Universal tensile Machine (UTM); and biological properties like cell viability and proliferation assay by 3-(4,5-dimethylthiazol-2-yl)-2, 5-diphenyltetrazolium bromide (MTT), cell attachment with FESEM and Confocal microscopy; Mineralization assay by Alizarin red S staining (ARS), and Von kossa staining.

In the present chapter, the various synthesis and characterization of experimental techniques have been explored with their principle, working and applications. The overview is given to understand the basic mechanisms behind the application of experimental techniques. The some of the specific experimentation and techniques are explained are explained in this chapter.

3.2 Electrospinning:

There are many methods for fabrication of scaffolds in tissue engineering but electrospinning is the simple, versatile, cost-effective, most popular cutting-edge technology. Electrospinning can be scaled for larger production and is easily replicable. It creates the fibre structures with controllable fibre size with interconnected pores. These properties mimic the extracellular matrix (ECM) of connective tissue. It allows the dissolution of nutrients and growth factors throughout the scaffolds and helps in cell-scaffold integration^{1,2}.

The surface of the electrospun scaffolds can be modified by various surface medication techniques like a chemical modification or bio-functionalization, etc. The understanding of cell adhesion, cell infiltration, proliferation, differentiation and vascularization on the surface of scaffolds are crucial for the development of tissue engineering.

Electrospinning (Figure 3.1) set-up consists of a supplier of high voltage, a syringe pump, a syringe with a needle (as a positive electrode), and a metal collector (as a negative electrode). A polymer solution filled syringe ejects the solution on the applied voltage and forms the Taylor cone at the tip of the needle. The formation of Taylor cone confirms the formation of fibres. As the voltage increases, at a certain point, repulsive electrostatic force overcomes the surface tension of solution and a charged jet of polymer in the form of fiber is ejected from the tip of the Taylor cone and travel toward the collector and deposits on it¹⁻⁴.

There are various electrospinning parameters which affect the process of electrospinning and fibre diameter. The applied voltage is an important factor in determining fibre diameter. There is a decrease in fibre diameter with an increase in voltage. The flow rate is kept lower as it provides more time for evaporation of solvent so that uniform and smooth fibre mesh is formed. There is a decrease in the fibre diameter with an increase in the flow rate. If there is too high flow rate then there is the formation of the bead in the fibre mesh or scaffolds. The distance between the needle tip and the collector is often called spinning distance. There is a minimum distance required between the tip of the needle and the collector so that it will provide sufficient time for stretching and drying of fibres before they reach collector. There is a decrease in fibre diameter with an increase in spinning distance. Also, bead formation occurs if there is too long or too short spinning distance³⁻⁶.

The polymer concentration determines the spinnability of a solution. With certain critical level concentration fibres are formed. There is an increase in fibre diameter with an increase in the concentration of the polymer solution. The very high concentration solutions are difficult to process because of the high viscosity of the solution. The molecular weight of a polymer also determines the electrical and rheological properties of the solution. In general, high molecular weight solution used to fabricate high diameter

fibres whereas low molecular weight solution tends to give bead formation. The viscosity of solution depends on the molecular weight and concentration of the polymer. A very low viscosity solution can't form uniform and smooth fibres whereas high viscosity can be difficult to obtain the continuous jet forming fibres^{1,5,6}.

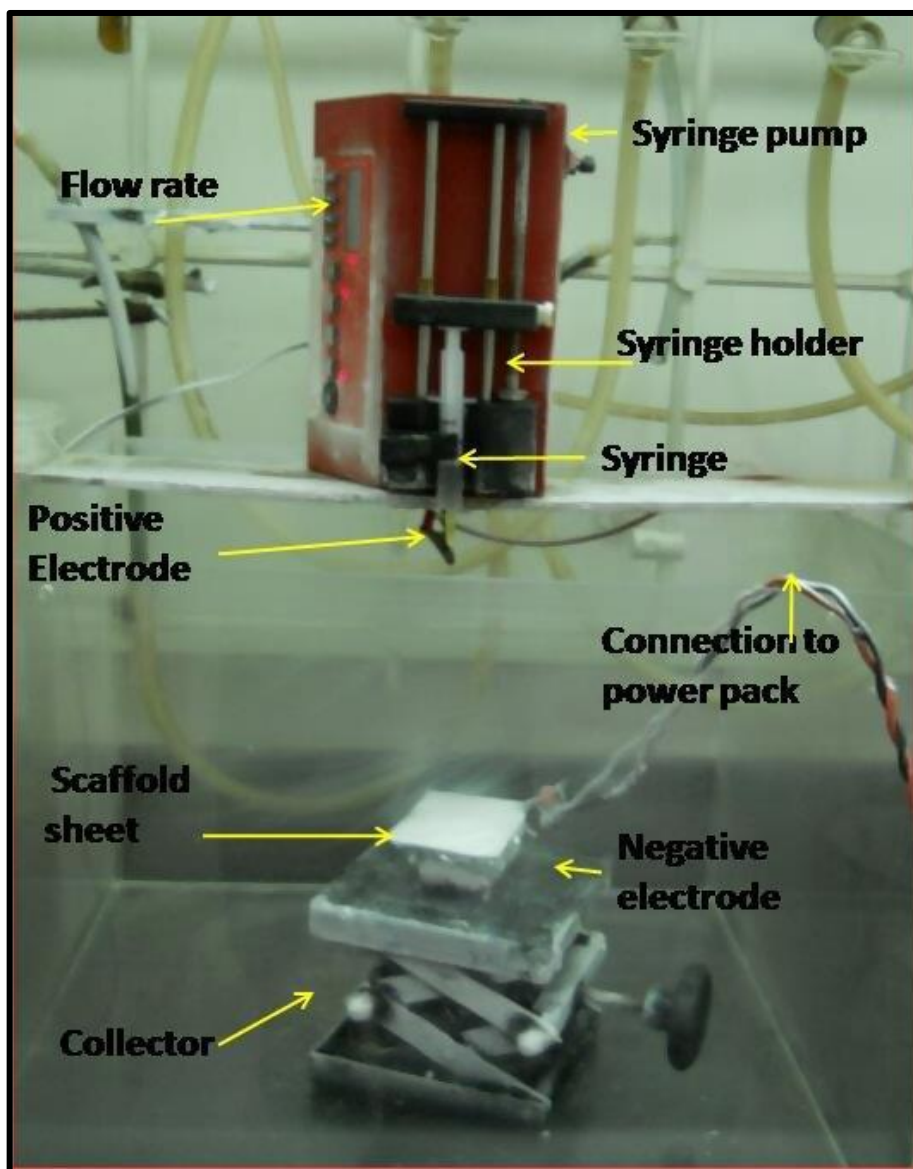


Figure 3.1: An Electrospinning Assembly

The formation of droplets, beads and fibres depends on the surface tension of the polymeric solution. The higher surface tension of the polymeric solution affects the fibre formation where low surface tension can form uniform and smooth fibres. Temperature

and humidity, environmental factors also affect the process of electrospinning. The higher temperature and low humidity are suitable for electrospinning^{1,5-8}.

3.3 Surface Modification methods:

The interaction between tissue and foreign surface largely depends upon the surface properties of materials such as wettability, roughness or topography, surface charge and chemistry⁹. For better cell attachment scaffolds should possess adequate surface structure and chemistry¹⁰. For better cell adhesion and proliferation a concave surface is favoured than a convex surface. A concave surface is involved in the initiation of the bone formation¹¹. The cube or disc-shaped scaffold is more suitable for bone tissue engineering¹². The surface modification also helps in the improvement of the biological properties of scaffolds. The hydrophilic surfaces with positively charged amines negatively charged clean glass, surfaces with methyl silica gradients showed better cell attachment¹³. Surface properties like morphology, hydrophilicity and surface energy promote cell adhesion, migration, phenotype maintenance and intracellular signalling *in vitro* and recruitment of cells at the tissue-scaffold interface *in vivo*¹⁴. This type of modification has the advantage that chemically well-defined surfaces are prepared which are amenable to fundamental surface structure-surface property correlations. The practical approaches to polymer surface modification include flame treatment, corona discharge treatment, plasma modification, and surface graft polymerization. The disadvantage of this approach is that a chemically well-defined surface cannot be designed and prepared but the advantage is that they work to control the technologically significant properties of adhesion, wettability, biocompatibility, and gas permeability. Multiple chemical reactions will certainly not replace the simpler and practical approaches for most applications¹⁵.

The surface of the scaffolds was modified by using the layer by layer method and paint method.

3.3.1 Layer by layer method:

The layer by layer method offer advantages of both these approaches as a surface modification technique for polymers. It is a simple, relatively fast, environmentally benign, and potentially economic process¹⁵ to prepare uniform multilayer films on substrates from solution. It is fast and irreversible deposition, easy to control of the

deposited film thickness and uniform surface coverage¹⁶. Easily electrospinnable synthetic polymers such as PCL, PLA, etc are primarily hydrophobic. For application in tissue engineering, the hydrophobicity of the nanofibrous mesh should be modified to be partly hydrophilic. Introducing hydrophilic property to hydrophobic nanofibers has been attempted in various ways, e.g. plasma treatment¹⁷.

The poly (ethylene terephthalate) (PET) was modified with poly (allylamine hydrochloride) by layer by layer deposition. It significantly improved wettability and mechanical strength of the PET films¹⁵. An electrospun PCL - poly (ethyleneimine) (PEI) block copolymer was modified by poly(ethylene glycol) (PEG) to transform original hydrophobic mesh to hydrophilic mesh using the layer by layer method. There was an improvement in cell viability and cell attachment of epidermal cells¹⁷. The PLA-PEI films were also modified with GO¹⁸. The polyamic acid (PAA)-PEI-GO films were prepared by layer by layer method¹⁶.

Preparation of PCL- GO, PCL- GO-CQ, PCL- GP, PCL- GP-CQ scaffolds were carried out by repetitive dipping of 2 minutes and air drying of these sheets for multiple cycles as 30, 60 cycles and with final overnight dipping. There is an alternative layer of GO/GP and CQ deposited on the PCL- GO-CQ and PCL- GP-CQ scaffolds.

3.3.2 Paint method:

The paint method is very simple and easy to apply for modification of scaffolds as compared to plasma treatment, spin coating, etc. It is very similar to ordinary painting; here we have used the respective paints of GP, GO, and CQ callus extract and their respective combinations to paint the electrospun PCL scaffold sheets.

3.4 Scanning electron microscopy:

Scanning electron microscopy (SEM) is one of the most common methods for imaging microstructures and morphology of biomaterials at higher magnification. It is used to characterize different types of materials from the nanometre to micrometre scale¹⁹. The sample is bombarded with the electron beam, the interaction between sample-electron beam generate various emissions which are detected by the specific type

detectors used in the form of secondary electrons, backscattered electrons, X rays, Auger electrons, visible photons and so on. The backscattered electrons are crucial.

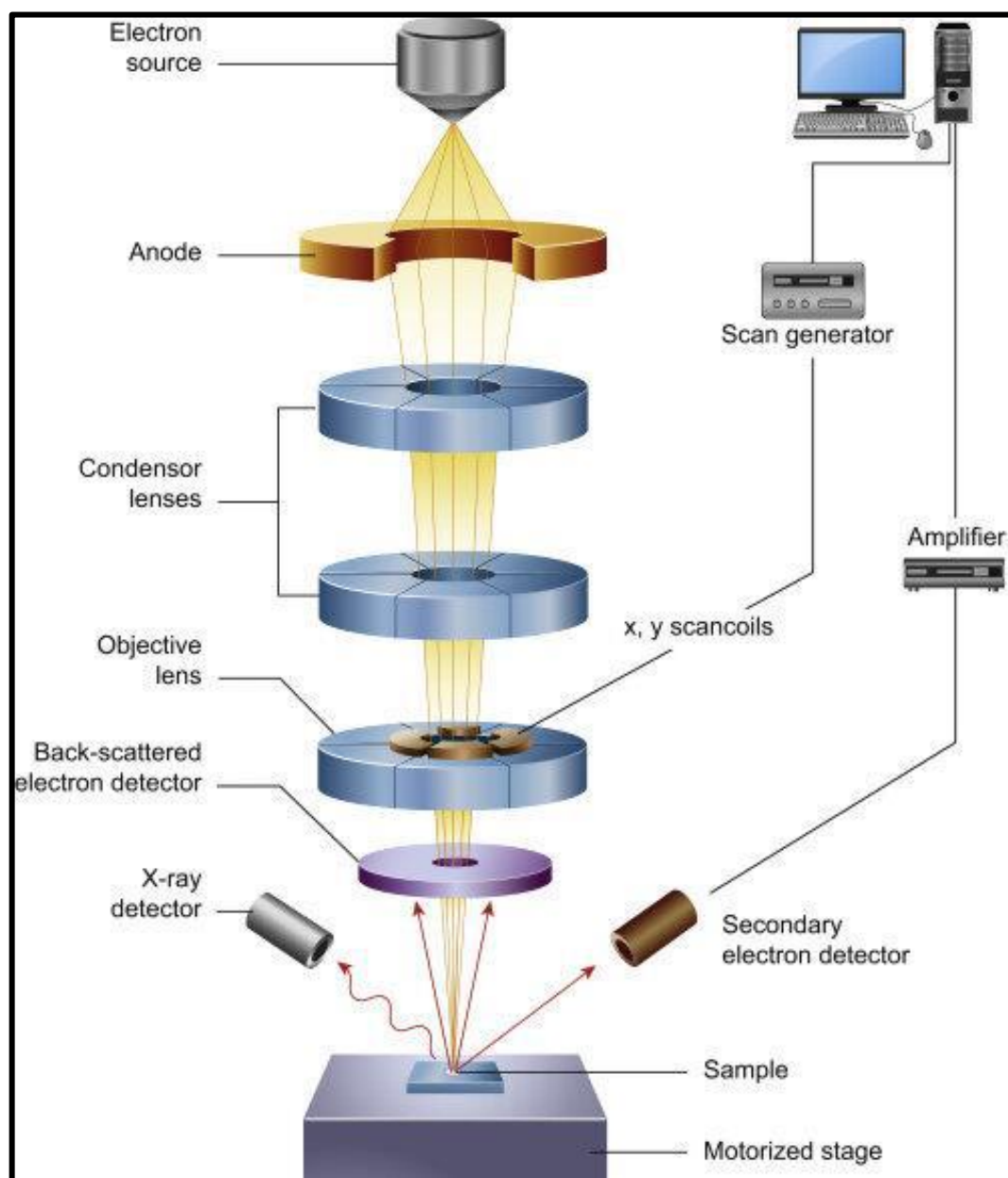


Figure 3.2: A schematic diagram of Scanning Electron Microscopy [source: <https://www.scimed.co.uk/sem-scanning-electron-microscopy/> (accessed 10 September 2018)]

There are two types of electron guns as thermionic electron gun with a diameter of electron beam about 20-50 μm and field emission electron gun with a diameter of the electron beam of about 10 nm. Therefore, the field emission SEM (FESEM) is mostly

used for high-resolution SEM images¹⁹⁻²¹. The basics are explained in Figure 3.2 adapted from²².

In SEM, specimens can be observed in the high and low vacuum, therefore, the samples should be dry. Samples should be electrically conductive and properly grounded to prevent accumulation of electrostatic charges on the surface. The non-conductive samples can charge when bombarded with an electron beam and therefore, usually coated with a thin coating of electrically conductive materials such as palladium, gold or carbon^{20,21,23,24}.

Energy Dispersive X-ray Spectroscopy (EDAX/EDS):

Elemental analysis and chemical information of biomaterials can be done with the help of X-rays or Auger electrons emitted from the sample under electron beam generally from SEM¹⁹.

The morphologies of the electrospun pure polymeric and composite scaffolds were examined by field emission scanning electron microscope (FESEM, Carl Zeiss, Germany) at an accelerating voltage of 15 kV. For FESEM, the samples were cut into 5X5 mm squares, mounted on to sample stubs; sputter coated with gold/palladium using an SC 7640 Sputter Coater (Quorum Technologies Ltd, UK). The coated GO were analysed on the electrospun fibres of PCL. The pore size and fibre diameter range of the scaffolds were calculated from the FESEM micrographs using image analysis software (ImageJ, National Institutes of Health, Bethesda, USA).

3.5 Atomic force microscopy:

Atomic force microscopy (AFM) is one of the powerful tool used for surface characterization of scaffolds like surface topography and surface roughness. The high resolution ($\sim 2 \text{ \AA}$) and magnification ($\sim 10^7\times$) gives a better idea of the topography of the surface of the scaffold. It is a quantitative technique used to measure nanoscale surface roughness and surface texture of different type of material surface like polymers and composites^{20,23}.

A typical AFM instrument consists of a cantilever with a sharp tip at its end for scanning the specimen surface. The cantilever is usually of silicon or silicon nitride. It has

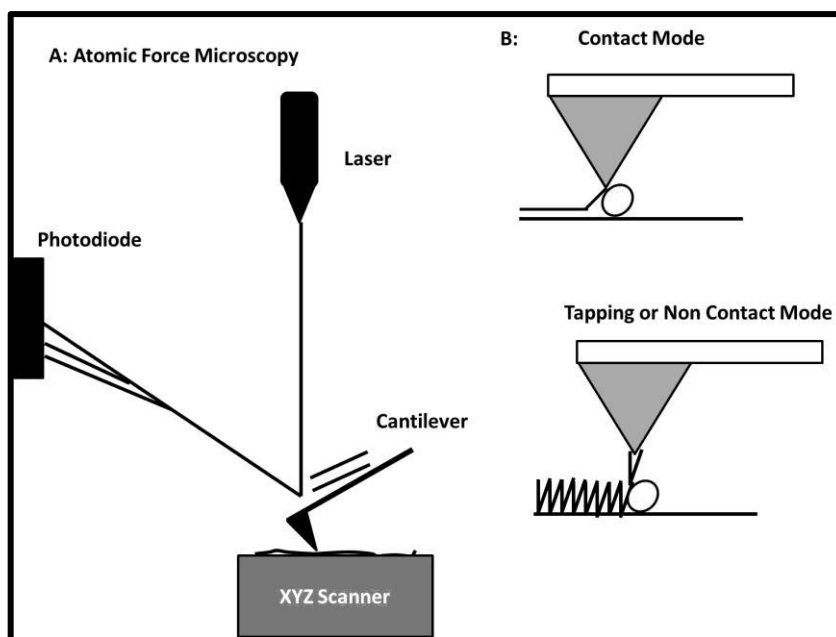


Figure 3.3: A: A schematic diagram of Atomic Force Microscopy; B: A representation of AFM imaging modes

a tip radius of curvature of about nanometers. When the tip is carried nearby to the surface of the sample, the force between the tip of cantilever and surface of the sample directs to a deflection of the cantilever with respect to Hooke's law. The deflection is calculated by a laser reflected from the top surface of the cantilever into an array of photodiodes. As per the application, the mechanical contact force, van der Waals force, capillary force, chemical bonding, electrostatic force, magnetic force, etc. measured in AFM¹⁹. As compared to other imaging techniques SEM or TEM, sample preparation in AFM with regard to biomaterials is quite easier. Also, it is affordable and time-saving. There is no requirement of a vacuum and samples can be imaged in ambient air or liquid. AFM gives three-dimensional topographical images rather than two-dimensional images.

There are three different modes of AFM operation as contact mode, non-contact mode and tapping mode. In the contact mode, the cantilever remains in contact with the surface during scanning. The sample-tip distance is so small that the important force is the core-core repulsive force. The cantilever is in continuous contact with the sample so there is the possibility of damage to the surface which can alter both the resulting image and properties of the material. Contact mode AFM is not suitable for soft materials¹⁹.

In the non-contact mode, there is no direct contact between cantilever tip and sample surface. The important force is the van der Waals which can achieve resolution of nearly 1 nm. The non-contact mode AFM is preferable over contact mode AFM in which sometimes, sample damage with a tip or sample degradation effects may occur due to contact. However, non-contact AFM is not commonly used for biomaterials because most biomaterials are hydrophilic and develop a liquid meniscus layer under ambient conditions. The tip sticking may occur resulting in low-resolution imaging^{19,20}.

In the tapping mode (Figure 3.3), when the tip begins to lightly touch the surface, a sensor reverses the motion of the cantilever to continue the oscillation. The tip then intermittently touches the surface, instead of being dragged avoiding damages. Therefore, the tapping mode is also called intermittent contact mode. The cantilever is oscillating at a frequency as it scans the surface of the sample. When it encounters bumps on the surface, the amplitude of oscillation is reduced, while, valleys or depressions cause the amplitude to increase. The important force is van der Waals forces, electrostatic force, etc. The amplitude of this oscillation is much greater than 10 nm, typically 100-200 nm. By recording these changes, an accurate topographical map can be produced. The tapping mode AFM is mostly used in the characterization of biomaterials. However there is mechanical contact, loss to the sample surface is minimized due to unequal contact and there is no lateral friction force employed to the sample. Tapping mode AFM can provide topographical information with superior resolution on biomaterials¹⁹⁻²¹.

Surface properties of the modified surface of PCL sheets were analysed by AFM (Asylum Research) by tapping mode. The scaffolds were cut into small pieces and stuck on a glass slide by cellophane tape. The Scan rate of 1.0 Hz and a scan area of 10 μm were used for imaging.

3.6 Confocal microscopy:

Confocal microscopy is a powerful choice for researchers interested in serious imaging of cell structure, function and unravelling the complexities of the morphology and dynamics of cells and tissues^{25,26}. There are other several advantages of confocal microscopy over conventional light and electron microscopy. The lateral resolution, out of focus information elimination and imaging of very thin sections are offered by

confocal microscopy²⁷. The use of confocal microscopy in the field of biomedical and biological sciences increased due to the enhanced imaging capability^{19,27}. In the field of tissue engineering, the challenge for imaging in the microscope is the two or three-dimensional biomaterials samples with different composite polymers, ceramics, etc., containing cells or extracellular matrix (ECM). The cells may be seeded deeply within or around the scaffolds/biomaterials^{28,29}.

The imaging of cell growth on opaque biomaterials, fluorescence technique is used to label the cells. Fluorescence microscopy has limitations where many cell layers are present; the resolution of the image will suffer due to the contribution of the glare from out of focus information to the image. In the rough scaffolds or surfaces, cell growth is deeper in grooves or pores will not be easily imaged by higher magnification lenses as they will be out of the range of working distance of the lens. In these cases, 3D information is required, confocal microscopy is the routine cellular imaging technique^{19,29}.

The study of fluorescently labelled samples is carried out by a confocal laser scanning microscope (CLSM) (Figure 3.4) where the sample is fixed and the laser scans the sample. The excitation of the fluorescent label is achieved by a laser specific to the excitation maxima of the dye. It has the advantage of maximising the signal to background ratio. The inclusion of confocally aligned pinholes in the optical path, assures only information from the plane of focus of microscope is collected. The 90% of the emission light can be filtered out by the pinhole. The specific wavelength lasers are used as light sources which are extremely bright and monochromatic. Therefore, the out of focus light is eliminated and produces images with clarity, high contrast²⁷. The laser beam is scanned across the specimen by scanning mirrors. The emitted light passing through the detector pinhole is transformed into electrical signals by a photomultiplier and displayed on a computer monitor²⁴. The study of fluorescently labelled samples is carried out by a confocal laser scanning microscope (CLSM) (Figure 3.4) where the sample is fixed and the laser scans the sample. The excitation of the fluorescent label is achieved by a laser specific to the excitation maxima of the dye. It has the advantage of maximising the signal to background ratio. The inclusion of confocally aligned pinholes in the optical path, assures only information from the plane of focus of microscope is collected.

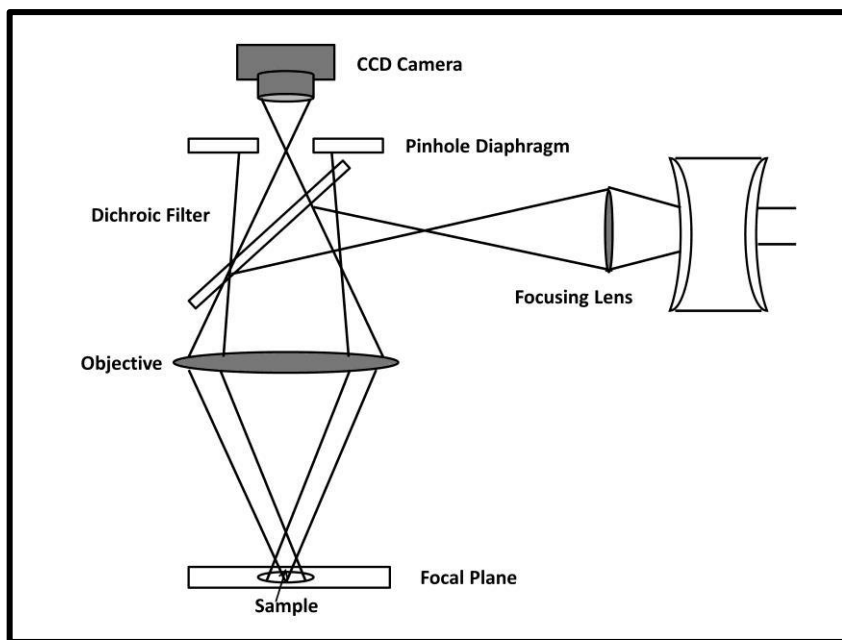


Figure 3.4: A schematic diagram of confocal laser scanning microscope.
 [Source: <http://www.cnilaser.com/clsm.html> (accessed 20 January 2019)]

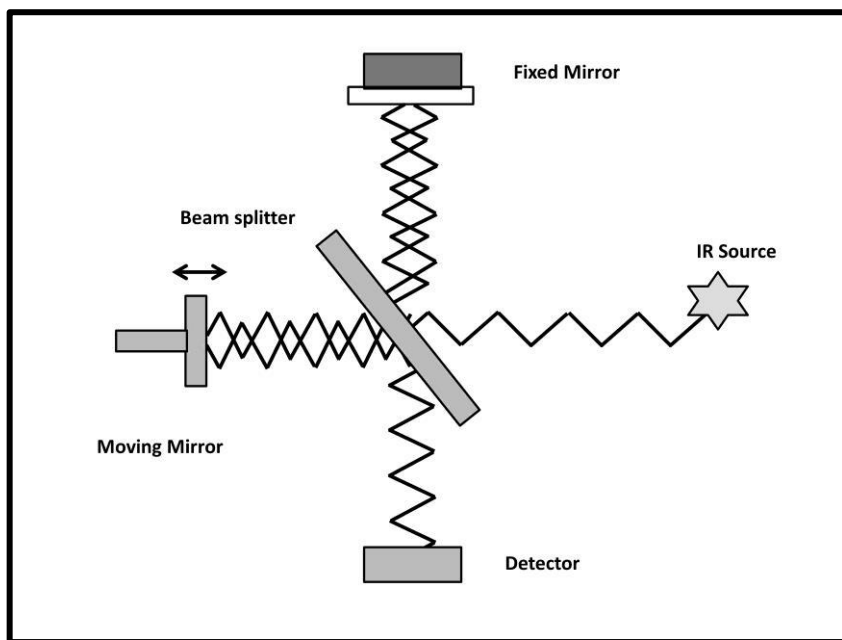


Figure 3.5: A schematic diagram of Fourier Transform Infrared Spectroscopy
 [Source: <http://crf.iitd.ac.in/Facility-FTIR.html> (accessed 20 January 2019)]

The 90% of the emission light can be filtered out by the pinhole. The specific wavelength lasers are used as light sources which are extremely bright and monochromatic.

Therefore, the out of focus light is eliminated and produces images with clarity, high contrast²⁷. The laser beam is scanned across the specimen by scanning mirrors. The emitted light passing through the detector pinhole is transformed into electrical signals by a photomultiplier and displayed on a computer monitor²⁴. The digital images collected are easily quantifiable. By altering the plane of focus stepwise a series of images, all in focus, can be collected throughout the depth of the sample, this is called optical sectioning. As it offers optical sectioning of the specimens, which is relatively noninvasive, living as well as fixed samples can be observed with greater clarity. Optical sectioning allows images to be collected at a relatively shallow depth of field (0.5-1.5 μm) within the tissue from a well-defined plane (z-series). The optical sections can be taken in different planes, as the x y plane, y z and x z planes (vertical sectioning) along with cells can be scanned in depth (z-axis) as well as laterally (x or y-axis)²⁵. These can be displayed as a gallery of optical sections showing the depth of cell ingress into a scaffold. This is useful for tissue engineering, as it allows cells growing on an uneven surface represented in one image^{24,28,29}.

3.7 Fourier Transform Infrared Spectroscopy:

Fourier Transform Infrared Spectroscopy (FTIR) (Figure 3.5), a form of vibrational spectroscopy, is fast, relatively inexpensive and widely used analytical technique for the characterization of biomaterials. It is established on the vibrations of the atoms inside a molecule. The infrared radiation passed through the sample and particular fraction of the incident radiations absorbed at a particular energy at which particular peaks appear corresponding to the frequency of a vibration of a part of a sample molecule. The molecular vibration is of two types of stretching vibrations that change the bond length and bending vibrations that change the bond angle. The stretching vibrations are generally giving stronger peaks as that of bending vibration. The weaker bending vibrations can be useful in the differentiating similar types of bonds. These changes are collected and analysed in the form of the spectrum^{20,21}.

In FTIR, virtually any sample in nearly any state can be studied. Liquids, films, fibres, gases, solutions, pastes, powders, and surfaces can be examined by a judicious choice of the sampling technique.

FTIR spectra were recorded for all scaffolds using (FTIR, Bruker, Germany). The spectra were obtained with 30 scans per sample ranging from 4000 to 500 cm^{-1} . The FTIR was carried out for the study of the potential existence of C=O, C=C, and asymmetric C-O-C stretching in the electrospinning PCL sheet; The C=O, C=C, C-H stretching for GO; C-C, C-OH, C-H stretching for GP; and C=O, C-N, C-H, C=S stretching for CQ.

3.8 Thermogravimetric analysis:

Thermal analysis is an analytical technique used to investigate the behaviour of a sample as a function of temperature. The commonly used thermal analysis techniques are differential thermal analysis, differential scanning calorimetry, thermogravimetry, thermomechanical analysis, etc.

Thermogravimetry (TG) is the branch of thermal analysis which examines the mass change of a sample as a function of temperature in the scanning mode or as a function of time in the isothermal mode. The change in mass may be due to thermal events like desorption, absorption, sublimation, vaporization, oxidation, reduction and decomposition. TG used to characterize the decomposition, thermal stability, examine the kinetics of the physic-chemical processing occurring in the sample. The sample is placed in the thermal microbalance and heated at a predetermined rate, and then a change in weight of the sample is detected. Mass changes occur in a variety of ways and this produces steps in the thermogravimetric analysis (TGA) (Figure 3.6). TGA is normally carried out in air or an inert atmosphere such as Helium or Argon. The analyser consists of a balance with a platinum pan where we can load the sample. The pan is placed in an electrically heated oven with a thermocouple to measure the temperature accurately. The reaction atmosphere is purged with an inert gas to prevent oxidation or other in desired reactions.

The thermal degradation behaviours of scaffolds were studied with a thermogravimetric analyser (Universal V4.7A TA Instrument); instrument under the nitrogen atmosphere in the temperature range from 30⁰C to 800⁰C at a heating rate of 10⁰C/min.

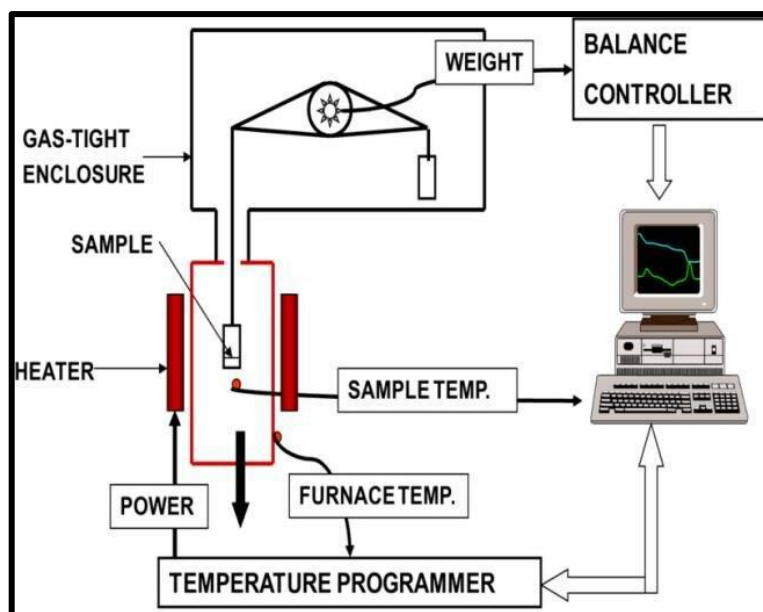


Figure 3.6: A schematic diagram of thermo gravimetric analyser

3.9 Mechanical Testing:

The Universal Testing Machine (UTM) is used to test the tensile and compressive properties of the material. Tensile properties are the most important single indication of strength in a material. The force required to strain the specimen apart is decided by how much the material extends before it fractures.

During tensile test, the sample is held in machine jaws and the load is employed via a screw gear mechanism by adjustable crosshead jaw. When a load is applied, sample gets stretched. The load cell is joined to the moving crosshead which is run by electric motors. A load cell in series with the grip measures the force, which can be displayed on a digital display. The obtained stress-strain graph gives the yield strength and tensile strength of the specimen.

The stress at the point of yielding (y) is termed the yield strength (σ_y or Y) and is typically reported in MPa or kPa. But there is a gradual transition from elastic to plastic deformation, so, the yield point is often not obvious. Therefore, the yield stress is often more accurately and reproducibly measured. The stress at the ultimate point (u) is termed the ultimate strength or tensile strength (σ_u or UTS) and is typically reported in MPa or kPa³⁰, Figure 3.7 shows the Y and UTS.

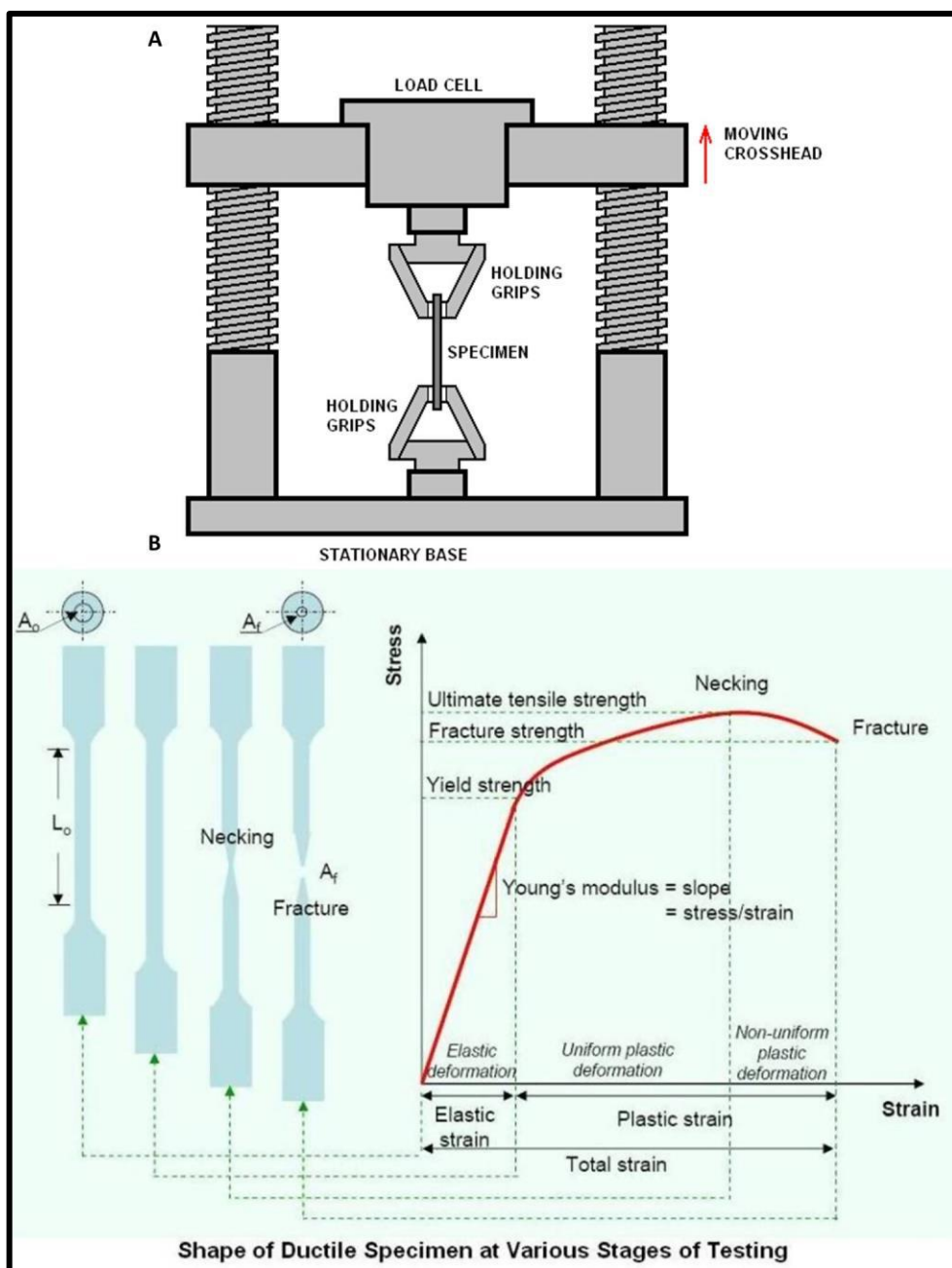


Figure 3.7: A: A schematic diagram of Universal testing machine for tensile testing; B: A typical stress-strain graph showing ductile specimen

Tensile properties were calculated at room temperature with UTM. Scaffold cut in to cylinders ($n=3$) were tested. The loading was 100 N and crosshead speed (strain rate) was 5mm/min. From the resulting stress-strain curves, Yield strength and tensile strength were calculated.

3.10 Contact angle measurement:

The angle between the material surface and the tangent line at the contact point of the drop with the surface is called the contact angle (CA, θ) (Figure 3.8)³¹. CA measurement is a simple, sensitive, reliable, inexpensive thermodynamic method for determination of quantitative value to determine the hydrophobicity of the material surface. Functions like protein adhesion, cell adhesion, and cell spreading¹⁹⁻²¹ are dependent on hydrophilicity. With increasing surface roughness there is a decrease in CA for hydrophilic surfaces while with an increase in surface roughness there is an increase in CA for hydrophobic surfaces. If CA of a substrate is ($\theta < 90^\circ$), then it is hydrophilic or wetting while if ($\theta > 90^\circ$), then it is hydrophobic or non-wetting. The CA can be explained using Young's equation as

$$\gamma_{lv} \cos\theta = \gamma_{sv} - \gamma_{sl} \text{-----} (3.1)$$

Where γ_{lv} = liquid-vapour interfacial tension,

γ_{sv} = Solid-vapour interfacial tension,

γ_{sl} = Solid-liquid interfacial tension,

θ = Young' Contact angle.

CA measurement is quite a simple method for solid samples and no special sample preparation is required. The samples characterized should be clean and do not swell and or dissolve in the test liquid. The small surface substrates up to few millimetres and small amounts of liquid up to few microliters required for measuring CA. There are several methods of CA measurement as most common Wilhelmy method, sessile drop method and captive bubble method¹⁹.

Wilhelmy method:

It is a dynamic method by measuring the equilibrium surface or interfacial tension at the air-liquid or liquid-liquid interfaces¹⁹.

Sessile drop method:

There are two kinds of sessile drop methods, as a static sessile drop method and dynamic sessile drop method.

In the static sessile drop method, a droplet of pure liquid is deposited vertically on to the surface and CAs is measured by a CA goniometer using an optical subsystem. The angle formed between the solid/liquid interface and the liquid/gas interface is determined as the liquid CA.

In the dynamic sessile drop method, alike to sessile drop method except needs the drop to be customized. Both advancing angle (θ_A), the largest CA possible without increasing its solid/liquid interfacial area by adding volume dynamically and receding angle (θ_R), the smallest possible angle by removing the volume without decreasing its solid/liquid interfacial area are measured in dynamic sessile drop method. The difference between the advancing and receding angle is the hysteresis CA ($\theta_H = \theta_A - \theta_R$)²⁰.

Sessile drop method is most commonly used CA measurement for biomaterials as it is a straightforward approach revealing surface energetics of the sample. It is used to characterize the hydrophilicity and hydrophobicity of solid biomaterials with micro-/nano-structures. typically, pure water serves as the test liquid^{19–21}. The schematic diagram is explained in Figure 3.8:B.

Captive bubble method:

It measures the wettability of samples in a liquid, most commonly water. An air bubble is placed in contact with the sample immersed in a solution. After the contact, the drop profile of the air bubble is immersed using a charge-coupled device (CCD) camera and CA is calculated from the image. The interface between the solid sample and droplet is the solid/gas interface. The captive bubble method is not as popular as a sessile drop method; it is useful for hydrated biomaterials¹⁹.

3.11 Cell viability assay: MTT assay:

The cytotoxic effects of the material on the living organism is analysed by cytotoxicity assay, earliest and simplest *in vitro* technique for biocompatibility evaluation

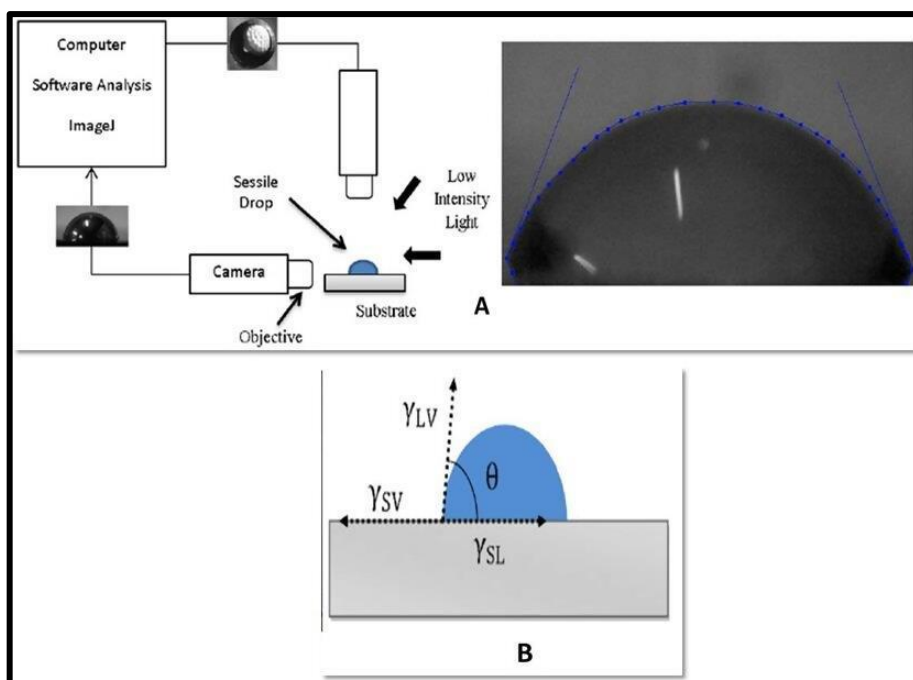


Figure 3.8: A: A scheme of the goniometer, planar and side view of sessile drop (left), and photograph of a drop during measurement of the contact angle in the software (right); B: A schematic of a contact angle of a liquid drop placed on a solid surface

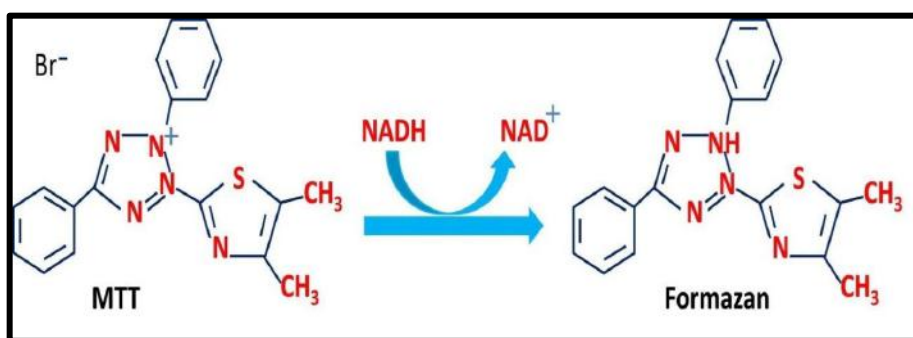


Figure 3.9: A schematic diagram representing reduction of MTT to formazan

of materials²⁰. Cell-based assays are versatile tools designed to measure cellular or biochemical functions of cells. These *in vitro* assays can be conducted to study the toxicity of test materials³². The understanding of biological interaction with materials is key to the development of materials for tissue engineering applications^{32,33}. The materials with cytotoxic effects are likely to affect the cell viability, including cellular metabolism, cell proliferation, and in many cases trigger programmed or necrotic cell death³². There is

a variety of methods for detecting viable eukaryotic cells. These include tetrazolium reduction, resazurin reduction, protease markers, ATP detection, etc. The most commonly used are tetrazolium salts, including, 3-(4,5-dimethylthiazol-2-yl)-2,5-diphenyltetrazolium bromide (MTT), 3-(4,5-dimethylthiazol-2-yl)-5-(3-carboxymethoxyphenyl)-2-(4-sulfophenyl)-2H-tetrazolium (MTS), and 2,3-bis-(2-methoxy-4-nitro-5-sulfophenyl)-2H-tetrazolium-5-carboxanilide (XTT).

MTT is one of the most widely used probes to study cell viability, cytotoxicity, proliferation, chemo and radiosensitivity *in vitro*³⁴. It is reduced to purple-coloured formazan derivatives by the action of nicotinamide adenine dinucleotide phosphate (NADPH)-dependent enzymes of the endoplasmic reticulum. MTT reduced to formazan by NADH transferring an electron to MTT (Figure 3.9). The metabolic activity is higher in actively proliferating cells under optimal cell culture conditions as compared to intoxicated cells³². The quantity of a purple coloured formazan, formed from tetrazolium reduction is directly proportional to metabolic active cells³²⁻³⁵.

For the MTT calorimetric assay, the tetrazolium dye is added to the cells after their incubation with material and is converted to an insoluble formazan derivative. This insoluble formazan derivative then solubilized prior to analysis. The assay is carried out in dark due to the light-sensitive nature of MTT. The absorbance of the solution is read using a spectrophotometer at (usually between 500 nm and 600 nm)^{32,35,36}.

The formazan, the insoluble product may accumulate in the cells or in the culture medium to stabilize colour, avoid evaporation and interference by the phenol red, formazan solubilized in the acidified isopropanol, DMSO, dimethylformamide, SDS, etc. Acidification changed phenol red to yellow colour less interfering with absorbance readings. The pH of the solubilizing solution can be adjusted for sensitivity issues^{33,37}.

3.11 Mineralization assay/ Osteoblastic differentiation assay:

Osteoblast differentiation *in vitro* and *in vivo* can be characterized by matrix mineralization in which Osteoblasts secrete and mineralize the bone matrix. The mineralized extracellular matrix is mainly composed of type I collagen, and smaller but significant amounts of osteocalcin, matrix gla protein, osteopontin, bone sialoprotein, BMPs, TGF- β , and the inorganic mineral hydroxylapatite which contains calcium

deposits. Calcium deposition can be visualized using adequate staining methods like alkaline phosphate staining, Alizarin red S staining, and Von kossa staining. The use Alizarin red S staining, and Von kossa staining for detection of mineralization used by various researchers such as differentiation of dental pulp stem cell osteogenic differentiation on fluorapatite modified PCL fibres³⁸. Calcium deposits are an indication of success *in vitro* bone formation and can specifically stain bright orange-red using Alizarin Red S or black precipitates using Von kossa staining³⁹.

3.11.1 Alizarin red S staining:

Alizarin red S (ARS) is typically used to visualize Ca^{2+} ion included in a hydroxyapatite that deposits during osteoblast differentiation⁴⁰. One mole of alizarin red has the capacity to bind 2 moles of calcium. The alizarin red gives a red colour when it binds to the mineralized matrix. The hMSCs cultured in osteoblastic differentiation media for 21 days, showed dark staining with ARS as compared to hMSCs cultured on MEM medium⁴¹. The ARS Assay showed more staining and higher absorbance value on phosphocreatine modified chitosan (CS_MP) seeded with FOB cells compared with pure chitosan group on the 14th day as compared to the 7th day. The calcium deposition was increased with time by cells cultured on CS_MP scaffolds⁴². Calvarial osteoblasts (OBs), bone marrow stromal cells (BMCs), periosteum-derived cells (PDCs) exhibited greater mineralization with ARS staining on osteoblastic medium than culture medium⁴³. ARS staining with calvarial primary osteoblasts cultured under static magnetic field and particularly with the presence of magnetic nanoparticles in the PCL scaffolds showed darker staining after 10th day⁴⁴. The BMPs were assessed for an osteoinduction of MSCs for 21 days of culture. There was significant mineralization and bone nodules formation when MSCs cultured with a combination of BMP-2+BMP-6+ BMP-9, confirmed by ARS staining⁴⁵.

3.11.2 Von kossa staining:

The Von kossa staining was used to evaluate the osteoblastic differentiation of MSCs through mineralization. After up to 24 days of culture of MSCs into osteoblastic induction medium, there was mineralization from 14 days onwards in increasing manner, as confirmed by Von kossa staining⁴⁶. The Foetal rat calvariae (FRC) cells were cultured

on osteoblastic medium showed mineralization or bone nodules formation on day 14, as confirmed by Von kossa staining⁴⁷. The BMPs were assessed for an osteoinduction of MSCs for 21 days of culture. There was significant mineralization and bone nodules formation when MSCs cultured with a combination of BMP-2+BMP-6+ BMP-9, confirmed by Von kossa staining⁴⁵. When MSCs cultured on biphasic calcium phosphate, calcium phosphate in presence of conditioned medium containing significant growth factors, mineralization was observed with positive Von kossa staining on 21 days of culture⁴⁸.

References:

- 1 A. Martins, R. L. Reis and N. M. Neves, *Int. Mater. Rev.*, 2008, **53**, 257–274.
- 2 H. Malshe, *Inquiry*, 2011, **12**, 70–76.
- 3 K. P. Feltz, E. A. G. Kalaf, C. Chen, R. S. Martin and S. A. Sell, *Electrospinning*, 2017, **1**, 46–61.
- 4 J. Cheng, Y. Jun, J. Qin and S. H. Lee, *Biomaterials*, 2017, **114**, 121–143.
- 5 N. M. N. Marta R. Casanova, Rui L. Reis, Albino Martins, *Adv. Exp. Med. Biol.*, 2018, **1058**, 11–16.
- 6 M. K. Leach, Z.-Q. Feng, S. J. Tuck and J. M. Corey, *J. Vis. Exp.*, 2011, **47**, 1–5.
- 7 S. Chen, R. Li, X. Li and J. Xie, *Adv. Drug Deliv. Rev.*, 2018, **132**, 188–213.
- 8 X. Cai, P. Zhu, X. Lu, Y. Liu, T. Lei and D. Sun, *J. Mater. Sci.*, 2017, **52**, 14004–14010.
- 9 W. M. Gallagher, I. Lynch, L. T. Allen, I. Miller, S. C. Penney, D. P. O’Connor, S. Pennington, A. K. Keenan and K. A. Dawson, *Biomaterials*, 2006, **27**, 5871–5882.
- 10 S. Yang, K. F. Leong, Z. Du and C. K. Chua, *Tissue Eng.*, 2001, **7**, 679–689.
- 11 A. Graziano, R. D’Aquino, M. G. C.-D. Angelis, F. De Francesco, A. Giordano, G. Laino, A. Piattelli, T. Traini, A. De Rosa and G. Papaccio, *J. Cell. Physiol.*, 2008, **214**, 166–172.
- 12 M. Patel and J. P. Fisher, *Pediatr. Res.*, 2008, **63**, 497–501.
- 13 K. Webb, V. Hlady and P. A. Tresco, *J. Biomed. Mater. Res.*, 1998, **41**, 422–430.
- 14 R. A. A. Muzzarelli, *Carbohydr. Polym.*, 2011, **83**, 1433–1445.
- 15 W. Chen and T. J. McCarthy, *Macromolecules*, 1997, **9297**, 78–86.
- 16 Y. Li, M. C. Choi, K. M. Jeong, J. H. Jeong, H. G. Lee, G. H. Kim and C. S. Ha,

- Macromol. Res.*, 2017, **25**, 496–499.
- 17 Y. J. Son, H. S. Kim and H. S. Yoo, *RSC Adv.*, 2016, **6**, 114061–114068.
 - 18 X. He, L. L. Wu, J. J. Wang, T. Zhang, H. Sun and N. Shuai, *High Perform. Polym.*, 2015, **27**, 318–325.
 - 19 B. Bandyopadhyay, Amit, Susmita, in *Characterization of Biomaterials*, Newnes, 2013, pp. 134–135.
 - 20 M. Omid, A. Fatehinya, M. Farahani, Z. Akbari, S. Shahmoradi, F. Yazdian, M. Tahriri and D. Vashaei, in *Characterization of Biomaterials*, Elsevier Ltd, 2017, pp. 97–115.
 - 21 T. S. Sampath Kumar, in *Physical and Chemical Characterization of Biomaterials*, Elsevier Ltd, 2013, pp. 11–47.
 - 22 B. J. Inkson, *Mater. Charact. Using Nondestruct. Eval. Methods*, 2016, 17–43.
 - 23 J. H. Warner, F. Schäffel, A. Bachmatiuk and M. H. Rummeli, *Graphene*, 2013, 229–332.
 - 24 M. Rohde, in *Methods in microbiology*, 2011, pp. 61–100.
 - 25 D. J. W. Wright, Shirley J., *Cell Biol. Appl. Confocal Microsc. Methods Cell Biol.*, 2002, **70**, 1–85.
 - 26 B. Coling, D., Kachar, *Curr. Protoc. Neurosci.*, 1997, **1**, 2–1.
 - 27 A. C. Bovik, in *Handbook of image and video processing*, Academic Press., 2nd edn., 2010, pp. 1291–1309.
 - 28 S. I. Anderson, *Tissue Eng. Using Ceram. Polym.*, 2014, 196–223.
 - 29 C. J. R. Sheppard, in *Confocal Microscopy- Principles , Practice and Options*, Academic Press., 2nd edn., 1999, pp. 303–309.
 - 30 R. K. Roeder, in *Characterization of Biomaterials*, Elsevier Inc, 2013, pp. 49–104.

-
- 31 J. M. Schuster, C. E. Schvezov and M. R. Rosenberger, *Procedia Mater. Sci.*, 2015, **8**, 742–751.
- 32 N. Ninan, H. Albrecht and A. Blencowe, in *Characterization of Nanomaterials*, Elsevier Ltd., 2018, pp. 129–166.
- 33 A. Sousa, S. C. Neves, I. C. Gonçalves and C. C. Barrias, in *Characterization of Polymeric Biomaterials*, Woodhead Publishing, 2017, pp. 285–315.
- 34 J. C. Stockert, R. W. Horobin, L. L. Colombo and A. Blázquez-Castro, *Acta Histochem.*, 2018, **120**, 159–167.
- 35 R. Scherließ, *Int. J. Pharm.*, 2011, **411**, 98–105.
- 36 *MTT Cell Proliferation Assay Instruction Guide*, American Type Culture Collection, 2011.
- 37 T. L. Riss, R. A. Moravec, A. L. Niles, H. A. Benink and T. J. Worzella, 2016, 1–31.
- 38 T. Guo, G. Cao, Y. Li, Z. Zhang, J. E. Nör, B. H. Clarkson and J. Liu, *J. Dent. Res.*, 2018, **97**, 1331–1338.
- 39 S. Terry, *J. Histochem. Cytochem.*, 1969, **17**, 110–124.
- 40 H. Tsutsumi, M. Kawamura and H. Mihara, *Bioorganic Med. Chem.*, 2018, **26**, 3126–3132.
- 41 N. A. Twine, L. Chen, C. N. Pang, M. R. Wilkins and M. Kassem, *Bone*, 2014, **67**, 23–32.
- 42 L. Liu, Y. He, X. Shi, H. Gao, Y. Wang and Z. Lin, *Appl. Mater. Today*, 2018, **12**, 21–33.
- 43 J. M. Rosales-Rocabado, M. Kaku, M. Kitami, Y. Akiba and K. Uoshima, *J. Oral Maxillofac. Surg.*, 2014, **72**, 1–9.
- 44 H. M. Yun, S. J. Ahn, K. R. Park, M. J. Kim, J. J. Kim, G. Z. Jin, H. W. Kim and
-

- E. C. Kim, *Biomaterials*, 2016, **85**, 88–98.
- 45 Y. Açil, A. A. Ghoniem, J. Wiltfang and M. Gierloff, *J. Cranio-Maxillofacial Surg.*, 2014, **42**, 2002–2009.
- 46 P. S. Hung, Y. C. Kuo, H. G. Chen, H. H. K. Chiang and O. K. S. Lee, *PLoS One*, 2013, **8**, 1–7.
- 47 N. Yamamoto, K. Furuya and K. Hanada, *Biol. Pharm. Bull.*, 2002, **25**, 509–515.
- 48 J. Wang, D. Liu, B. Guo, X. Yang, X. Chen, X. Zhu, Y. Fan and X. Zhang, *Acta Biomater.*, 2017, **51**, 447–460.

CHAPTER 4:

SYNTHESIS AND

CHARACTERIZATION OF

SCAFFOLDS

4.1 Introduction:

The bone tissue engineering has become one of the mainstream researches in the regeneration, repair or restructuring of bone tissues. A plethora of research methodologies have been bourgeoned with biomaterials and their applications in the field of tissue engineering and regenerative medicine. The various polymers like poly ϵ -caprolactone (PCL), poly-D, L-lactic acid (PDLLA)¹, poly (L/DL-lactide) (PLDL)², PLLA³, poly (DL-lactic-co-glycolic acid) (PLGA)⁴ shown to be a potential candidate with good mechanical properties like tensile strength, elastic modulus, biocompatibility, higher cellular properties and even bone formation in a rat model⁵. The PCL is biocompatible, biodegradable as well as FDA approved material and used extensively in tissue engineering applications. PCL along with Hydroxyapatite (HA)⁶. PCL-gelatin hybrid nanofibrous membranes⁷. PCL-(Poly-1,4- butylene adipate-co-polycaprolactam (PBAPCL)-HA composite scaffold⁸ were used in bone tissue engineering.

Easily electrospinnable synthetic polymers are primarily hydrophobic such as PCL, PLA, etc. For application in tissue engineering, the hydrophobicity of the nanofibrous mesh should be modified to be partly hydrophilic. Introduction of hydrophilic property to hydrophobic nanofibers has been attempted in various ways by surface modification, e.g. flame treatment, corona discharge treatment, plasma modification, and surface graft polymerization⁹. Surface modification is an important aspect in the field of tissue engineering to increase the cell attachment and cell proliferation. The surface modification also helps in improvement of the biological properties of scaffolds. The interaction between tissue and foreign surface largely depends upon the surface properties of materials such as wettability, roughness or topography, surface charge and chemistry^{10,11}.

The layer-by-layer method is a simple, relatively fast, environmentally benign, and potentially economic process¹² to prepare uniform multilayer films on substrates from solution. It is fast and irreversible deposition, easy to control the thickness of deposited film and uniform surface coverage¹³. The poly (ethylene terephthalate) (PET) was modified with poly (allylamine hydrochloride) using layer by layer deposition approach. It significantly improved wettability and mechanical strength of the PET films¹². An electrospun PCL-poly (ethyleneimine) (PEI) block copolymer was modified by poly

(ethylene glycol) (PEG) to transform original hydrophobic mesh to hydrophilic mesh using a layer by layer method. There was an improvement in cell viability and cell attachment of epidermal cells⁹. The PLA-PEI films were also modified with graphene oxide (GO)¹⁴. The polyamic acid (PAA)-PEI-GO films were prepared using layer by layer method¹³.

The carbon materials are considered as similar physical analogues of extracellular matrix (ECM) like that of collagen fibres⁵. The graphene oxide (GO) and graphene (GP) has become the biomaterial of the 21st century as being potential of applications in electronics to biomedical applications and tissue engineering. The extravagant mechanical properties, biocompatibility and osteoinductive properties of GO/GP would make them one of the most foreseen biomaterials in the regenerative medicine in coming years.



Figure 4.1: *Cissus quadrangularis* plant

A medicinal plant *Cissus quadrangularis* (CQ), (Figure 4.1) also known as Vajravalli in Sanskrit, in Hindi Hadjod, in Marathi Kandvel, and in English Edible Stemmed Vine. The medicinal properties of the plant have been described in the ancient book “BhawaPrakash”. The plant has immense medicinal potential with reported antimicrobial and antioxidant activity¹⁵. Methanolic extract of CQ revealed the faster bone healing in the experimentally fractured radius-ulna of the dog as well as complete

bone healing on the 21st day as compared to an untreated group of dogs¹⁶. CQ Stem extract has soaring calcium and phosphorous. Extract of this plant is proved to be useful for bone fracture healing¹⁷. The effective constituents of CQ may encourage proliferation and differentiation of MSCs into osteoblasts and bone formation via wnt-LRp5- β -catenin or MAPK dependent pathway¹⁸. The results showed that PCL-CQ-HA nano-fibrous scaffolds have appropriate surface roughness for the osteoblast adhesion, proliferation, and mineralization comparing with other scaffolds which makes them potentially biocompatible material for bone tissue engineering¹⁹. CQ fast-tracks fracture healing and also stimulate early bone remodelling. A plant based steroid is supposed to be the key component in CQ. It has been observed that CQ acts by stimulation of metabolism like the increased expression of osteopontin and increased uptake of the minerals calcium, sulphur, and strontium by the osteoblasts in fracture healing²⁰.

Here, porous PCL electrospun sheets were modified with GO/GP and CQ using the layer-by-layer method. Also, the ink of GO, GP and CQ callus culture extract and their respective combinations were prepared. Porous PCL electrospun sheets were modified with GO/GP and CQ ink by paint method. The paint method is novel and unique, similar to artwork painting. These composite scaffolds were characterized and studied for bone tissue engineering.

4.2 Materials and Methods:

4.2.1 Materials:

PCL (average Mol. Wt. 80000 gmol⁻¹), GP, GO (GO and GP prepared by Modified Hummer's method were supplied by Sachin Kochrekar, Department of Chemistry, Defence Institute of Advanced Technology, Girinagar, Pune), CQ plant, MS medium No.6, NAA (α -Naphthalene acetic acid), BAP (6-Benzylaminopurine), sucrose, Agar, 70% ethanol, 0.01% Hypo chloride (HgCl₂) solution (Himedia), Collagenase type IV, Dispase II, phosphate buffer saline (PBS), Trypsin (0.05% and) EDTA (0.02%) (Sigma Aldrich), Dulbecco's Modified Eagle's Medium (DMEM), Ham's F12 (DMEM: HF12, 1:1), (Invitrogen), Penicillin, streptomycin, human umbilical cord blood serum, (Sigma Aldrich).

4.2.2 Methods:

4.2.2.1 *Cissus quadrangularis* Callus Culture:

Plant callus is nothing but a mass of unorganised plant parenchyma cells made from structural tissue and not from individual cells. These cell mass can also be considered as stem cell pull of plant as they give rise to shoot or root of plant depending on their growth medium.

4.2.2.1.1 Cleaning of Glassware:

All the glasswares were cleaned using mild anionic detergent and dried in the oven. These glasswares were sterilized by autoclaving at 15 lbs/in², 121⁰ C for 20 min.

4.2.2.1.2 Preparation of Media:

The stocks of α -Naphthalene acetic acid (NAA) (1 mg/mL) and 6-Benzylaminopurine (BAP) (1 mg/mL) were prepared and stored at 4⁰ C in freeze and used for medium preparation. For preparation of callus induction medium, MS medium No.6 (2.26 g/l), NAA 2.5 mg/l, BAP 0.5 mg/l, sucrose 40 g/l, Agar 10 g/l were used. The pH of the medium was adjusted to 5.7 and then the agar was added to the medium. The medium was warmed to liquefy the agar. Medium distributed in test tubes and plugged with cotton. Medium was autoclaved at 15 lbs/inch², 125⁰C for 20 min. After autoclaving tubes were kept in slanting position & allow cooling and solidifying.

4.2.2.1.3 Explant sterilization:

The CQ plant was identified and confirmed in the surrounding region of Kolhapur, Maharashtra, India. The stem parts of the plant were isolated. Petioles were separated from stems. The stem of plant washed for 10 min in running tap water. The stem of fresh plant surface was sterilized by 70% ethanol (v/v) for 5 min. Stem explants immersed in 0.01% HgCl₂ (mercuric chloride) solution for 1.5 & 3 min. respectively. After that, these stem explants washed 5 times with distilled water. Stems cut into 10-13 mm pieces.

4.2.2.1.4 Inoculation of Explants:

These surface sterilized explants inoculated into the centre of media containing tubes with the help of sterilized forceps. The culture tubes or bottles mouth flame sterilized before and after inoculation of explants. Test tubes were plugged with cotton.

4.2.2.1.5 Culture of Explants:

The culture tubes stored at air-conditioned culture room at temp 28⁰C, 60% humidity and kept in dark. These cultures were observed on daily basis for callus formation. The contaminated culture tubes were immediately discarded. Further, all the precautionary measures were taken to avoid any contamination.

4.2.2.1.6 CQ callus powder extraction:

The fully grown callus from the 4-5 weeks grown culture was selected and dehydrated, dried and fine powder was made. The crude extract was prepared by using a Soxhlet apparatus with ethanol. The obtained extract again was partitioned with petroleum ether and the pure form of the extract was prepared.

4.2.2.1.7 Salkowski test:

The finally prepared pure callus extract was tested by Salkowski test to determine the presence of phytosterol, the main component responsible for the osteoinductive property. A small quantity of extract dissolved in 1mL of chloroform. Few drops of concentrated Sulphuric acid were added along the walls of the test tube. Formation of the brown ring at the bottom of the test tube indicates the presence of Phytosterol.

4.2.2.2 Preparation of scaffolds by electrospinning:

PCL solution (10% w/v) was prepared by 30 hours of magnetic stirring in the THF (Tetrahydrofuran): Methanol (3:1). The PCL scaffold sheets were fabricated by electrospinning with parameters of flow rate of 0.8 mL/h, voltage 12kv and 12.5 cm distance. The GO solutions (1 mg/mL), GP solutions (1 mg/mL), and CQ solution (1 mg/mL) were prepared by dispersing/dissolving in distilled water and sonication.

The ink of GO (1 mg/mL), GP (1 mg/mL), and CQ (1 mg/mL) were prepared by dispersing/dissolving components in distilled water and sonication then after. The GO-CQ and GP-CQ ink (1:1v/v) were also prepared.

4.2.2.3 Modification of scaffolds using layer by layer method:

The PCL scaffold sheets fabricated by electrospinning used for further surface modification of scaffolds. Preparation of PCL-GO, PCL-GO-CQ, PCL- GP, PCL- GP-CQ scaffolds were carried out by repetitive dipping of 2 minutes and air drying of these sheets for multiple cycles as 30, 60 cycles and overnight dipping. There is an alternative layer of GP and CQ deposited on the PCL-GP-CQ scaffolds. There is an alternative layer of GO and CQ deposited on the PCL-GO-CQ scaffolds. While there is a single layer of GP on the PCL-GP scaffolds and of GO on the PCL-GO scaffolds. The leaching of the additives (GO and GP) from the scaffolds was investigated as per ISO-10994-12. Experiments were performed in batch mode as incubated with extractants. The 0.1 g of scaffolds per 1 mL of distilled water was incubated at 37 °C for 72 hrs. The concentration of GO and GP in the obtained extracts was determined by measuring the absorbance at 233 nm and 263 nm for GO and GP respectively, using a UV-visible spectrophotometer. The standard calibration curve of GO and GP were also plotted to calculate their respective concentrations. Ultraviolet-visible (UV-Vis) absorption spectra were recorded using a 1cm path length quartz cuvette with distilled water as the reference on a U-2001 UV/Vis Spectrophotometer (Hitachi). Depending on the binding of these substrates scaffolds were selected for further study.

The leaching (Figure 4.2) is least in the overnight dipped samples then followed by 60 cycles. Leaching is higher as compared to 30 cycles. This could be due to more interaction between PCL and GO or GP in the 60 dipped cycles. In the overnight dipped samples, the deposition was not uniform. Therefore, we are choosing 60 cycles over 30 cycles and overnight dipped samples as because of more uniform deposition as well as less leaching. The leaching study is not significant as there is very small amount of GP/GO in the leached solution.

4.2.2.4 Modification of Scaffolds by Paint method:

The surface of PCL scaffold sheets fabricated by electrospinning was modified using yet another method to compare the best surface modification technique. Preparation of PCL-GO, PCL-GO-CQ, PCL-GP, PCL-GP-CQ scaffolds were carried out by a respective painting of the ink. The ink was simply single painted by acrylic painting brush (flat, midsize) with hands. After painting, these were allowed to dry at room temperature. The leaching study carried out for adhesion of GO and GP in painted scaffolds similar to layer by layer scaffolds. The leaching study (Figure 4.3) shows a small amount of GP leached from PCL-GP and PCL-GP-CQ scaffolds. There is a small amount of GO leaching from PCL-GO and PCL-GO-CQ scaffolds. The leaching study is not significant as there is a very small amount of GP, GO in the leached solution.

4.2.2.5 Characterization of Scaffolds:

The prepared scaffolds were characterized for morphological, chemical, physical, mechanical and biological properties.

4.2.2.5.1 Morphological analysis:

The morphologies of the electrospun pure polymeric and composite scaffolds were examined by field emission scanning electron microscope (FESEM, Carl Zeiss, Germany) at an accelerating voltage of 15 kV. For FESEM, the samples were cut into 5X5 mm squares, mounted on to sample stubs; sputter coated with gold/palladium using an SC 7640 Sputter Coater (Quorum Technologies Ltd, UK). The coated GO were analysed on the electrospun fibres of PCL. The pore size and fibre diameter range of the scaffolds were calculated from the FESEM micrographs using image analysis software (ImageJ, National Institutes of Health, Bethesda, USA).

Surface properties of the modified PCL surface sheets were analysed by atomic force microscopy (AFM, Asylum Research) by tapping mode. The scaffolds were cut into small pieces and stuck on a glass slide by cellophane tape. The scan rate of 1.0 Hz and a scan area of 10µm were used for imaging.

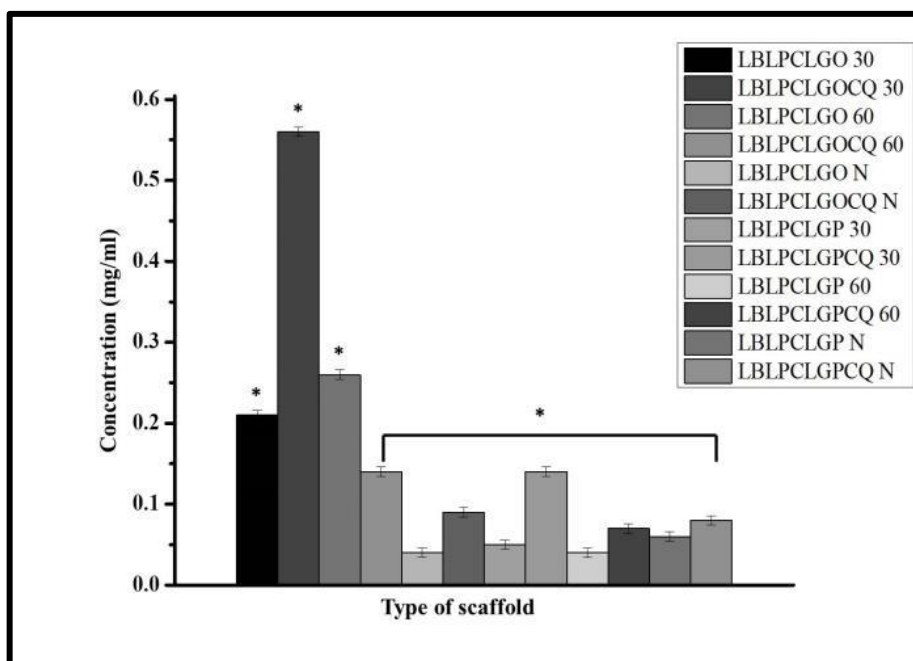


Figure 4.2: Leaching study of Layer by layer scaffolds (*p< 0.05)

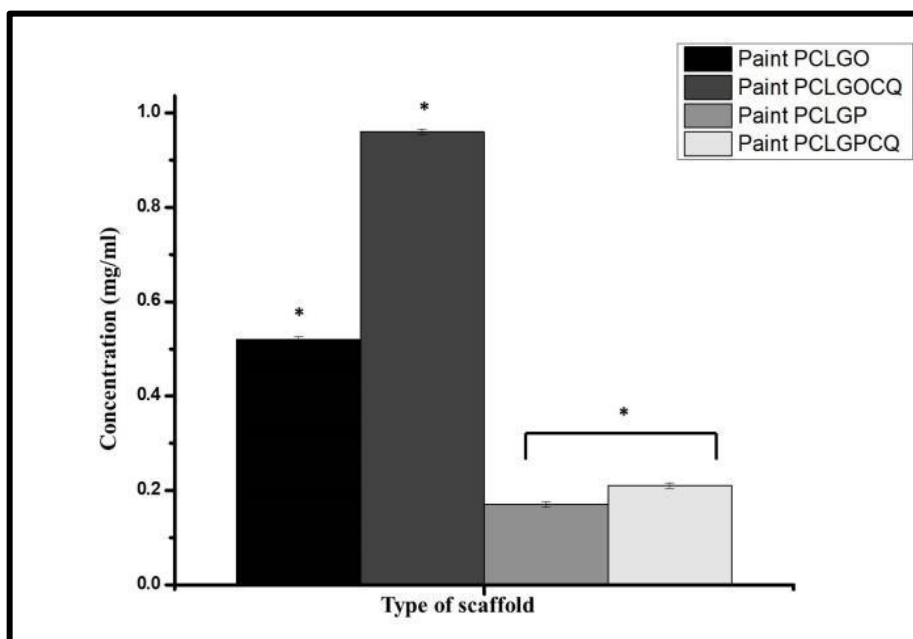


Figure 4.3: Leaching study of Paint scaffolds (*p< 0.05)

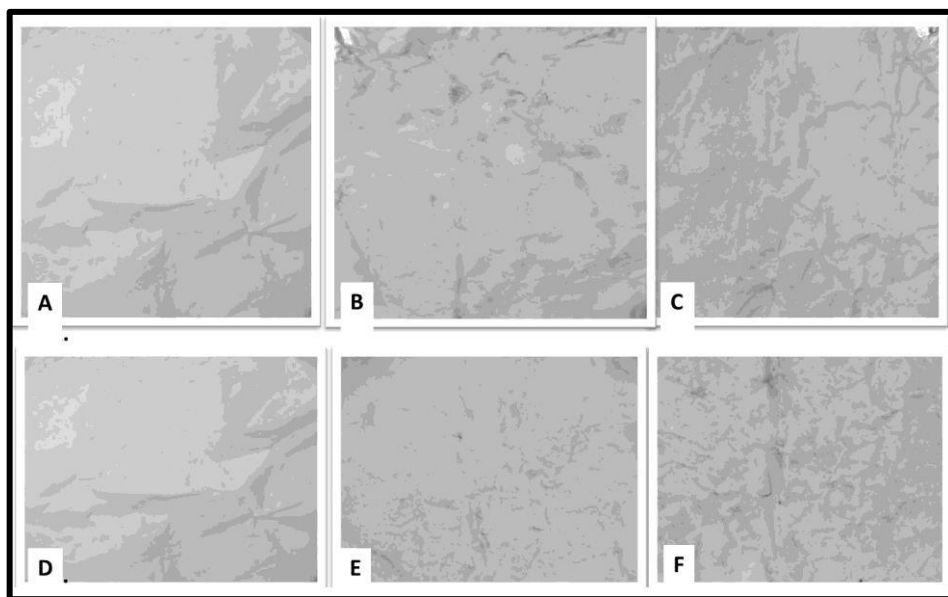


Figure 4.4 Layer by layer scaffolds. A. PCL; B: PCL-GP; C: PCL-GP-CQ; D. PCL; E: PCL-GO; F: PCL-GO-CQ

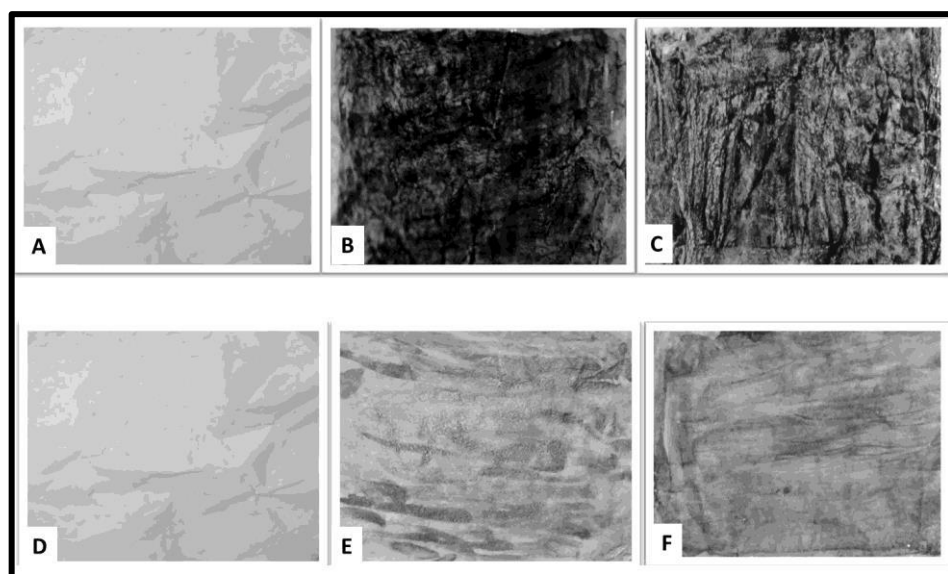


Figure 4.5 Paint scaffolds. A. PCL; B: PCL-GP; C: PCL-GP-CQ; D. PCL; E: PCL-GO; F: PCL-GO-CQ

4.2.2.5.2 Physical analysis:

FTIR spectra were recorded for all scaffolds (FTIR, Bruker, Germany). The spectra were obtained with 30 scans per sample ranging from 4000 to 500 cm^{-1} .

The TGA of scaffolds was studied with a thermogravimetric analyser (Universal V4.7A TA Instrument) instrument under the nitrogen atmosphere in the temperature range from 30°C to 800°C at a heating rate of 10°C/min.

4.2.2.5.3 Wetting properties:

The water contact angle was determined by sessile drop method and Drop shape image analysis using water as droplet with contact angle goniometer (KRUSS, Germany). Contact angle measurement of liquid droplets on a solid substrate (n=3) was used to characterize surface wettability, surface cleanliness and the hydrophilic/hydrophobic nature of the surface.

4.2.2.5.4 Mechanical Properties:

Tensile properties were calculated at room temperature with a UTM (STS 248, Star Testing Systems, India). Scaffold cut into cylinders (n=3) were tested. The loading was 100 N (maximum loading) and the crosshead speed (strain rate) was 5mm/min. From the resulting stress-strain curves, yield strength and tensile strength were calculated^{19,21,22}.

4.2.2.6 Isolation and Culture of hUCMSCs:

4.2.2.6.1 Collection of Human umbilical cords (HUCs):

The human umbilical cords were collected from caesarean deliveries with patient consent. The collected cord was stored in the L15 medium and transported to the lab. Collected HUCs were washed with PBS to remove cord blood and blood clots and surface disinfection was carried out using 10% betadine solution for 5 minutes. These cleaned cords were used to isolate human umbilical cord Wharton's Jelly mesenchymal stem cells (hUCMSCs).

4.2.2.6.2 Isolation and expansion of hUCMSCs:

In culture lab under strict sterilization, blood vessels were removed from cleaned cords and cords were chopped into pieces of 1-2 mm length using sterile surgical blade. The chopped cord tissue was digested with a mixture of enzymes Collagenase Type IV and Dispase II (7:1v/v) for 30 min at 400 rpm and 37°C on the magnetic orbital shaker.

Similarly the tissue was incubated with Trypsin (0.05%)-EDTA (0.02%) for 20 minutes. The homogenate was then filtered using a sterile muslin cloth and centrifuged at 1500 rpm for 10 minutes to isolate pellet. Then this pellet containing cells were washed and cultured in the Dulbecco's Modified Eagle's Medium (DMEM), Ham's F12 (DMEM: HF12, 1:1) medium supplemented with 10% serum and penicillin (100 units/mL) and streptomycin (100 µg/mL). The cells were incubated for 48 hours at 37°C, 5% CO₂. The medium was changed after every 48 hrs and the first passage was carried out after 8 days and then after every 4 days. The isolated hUCMSCs were cryopreserved using 10% DMSO with standard protocol²³.

4.2.2.7 *In Vitro* Studies:

4.2.2.7.1 Cell Seeding

Scaffolds were cut appropriately to fit in 48 well plate. These scaffolds were washed with PBS thrice and then sterilized by ethylene oxide (EtO). The T 75 culture flasks of 80-90 % confluent with hUCMSCs were taken, medium removed and cells were trypsinized. The 2mL of DMEM was added to each flask and 100µl of this suspension taken for cell count. The 1.0×10^4 cells/mL were seeded into each well. Cell suspension kept on scaffolds centrally. These cell seeded plates incubated for 2 hrs at 37 °C, 5% CO₂ for good cell attachment. After this incubation, DMEM medium was added to each well and incubated these plates at 37°C, 5% CO₂. According to the kind of cell study, cell-seeded scaffolds were incubated for 1, 4 and 7 days for cell attachment, cytotoxicity and proliferation studies.

4.2.2.7.2 MTT Cell Viability and Proliferation Assay:

MTT (3-(4, 5-dimethylthiazol-2yl)-2, 5-diphenyltetrazolium bromide) is prepared in DMEM at the final concentration of 5mg/mL (pH=7.4), filter sterilized through 0.2 µM filter in to sterile, light-protected container. 50 µl MTT solutions were added into each well-containing cells seeded scaffolds. Dimethyl sulfoxide (DMSO) was added to each well after incubation of 3 hrs, to dissipate formazan crystals. The quantity of a purple coloured formazan, formed from tetrazolium reduction is directly proportional to metabolically active viable cells. The absorbance was measured at 570 nm using a plate

reader spectrophotometer. Reference was set at 650 nm²⁴. The same procedure was followed for 4th and 7th day.

4.2.2.7.3 Cell Attachment Study:

Cell-seeded scaffolds incubated for 24 hours were taken out from the incubator at respective time intervals and aspirated the medium from plates, washed two times with PBS. Cells were fixed on scaffolds with 4% paraformaldehyde. Plates were kept in freeze and then analysed with FESEM.

4.2.2.7.4 Confocal Microscopy Imaging:

Cell-seeded scaffolds incubated for 1, 4 and 7 days were also fixed with 4% paraformaldehyde and cells were permeabilized using permeabilization buffer. Cell-seeded scaffolds then stained with DAPI for nuclear visualization. Slides were mounted on mounting media and images were taken with a confocal microscope (Zeiss, Germany). The images were analysed with Zen Software (Zeiss).

4.2.2.7.5 Osteoblastic Differentiation:

4.2.2.7.5.1 Alizarin Red S staining for calcium:

The calcium deposition was analysed by Alizarin Red S staining. The specimens were prepared by fixing the cells with 10% formalin. The 2% Alizarin Red S stain (pH 4.2) was added enough to cover cell monolayer and incubated at room temperature for 45 minutes at dark. After this, the scaffolds were cleansed with PBS. The samples were observed by using Inverted Phase contrast microscope equipped with a digital camera. These scaffolds quantified using a solution of 10% acetic acid. After 30 min incubation with acetic acid, the scaffolds were placed into a microcentrifuge tube, heated at 85 °C for 10 min, cooled, and centrifuged at 10,000g for 15 min; 500 µl of the above solution was taken and neutralized with 10% ammonium hydroxide. The 150 µl of this solution was transferred to a 96 well plate and the quantity of Alizarin Red S was determined by measuring absorbance at 405 nm²⁵⁻²⁷.

4.2.2.7.5.2 Von Kossa staining for calcium:

The scaffolds also evaluated for calcium deposition by using Von Kossa staining. The samples were fixed by 10% formalin and then 1mL of 5% silver nitrate (AgNO_3) solution used to stain the samples at room temperature for 60 min. in UV light. The stain was removed and the samples were visualized under Inverted phase contrast microscope and images were taken.

4.3 Statistical analysis:

Statistical analysis of all data was performed using the Origin Pro 8.5 software. Data are presented as the Mean \pm standard deviation. Statistical significance was assessed by student's t-test. ($P \leq 0.05$ *; $P \leq 0.005$ **)

References:

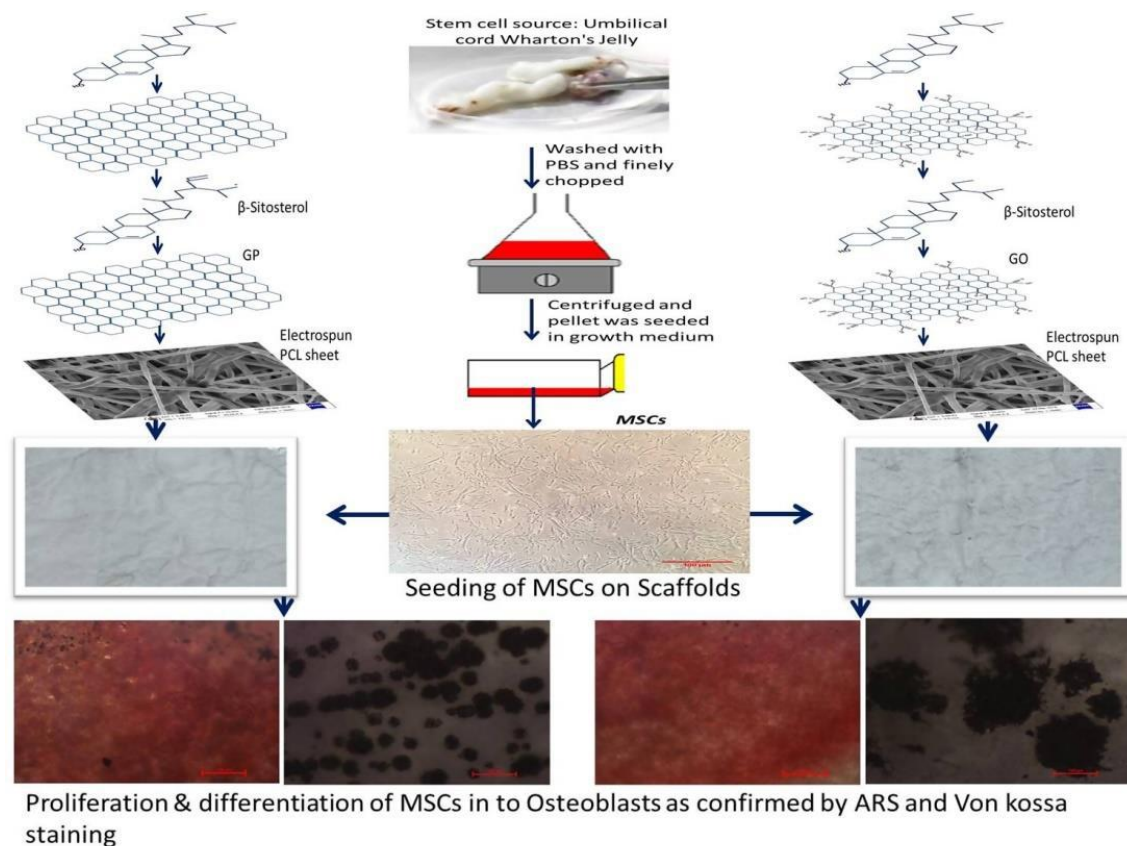
- 1 A. Alves, A. R. C. Duarte, J. F. Mano, R. A. Sousa and R. L. Reis, *J. Supercrit. Fluids*, 2012, **65**, 32–38.
- 2 I. Rajzer, E. Menaszek, R. Kwiatkowski and W. Chrzanowski, *J. Mater. Sci. Mater. Med.*, 2014, **25**, 1239–1247.
- 3 X. Liu and P. Ma, *Ann. Biomed. Eng.*, 2004, **32**, 477–486.
- 4 J. Qian, W. Xu, X. Yong, X. Jin and W. Zhang, *Mater. Sci. Eng. C. Mater. Biol. Appl.*, 2014, **36**, 95–101.
- 5 S. Kashte, A. K. Jaiswal and S. Kadam, *Tissue Eng. Regen. Med.*, 2017, **14**, 1–14.
- 6 B. Chuenjitkuntaworn, T. Osathanon, N. Nowwarote, P. Supaphol and P. Pavasant, *J Biomed Mater Res Part A*, 2015, **104**, 264–271.
- 7 K. Ren, Y. Wang, T. Sun, W. Yue and H. Zhang, *Mater. Sci. Eng. C*, 2017, **78**, 324–332.
- 8 V. Y. Chakrapani, T. S. S. Kumar, D. K. Raj and T. V Kumary, *J. Nanosci. Nanotechnol.*, 2017, **17**, 2320–2328.
- 9 Y. J. Son, H. S. Kim and H. S. Yoo, *RSC Adv.*, 2016, **6**, 114061–114068.
- 10 W. M. Gallagher, I. Lynch, L. T. Allen, I. Miller, S. C. Penney, D. P. O'Connor, S. Pennington, A. K. Keenan and K. A. Dawson, *Biomaterials*, 2006, **27**, 5871–5882.
- 11 S. Yang, K. F. Leong, Z. Du and C. K. Chua, *Tissue Eng.*, 2001, **7**, 679–689.
- 12 W. Chen and T. J. McCarthy, *Macromolecules*, 1997, **9297**, 78–86.
- 13 Y. Li, M. C. Choi, K. M. Jeong, J. H. Jeong, H. G. Lee, G. H. Kim and C. S. Ha, *Macromol. Res.*, 2017, **25**, 496–499.
- 14 X. He, L. L. Wu, J. J. Wang, T. Zhang, H. Sun and N. Shuai, *High Perform. Polym.*, 2015, **27**, 318–325.

- 15 G. Mishra, S. Srivastava and B. P. Nagori, *Int. J. PharmTech Res.*, 2010, **2**, 1298–1310.
- 16 D. K. Deka, L. C. Lahon, A. Saikia and Mukit, *Indian J Pharmacol*, 1994, **26**, 44–45.
- 17 M. S. Rao, P. Bhagath Kumar, V. B. Narayana Swamy and N. Gopalan Kutty, *Pharmacologyonline*, 2007, **3**, 190–202.
- 18 B. K. Potu, M. S. Rao, N. G. Kutty, K. M. R. Bhat, M. R. Chamallamudi and S. R. Nayak, *Clinics (Sao Paulo)*., 2008, **63**, 815–820.
- 19 S. Suganya, J. Venugopal, S. Ramakrishna, B. S. Lakshmi and V. R. Giri Dev, *J. Appl. Polym. Sci.*, 2014, **131**, 1–11.
- 20 N. Singh, V. Singh, R. Singh, A. Pant, U. Pal, L. Malkunje and G. Mehta, *Natl. J. Maxillofac. Surg.*, 2013, **4**, 52–56.
- 21 K. Parvathi, A. G. Krishnan, A. Anitha, R. Jayakumar and M. B. Nair, *Int. J. Biol. Macromol.*, 2018, **110**, 514–521.
- 22 T. Zhou, G. Li, S. Lin, T. Tian, Q. Ma, Q. Zhang, S. Shi, C. Xue, W. Ma, X. Cai and Y. Lin, *ACS Appl. Mater. Interfaces*, 2017, **9**, 42589–42600.
- 23 S. Kadam and R. Bhonde, *Islets*, 2010, **2**, 112–120.
- 24 A. K. Jaiswal, S. S. Kadam, V. P. Soni and J. R. Bellare, *Appl. Surf. Sci.*, 2013, **268**, 477–488.
- 25 N. Thadavirul, P. Pavasant and P. Supaphol, *Macromol. Mater. Eng.*, 2017, **302**, 1–17.
- 26 K.-Y. Tsai, H.-Y. Lin, Y.-W. Chen, C.-Y. Lin, T.-T. Hsu and C.-T. Kao, *Materials (Basel)*., 2017, **10**, 65–72.
- 27 H. Chhabra, J. Kumbhar, J. Rajwade and S. Jadhav, *J. Bioact. Compat. Polym.*, 2016, **31**, 273–290.

CHAPTER 5:

LAYER BY LAYER

SCAFFOLDS



5.1 Introduction:

Bone is the second utmost transplanted tissue following blood¹. The bone tissue engineering has become one of the mainstream researches in the regeneration, repair or restructuring of bone tissues. A plethora of research methodologies have been bourgeoned with biomaterials and their applications in the field of tissue engineering and regenerative medicine. The various polymers like poly ϵ -caprolactone (PCL), poly-d, l-lactic acid (PDLA)², poly (L/DL-lactide) (PLDL)³, PLLA⁴, poly (DL-lactic-co-glycolic acid) (PLGA)⁵ have showed to be potential with its mechanical properties like tensile strength, elastic modulus, biocompatible, higher cellular properties and even bone formation in rat model¹. The PCL is biocompatible, biodegradable and FDA approved material and used extensively in tissue engineering applications. PCL along with Hydroxyapatite (HA)⁶, PCL-gelatin hybrid nanofibrous membranes⁷, PCL-(Poly-1,4- butylene adipate-co-polycaprolactam (PBAPCL)-HA composite scaffold⁸, are used in bone tissue engineering.

Easily electrospinnable synthetic polymers are primarily hydrophobic such as PCL, PLA, etc. For application in tissue engineering, the hydrophobicity of the nanofibrous mesh should be modified to be partly hydrophilic. An introducing hydrophilic property to hydrophobic nanofibers has been attempted in various ways by Surface modification, e.g. flame treatment, corona discharge treatment, plasma modification, and surface graft polymerization⁹. Surface modification is an important aspect in the field of tissue engineering to cell attachment and cell proliferation. The surface modification also helps in the improvement of biological properties of scaffolds. The interaction between tissue and foreign surface largely depends upon surface properties of materials such as wettability, roughness or topography, surface charge and chemistry^{10,11}.

A layer-by-layer method is a simple, relatively fast, environmentally benign, and potentially economic process¹² to prepare uniform multilayer films on substrates from solution. It is fast and irreversible deposition, easy to control of the deposited film thickness and uniform surface coverage¹³. The poly (ethylene terephthalate) (PET) is modified with poly (allylamine hydrochloride) by layer by layer deposition. It significantly improved wettability and mechanical strength of the PET films¹². An electrospun PCL-poly (ethyleneimine) (PEI) block copolymer is modified by poly (ethylene glycol) (PEG) to transform original hydrophobic mesh to hydrophilic mesh

using layer by layer method. There is an improvement in cell viability and cell attachment of epidermal cells⁹. The PLA-PEI films are also modified with GO¹⁴. The polyamic acid (PAA)-PEI-GO films are prepared by layer by layer method¹³.

The carbon materials are considered to be a similar physical analogue of extracellular matrix (ECM) like that of collagen fibers¹. The graphene oxide (GO) and graphene (GP) has become the biomaterial of the 21st century as being potential of applications in electronics to biomedical applications and tissue engineering. The extravagant mechanical properties, biocompatibility and osteoinductive properties of GO/GP would make them one of the most foreseen biomaterials in the regenerative medicine in coming years.

The medicinal properties of the *Cissus quadrangularis* (CQ) plant have been described in the ancient book Bhawa Prakash. The plant has immense medicinal potential with reported antimicrobial and antioxidant activity¹⁵. Methanolic extract of CQ has revealed the faster bone healing in the experimentally fractured radius-ulna of the dog as well as complete bone healing on the 21st day as compared to an untreated group of dogs¹⁶. CQ Stem extract has soaring calcium and phosphorous. Extract of this plant is proved to be useful for bone fracture healing¹⁷. The active constituents of CQ may promote proliferation and differentiation of MSCs into osteoblasts and bone formation via wnt-LRp5- β -catenin or MAPK dependent pathway¹⁸. The results show that PCL-CQ-HA nano-fibrous scaffolds have appropriate surface roughness for the osteoblast adhesion, proliferation, and mineralization comparing with other scaffolds, making them potential biocompatible material for bone tissue engineering¹⁹. CQ fast-tracks fracture healing and also stimulate early bone remodelling. A plant-based steroid is supposed to be the key component in CQ. It has been observed that CQ acts by stimulation of metabolism like an increased expression of osteopontin and increased uptake of the minerals calcium, sulphur, and strontium by the osteoblasts in fracture healing²⁰.

Here, porous PCL electrospun sheets are modified with GO or GP and CQ by a layer-by-layer method. These composite scaffolds are characterized and studied for bone tissue engineering.

5.2 Results and Discussion:

5.2.1 CQ callus culture and powder extraction:

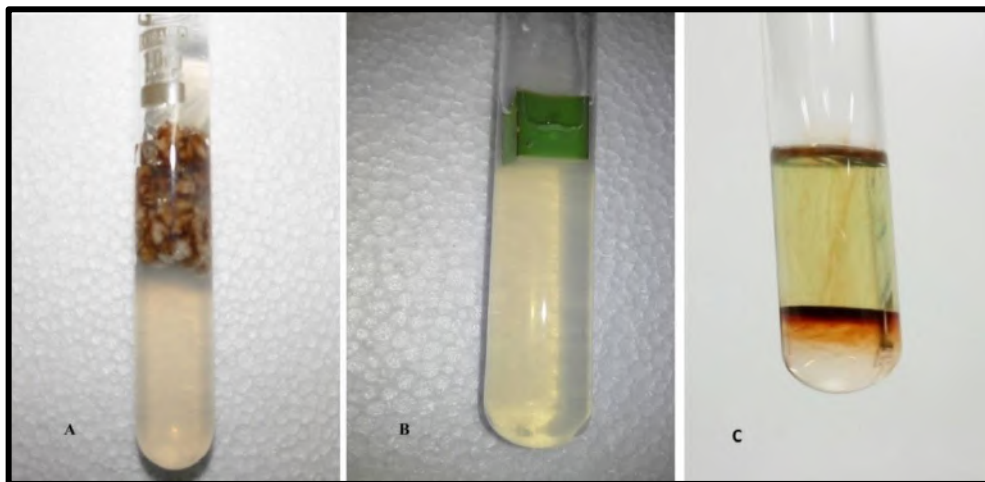


Figure 5.1: CQ callus culture. A: Callus formed from CQ stem explant; B: Control CQ stem explant; C: Salwoski test. The brown ring formed at the bottom of the test tube confirms the presence of phytosterols in the callus extract.

The brown coloured callus is observed after the 4 weeks of culture (Figure 5.1: A)^{21,22}. The extracted CQ callus extract shows the presence of Phytosterol, is confirmed by the formation of the brown ring at the bottom of test tube as indicated in Salkowski test (Figure 5.1: C), similar to shown elsewhere¹⁹. The Phytosterols are osteoinductive in nature¹⁹. These phytosterols stimulate increased expression of osteopontin and increased uptake of the minerals such as calcium, sulphur, by the osteoblasts in fracture healing, acting as the main component in bone regeneration²⁰.

5.2.2 Preparation and Characterization of Scaffolds:

5.2.2.1 Morphological analysis:

The SEM analysis is performed for the morphological analysis of the electrospun PCL and LBL composite scaffolds. SEM images (Figure 5.2) shows the electrospun PCL scaffolds with smooth fibre structures while that of LBL scaffolds are decorated with the GP-CQ and GO-CQ are rough in nature. The fibre diameter (Table 5.1) is increased in the PCL-GO and PCL-GP scaffolds as compared to PCL scaffolds. The Fibre diameter is

significantly increased in the PCL-GO-CQ scaffolds. The GO layers on the PCL-GO, PCL-GO-CQ and GP layers on the PCL-GP, PCL-GP-CQ scaffolds are randomly distributed throughout the PCL sheet. The enhanced rough surface and fiber diameter is helpful for protein adhesion, cell adhesion and cell proliferation¹⁹.

Surface properties of the PCL and surface modified PCL sheets are analysed by atomic force microscopy (AFM) by tapping mode. The AFM images (Figure 5.3) reveals the rough surface of the scaffolds. The root mean square roughness (RMS) values are PCL (146 ± 10 nm), PCL-GO (222 ± 8 nm), PCL-GO-CQ (341 ± 9 nm), PCL-GP (270 ± 10 nm) and PCL-GP-CQ (278 ± 11 nm). The modified scaffolds PCL-GO and PCL-GP are rough as compared to the PCL scaffold. The PCL-GO-CQ scaffolds show highest roughness as compared to other scaffolds.

The rough surface is beneficial in cell attachment and proliferation. Surface roughness affects the adsorption of fibronectin and albumin *in vitro*²³ and promotes cell attachment and adhesion on the surfaces of composites and osteoblast proliferation, differentiation and matrix synthesis and local factor production²⁴. Surface roughness has a positive effect on bioactivity, water uptake and cytocompatibility of the composites²⁵. The similar results are analysed by other researchers. The coating of polyethyleneimine-GO on PLA films have showed rough, uneven, mountain-like topography compared to uncoated PLA films¹⁴. The GO films on Si/SiO₂ have showed nanoripples with high density²⁶.

5.2.2.2 Physical analysis:

The FTIR spectra (Figure 5.4) show the presence of PCL, GO, GP and CQ in the respected scaffolds. Distinctive absorption peaks of asymmetric CH₂ stretching at 2926 cm^{-1} and symmetric CH₂ stretching at 2860 cm^{-1} , C=O/carbonyl stretching at 1720 cm^{-1} , C-O and C-C stretching at 1293 cm^{-1} , asymmetric C-O-C stretching at 1240 cm^{-1} are for PCL. Carboxylic C=O bend at 1719 cm^{-1} , C=C bend at 1569 cm^{-1} , C-O bend at 1220 cm^{-1} for GO, C-C stretching at 1576 cm^{-1} , C-OH stretching at 1365 cm^{-1} , alkoxy C-O stretching at 1150 cm^{-1} and 1069 cm^{-1} for GP. Alkane asymmetric C-H stretching at 2920 cm^{-1} , alkane symmetric C-H stretching at 2847 cm^{-1} , C=O stretching at 1708 cm^{-1} and

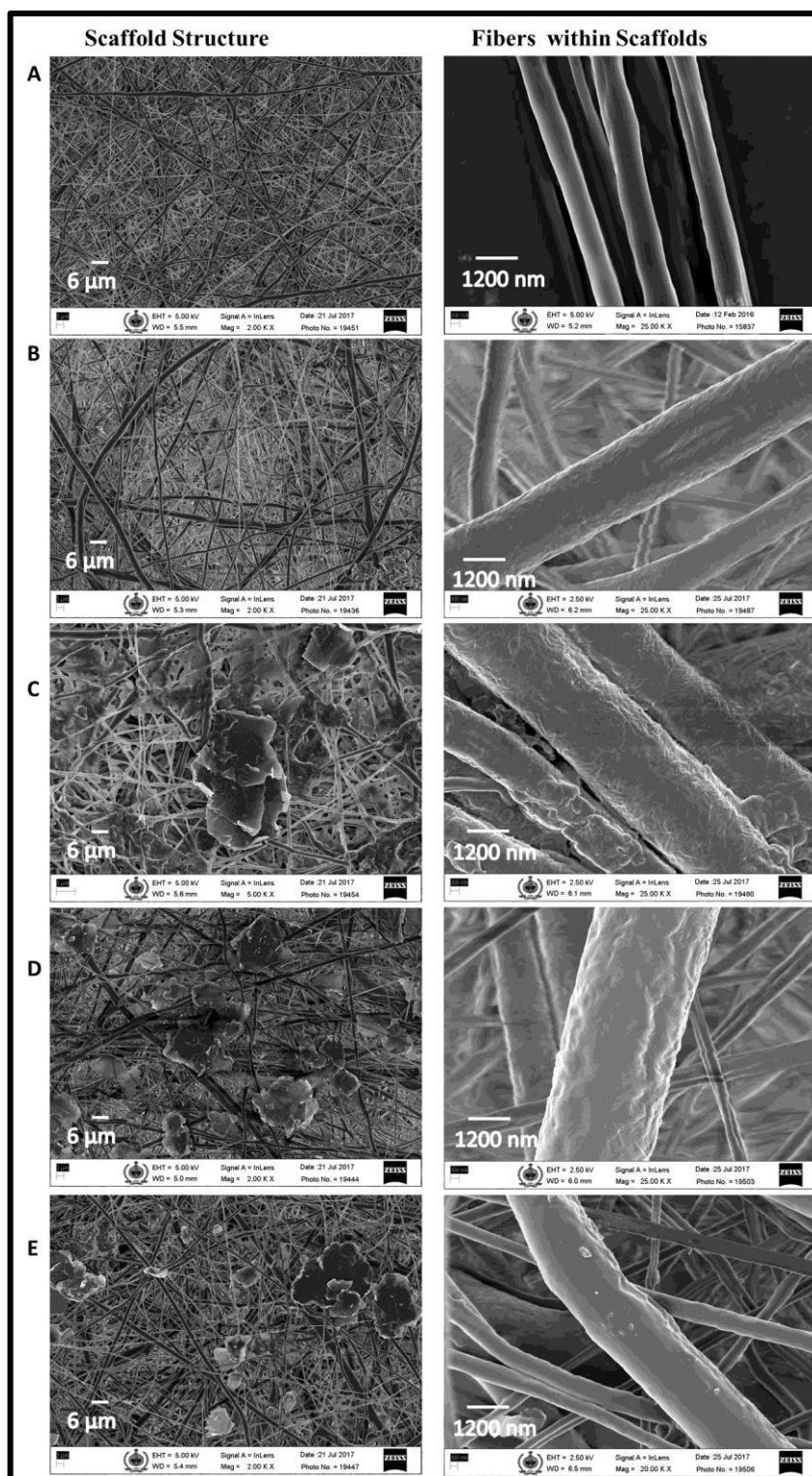


Figure 5.2: Field emission scanning electron microscope (FESEM) images. A: PCL; B: PCL-GO; C: PCL-GO-CQ; D: PCL-GP; E: PCL-GP-CQ; Scale bar 3μm& 300nm

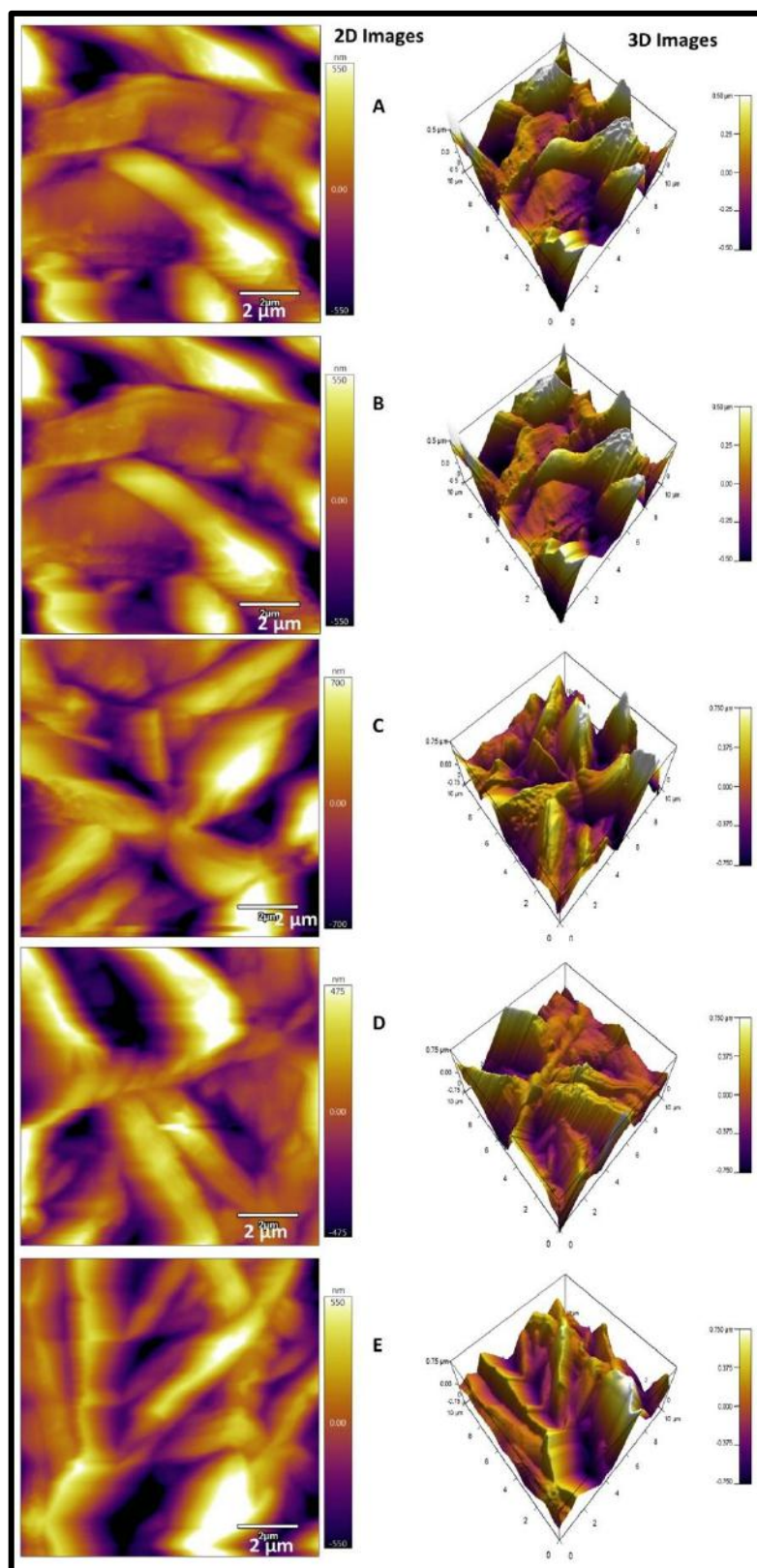


Figure 5.3: Atomic force microscopy (AFM) 2D and 3D images. A: PCL; B: PCL-GO; C: PCL-GO-CQ; D: PCL-GP; E: PCL-GP-CQ; Scale bar 2μm

1459 cm^{-1} , Alkane C-H bending at 1377 cm^{-1} and 1163 cm^{-1} , C-N stretching at 1150 cm^{-1} -1000 cm^{-1} , C=S stretching at 1032 cm^{-1} for CQ.

The FTIR spectra (Figure 5.4) confirm the interaction of PCL with GP, GO and CQ in the respective scaffolds. In the composite scaffolds there are many overlapping peaks observed between PCL, GP, GO and CQ, therefore could not be clearly differentiated. However, integrating and or broadening of peaks confirm the presence of these multiple components. Similar kind of results obtained elsewhere^{19,27}.

Thermal degradation of scaffolds (Figure 5.5) is studied by determining the weight loss of sample with increasing temperature. The PCL scaffold displays one main degradation at 433 $^{\circ}\text{C}$ (88 % weight loss) and 487 $^{\circ}\text{C}$ (10 % weight loss) with 2% residue ; PCL-GO: 431 $^{\circ}\text{C}$ (88 % weight loss) and 526 $^{\circ}\text{C}$ (12 % weight loss) with complete degradation; PCL-GO-CQ: 431 $^{\circ}\text{C}$ (87 % weight loss) and 586 $^{\circ}\text{C}$ (13 % weight loss) with complete degradation; PCL-GP: 430 $^{\circ}\text{C}$ (76 % weight loss) and 578 $^{\circ}\text{C}$ (13 % weight loss) with 11% residue; PCL-GP-CQ: 429 $^{\circ}\text{C}$ (84 % weight loss) and 505 $^{\circ}\text{C}$ (15 % weight loss) with 1% residue. There is complete degradation of PCL-GO and PCL-GO-CQ scaffolds. It could be due to pyrolysis of liable oxygen-containing groups in GO, or phytosterols. The similar results are found in GO incorporated PLGA scaffolds²⁸, PCL scaffolds²⁹. The incorporation of polyethyleneimine-GO into PLA films they are majorly degraded¹⁴. There is residue remaining in PCL-GP, PCL-GP-CQ scaffolds. It could be due to GP has lower activation energies for oxidation. The amorphous carbon is likely to to be oxidized at around 500 $^{\circ}\text{C}$ ³⁰. Also fluctuations in the degradation temperature could occur due to different heating rates³¹.

5.2.2.3 Wetting properties:

The water contact angles of PCL and modified PCL-GO, PCL-GO-CQ and PCL-GP, PCL-GP-CQ are shown in Figure 5.6 and Table 5.2. The plain PCL scaffolds are hydrophobic while LBL modified scaffolds PCL-GP, PCL-GP-CQ, PCL-GO, and PCL-GO-CQ are hydrophilic in nature. The PCL-GO-CQ scaffolds show the lowest water contact angle and the highest hydrophilicity. The incorporation of GO, GP and CQ into the respective scaffolds have increased the hydrophilicity of the scaffolds.

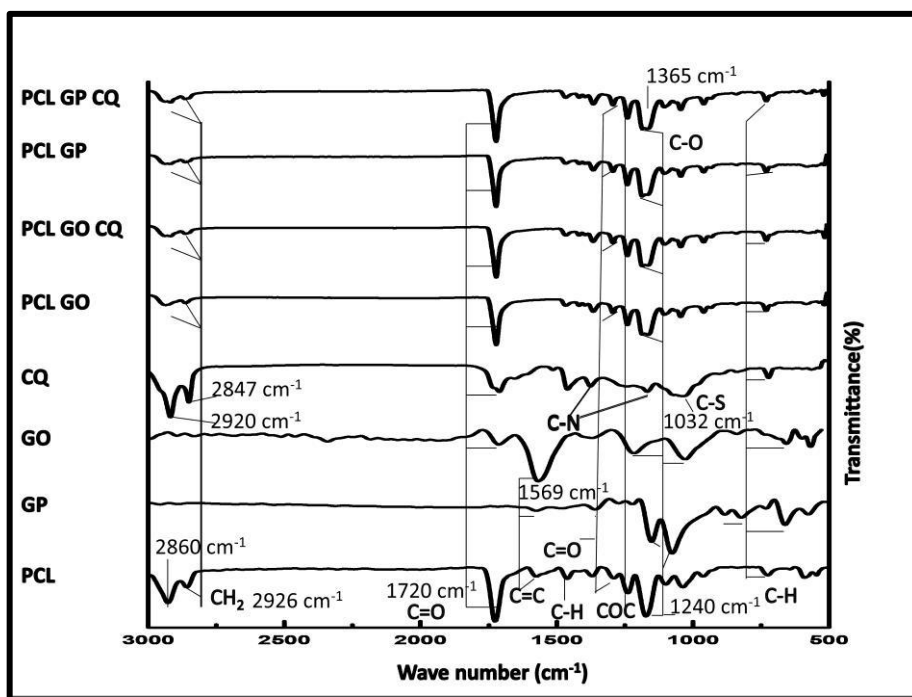


Figure 5.4: Fourier Transform Infra-Red (FTIR) spectra of the scaffolds.

Table 5.1: Properties of scaffolds. Fiber diameters are mentioned in the table.

Sl. No.	Type of Scaffolds	Fibre Diameter (nm)
		(Mean \pm SD)
1	PCL	226.37 \pm 16.92
2	PCL GO	1929.64 \pm 694.94
3	PCL GOCQ	2369.74 \pm 681.45
4	PCL GP	1029.5 \pm 183.51
5	PCL GPCQ	1374.66 \pm 224.25

This is because of the nature of GO and CQ possessing hydrophilic carboxylic and hydroxyl containing functional groups³². The hydrophilic surface provides better cell attachment, spreading and proliferation of cells than hydrophobic surfaces. The hydrophilic surface allows absorption of fibronectin which is important in osteoblast adhesion *in vitro*²⁴. A similar decrease in hydrophilicity is observed elsewhere. The contact angle of Poly (3-hydroxybutyrate-co-4-hydroxybutyrate) is also decreased on the addition of GO making hydrophobic to hydrophilic. It also have showed the increasing concentration of GO decreases the contact angle³². The contact angle of PLA decreased in

the addition of GO^{33,14}. The hydrogen bond interactions between oxygen-containing groups present in GO and water can explain this behaviour. The contact angle of poly(lactic co glycolic acid) (PLGA) is also decreased in the addition of GO²⁸. The hydrophilicity of PLLA²⁷ is also increased on the addition of CQ crude extract. The contact angle of PCL is decreased from 133 to 37 on the addition of CQ¹⁹.

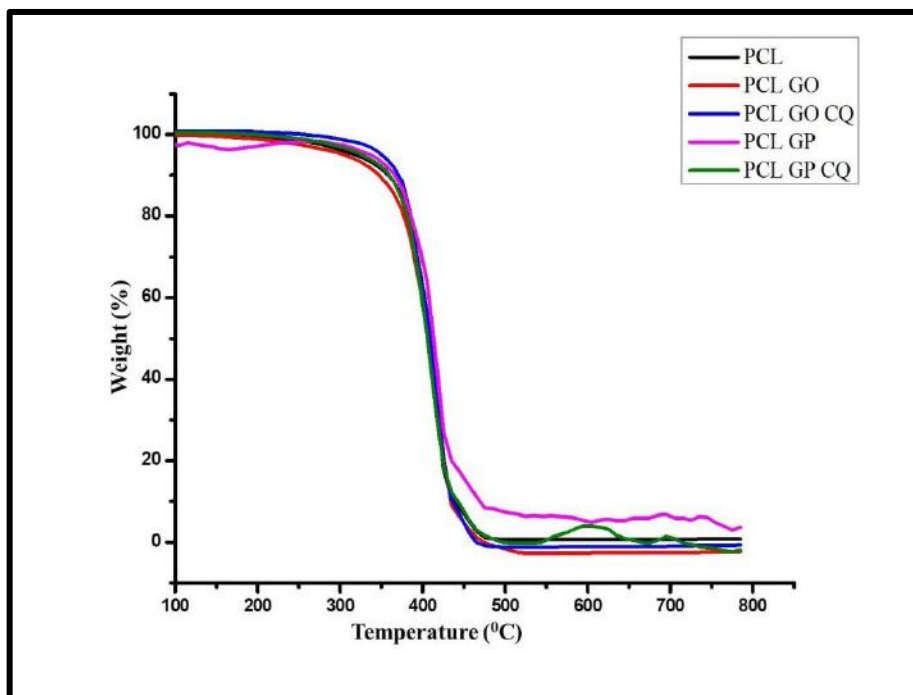


Figure 5.5: The Thermogravimetric analysis (TGA) of scaffolds

Table 5.2: Properties of scaffolds. The contact angle and mechanical properties are mentioned in the table.

Sl. No.	Type of Scaffolds	Contact angle (Mean \pm SD)	Nature of Scaffolds	Tensile strength (MPa) (Mean \pm SD)	Yield strength (MPa) (Mean \pm SD)
1	PCL	126.5 \pm 0.28	Hydrophobic	0.85 \pm 0.11	0.46 \pm 0.01
2	PCL GO	58.9 \pm 0.55	Hydrophilic	1.21 \pm 0.01	0.51 \pm 0.02
3	PCL GO CQ	55.7 \pm 0.51	Hydrophilic	3.02 \pm 0.04	1.51 \pm 0.02
4	PCL GP	77.4 \pm 0.34	Hydrophilic	0.86 \pm 0.01	0.49 \pm 0.01
5	PCL GP CQ	67.7 \pm 0.4	Hydrophilic	2.16 \pm 0.01	0.95 \pm 0.01

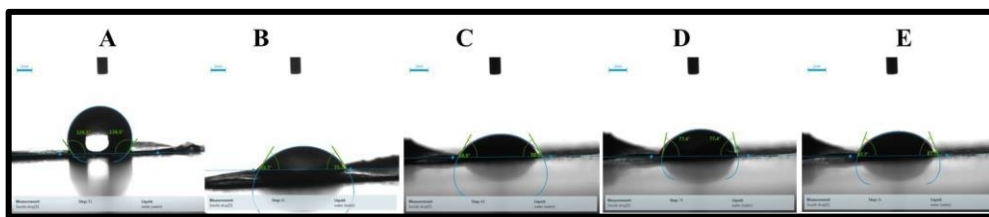


Figure 5.6: The water contact angle of scaffolds. A: PCL; B: PCL-GO; C: PCL-GO-CQ; D: PCL-GP; E: PCL-GP-CQ

5.2.2.4 Mechanical Properties:

Tensile strength and yield strength of scaffolds are mentioned in Table 5.2. Both tensile strength and yield strength of scaffolds have increased with the addition of GP and CQ into the PCL sheets (in PCL-GP-CQ scaffold) and the addition of GO and CQ into the PCL sheets (in PCL-GO-CQ scaffold). The PCL-GO-CQ scaffolds show highest tensile strength and yield strength as compared to other scaffolds.

All the composite scaffolds PCL-GO, PCL-GO-CQ and PCL-GP, PCL-GP-CQ have increased tensile strength and yield strength as compared to PCL alone (Table 5.2). The increase in the concentration of GO, GP and CQ in the respective scaffolds increases the tensile strength and yield strength of the scaffolds. It has been previously documented. Also, tensile strength and young's modulus of the PLLA have increased on the addition of CQ²⁷. Tensile strength of PCL nanofibers also improved from 0.79 MPa to 2.92 MPa by addition of CQ¹⁹. The scaffolds with higher mechanical strength support cell-based bone regeneration via an endochondral ossification³⁴. The scaffolds should be mechanically stable so that it will retain its structure after *in vivo* implantation in load-bearing tissues such as bones^{11,35}. Therefore, the mechanical properties of implanted scaffolds should be comparable with the native tissue^{36,37}.

5.2.3 Isolation and Culture of HUCMSCs:

The hUCMSCs (Figure 5.7) are successfully isolated from human umbilical cord Wharton's Jelly with a mixture of enzymes Collagenase Type IV and Dispase (7:1v/v) and Trypsin-EDTA. These hUCMSCs are used for further studies.

5.2.4 *In Vitro* Studies:

5.2.4.1 MTT Cell Proliferation Assay:

The proliferation of hUCMSCs on different scaffolds is evaluated by MTT assay at different time point 1st, 4th, and 7th day. From (Figure 5.8), it is evident that the proliferation of the cells, as determined by the absorbance, increases from day 1 to day 7 for all scaffolds. This shows the proficiency of all the scaffolds to support the proliferation of hUCMSCs. Cell proliferation on all the scaffolds is found to be higher as compared to control. Cell proliferation on PCL-GP-CQ is slightly higher than PCL-GO-CQ and as compared to other scaffolds. Cell culture experiments exhibit improved biocompatibility of PCL-GO, PCL-GO-CQ and PCL-GP, PCL-GP-CQ composite scaffolds as compared to PCL alone (Figure 5.8).

The improved biocompatibilities of scaffolds are due to the improved hydrophilic and rough surfaces. The presence of GO on the surface of the scaffold has improved hydrophilicity which is required for the cell adhesion and protein adsorption. The vitronectin and fibronectin protein adhesion are increased in hydrophilic surfaces. Also, similar results are observed in the PLA/GO and PLA-GNP (graphene nano-platelets). There is significantly higher MG 63 cell proliferation on GO and GNP containing PLA scaffolds³³. The human osteosarcoma cells (HOS) have showed good biocompatibility on Poly(1,4-butylen adipate-co-polycaprolactam) (PBA)-PCL blended with HA⁸. The MTT assay have showed that there is an equivalent growth of cells on GP coated substrate like that of a glass slide or Si/SiO₂²⁶. The PCL-CQ scaffolds have showed good growth and proliferation of human fetal osteoblast cells (hFOB) compared to PCL alone¹⁹.

5.2.4.2 Cell Adhesion study:

The hUCMSCs on the scaffolds appear after 24 hours of culture days (Figure 5.9). The cells are attached on the PCL-GO, and PCL-GO-CQ, PCL-GP, PCL-GP-CQ scaffolds. The hUCMSCs are well spread and attached on PCL-GO-CQ and PCL-GP-CQ scaffolds. The morphology of the cells is fibroidal in nature. The filopodia of the cells are attached to the surface of the scaffold. The rough surface and hydrophilic nature of scaffolds have contributed to the good attachment and spreading of cells on the surfaces. (Figure 5.9). The obtained results are similar to shown elsewhere. HOS cells have showed

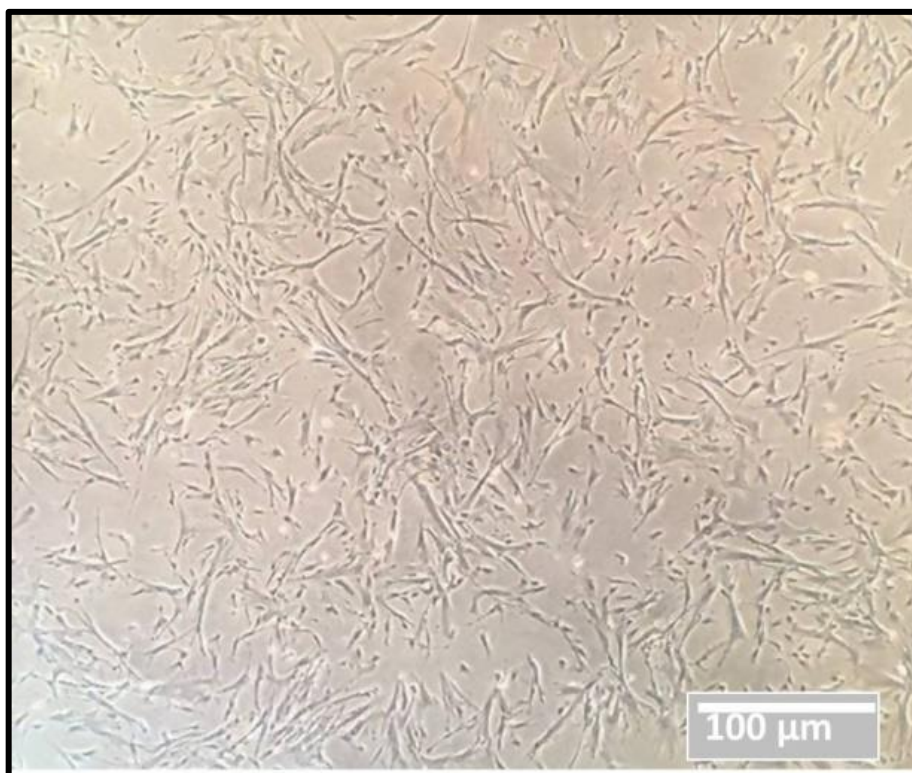


Figure 5.7: Isolated human umbilical cord Wharton's Jelly mesenchymal stem cells (HUCMSCs). Scale bar 100μm

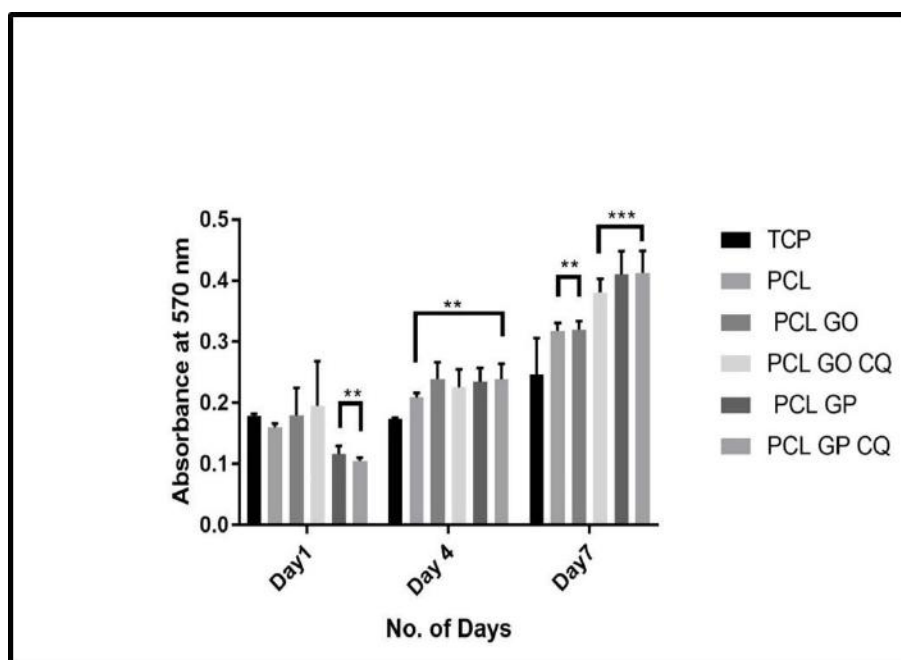


Figure 5.8: The cell viability and proliferation of hUCMSCs on the scaffolds for 1, 4, and 7 days of culture studied with MTT assay (p < 0.01, ***p < 0.001).**

flat morphologies as they adhere and spread on (PBA)-PCL blended with HA scaffolds⁸. The hFOB cells cuboidal osteoblast-like morphology with filopodia and bridging each other with the ECM, also there is a formation of the mineral particle on cell surfaces after 10 and 15 days of culture¹⁹.

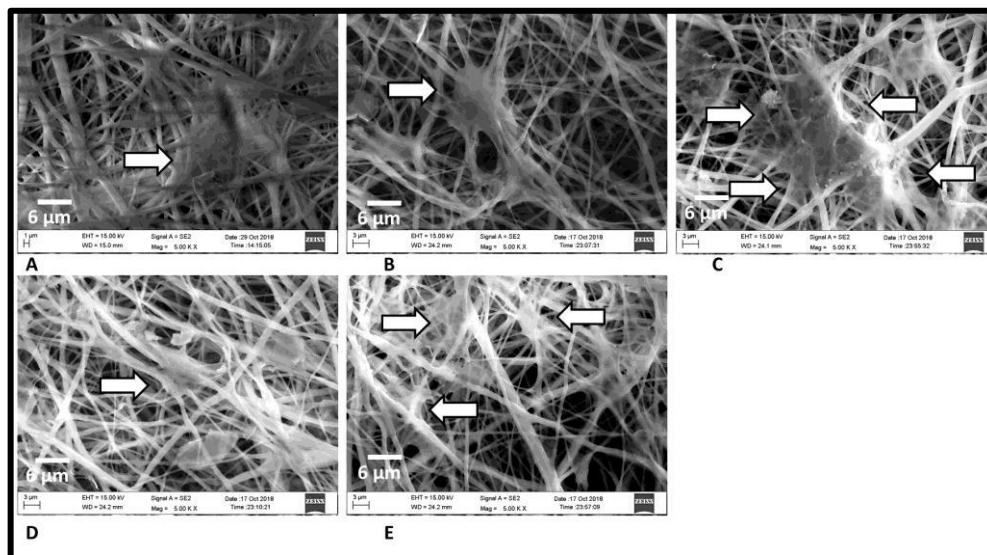


Figure 5.9: The FESEM images of cell attachment with Scaffolds. A: PCL; B: PCL-GO; C: PCL-GO-CQ; D: PCL-GP; E: PCL-GP-CQ; (Arrow showing cell attachment with fibers), scale bar 3μm

5.2.4.3 Confocal Microscopy Imaging:

Cell-seeded scaffolds incubated for 1, 4 and 7 days are also stained with DAPI for nuclear visualization shown in (Figure 5.10). The cells are in a progressive manner from 1st day to 7th day of culture. The Z stack images showed the cell attachment and cell movement deep into the scaffold and not only on the surface. Cell count with ImageJ software show that on 1st, 4th and 7th day no. of cells on PCL (884, 2683, 2773), PCL-GO (20, 578, 2690), and PCL-GO-CQ (94, 2164, 4612), PCL-GP (78, 232, 2615), and PCL-GP-CQ (76, 323, 2435) are respectively.

It shows the good proliferation and penetration of cells on these scaffolds. It again shows the resemblance with the cell viability and cell attachment of the cells on these scaffolds. The rough surface and hydrophilic nature of scaffolds have contributed to the proliferation of cells. All the composite scaffolds show the highest cell proliferation on

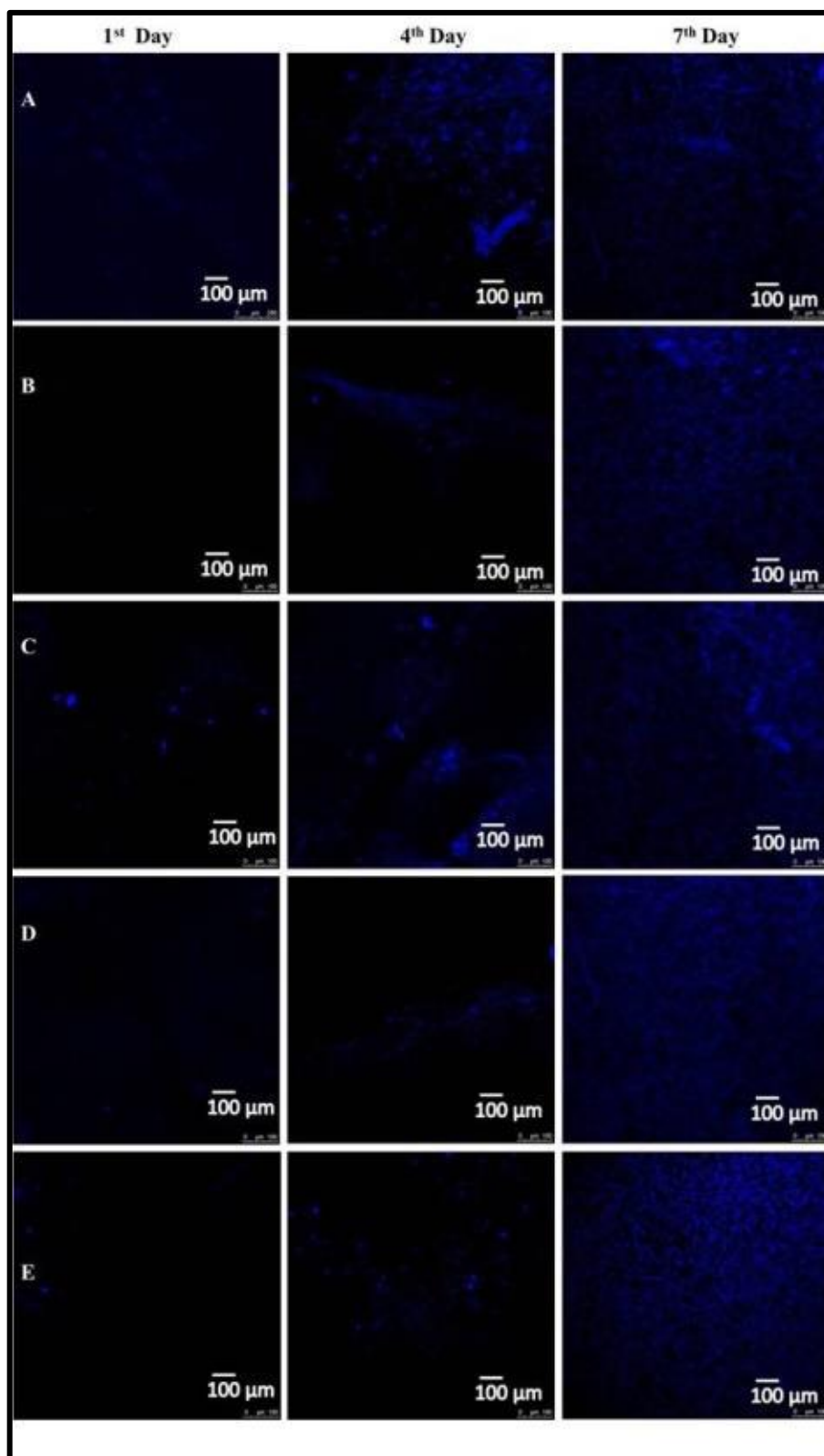


Figure 5.10: Confocal Microscopy Imaging from 1st day to 7th day of culture. A: PCL; B: PCL-GO; C: PCL-GO-CQ; D: PCL-GP; E: PCL-GP-CQ; scale bar 100μm

the 7th day as compared to PCL scaffolds. PCL-GO-CQ scaffold show the highest cell proliferation (Figure 5.10). The higher proliferation is due to the hydrophilic and rough surfaces of the scaffolds. They allow absorption of fibronectin which is important in osteoblast adhesion *in vitro*^{23,24} and promotes cell attachment on the surfaces of composites and osteoblast proliferation, differentiation. They also have a positive effect on bioactivity, water uptake and cytocompatibility of the composites²⁵. Similar results are found in GO and GP containing other scaffolds. The GP and GO films have showed the progressive proliferation of MSCs from day 1 to day 7. There is a higher density of blue stained nuclei on GP and GO films compared to PDMS (polydimethylsiloxane) or Si/SiO₂³⁸. HOS cells also have showed adherence and high density on (PBA)-PCL blended with HA scaffolds via nuclei staining⁸.

5.4.4 Osteoblastic Differentiation:

5.2.4.4.1 Alizarin Red S staining for calcium:

Alizarin Red S staining is used to evaluate calcium deposits in differentiated cells. There is a red-orange complex formed with Alizarin Red S staining show the presence of secreted mineralization. The differentiation of hUCMSCs into osteoblasts is observed from 14 days onwards. There is mineralization on PCL-GO, PCL-GO-CQ, PCL-GP, PCL-GP-CQ scaffolds after 21 days of culture.

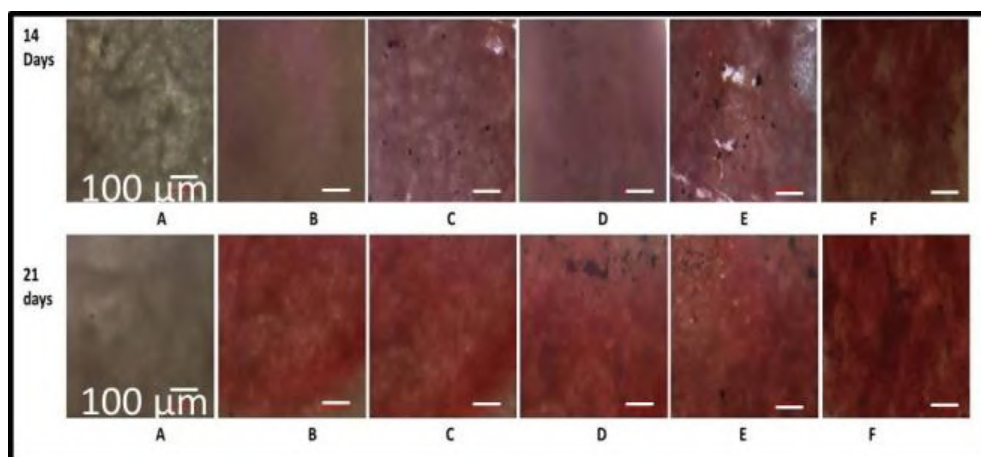


Figure 5.11: Alizarin Red S staining of Layer by layer scaffolds after 14 days and 21 days of differentiation of HUCMSCs. A A: PCL; B: PCL-GO; C: PCL-GO-CQ; D: PCL-GP; E: PCL-GP-CQ; (A to E: without Osteoblastic differentiation medium); F: Tissue culture plate; scale bar 100μm

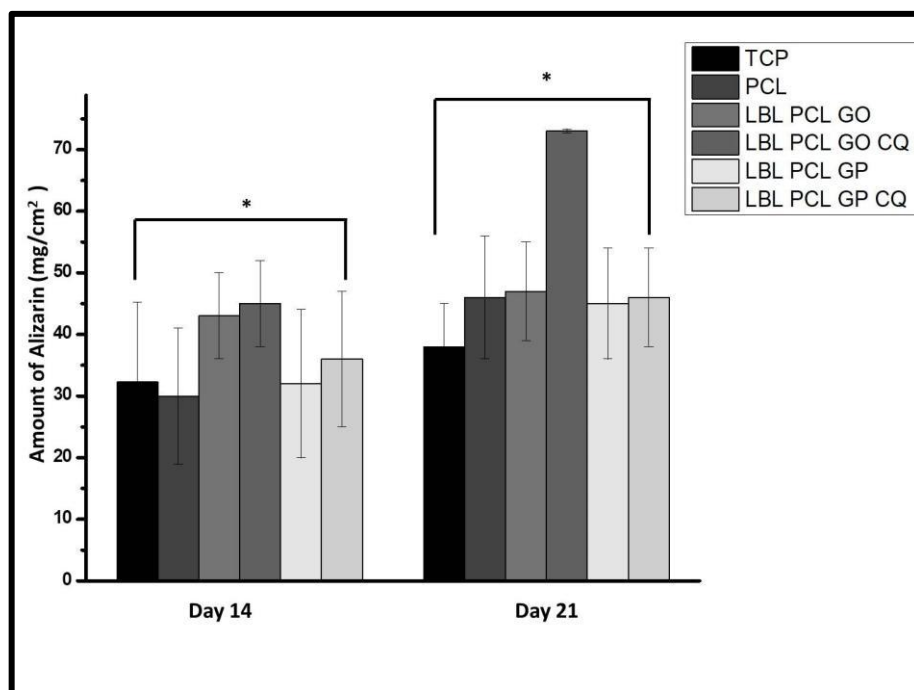


Figure 5.12: Alizarin Red S staining quantification of Layer by layer scaffolds after 14 days and 21 days of differentiation of hUCMSCs (* $p < 0.05$).

The maximum differentiation of hUCMSCs into osteoblasts is confirmed after 21 days of culture on the modified scaffolds of PCL-GO-CQ. These results indicate that the synergistic effect of GO and CQ extract could enhance the expression of the osteogenic differentiation markers and can stimulate calcium deposition (Figure 5.11 and Figure 5.12). The hUCMSCs differentiated on the scaffolds (Figure 5.11.A to E) without an osteogenic medium is comparable with that to the control tissue culture plate (Figure 5.11.F) with an osteogenic medium. The least mineralization is on the PCL scaffolds without an osteogenic medium. These results suggest that these scaffolds have great potential for osteogenic differentiation of hUCMSCs.

5.2.4.4.2 Von Kossa staining for calcium:

The Von Kossa staining also is used to evaluate secreted calcium deposits in differentiated cells (Figure 5.13). The appearance of black precipitates confirms the positive Von Kossa staining with secreted mineral deposition. The black precipitates are observed from 14 days onwards and are maximum and broad after 21 days of culture on the modified scaffolds of PCL-GO-CQ as compared to other scaffolds. The hUCMSCs

differentiated on the scaffolds (Figure 5.13.A to E) without an osteogenic medium is comparable with that to the control tissue culture plate (Figure 5.13.F) with an osteogenic medium. The least mineralization is on the PCL scaffolds without an osteogenic medium. The similar results as that of Alizarin Red S staining confirm the differentiation of hUCMSCs into osteoblasts. The osteogenic differentiation of MSCs is shown in the presence of serum and human plasma after 28 days of culture in osteogenic media³⁹. Mesenchymal stem cells (MSCs) cultured on biphasic calcium phosphate, calcium phosphate in the presence of conditioned medium containing significant growth factors, mineralization is observed with positive Von kossa staining on 21 days of culture⁴⁰. The Von kossa staining is used to evaluate the osteoblastic differentiation of MSCs through mineralization. After 24 days of culture of MSCs into osteoblastic induction medium, there is mineralization from 14 days onwards in an increasing manner, as confirmed by Von kossa staining⁴¹.

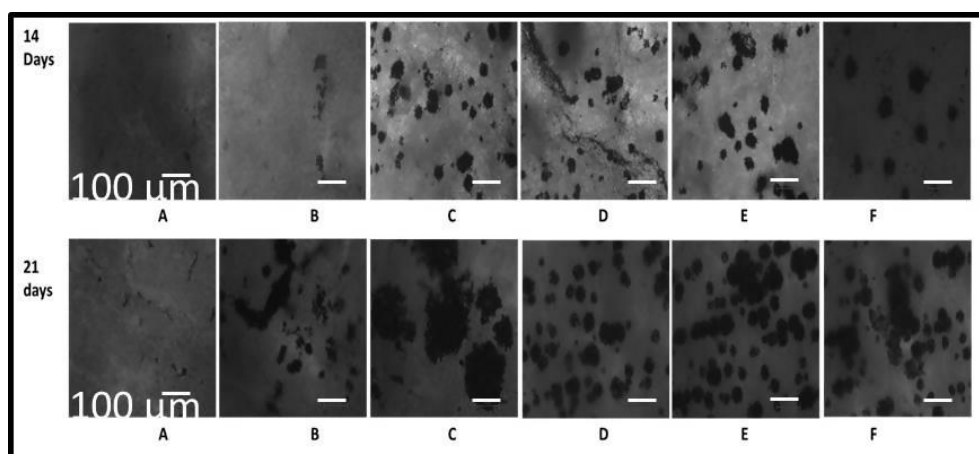


Figure 5.13: Von Kossa staining after 14 days and 21 days of differentiation of hUCMSCs. A: PCL; B: PCL-GO; C: PCL-GO-CQ; D: PCL-GP; E: PCL-GP-CQ; (A to E: without Osteoblastic differentiation medium); F: Tissue culture plate with Osteoblastic differentiation; scale bar 100μm

The Foetal Rat Calvariae (FRC) cells were cultured on osteoblastic medium have showed mineralization or bone nodules formation on day 14, as confirmed by Von kossa staining⁴². The BMPs were assessed for an osteoinduction of MSCs for 21 days of culture. There is significant mineralization and bone nodules formation when MSCs cultured with a combination of BMP-2+BMP-6+ BMP-9, confirmed by Von kossa staining⁴³.

5.3 Conclusions:

The prepared PCL-GO-CQ scaffold is novel, herbal, and biocompatible, with an osteoinductive nature. Their porous, rough, hydrophilic nature, and mechanically stable character helped the hUCMSCs to adhere, spread, proliferates and differentiates into osteoblast-like cells. The synergistic effect of GO and CQ in the PCL-GO-CQ scaffold enhanced the roughness, thermal and mechanical properties and wettability of the scaffolds. Mainly GO and CQ callus extract provided osteoinductive properties to scaffold that helps hUCMSCs to spontaneously differentiate into osteoblast without any osteogenic media or growth factors or added external stimuli. This property will help the scaffold in speedy *in vivo* bone formation upon transplantation, thus saving *in vitro* differentiation time before transplantation. Thus, the novel PCL-GO-CQ scaffolds which is prepared using the layer by layer method shows tremendous potential for *in vivo* bone tissue engineering and further studies to regenerate bone tissues.

References:

- 1 S. Kashte, A. K. Jaiswal and S. Kadam, *Tissue Eng. Regen. Med.*, 2017, **14**, 1–14.
- 2 A. Alves, A. R. C. Duarte, J. F. Mano, R. A. Sousa and R. L. Reis, *J. Supercrit. Fluids*, 2012, **65**, 32–38.
- 3 I. Rajzer, E. Menaszek, R. Kwiatkowski and W. Chrzanowski, *J. Mater. Sci. Mater. Med.*, 2014, **25**, 1239–1247.
- 4 X. Liu and P. Ma, *Ann. Biomed. Eng.*, 2004, **32**, 477–486.
- 5 J. Qian, W. Xu, X. Yong, X. Jin and W. Zhang, *Mater. Sci. Eng. C. Mater. Biol. Appl.*, 2014, **36**, 95–101.
- 6 B. Chuenjitkuntaworn, T. Osathanon, N. Nowwarote, P. Supaphol and P. Pavasant, *J Biomed Mater Res Part A*, 2015, **104**, 264–271.
- 7 K. Ren, Y. Wang, T. Sun, W. Yue and H. Zhang, *Mater. Sci. Eng. C*, 2017, **78**, 324–332.
- 8 V. Y. Chakrapani, T. S. S. Kumar, D. K. Raj and T. V Kumary, *J. Nanosci. Nanotechnol.*, 2017, **17**, 2320–2328.
- 9 Y. J. Son, H. S. Kim and H. S. Yoo, *RSC Adv.*, 2016, **6**, 114061–114068.
- 10 W. M. Gallagher, I. Lynch, L. T. Allen, I. Miller, S. C. Penney, D. P. O'Connor, S. Pennington, A. K. Keenan and K. A. Dawson, *Biomaterials*, 2006, **27**, 5871–5882.
- 11 S. Yang, K. F. Leong, Z. Du and C. K. Chua, *Tissue Eng.*, 2001, **7**, 679–689.
- 12 W. Chen and T. J. McCarthy, *Macromolecules*, 1997, **9297**, 78–86.
- 13 Y. Li, M. C. Choi, K. M. Jeong, J. H. Jeong, H. G. Lee, G. H. Kim and C. S. Ha, *Macromol. Res.*, 2017, **25**, 496–499.
- 14 X. He, L. L. Wu, J. J. Wang, T. Zhang, H. Sun and N. Shuai, *High Perform. Polym.*, 2015, **27**, 318–325.

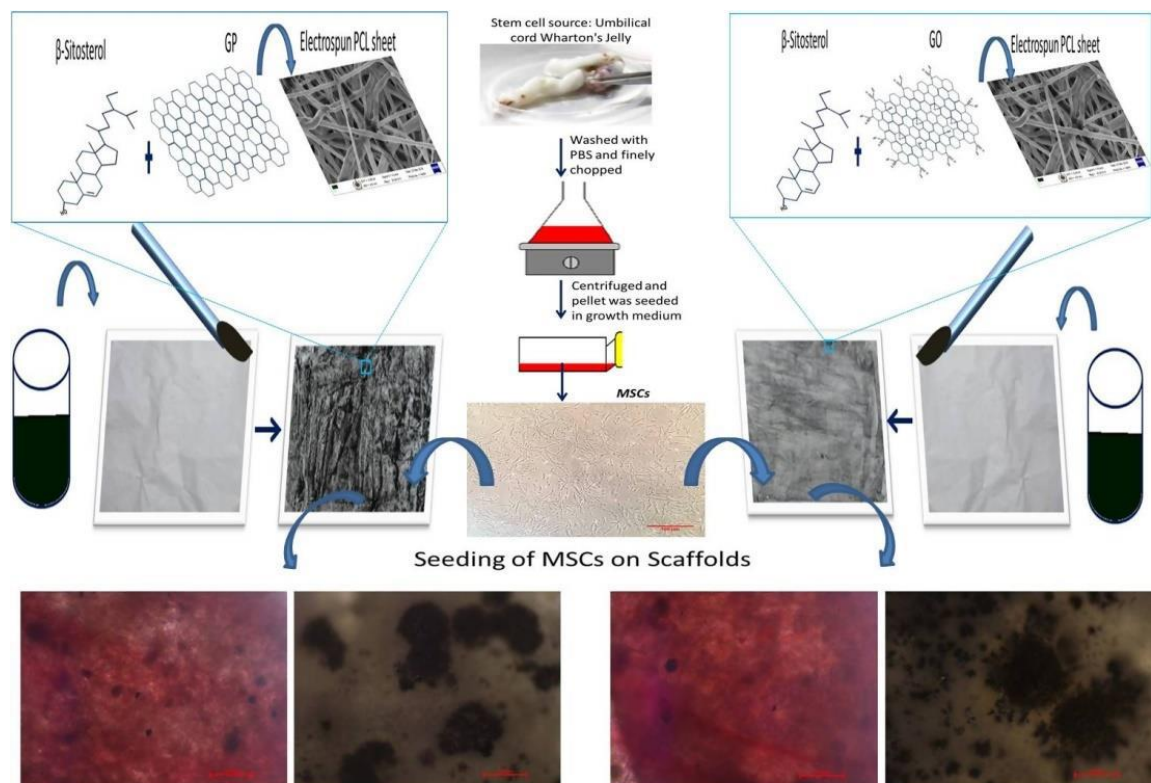
- 15 G. Mishra, S. Srivastava and B. P. Nagori, *Int. J. PharmTech Res.*, 2010, **2**, 1298–1310.
- 16 D. K. Deka, L. C. Lahon, A. Saikia and Mukit, *Indian J Pharmacol*, 1994, **26**, 44–45.
- 17 M. S. Rao, P. Bhagath Kumar, V. B. Narayana Swamy and N. Gopalan Kutty, *Pharmacologyonline*, 2007, **3**, 190–202.
- 18 B. K. Potu, M. S. Rao, N. G. Kutty, K. M. R. Bhat, M. R. Chamallamudi and S. R. Nayak, *Clinics (Sao Paulo)*., 2008, **63**, 815–820.
- 19 S. Suganya, J. Venugopal, S. Ramakrishna, B. S. Lakshmi and V. R. Giri Dev, *J. Appl. Polym. Sci.*, 2014, **131**, 1–11.
- 20 N. Singh, V. Singh, R. Singh, A. Pant, U. Pal, L. Malkunje and G. Mehta, *Natl. J. Maxillofac. Surg.*, 2013, **4**, 52–56.
- 21 P. Garg and C. P. Malik, *Int. J. Pharm. Clin. Res.*, 2012, **4**, 4–10.
- 22 P. S. R Mehta, K Teware, *Int. J. Ayurvedic Herb. Med.*, 2012, **2**, 229–233.
- 23 D. Deligianni, N. Katsala, S. Ladas, D. Sotiropoulou, J. Amedee and Y. Missirlis, *Biomaterials*, 2001, **22**, 1241–1251.
- 24 M. Yang, S. Zhu, Y. Chen, Z. Chang, G. Chen, Y. Gong, N. Zhao and X. Zhang, *Biomaterials*, 2004, **25**, 1365–1373.
- 25 S. K. Misra, T. Ansari, D. Mohn, S. P. Valappil, T. J. Brunner, W. J. Stark, I. Roy, J. C. Knowles, P. D. Sibbons, E. V. Jones, A. R. Boccaccini and V. Salih, *J. R. Soc. Interface*, 2010, **7**, 453–465.
- 26 T. R. Nayak, H. Andersen, V. S. Makam, C. Khaw, S. Bae, X. Xu, P.-L. R. Ee, J.-H. Ahn, B. H. Hong, G. Pastorin and B. Özyilmaz, *ACS Nano*, 2011, **5**, 4670–4678.
- 27 K. Parvathi, A. G. Krishnan, A. Anitha, R. Jayakumar and M. B. Nair, *Int. J. Biol. Macromol.*, 2018, **110**, 514–521.

-
- 28 E. J. Lee, J. H. Lee, Y. C. Shin, D. Hwang, J. S. Kim, O. S. Jin, L. Jin, S. W. Hong and D. Han, *Biomater. Res.*, 2014, **18**, 18–24.
- 29 S. K. Bhullar, D. Rana, H. Lekesiz, A. C. Bedeloglu, J. Ko, Y. Cho, Z. Aytac, T. Uyar, M. Jun and M. Ramalingam, *Mater. Sci. Eng. C*, 2017, **81**, 334–340.
- 30 N. Abdullah, A. Hakim and M. Kubo, *ARPN J. Eng. Appl. Sci.*, 2016, **11**, 9582–9585.
- 31 Olivier Persenaire, Michaël Alexandre, A. Philippe Degée and P. Dubois†, *Biomacromolecules*, 2001, **2**, 288–294.
- 32 T. Zhou, G. Li, S. Lin, T. Tian, Q. Ma, Q. Zhang, S. Shi, C. Xue, W. Ma, X. Cai and Y. Lin, *ACS Appl. Mater. Interfaces*, 2017, **9**, 42589–42600.
- 33 A. M. Pinto, S. Moreira, I. C. Gonçalves, F. M. Gama, A. M. Mendes and F. D. Magalhães, *Colloids Surfaces B Biointerfaces*, 2013, **104**, 229–238.
- 34 H. Sun, F. Zhu, Q. Hu and P. H. Krebsbach, *Biomaterials*, 2014, **35**, 1176–1184.
- 35 C. Y. Lin, N. Kikuchi and S. J. Hollister, *J. Biomech.*, 2004, **37**, 623–636.
- 36 M. Tarik Arafat, I. Gibson and X. Li, *Rapid Prototyp. J.*, 2014, **20**, 13–26.
- 37 J. Wang and X. Yu, *Acta Biomater.*, 2010, **6**, 3004–3012.
- 38 W. C. Lee, C. H. Y. X. Lim, H. Shi, L. A. L. Tang, Y. Wang, C. T. Lim and K. P. Loh, *ACS Nano*, 2011, **5**, 7334–7341.
- 39 T. Felka, R. Schfer, P. De Zwart and W. K. Aicher, *Cytotherapy*, 2010, **12**, 143–153.
- 40 J. Wang, D. Liu, B. Guo, X. Yang, X. Chen, X. Zhu, Y. Fan and X. Zhang, *Acta Biomater.*, 2017, **51**, 447–460.
- 41 P. S. Hung, Y. C. Kuo, H. G. Chen, H. H. K. Chiang and O. K. S. Lee, *PLoS One*, 2013, **8**, 1–7.
- 42 N. Yamamoto, K. Furuya and K. Hanada, *Biol. Pharm. Bull.*, 2002, **25**, 509–515.
-

- 43 Y. Açil, A. A. Ghoniem, J. Wiltfang and M. Gierloff, *J. Cranio-Maxillofacial Surg.*, 2014, **42**, 2002–2009.

CHAPTER 6:

PAINT SCAFFOLDS



Proliferation & differentiation of MSCs into Osteoblasts as confirmed by ARS and Von Kossa staining

6.1 Introduction:

Bone healing is a complex process of biology and biomechanics to restore the healthy form and function of the bone¹. Earlier, bone regeneration is achieved through natural grafts such as autografts, allografts, and xenografts but with limitations. These drawbacks push the endeavour to design bone graft alternatives, using the doctrines of biomaterials and tissue engineering. A variety of biomaterials such as metals (stainless steel, Cobalt-Chromium (Co-Cr) alloys and Titanium (Ti) alloys, etc.)², ceramics (Hydroxyapatite (HA), tri-calcium phosphate (TCP), etc.)³, natural polymers (collagen, fibrin, chitosan, etc.)⁴ and synthetic polymers (poly (lactic acid) (PLA), poly (glycolic acid) (PGA), etc.) and their combinations have been explored for replacement and repair of damaged or traumatized bone tissues.

The poly ϵ -caprolactone (PCL), an FDA approved polymer used for fabrication of scaffold sheets by electrospinning, the most common and versatile technique. PCL is biocompatible, biodegradable and used largely in tissue engineering applications. In various studies, PCL along with Hydroxyapatite (HA)⁵, PCL-gelatin hybrid nanofibrous membranes⁶, PCL-(Poly-1,4-butylene adipate-co-polycaprolactam (PBAPCL)-HA composite scaffold⁷, PCL has shown its potential in bone tissue engineering applications. However, electrospinnable synthetic polymers such as PCL, PLA, etc. are mainly hydrophobic. Therefore, they are not sufficient to perform all the necessary functions in the process of bone tissue engineering.

The application of these materials in tissue engineering can be advanced through the modification of surfaces from hydrophobic to be partly hydrophilic. Introducing hydrophilic property to hydrophobic nanofibres has been attempted in various ways by surface modification technologies, e.g. flame treatment, corona discharge treatment, plasma modification, and surface graft polymerization⁸. Surface modification is an important aspect in the field of tissue engineering to cell attachment and cell proliferation. Rough surfaces with porosity are significant in cell behaviour.

Therefore, along with PCL, we used graphene oxide (GO), graphene(GP) and *Cissus quadrangularis* (CQ) callus culture extract as physical, chemical, and biological property enhancers in the preparation of scaffolds for bone tissue engineering. GP has

gained attraction in bone tissue engineering because of its large surface area, low biological toxicity and osteoinductive nature⁹. GP-chitosan films¹⁰, GP coated cobalt-chromium-molybdenum-based alloy¹¹, GP nanosheets coated titanium alloys¹² have showed biocompatibility and its potential in tissue engineering. On the other hand, GO has more hydrophilic groups and easy dispersion ability as compared to GP¹³. GO along with HA and chitosan functionalized graphene nanoplatelets reinforced with polyvinyl alcohol¹⁴, GO with Polylactic acid and HA¹⁵, GO doped poly (lactic-co-glycolic acid) (PLGA) scaffolds¹³. GO-poly-L-lysine composites¹⁶ used for bone tissue engineering. GP and GO most fascinating materials of today, and their interaction with stem cells channelled cell attachment, cell proliferation and differentiation into various lineages like osteoblasts, chondroblasts, and neurons^{11,12,17}.

Cissus quadrangularis (CQ) is used in Ayurveda as Asthiyuk (bone strengthener)¹⁸. The stem extract of this plant which contains high calcium ions (4% weight) and phosphorous¹⁹ and ethanolic extract possess triterpenes, β -sitosterol, α and β - amyrins, ketosteroids, phenols, tannins, carotene and vitamin C¹⁸, is proved to be useful for bone fracture healing. The effective constituents of CQ may encourage proliferation and differentiation of MSCs into osteoblasts and bone formation via wnt-LRp5- β -catenin or MAPK dependent pathway. CQ found to increase the activity of the proliferation and differentiation of BM MSCs into osteoblasts²⁰. The isolated phytochemical steroid is believed to be the main constituent in CQ²¹. Methanolic extract of CQ²² and its use in fracture healing is proven. PCL-CQ-HA nano-fibrous scaffolds found to be a potential biocompatible material for bone tissue engineering²³. We have used CQ callus culture extract obtained from callus culture, a plant tissue culture technique used to propagate the plant in vitro. The obtained callus is brown in colour and contains a high amount of phytosterols. Therefore, callus culture extract contains a pure and higher amount of metabolites rather than crude stem extract of the plant.

The purpose of this study is to investigate the osteoblastic differentiation potential of hUCMSCs induced by GO, GP, and CQ callus culture extract. Therefore, different combinations of PCL-GO, PCL-GO-CQ, PCL-GP and PCL-GP-CQ scaffolds are evaluated for osteoinductive potential.

6.2 Results and Discussion:

6.2.1 CQ callus culture and powder extraction:

The brown coloured callus is observed after the 4 weeks of culture (Figure 6.1: A, B) similar to mentioned elsewhere^{24,25}. From the 4-5 weeks of fully grown, dehydrated and dried callus, the fine powder is made. The crude extract is prepared by using a Soxhlet apparatus with ethanol. The 50 g callus powder of CQ yielded 3 g of extract which then dissolved in water, partitioned with petroleum ether yielding 0.5 g of extract.

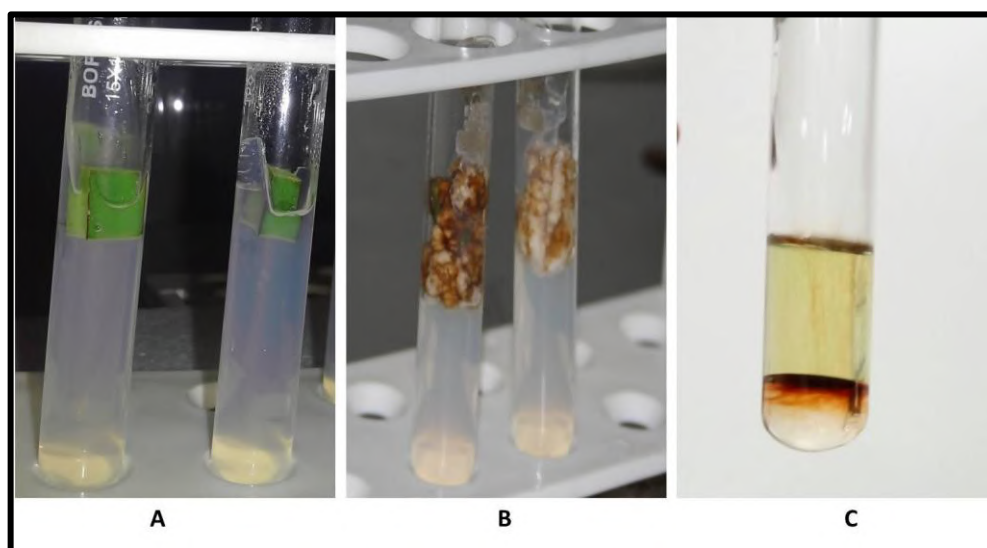


Figure 6.1: CQ callus culture. A: Callus formed from CQ stem explant; B: Control CQ stem explant; C: Salwoski test. The brown ring formed at the bottom of the test tube confirms the presence of phytosterols in the callus extract.

The CQ callus extract shows the presence of Phytosterol, confirmed by the formation of the brown ring at the bottom of test tube as indicated in Salkowski test (Figure 1: C), similar to shown elsewhere²³. The CQ callus extract is preferred over crude stem extract because of its high content of phytosterols. The phytosterols are osteoinductive in nature²³. These phytosterols stimulate increased expression of osteopontin and increased uptake of the minerals such as calcium, sulphur, by the osteoblasts in fracture healing²¹, acting as the main component in bone regeneration.

6.2.2 Preparation and Characterization of Scaffolds:

6.2.2.1 Morphological analysis:

The FESEM analysis is done for the morphological analysis of the electrospun PCL and painted scaffolds. FESEM images (Figure 6.2) show the electrospun PCL scaffolds with smooth fibre structures while that of painted scaffolds are decorated with the GO, GP and CQ are rough in nature. The Fibre diameter (Table 6.1) is significantly increased with GO, GP and further increased with CQ. The fibre diameter is increased in the PCL-GO and PCL-GP scaffolds as compared to PCL scaffolds. The Fibre diameter is significantly increased in the PCL-GP-CQ and PCL-GO-CQ scaffolds.

Surface properties of the PCL and surface modified PCL sheets are analysed by AFM by tapping mode. The AFM images (Figure 6.3) show the rough surface of the scaffolds. The modified scaffolds PCL-GO and PCL-GP are rough as compared to the PCL scaffold. The PCL-GP-CQ and PCL-GO-CQ scaffolds show higher roughness as compared to other scaffolds. The root mean square roughness (RMS) values are PCL (146 ± 10 nm), PCL-GO (201 ± 9 nm), PCL-GO-CQ (231 ± 9 nm), PCL-GP (330 ± 12 nm) and PCL-GP-CQ (382 ± 11 nm).

The rough surface is helpful in cell attachment and proliferation. Surface roughness has a positive effect on bioactivity, water uptake and cytocompatibility of the composites²⁶. Alike results are analysed by various researchers. The coating of polyethyleneimine-GO on PLA films also have showed rough, uneven, mountain-like topography compared to uncoated PLA films²⁷. The GO films on Si/SiO₂ have showed nanoripples with high density²⁸. The root mean square roughness of the rGO coated on Ti alloys and GO coated on Ti alloys is higher than Ti alloys alone¹².

6.2.2.2 Physical analysis:

The FTIR spectra (Figure 6.4) show distinctive absorption peaks of asymmetric CH₂ stretching at 2926 cm^{-1} and symmetric CH₂ stretching at 2860 cm^{-1} , C=O stretching at 1720 cm^{-1} , C-O and C-C stretching at 1293 cm^{-1} , asymmetric C-O-C stretching at 1240 cm^{-1} for PCL. Carboxylic C=O bend at 1719 cm^{-1} , C=C bend at 1569 cm^{-1} , C-O bend at 1220 cm^{-1} and 1029 cm^{-1} , for GO. C-C stretching at 1576 cm^{-1} , C-OH stretching at 1365

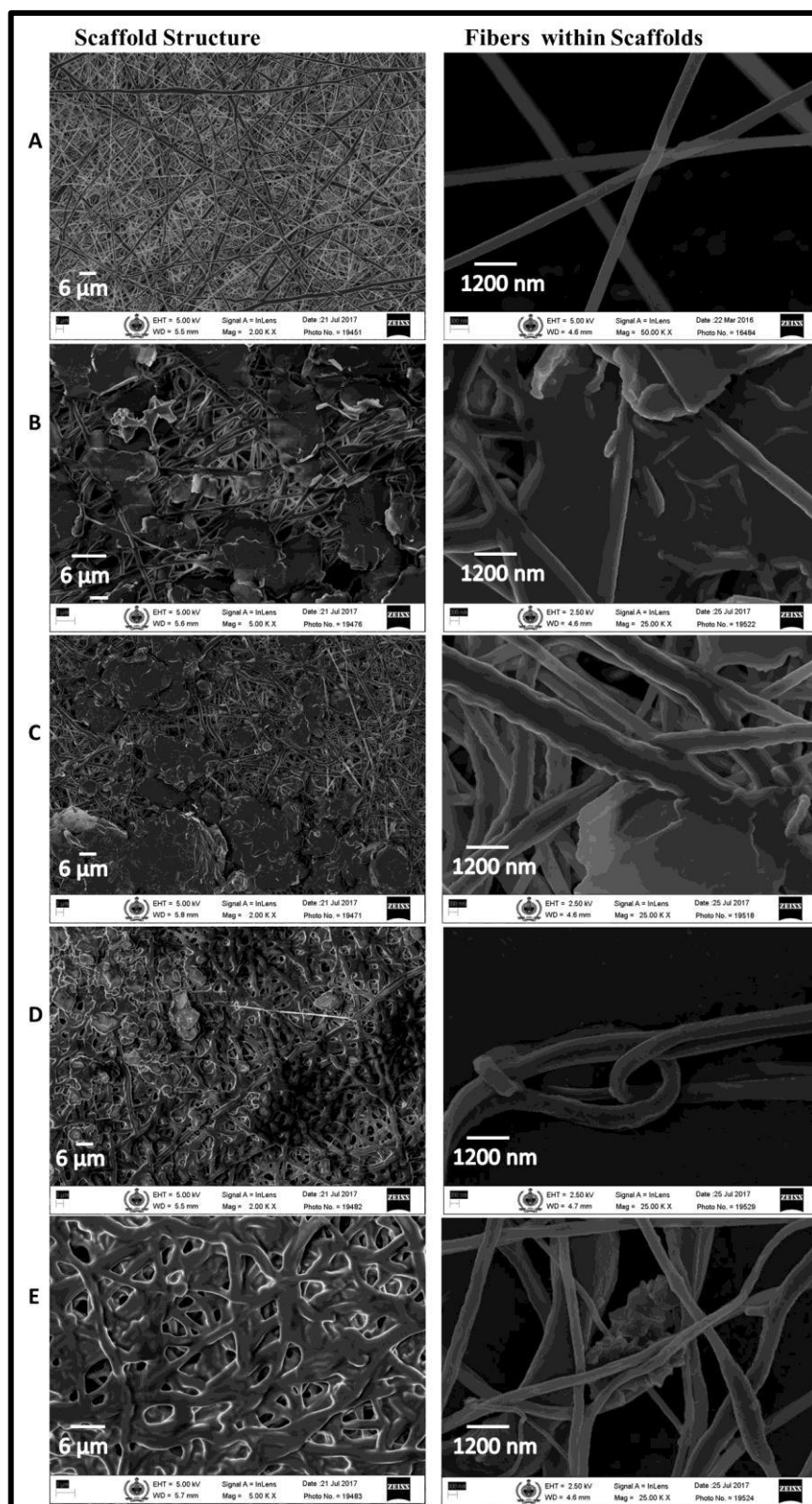


Figure 6.2: Field emission scanning electron microscope (FESEM) images. A: PCL; B: PCL-GO; C: PCL-GO-CQ; D: PCL-GP; E: PCL-GP-CQ. Scale bar 3μm& 300nm

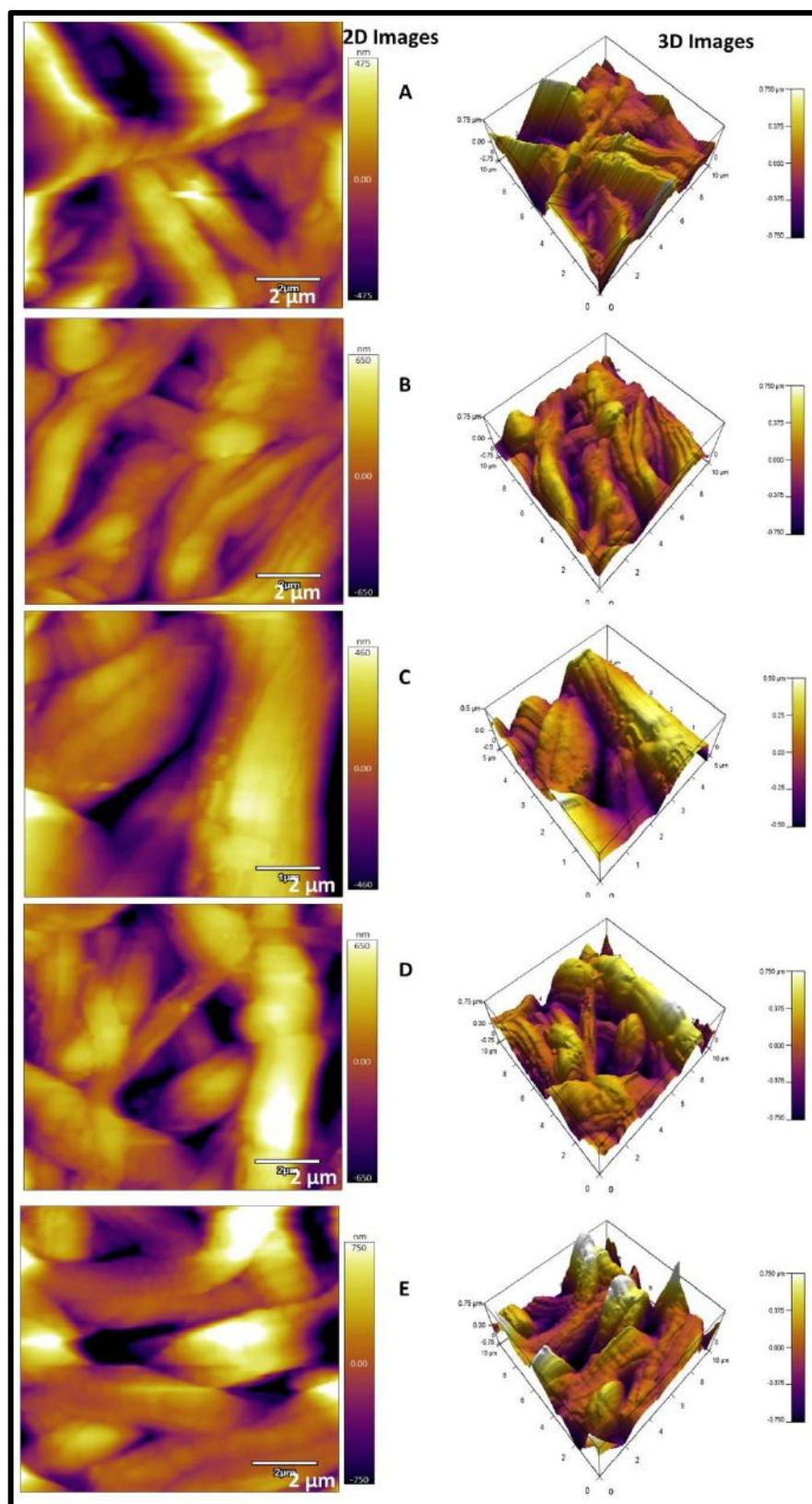


Figure 6.3: Atomic force microscopy (AFM) 2D and 3D images. A: PCL; B: PCL-GO; C: PCL-GO-CQ; D: PCL-GP; E: PCL-GP-CQ; Scale bar 2μm

cm^{-1} , alkoxy C-O stretching at 1150 cm^{-1} and 1069 cm^{-1} , for GP. Alkane asymmetric C-H stretching at 2920 cm^{-1} , alkane symmetric C-H stretching at 2847 cm^{-1} , C=O stretching at 1708 cm^{-1} and 1459 cm^{-1} , Alkane C-H bending at 1377 cm^{-1} and 1163 cm^{-1} , C-N stretching at 1150 cm^{-1} - 1000 cm^{-1} , C=S stretching at 1032 cm^{-1} for CQ.

The FTIR spectra (Figure 6.4) confirm the interaction of PCL with GP, GO and CQ in the respective scaffolds. The peaks obtained here are similar to that of PCL^{6,7,29}, GP, GO^{12,14,30} and CQ^{18,23,31,32} obtained elsewhere. In the composite scaffolds, the interaction could be due to the hydrogen bonds and/or van der Waals forces^{23,31}. There are many overlapping peaks between PCL, GP, GO and CQ, therefore, they could not be differently differentiated. But integrating and or reduction or broadening of peaks could confirm the presence of these multiple components. Similar kind of results obtained elsewhere^{23,31}.

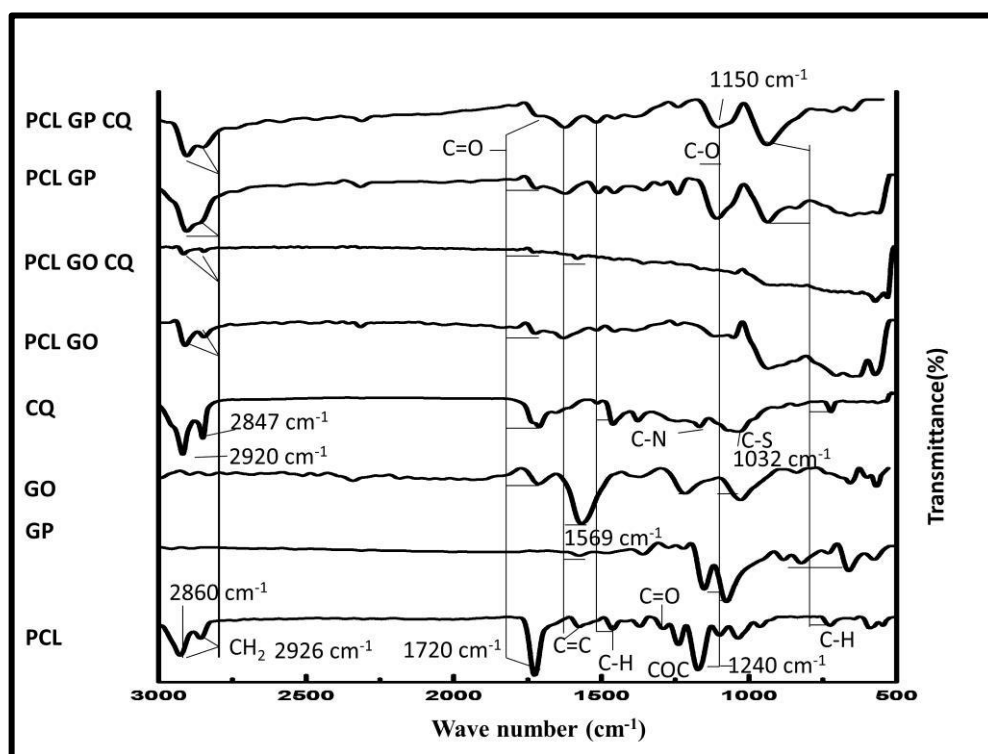


Figure 6.4: Fourier Transform Infra-Red (FTIR) spectra of the scaffolds.

Thermal degradation of scaffolds is studied by determining weight loss of sample upon linearly increasing temperature. In Figure 6.5, PCL TGA curve displays main degradation at $250\text{--}433^\circ\text{C}$ (88 % weight loss) with 2% residue; PCL-GO: $213\text{--}434^\circ\text{C}$ (88

% weight loss) with complete degradation; PCL-GO-CQ: 187-433 °C (87 % weight loss) with complete degradation; PCL-GP: 313-451 °C (76 % weight loss) with 11% residue; PCL-GP-CQ: 235- 498 °C (85 % weight loss).

Table 6.1: Properties of scaffolds. Fiber diameter of the scaffolds.

Sl. No.	Type of Scaffolds	Fibre Diameter (nm) (Mean \pm SD)
1	PCL	226 \pm 16
2	PCL-GO	1029 \pm 183
3	PCL-GO-CQ	1374 \pm 224
4	PCL-GP	823 \pm 124
5	PCL-GP-CQ	1319 \pm 680

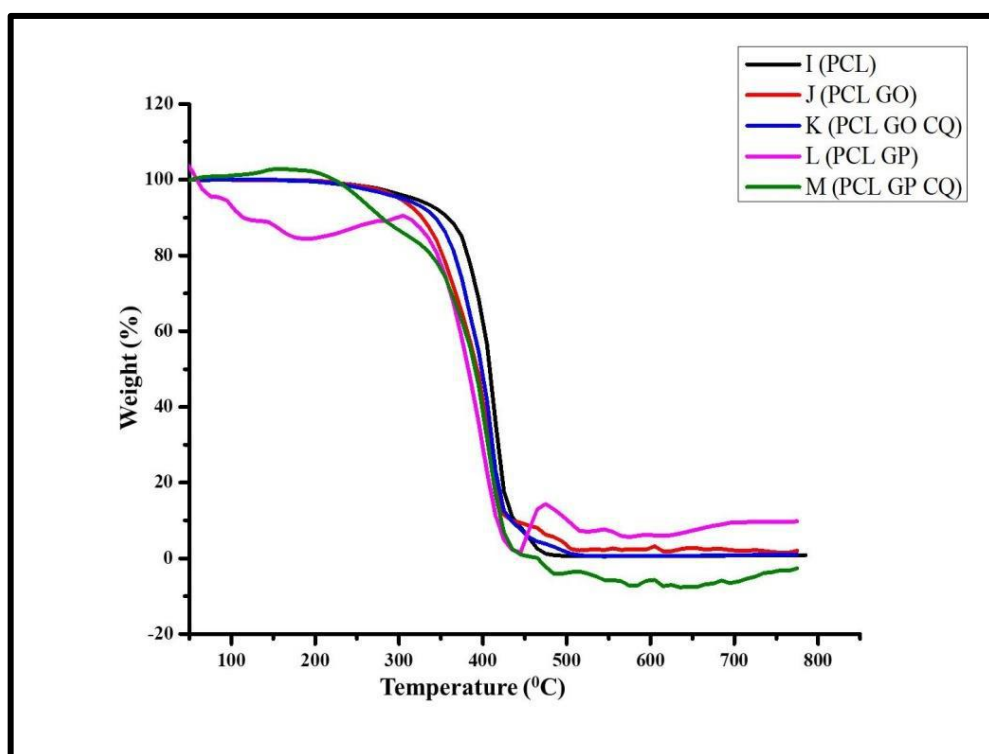


Figure 6.5: Thermogravimetric analysis (TGA) of scaffolds

There is complete degradation of PCL-GO and PCL-GO-CQ scaffolds. It could be due to pyrolysis of liable oxygen-containing groups in GO, or phytosterols. The similar results are found in GO incorporated PLGA scaffolds³³, PCL scaffolds³⁴. The incorporation of polyethyleneimine-GO into PLA films they are majorly degraded²⁷. There is residue remaining in PCL-GP scaffolds. It could be due to GP has lower activation energies for oxidation. The amorphous carbon is likely to be oxidized at around 500 °C³⁵. Also fluctuations in the degradation temperature could occur due to different heating rates³⁶.

6.2.2.3 Wetting properties:

The water contact angles of PCL, and modified PCL-GO, PCL-GO-CQ and PCL-GP, PCL-GP-CQ are represented in Figure 6.6 and Table 6.2. The plain PCL scaffolds are hydrophobic while painted scaffolds PCL-GP, PCL-GP-CQ, PCL-GO, and PCL-GO-CQ are hydrophilic in nature. The PCL-GO-CQ scaffolds show the lowest water contact angle and the highest hydrophilicity. The incorporation of GO, GP and CQ into the respective scaffolds increased the hydrophilicity of the scaffolds. This is because of the nature of most, GO and CQ possessing hydrophilic carboxylic and hydroxyl containing functional groups³⁷. The hydrophilic surface provides better cell attachment, spreading and proliferation of cells than hydrophobic surfaces. The hydrophilic surface allows absorption of fibronectin which is important in osteoblast adhesion *in vitro*³⁸. A similar decrease in hydrophilicity observed elsewhere. The contact angle of Poly (3-hydroxybutyrate-co-4-hydroxybutyrate) also decreased on the addition of GO making hydrophobic to hydrophilic. It also have showed the increasing concentration of GO decreases the contact angle³⁷. The contact angle of PLA decreased in the addition of GO^{27,39}. The hydrogen bond interactions between oxygen-containing groups present in GO and water can explain this behaviour. The contact angle of poly(lactic co glycolic acid) (PLGA) is also decreased in the addition of GO³³. The hydrophilicity of PLLA³¹ is increased on the addition of CQ crude extract. The contact angle of PCL also decreased drastically on the addition of CQ²³. The super-hydrophilic nature observed with rGO Ti and GO Ti alloys films, the water droplets on contact with the surfaces, disappear and infiltrate inside the samples completely¹².

Table 6.2: Properties of scaffolds. The contact angle and mechanical properties are mentioned in the table.

Sl. No	Type of Scaffolds	Contact angle (Mean \pm SD)	Nature of Scaffolds	Tensile strength (MPa) (Mean \pm SD)	Yield strength (MPa) (Mean \pm SD)
1	PCL	126.5 \pm 0.28	Hydrophobic	0.85 \pm 0.11	0.46 \pm 0.01
2	PCL-GO	55.6 \pm 0.72	Hydrophilic	1.72 \pm 0.02	0.53 \pm 0.01
3	PCL-GO-CQ	47.6 \pm 0.72	Hydrophilic	2.84 \pm 0.01	1.00 \pm 0.01
4	PCL-GP	68.1 \pm 0.95	Hydrophilic	1.63 \pm 0.03	0.81 \pm 0.01
5	PCL-GP-CQ	51.6 \pm 0.72	Hydrophilic	2.44 \pm 0.03	1.04 \pm 0.01

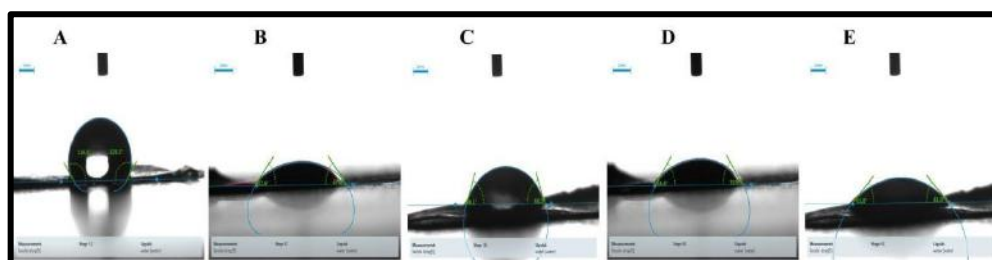


Figure 6.6: The water contact angle of scaffolds. A: PCL; B: PCL-GO; C: PCL-GO-CQ; D: PCL-GP; E: PCL-GP-CQ

6.2.2.4 Mechanical Properties:

Tensile strength and yield strength of scaffolds have shown in Table 6.2. Both Tensile strength and Yield strength of scaffolds have increased with the addition of GP and CQ into the PCL sheets (in PCL-GP-CQ scaffold) and the addition of GO and CQ into the PCL sheets (in PCL-GO-CQ scaffold) increased the mechanical strength of scaffolds. The PCL-GO-CQ scaffolds show highest tensile strength and yield strength as compared to other scaffolds. The painted composite scaffolds PCL-GO, PCL-GO-CQ and PCL-GP, PCL-GP-CQ have showed increased tensile strength and yield strength as

compared to PCL alone (Table 6.2). The increase of GO, GP and CQ concentration in the respective scaffolds increases the tensile strength and yield strength of the scaffolds has been also previously documented.

The tensile strength of PCL-PMMA increased from 101 MPa to 137 MPa on the addition of GO²⁹. The tensile strength of PCL nanofibers also improved from 0.79 MPa to 2.92 MPa by addition of CQ²³. The mechanical properties of GP-chitosan are higher than chitosan alone¹⁰. The scaffolds with higher mechanical strength support cell-based bone regeneration via an endochondral ossification⁴⁰. The scaffolds should be mechanically stable so that will retain its structure after *in vivo* implantation in load-bearing tissues such as bones^{4,41}. Therefore, the mechanical properties of implanted scaffolds should be comparable with the native tissue^{42,43}.

6.2.3 Isolation and Culture of hUCMSCs:

The hUCMSCs (Figure 6.9) are successfully isolated from human umbilical cord Wharton's Jelly with a mixture of enzymes Collagenase Type IV and Dispase (7:1v/v) and Trypsin-EDTA. The morphology of hUCMSCs exhibits spindle-shaped fibroblast-like morphology. These cells used for further *in vitro* studies.

6.2.4 In Vitro Studies:

6.2.4.1 MTT Cell Proliferation Assay:

The proliferation of hUCMSCs on different scaffolds is evaluated by MTT assay at different time point 1st, 4th, and 7th day. From (Figure 6.8) it is evident that the proliferation of the cells, as determined from the absorbance, increases from day 1 to day 7 for all substrates. This shows the proficiency of all the scaffolds to support the proliferation of hUCMSCs. Cell proliferation on all the modified scaffolds is higher as compared to control. Cell proliferation on PCL-GO-CQ is highest as compared to other scaffolds. The presence of GO on the surface has improved hydrophilicity which is required for the cell adhesion and protein adsorption. The vitronectin and fibronectin protein adhesion are increased in hydrophilic surfaces. Also, similar results are found in the PLA/GO and PLA/GNP (graphene nano-platelets).

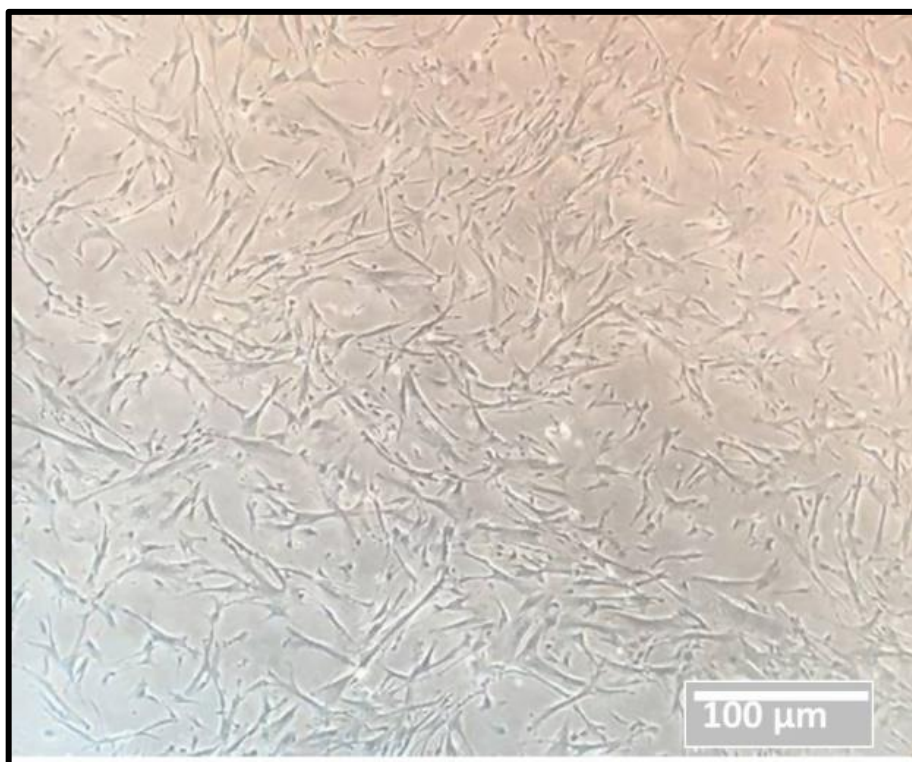


Figure 6.7: Isolated human umbilical cord Wharton's Jelly mesenchymal stem cells (hUCMSCs). Scale bar 100μm

There is significantly higher MG 63 cell proliferation on GO and GNP containing PLA scaffolds³⁹. Similarly, human osteosarcoma cells (HOS) have showed good biocompatibility on Poly(1,4-butylene adipate-co-polycaprolactam) (PBA)-PCL blended with HA⁷. The MTT assay have showed that there is an equivalent growth of cells on GP coated substrates like that of a like glass slide or Si/SiO₂²⁸. The PCL-CQ scaffolds have showed good growth and proliferation of human fetal osteoblast cells (hFOB) compared to PCL alone²³. The GP-Chitosan films have showed good biocompatibility with L929 cell lines. There is no visible reduction in viability after 24 and 48 hrs of MTT study¹⁰. The MG63 cells seeded on PCL-PMMA-GO have showed no cytotoxicity over a period of 1 to 7 days. There is an improvement in cell viability as compared to PCL-PMMA films²⁹. The MSCs cultured on calcium phosphate and biphasic calcium phosphate have showed viability with MTT assay through day 3 and day 7⁴⁴.

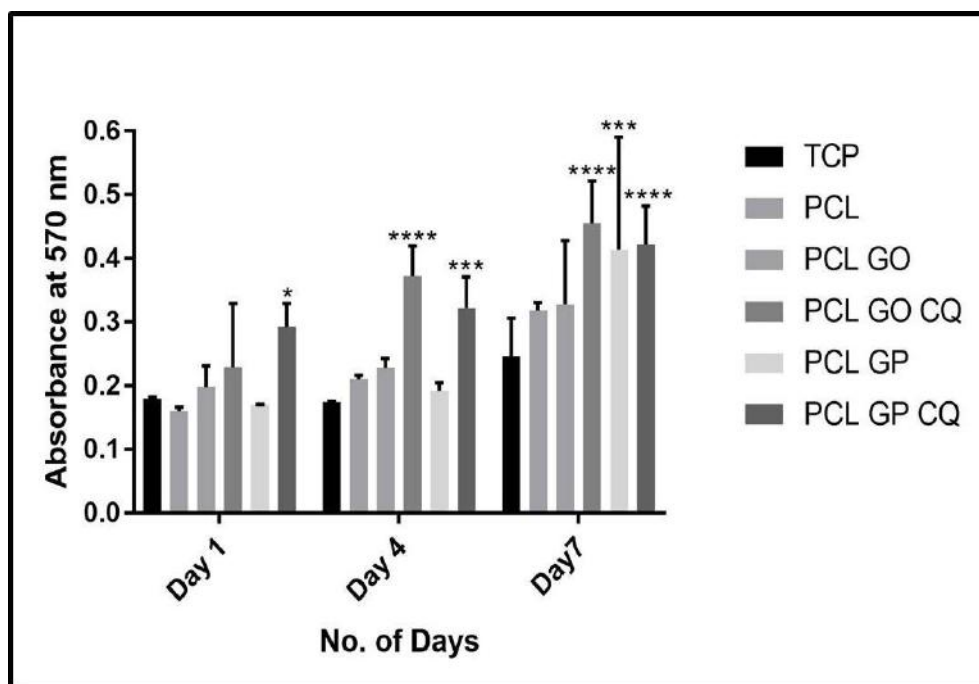


Figure 6.8: The cell viability and proliferation of hUCMSCs on the scaffolds for 1, 4, and 7 days of culture studied with MTT assay (p < 0.01, ***p < 0.001).**

6.2.4.2 Cell Adhesion study:

The cells on the scaffolds appear after 24 hrs of culture days (Figure 6.9). The cells are attached on the PCL-GO, and PCL-GO-CQ, PCL-GP, PCL-GP-CQ scaffolds. The morphology of the cells is fibroidal in nature. The filopodia of the cells are attached to the surface of the scaffold. The rough surface and hydrophilic nature of scaffolds have contributed to the good attachment and spreading of cells on the surfaces.

Alike results are analysed by various researchers. The hFOB cells cuboidal osteoblast-like morphology with filopodia and bridging each other with the extracellular matrix, also there is the formation of a mineral particle on cell surfaces after 10 and 15 days of culture²³. HOS cells have showed flat morphologies as adherence and spread on (PBA)-PCL blended with HA scaffolds⁷. BMSCs cultured on GP-Co-Cr-Mo, there is an increase in cells with increasing time of culture. The appearance of the BMSCs is flat and polygonal, ovoid or fusiform and displayed many cytoplasmic lamellipodia. On days 3 and 5, cells are colonized more densely¹¹. The MG63 cells seeded on PCL-PMMA-GO have showed well anchored and cells spread after 7 days of culture. The quick interaction

due to nanoroughness has a favourable impact on cell attachment, cell survival and proliferation²⁹.

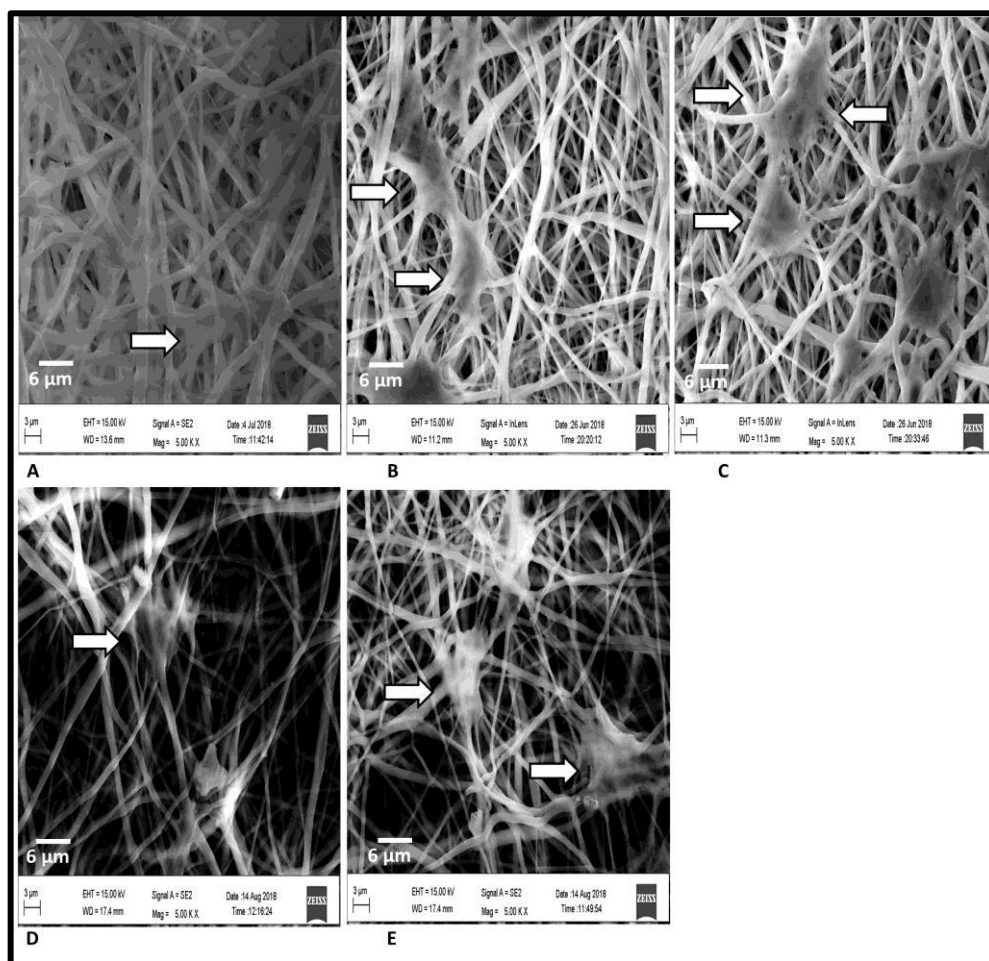


Figure 6.9: The FESEM images of cell attachment with Scaffolds. A: PCL; B: PCL-GO; C: PCL-GO-CQ; D: PCL-GP; E: PCL-GP-CQ;(Arrow showing cell attachment with fibers), Scale bar 3μm

6.2.4.3 Confocal microscopy imaging:

Cell-seeded scaffolds incubated for 1, 4 and 7 days are also stained with DAPI for nuclear visualization shown in (Figure 6.10). The cells are in a progressive manner from 1st day to 7th day of culture. The Z stack images show the cell attachment and cell movement deep into the scaffold and not only on the surface. Cell count with ImageJ software show that on 1st, 4th and 7th day no. of cells on PCL (884, 2683, 2773), PCL-GO (223, 474, 2933), and PCL-GO-CQ (247, 274, 3194), PCL-GP (138, 382, 1793), and PCL-GP-CQ (134, 186, 2081) are respectively.

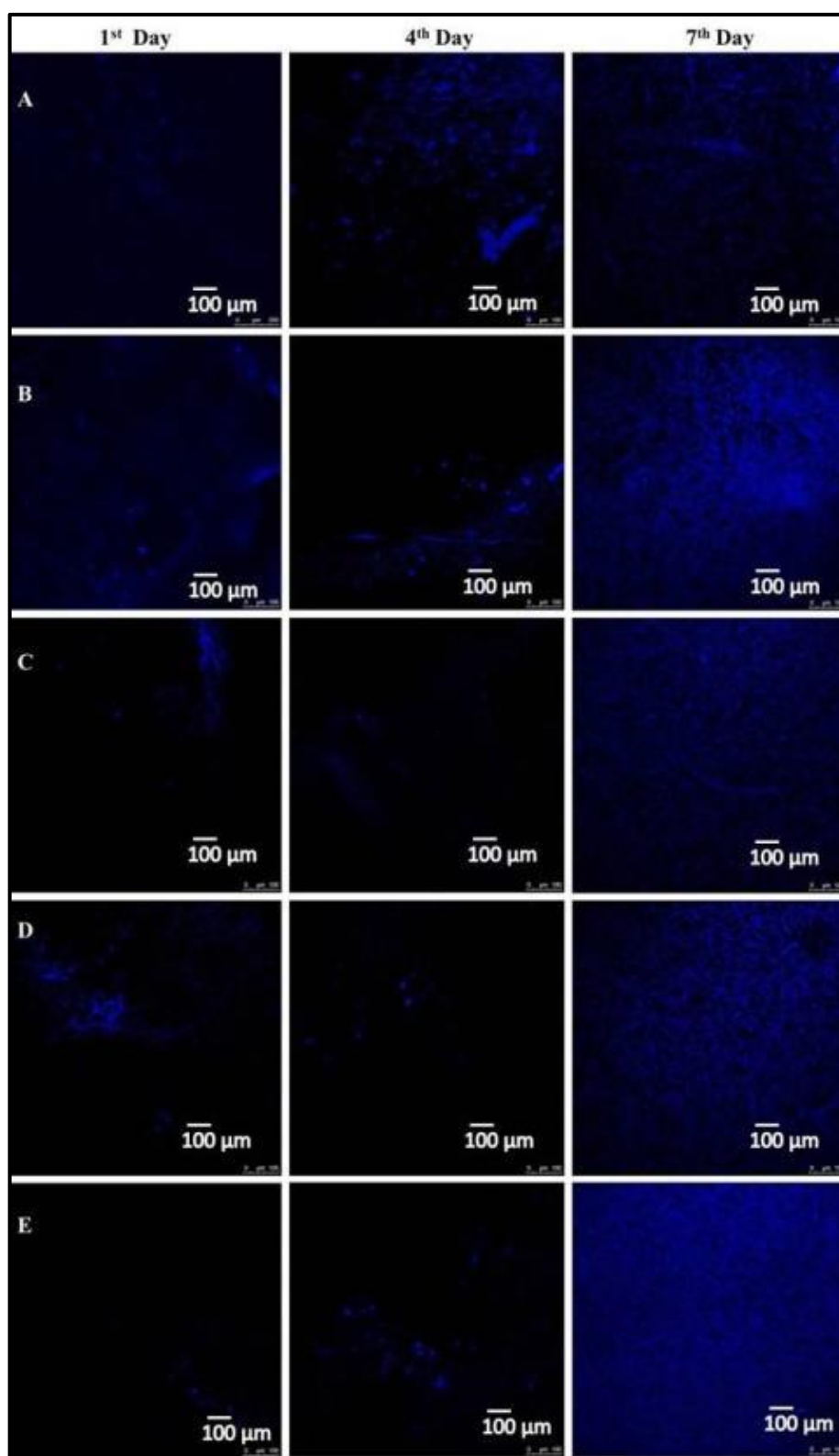


Figure 6.10: Confocal microscopy imaging from 1st day to 7th day of culture.
A: PCL; B: PCL-GO; C: PCL-GO-CQ; D: PCL-GP; E: PCL-GP-CQ; Scale bar
100μm

It shows the good proliferation and penetration of cells on these scaffolds. All the composite scaffolds show the highest cell proliferation on the 7th day as compared to PCL scaffolds. The PCL-GO-CQ followed by PCL-GP-CQ scaffolds show the highest cell proliferation. It again shows the resemblance with the cell viability and cell attachment of the cells on these scaffolds. The rough surface and hydrophilic nature of scaffolds have contributed to the proliferation of cells. They allow absorption of fibronectin which is important in osteoblast adhesion *in vitro*^{45,38} and promotes cell attachment on the surfaces of composites and osteoblast proliferation, differentiation. They also have a positive effect on bioactivity, water uptake and cytocompatibility of the composites²⁶. There is a higher density of blue stained nuclei on GP and GO films compared to PDMS (polydimethylsiloxane) or Si/SiO₂⁴⁶. The MG63 cells seeded on PCL-PMMA-GO have showed good attachment and proliferation on DAPI staining of cell nuclei²⁹. HOS cells also have showed adherence and high density on (PBA)-PCL blended with HA scaffolds via nuclei staining⁷. The BMSCs culture on rGOTi and GOTi films have showed better cell adhesion and spreading after 24 hrs of DAPI staining¹².

6.2.4.4 Osteoblastic Differentiation:

6.2.4.4.1 Alizarin Red S staining for calcium:

Alizarin Red S staining is used to evaluate calcium deposits in differentiated cells. There is a red-orange complex formed with Alizarin Red S staining shows the presence of secreted mineralization. The differentiation of hUCMSCs into osteoblasts is observed from 14 days onwards. There is mineralization on PCL-GO, PCL-GO-CQ, PCL-GP, PCL-GP-CQ scaffolds after 21 days of culture. The maximum differentiation of hUCMSCs into osteoblasts is confirmed after 21 days of culture on the modified scaffolds of PCL-GO-CQ. These results indicate that the synergistic effect of GO and CQ extract could enhance the expression of the osteogenic differentiation markers and can stimulate calcium deposition (Figure 6.11 and Figure 6.12). The hUCMSCs differentiated on the scaffolds (Figure 6.11.A to E) without an osteogenic medium is comparable with that to the control tissue culture plate (Figure 6.11.F) with the osteogenic medium. The least mineralization is on the PCL scaffolds without an osteogenic medium. These results suggest that these scaffolds have great potential for osteogenic differentiation of

hUCMSCs. Also, there is a higher amount of mineralization on PCL-GO-CQ and PCL-GP-CQ scaffold. There is increased activity on PCL-GO-CQ scaffolds as compared to

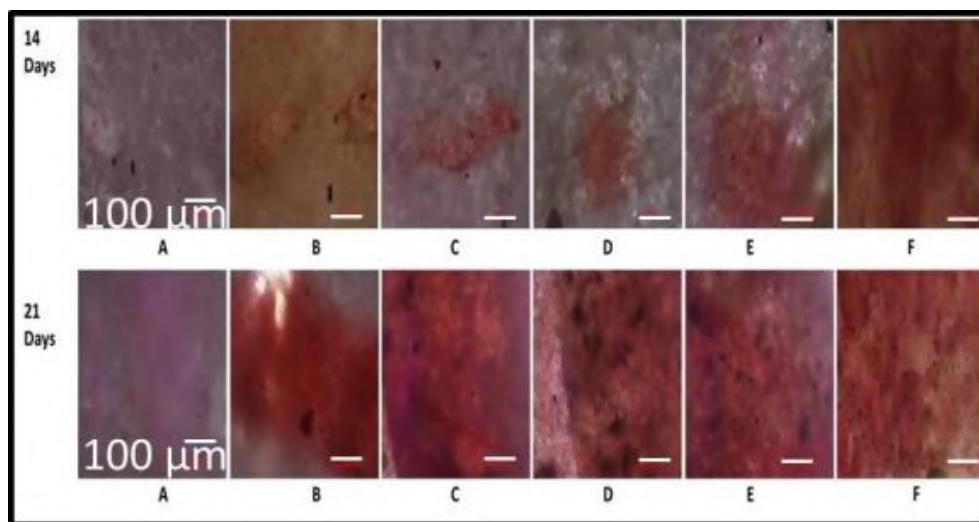


Figure 6.11: Alizarin Red S staining of Paint scaffolds after 14 days and 21 days of differentiation of hUCMSCs. A: PCL; B: PCL-GO; C: PCL-GO-CQ; D: PCL-GP; E: PCL-GP-CQ; (A to E: without Osteoblastic differentiation medium); F: Tissue culture plate. Scale bar 100μm

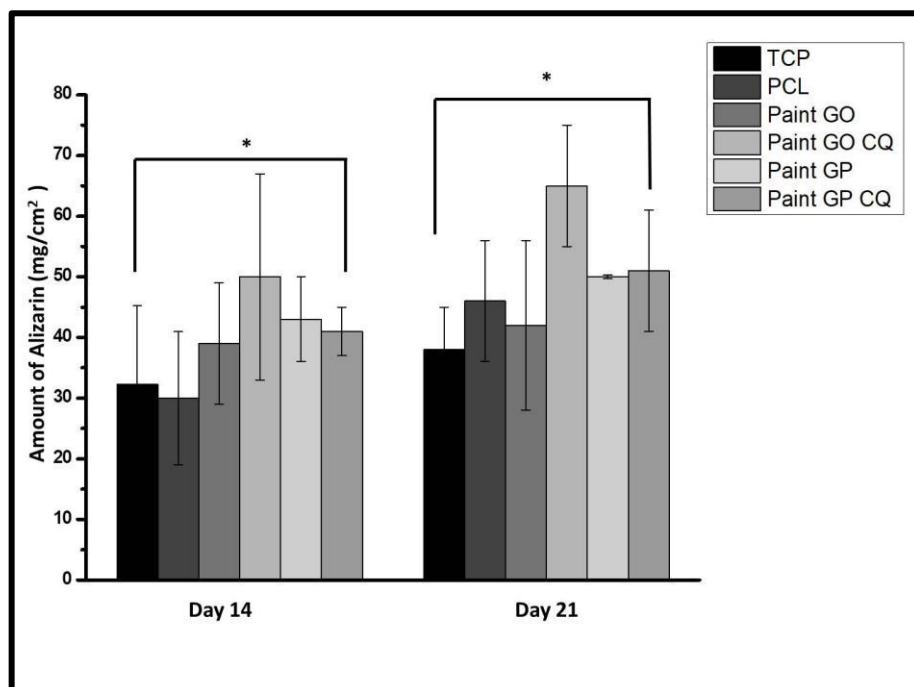


Figure 6.12: Alizarin Red S staining quantification of Paint scaffolds after 14 days and 21 days of differentiation of hUCMSCs (*p< 0.05).

PCL-GP-CQ scaffolds. Alizarin Red S staining confirmed calcium deposition due to the osteoblastic differentiation of hUCMSCs after 21 days on the PCL GO CQ scaffolds (Figure 6.11, 6.12). It may be due to the secretion of osteocalcin by differentiated osteoblasts. Osteocalcin plays an important role in bone metabolic activities and bone building²³. It shows PCL-GO-CQ scaffolds as the potential bone regenerative scaffold.

The Alizarin red S staining and Von kossa staining for detection of mineralization are used by various researchers as differentiation of dental pulp stem cell osteogenic differentiation on fluorapatite modified PCL fibres⁴⁷. The PLLA-CQ scaffolds also have showed mineralization with simulated body fluid/(SBF) after 14 days of incubation with Alizarin Red S staining³¹. The human fetal osteoblast cells also have showed the good intensity of mineralization on CQ containing scaffolds on the 15th day of culture²³. The GP proved as the alternative to BMP-2 (Bone morphogenic growth factor-2) as GP have showed the equivalent amount of hMSCs differentiation into osteoblastic cells, with a significant amount of osteocalcin secretion on the 15th day as that of BMP-2 in the presence of osteogenic media²⁸. Also, GP and GO have showed differentiation of MSCs into osteoblasts by mineralization on the 12th day in the presence of osteogenic media. It also reported higher osteoblastic differentiation potential of GP due to its ability to preconcentrate dexamethasone and β -glycerophosphate⁴⁶. The BMPs are assessed for an osteoinduction of MSCs for 21 days of culture. There is significant mineralization and bone nodules formation when MSCs cultured with a combination of BMP-2+BMP-6+BMP-9, confirmed by ARS staining⁴⁸. MC3T3-E1 cells seeded on PCL-rGO-Cu have showed mineralization on the 14th day in the presence of osteogenic media¹⁷.

6.2.4.4.2 Von Kossa staining for calcium:

The Von Kossa staining is also used to evaluate secreted calcium deposits in differentiated cells (Figure 6.13). The appearance of black precipitates confirms the positive Von Kossa staining with secreted mineral deposition. The black precipitates are observed from 14 days onwards and are maximum and broad after 21 days of culture on the modified scaffolds of PCL-GO-CQ as compared to other scaffolds. The hUCMSCs differentiated on the scaffolds (Figure 6.13.A to E) without osteogenic medium are comparable with that to the control tissue culture plate (Figure 6.13.F) with an osteogenic medium. The least mineralization is on the PCL scaffolds without an osteogenic medium.

The similar results as that of Alizarin Red S staining confirm the differentiation of hUCMSCs into osteoblasts.

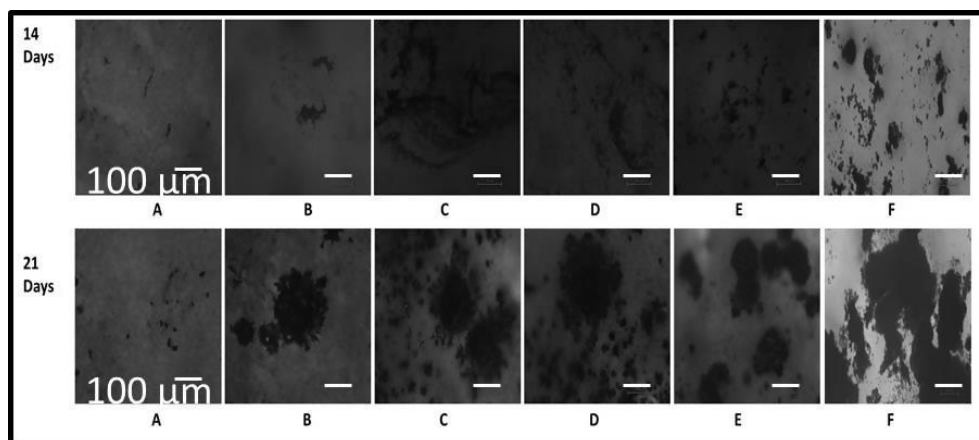


Figure 6.13: Von Kossa staining after 14 days and 21 days of differentiation of hUCMSCs. A: PCL; B: PCL-GO; C: PCL-GO-CQ; D: PCL-GP; E: PCL-GP-CQ; (A to E: without Osteoblastic differentiation medium); F: Tissue culture plate with Osteoblastic differentiation. Scale bar 100μm

Similar results are observed when MSCs cultured on biphasic calcium phosphate, calcium phosphate in the presence of conditioned medium containing significant growth factors, mineralization is observed with positive Von kossa staining on 21 days of culture⁴⁴. The Von kossa staining is used to evaluate the osteoblastic differentiation of MSCs through mineralization. After up to 24 days of culture of MSCs into osteoblastic induction medium, there is mineralization from 14 days onwards in an increasing manner, as confirmed by Von kossa staining⁴⁹. The BMPs are assessed for an osteoinduction of MSCs for 21 days of culture. There is significant mineralization and bone nodules formation when MSCs cultured with a combination of BMP-2+BMP-6+ BMP-9, confirmed by Von kossa staining⁴⁸. The Fetal rat calvariae (FRC) cells are cultured on osteoblastic medium have showed mineralization or bone nodules formation on day 14, as confirmed by Von kossa staining⁵⁰.

6.3 Conclusions:

The PCL, PCL-GO, PCL-GO-CQ and PCL-GP, PCL-GP-CQ scaffolds are prepared by the paint method, of which PCL-GO-CQ and PCL-GP-CQ scaffolds show promising

results. The PCL-GO-CQ scaffolds show higher biocompatibility, with higher roughness, hydrophilic nature and mechanically stable character as compared to PCL-GP-CQ and other scaffolds. These improved characteristics could be due to the synergistic effect of GO and CQ that helped the hUCMSCs to adhere, spread, proliferates and differentiates into osteoblast-like cells. Mainly GO and CQ callus extract provided osteoinductive properties to scaffold that helps hUCMSCs to spontaneously differentiate into osteoblast without any osteogenic media or growth factors or added external stimuli. This property will help the scaffold in speedy *in vivo* bone formation upon transplantation, thus saving *in vitro* differentiation time before transplantation. Thus, the novel PCL-GO-CQ scaffolds which is prepared using the paint method shows tremendous potential for *in vivo* bone tissue engineering and further studies to regenerate bone tissues.

References:

- 1 A. R. Shrivats, P. Alvarez, L. Schutte and J. O. Hollinger, in *Principles of Tissue Engineering*:, Elsevier, 4th edn., 2013, pp. 1201–1221.
- 2 J. E. L. Buddy D. Ratner, Allan S. Hoffman, Frederick J. Schoen, in *Biomaterials science: an introduction to materials in medicine.*, Elsevier Inc, 1996, pp. 415–455.
- 3 F. J. O’Brien, *Mater. Today*, 2011, **14**, 88–95.
- 4 S. Yang, K. F. Leong, Z. Du and C. K. Chua, *Tissue Eng.*, 2001, **7**, 679–689.
- 5 B. Chuenjitkuntaworn, T. Osathanon, N. Nowwarote, P. Supaphol and P. Pavasant, *J Biomed Mater Res Part A*, 2015, **104**, 264–271.
- 6 K. Ren, Y. Wang, T. Sun, W. Yue and H. Zhang, *Mater. Sci. Eng. C*, 2017, **78**, 324–332.
- 7 V. Y. Chakrapani, T. S. S. Kumar, D. K. Raj and T. V Kumary, *J. Nanosci. Nanotechnol.*, 2017, **17**, 2320–2328.
- 8 Y. J. Son, H. S. Kim and H. S. Yoo, *RSC Adv.*, 2016, **6**, 114061–114068.
- 9 P. Yu, R. Y. Bao, X. J. Shi, W. Yang and M. B. Yang, *Carbohydr. Polym.*, 2017, **155**, 507–515.
- 10 H. Fan, L. Wang, K. Zhao, N. Li, Z. Shi, Z. Ge and Z. Jin, *Biomacromolecules*, 2010, **11**, 2345–2351.
- 11 Q. Zhang, K. Li, J. Yan, Z. Wang, Q. Wu, L. Bi, M. Yang, K. Li, J. Yan, Z. Wang, Q. Wu, L. Bi, M. Yang and Y. Han, *Biochem. Biophys. Res. Commun.*, 2018, **497**, 1011–1017.
- 12 J. Qiu, J. Guo, H. Geng, W. Qian and X. Liu, *Carbon N. Y.*, 2017, **125**, 227–235.
- 13 Y. Luo, H. Shen, Y. Fang, Y. Cao, J. Huang, M. Zhang, J. Dai, X. Shi and Z. Zhang, *ACS Appl. Mater. Interfaces*, 2015, **7**, 6331–6339.

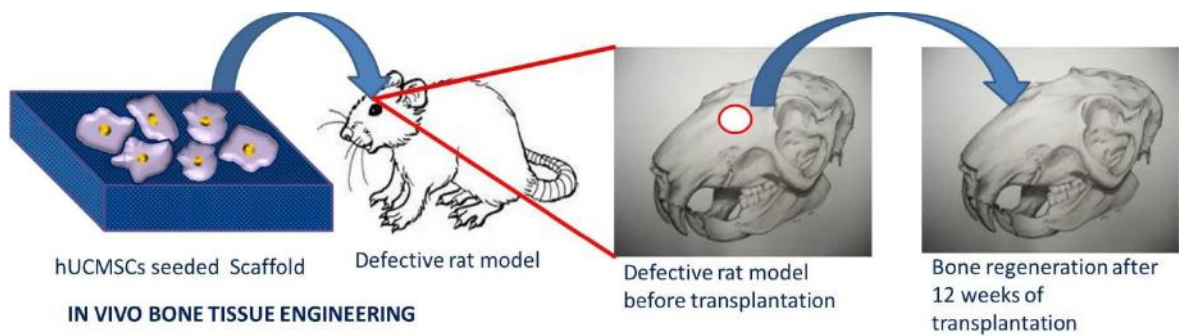
-
- 14 T. Kaur, A. Thirugnanam and K. Pramanik, *Mater. Today Commun.*, 2017, **12**, 34–42.
 - 15 H. Ma, W. Su, Z. Tai, D. Sun, X. Yan, B. Liu and Q. Xue, *Chinese Sci. Bull.*, 2012, **57**, 3051–3058.
 - 16 W. Qi, W. Yuan, J. Yan and H. Wang, *J. Mater. Chem. B*, 2014, **2**, 5461–5467.
 - 17 L. R. Jaidev, S. Kumar and K. Chatterjee, *Colloids Surfaces B Biointerfaces*, 2017, **159**, 293–302.
 - 18 A. Siddiqua and S. Mittapally, *Int. Res. J. Pharm. Biosci.*, 2017, **4**, 9–29.
 - 19 M. S. Rao, P. Bhagath Kumar, V. B. Narayana Swamy and N. Gopalan Kutty, *Pharmacologyonline*, 2007, **3**, 190–202.
 - 20 B. K. Potu, M. S. Rao, N. G. Kutty, K. M. R. Bhat, M. R. Chamallamudi and S. R. Nayak, *Clinics (Sao Paulo)*, 2008, **63**, 815–820.
 - 21 N. Singh, V. Singh, R. Singh, A. Pant, U. Pal, L. Malkunje and G. Mehta, *Natl. J. Maxillofac. Surg.*, 2013, **4**, 52–56.
 - 22 D. K. Deka, L. C. Lahon, A. Saikia and Mukit, *Indian J Pharmacol*, 1994, **26**, 44–45.
 - 23 S. Suganya, J. Venugopal, S. Ramakrishna, B. S. Lakshmi and V. R. Giri Dev, *J. Appl. Polym. Sci.*, 2014, **131**, 1–11.
 - 24 P. Garg and C. P. Malik, *Int. J. Pharm. Clin. Res.*, 2012, **4**, 4–10.
 - 25 P. S. R Mehta, K Teware, *Int. J. Ayurvedic Herb. Med.*, 2012, **2**, 229–233.
 - 26 S. K. Misra, T. Ansari, D. Mohn, S. P. Valappil, T. J. Brunner, W. J. Stark, I. Roy, J. C. Knowles, P. D. Sibbons, E. V. Jones, A. R. Boccaccini and V. Salih, *J. R. Soc. Interface*, 2010, **7**, 453–465.
 - 27 X. He, L. L. Wu, J. J. Wang, T. Zhang, H. Sun and N. Shuai, *High Perform. Polym.*, 2015, **27**, 318–325.
-

-
- 28 T. R. Nayak, H. Andersen, V. S. Makam, C. Khaw, S. Bae, X. Xu, P.-L. R. Ee, J.-H. Ahn, B. H. Hong, G. Pastorin and B. Özyilmaz, *ACS Nano*, 2011, **5**, 4670–4678.
- 29 F. Pahlevanzadeh and E. Hamzah, *J. Mech. Behav. Biomed. Mater.*, 2018, **82**, 257–267.
- 30 A. Oyefusi, O. Olanipekun, G. M. Neelgund, D. Peterson, J. M. Stone, E. Williams, L. Carson, G. Regisford, A. Oki, J. Qiu, J. Guo, H. Geng, W. Qian, X. Liu, L. R. Jaidev, S. Kumar, K. Chatterjee, K. Fujita, S. Take, R. Tani, J. Maru, S. Obara, S. Endoh, H. Elkhenany, S. Bourdo, S. Hecht, R. Donnell, D. Gerard, R. Abdelwahed, A. Lafont, K. Alghazali, F. Watanabe, A. S. Biris, D. Anderson, M. Dhar, Q. Zhang, K. Li, J. Yan, Z. Wang, Q. Wu, L. Bi, M. Yang, Y. Han, E. Paz, F. Forriol, J. C. del Real, N. Dunne, F. Pahlevanzadeh, H. R. Bakhsheshi-Rad and E. Hamzah, *Biochem. Biophys. Res. Commun.*, 2017, **132**, 410–416.
- 31 K. Parvathi, A. G. Krishnan, A. Anitha, R. Jayakumar and M. B. Nair, *Int. J. Biol. Macromol.*, 2018, **110**, 514–521.
- 32 S. Chanda, Y. Baravalia and K. Nagani, *J. Pharmacogn. Phytochem.*, 2013, **2**, 149–157.
- 33 E. J. Lee, J. H. Lee, Y. C. Shin, D. Hwang, J. S. Kim, O. S. Jin, L. Jin, S. W. Hong and D. Han, *Biomater. Res.*, 2014, **18**, 18–24.
- 34 S. K. Bhullar, D. Rana, H. Lekesiz, A. C. Bedeloglu, J. Ko, Y. Cho, Z. Aytac, T. Uyar, M. Jun and M. Ramalingam, *Mater. Sci. Eng. C*, 2017, **81**, 334–340.
- 35 N. Abdullah, A. Hakim and M. Kubo, *ARPN J. Eng. Appl. Sci.*, 2016, **11**, 9582–9585.
- 36 Olivier Persenaire, Michaël Alexandre, A. Philippe Degée and P. Dubois†, *Biomacromolecules*, 2001, **2**, 288–294.
- 37 T. Zhou, G. Li, S. Lin, T. Tian, Q. Ma, Q. Zhang, S. Shi, C. Xue, W. Ma, X. Cai and Y. Lin, *ACS Appl. Mater. Interfaces*, 2017, **9**, 42589–42600.
-

-
- 38 M. Yang, S. Zhu, Y. Chen, Z. Chang, G. Chen, Y. Gong, N. Zhao and X. Zhang, *Biomaterials*, 2004, **25**, 1365–1373.
- 39 A. M. Pinto, S. Moreira, I. C. Gonçalves, F. M. Gama, A. M. Mendes and F. D. Magalhães, *Colloids Surfaces B Biointerfaces*, 2013, **104**, 229–238.
- 40 H. Sun, F. Zhu, Q. Hu and P. H. Krebsbach, *Biomaterials*, 2014, **35**, 1176–1184.
- 41 C. Y. Lin, N. Kikuchi and S. J. Hollister, *J. Biomech.*, 2004, **37**, 623–636.
- 42 M. Tarik Arafat, I. Gibson and X. Li, *Rapid Prototyp. J.*, 2014, **20**, 13–26.
- 43 J. Wang and X. Yu, *Acta Biomater.*, 2010, **6**, 3004–3012.
- 44 J. Wang, D. Liu, B. Guo, X. Yang, X. Chen, X. Zhu, Y. Fan and X. Zhang, *Acta Biomater.*, 2017, **51**, 447–460.
- 45 D. Deligianni, N. Katsala, S. Ladas, D. Sotiropoulou, J. Amedee and Y. Missirlis, *Biomaterials*, 2001, **22**, 1241–1251.
- 46 W. C. Lee, C. H. Y. X. Lim, H. Shi, L. A. L. Tang, Y. Wang, C. T. Lim and K. P. Loh, *ACS Nano*, 2011, **5**, 7334–7341.
- 47 T. Guo, G. Cao, Y. Li, Z. Zhang, J. E. Nör, B. H. Clarkson and J. Liu, *J. Dent. Res.*, 2018, **97**, 1331–1338.
- 48 Y. Açil, A. A. Ghoniem, J. Wiltfang and M. Gierloff, *J. Cranio-Maxillofacial Surg.*, 2014, **42**, 2002–2009.
- 49 P. S. Hung, Y. C. Kuo, H. G. Chen, H. H. K. Chiang and O. K. S. Lee, *PLoS One*, 2013, **8**, 1–7.
- 50 N. Yamamoto, K. Furuya and K. Hanada, *Biol. Pharm. Bull.*, 2002, **25**, 509–515.
-

CHAPTER 7:

IN VIVO BONE TISSUE ENGINEERING



7.1. Introduction:

The critical size calvarial bone defects and their repair is the major treatment challenge in orthopaedic surgery. A critical-sized segmental bone defect is defined as the smallest osseous defect in a particular bone and species of animal that will not heal spontaneously during the lifetime of the animal or shows less than 10% bony regeneration during the lifetime of the animal. These critical size defects are particularly problematic for severe trauma. It affects the quality of life of patients. It entails long and postoperative therapies expense and also causes large surgical, socio-economic problems^{1,2}.

Although Autografts and allografts are widely used for repair of osseous defects, their use is limited due to tissue availability, disease transmission, donor morbidity and high cost. Bone tissue engineering is emerging as the treatment of choice in the repair of bone defects with different combinations such as scaffolds, stem cells, and growth factors³.

The scaffolds are of great importance as they provide a temporary framework for cell adhesion, growth and their proliferation and differentiation. It assists in tissue repair. The various polymers like poly ϵ -caprolactone (PCL), poly-D, L-lactic acid (PDLLA)⁴, poly (L/DL-lactide) (PLDL)⁵, PLLA⁶, poly (DL-lactic-co-glycolic acid) (PLGA)⁷ shown to be potential with its properties like tensile strength, biocompatible, higher cellular properties and even bone formation in rat model³. The PCL is biocompatible, biodegradable and FDA approved material and used extensively in tissue engineering applications. PCL along with Hydroxyapatite (HA)⁸, PCL-gelatin hybrid nanofibrous membranes⁹, PCL-(Poly-1,4- butylene adipate-co-polycaprolactam (PBAPCL)- HA composite scaffold¹⁰, are used in bone tissue engineering. The graphene oxide (GO) has become the biomaterial of the 21st century as being potential of applications in electronics to biomedical applications and tissue engineering. The extravagant mechanical properties, biocompatibility and osteoinductive properties of GO would make them one of the most foreseen biomaterials in the regenerative medicine in coming years. *Cissus quadrangularis* (CQ) plant has immense medicinal potential with reported antimicrobial and antioxidant activity¹¹. Methanolic extract of CQ revealed the faster bone healing in the experimentally fractured radius-ulna of dog as well as complete bone healing as compared to an untreated group of dogs¹². The effective ingredients of CQ may

encourage proliferation and differentiation of MSCs into osteoblasts and bone tissue formation via wnt-LRp5- β -catenin or MAPK dependent pathway¹³. The results have showed that PCL-CQ-HA nano-fibrous scaffolds had appropriate surface roughness for the osteoblast adhesion, proliferation, and mineralization comparing with other scaffolds, making them potential biocompatible material for bone tissue engineering¹⁴.

Mesenchymal stem cells (MSCs) are known to differentiate into matured cells like osteoblasts, chondroblasts and chondrocytes on external stimuli (like the addition of ascorbic acid, β -glycerophosphate, dexamethasone)¹⁵. Bone marrow and peripheral blood are traditional sources for MSCs. MSCs isolated from peripheral blood of rabbit have been differentiated into osteoblasts, chondrocytes and healed critical-sized bone defects in rabbit models with the use of porous calcium phosphate resorbable substitute¹⁶. The transplantation of bone marrow-derived rat MSCs on electrospun nanofiber scaffolds poly ϵ -caprolactone (PCL) fibers have showed bone formation in rat model¹⁵.

We have used the PCL scaffolds prepared by electrospinning. These PCL sheets then modified by layer by layer method to prepare PCL-GO, PCL-GO-CQ scaffolds. These scaffolds are porous, rough in surface, hydrophilic in nature, and mechanically stable. The human umbilical cord-derived mesenchymal stem cells (hUCMSCs) adhere, spread, proliferate and differentiate into osteoblast-like cells without any osteogenic media or growth factors on the PCL-GO, PCL-GO-CQ scaffolds. These scaffolds are biocompatible and osteoinductive in nature.

The aim of this study is to evaluate the potential of the PCL, PCL- hUCMSCs, PCL-GO, PCL-GO-CQ, PCL-GO-CQ-hUCMSCs to heal critical size calvarial bone defect in the rat models. The *in vivo* bone tissue engineering is evaluated by creating critical size calvarial defect of 8mm in the rat skull. These calvarial bone defects are treated with these scaffolds for 6 weeks and 12 weeks. The new bone regeneration is analysed by digital radiography and micro CT.

7.2. Materials and Methods:

7.2.1 Animals and housing:

The animal experiments were executed with prior approval from Institutional Animal Ethics Committee of the National Institute for Research in Reproductive Health (NIRRH approval no. NIRRH/IAEC/11/18).

The animal study was carried out in acquiescence with the guiding principle of the Committee for the Purpose of Control and Supervision of Experimental Animals (CPCSEA), India. Six to eight-week-old healthy adult Wister female rats with average body weight (BW) of 270 ± 50 g were used in this study. All animals used in the Institute of NIRRH and were accommodated in polypropylene cages was monitored temperature of $23 \pm 1^{\circ}\text{C}$, the humidity of $55 \pm 5\%$ and 14 h light/10h dark cycle. Sterile paddy husk was used as bedding material that was replaced every week. During the study, soy-free, in house made pelleted forage and filtered drinking water ad libitum were given to the animals.

7. 2.2 Study design and surgical procedures:

Six different types of groups were studied such as Sham, PCL, PCL-hUCMSCs, PCL-GO, PCL-GO-CQ and PCL-GO-CQ-hUCMSCs. The scaffolds were implanted on the defect created sites over the period of 6 weeks and 12weeks. All the scaffolds were EtO sterilized and then seeded with hUCMSCs for 24 hours. The scaffolds then were washed with PBS to remove traces of culture medium. These scaffolds then implanted at defect sites. Animals were sedated by intraperitoneal injection with a combination of ketamine HCL (60 mg/kg, Intas pharma Ltd., India) and xylazine (7mg/kg, Themis Medicare Ltd., India). The site of the surgery was clean-shaven and sterilized with betadine (G.S. Pharmbutor Pvt. Ltd., India) and 70% ethanol after sedation of the animal. The soft tissue and periosteum were uplifted to reveal the calvarial surface on the sagittal suture line. On the sagittal suture line of parietal bones, the critical size bone defects (8mm diameter) were crafted with a trephine bur accompanying to a dental hand piece with the micro motor. To get rid of heat generation sterile saline was constantly irrigated during defect crafting. The utmost precaution was taken to avert damage to both the sagittal suture and the brain. The scaffolds were implanted into the defect site in

respective animal groups for 6 weeks and 12 weeks. The Sham group was kept empty without any scaffold. The pericranium and skin were sealed. After surgery, each rat was caged individually. These animals were examined for clinical indications and symptoms. The weights of animals before and after surgery (transplantation of scaffold) were taken before and after the surgery at 6 weeks and 12 weeks' time points. Also, the weight of essential organs was taken after the surgery at both 6 weeks and 12 weeks.

Table 7.1: Experimental Groups:

Sl. No.	Group name	6 Weeks	12 Weeks
1.	Sham	N= 5	N= 5
2.	PCL	N= 5	N= 5
3.	PCL-hUCMSCs	N= 5	N= 5
4.	PCL-GO	N= 5	N= 5
5.	PCL-GO-CQ	N= 5	N= 5
6.	PCL-GO-CQ-hUCMSCs	N= 5	N= 5



Figure 7.1: Operating rat during *In Vivo* Study

7.2.3 Blood Collection, Haematology and Serum Biochemistry:

The clinical pathology and examination were done for any inflammatory reactions after implantation of scaffolds, through a complete blood count (CBC). After 6 weeks and 12 weeks of transplantation, animals were bled from retro-orbital sinus and 1ml blood

was collected in two vials with and without heparin. The heparin (2IU/ml) containing vial was utilized for evaluation of haematological parameters like haemoglobin (Hb; g/dl), packed cell volume (PCV; %), total red cell count (RBC), total white cell count (WBC), absolute erythrocyte indices, differential WBC count. The other vial without heparin was utilized for evaluation of serum biochemistry parameters such as serum glutamic pyruvic transaminase (SGPT), serum glutamic oxaloacetic transaminase (SGOT), alkaline phosphatase (ALP), creatinine and urea. The concentrations of Osteocalcin (OCN) were measured using an enzyme-linked immunoassay kit (Invitrogen, USA). The coating buffer used to coat the microwell plate prior to addition of samples. The blocking buffer used to block the other active sites. The samples then incubated with primary antibody Antihuman Osteocalcin for one hour at room temperature and then HRP conjugated secondary antibody for one hour at room temperature. The substrate 3,3',5,5'-tetramethylbenzidine (TMB) added into each well and incubated for 30 minutes. The reaction is ended by adding stop solution. The absorbance was measured at 450 nm. The lower detection limit of the OCN concentrations was 1.0 ng/ml.

A differential WBC count (lymphocytes, monocytes, neutrophils, eosinophiles, and basophiles) was calculated morphologically by blood smears. CBC was performed using Abacus (Diatron MI PLC, Hungary) haematology analyser, while serum biochemistry evaluation was done on ERba Chem 7 (Erba Mannheim, Germany) semi-autoanalyzer using commercial reagent kits.

7.2.4 X-ray and micro-CT analysis:

Rat calvaria was harvested from rat skull and imaged using a digital X-ray machine at 30 kV and 3 mA for 1.5 min. Rat skulls after euthanasia were fixed in ethanol and washed before scanning on an animal micro-computed tomography (CT) scanner (FLEX Triumph micro-PET/SPECT/CT scanner, Gamma Medica-Ideas, USA) using an X-ray tube potential of 75 kV and a tube current of 100 μ A. The scanner equipped with an X-ray source and a detector system. It turns around a bed having the calvaria. The data was acquired over 360⁰ producing 1024 views. Each frame was exposed for 2000 milli sec. The total image acquisition was 45 min and images were reconstructed using a modified cone-beam algorithm with an isotropic voxel spacing of 0.045X 0.045 X 0.045 mm³ over a region of interest.

Furthermore, micro-CT scan was also performed on rat skulls isolated from the Sham control as the negative control. All the factors and circumstances were kept constant for all samples.

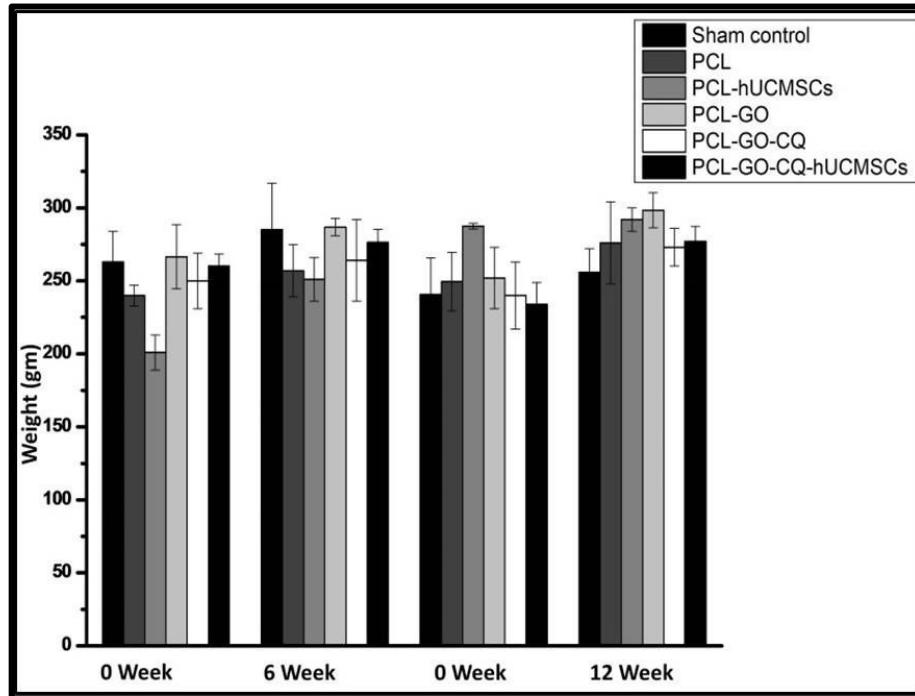


Figure 7.2: Animal weight before transplantation of scaffold (0 Week) and after transplantation of scaffold (6 Weeks and 12 Weeks). All animals have their weight in the normal range.

Bone Mineral Density (BMD): Bone quality analysis in terms of bone mineral density (mg/mm^2) was analysed using MicroView software to evaluate the quality of bone formed after 12 weeks of transplantation of scaffolds. The harvested calvaria was scanned for BMD in the region of interest (ROI). The normal calvaria was scanned to have BMD control values for comparison with test groups.

7.2.5 Histological Analysis:

Post-harvest, cranium samples were fixed in neutral buffered formalin (NBF) at 4°C for 48 hrs. The calvaria were decalcified in HCl for 3 weeks. These decalcified calvaria were processed and embedded in paraffin. The blocks were trimmed and sectioned with a microtome (Leica RM2156; Leica, Germany) equipped with a tungsten carbide knife. The

sections were stained with haematoxylin and eosin (H&E). The histological analysis of the bone tissues was performed using an optical microscope (Carl Zeiss, Germany).

7.3 Statistical Analysis:

Statistical analysis of data was evaluated by Origin Pro 8.5 software. Data were presented as the Mean \pm standard deviation. Statistical analysis was performed by using a one-way analysis of variance (ANOVA). A value ($p < 0.05$) was considered to be statistically different.

7.4. Results and Discussion:

7.4.1 Animal Weight and Organ weight:

The weights of animals before and after 6- or 12-weeks post-surgery (transplantation of scaffold) are in normal range with no significant weight loss (Figure 7.2). Also, the weight of essential organs i.e. Liver, Kidney, Heart, Spleen Lungs (Figure 7.3) and their respective relative (Rel) weights to the body weights (Figure 7.4) are in the normal range. The similar body weights, organ weights and their Rel weights are mentioned elsewhere¹⁷⁻¹⁹. The body weight, weight of essential organs and their respective Rel weight in the normal range show that there is no adverse effect of the transplanted scaffolds on these organs or on the animal itself.

7.4.2 Blood Collection, Haematology and Serum Biochemistry:

The blood haematological parameters are evaluated to assess any possible infections due to implantation of scaffolds in rat skull defects. CBCs and differential leukocytes counts among all the groups are within the normal range after 6 and 12 weeks (Figure 7.5, 7.6, 7.7, 7.8). This indicates that scaffold transplantation did not evoke an inflammatory response. The similar results are observed when poly (L-lactic acid)-hydroxyapatite- gelatin and poly (L-lactic acid)-hydroxyapatite scaffolds are implanted in critical size calvarial bone defects for 6 weeks and 10 weeks²⁰. Also there is no inflammatory reaction when PCL- hydroxyapatite and PCL-hardystonite scaffolds are implanted for 6 weeks and 12 weeks in rat calvarial defects²¹. Also, a similar range of haematological parameters are mentioned elsewhere¹⁸.

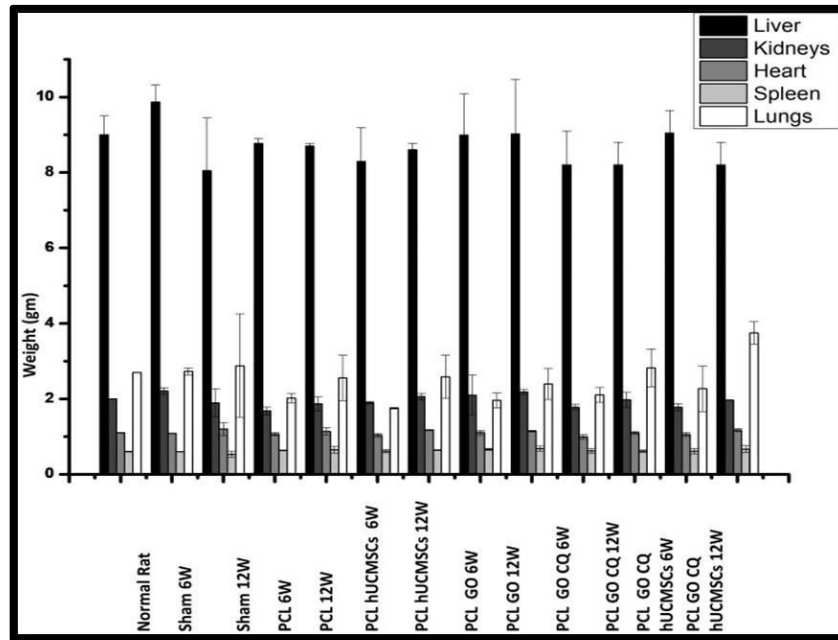


Figure7.3: Essential Animal organ weight after transplantation of scaffold (6 W (week) and 12 W (week)). All Essential organs of animals have their weight in the normal range. There is no significant difference among the groups ($p > 0.05$).

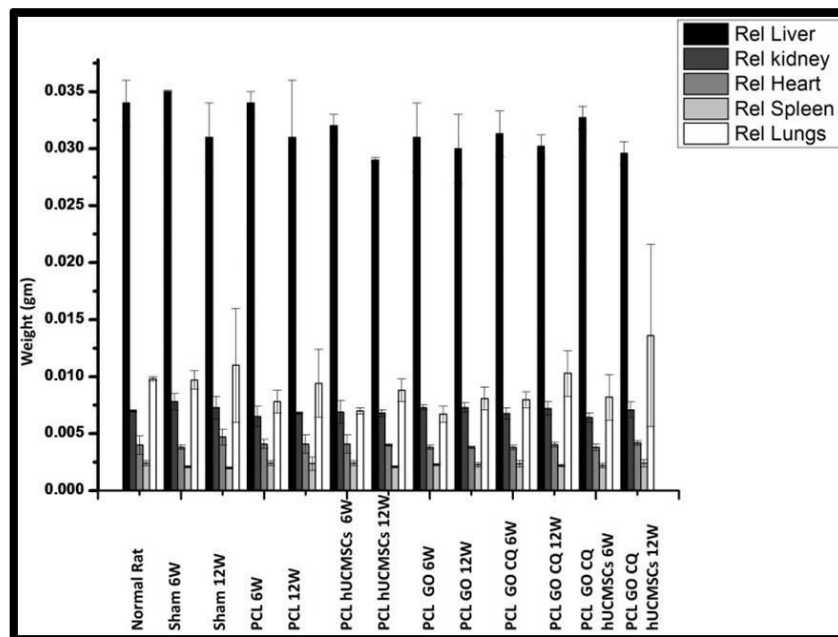


Figure7.4: Rel (Relative) weight of Essential organ after transplantation of scaffold (6 W (week) and 12 W (week)). All Rel weight of Essential organ of animals has their weight in the normal range. There is no significant difference among the groups ($p > 0.05$).

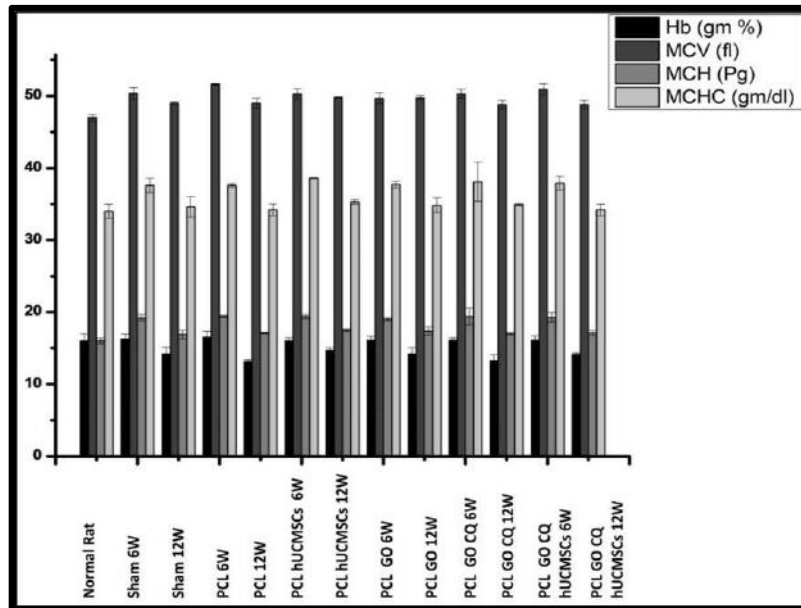


Figure 7.5: Hematological parameters of the samples collected before the sacrifice. Hb: Hemoglobin; MCV Mean Corpuscular Volume; MCH: Mean Corpuscular Hemoglobin; MCHC: Mean Corpuscular Hemoglobin Concentration. There is no significant difference among the groups ($p > 0.05$).

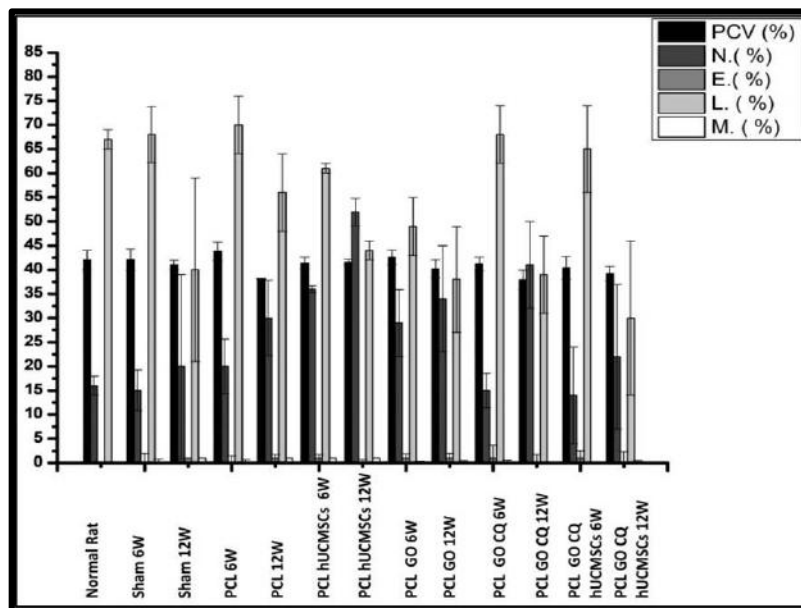


Figure 7.6: Hematological parameters of the samples collected before the sacrifice. PCV: Packed Cell Volume; N: Neutrophils; E: Eosinophils; L: Lymphocytes; M: Monocytes. There is no significant difference among the groups ($p > 0.05$).

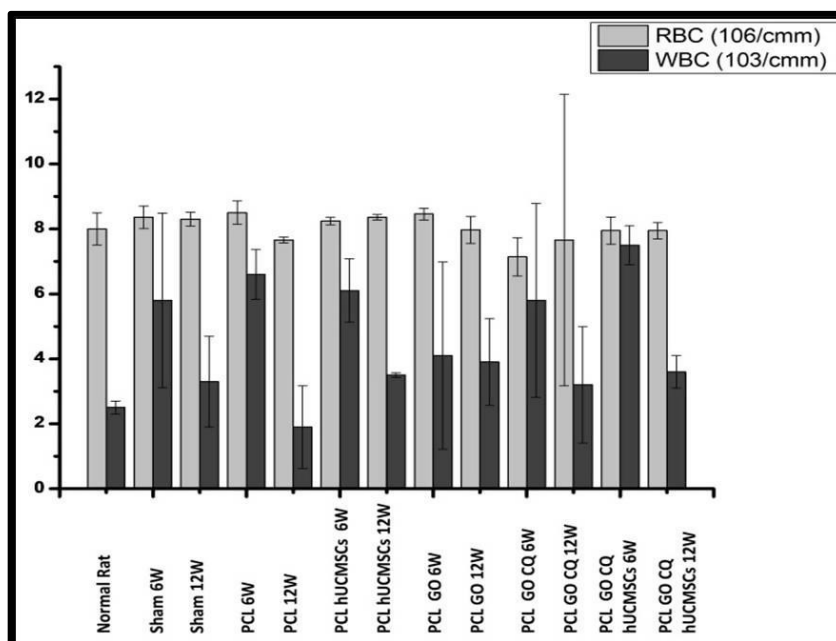


Figure 7.7: Hematological parameters of the samples collected before the sacrifice. RBC: Red Blood Cell; WBC: White Blood Cell. There is no significant difference among the groups ($p > 0.05$).

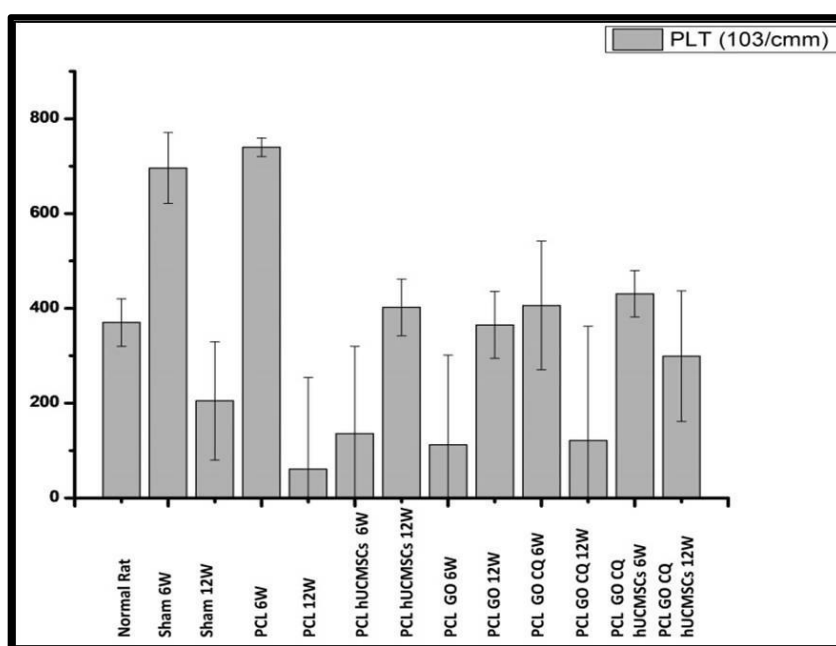


Figure 7.8 Hematological parameters of the samples collected before the sacrifice. PLT: Platelets. There is no significant difference among the groups ($p > 0.05$).

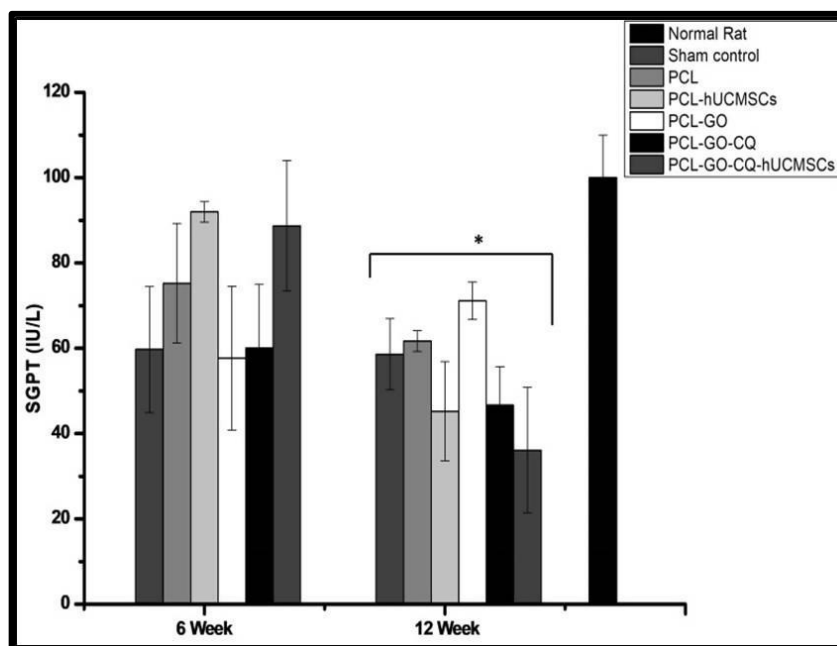


Figure 7.9: SGPT values described for 6 weeks and 12 weeks. SGPT values are in the normal range. There is a significant difference in 12 weeks among the groups ($p < 0.05$).

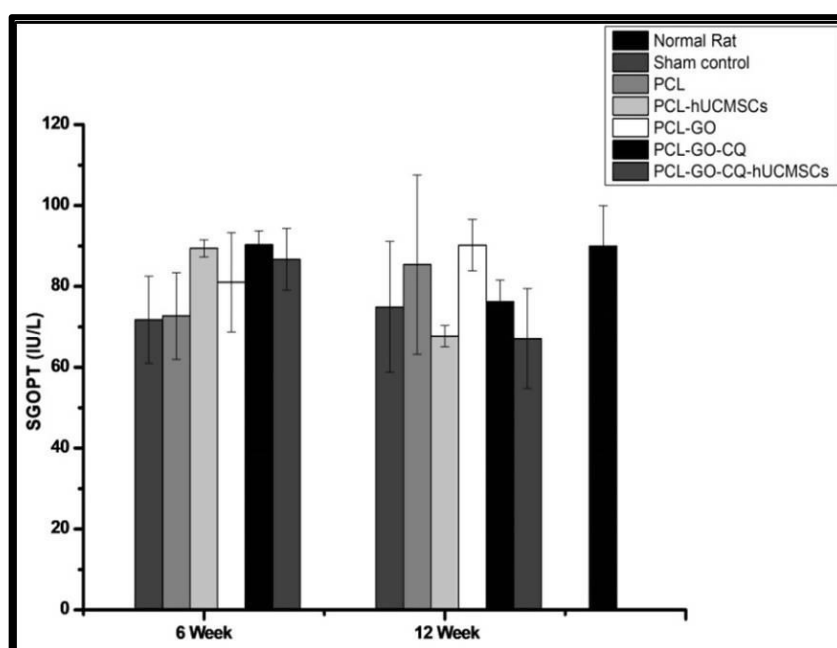


Figure 7.10: SGOPT values described for 6 weeks and 12 weeks. SGOPT values are in the normal range. There is no significant difference among the groups ($p > 0.05$).

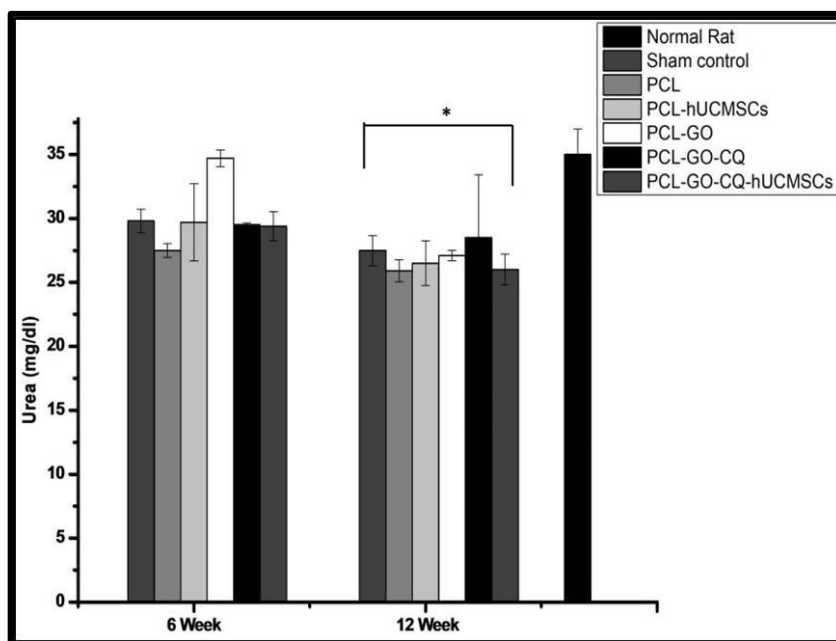


Figure 7.11: Urea values described for 6 weeks and 12 weeks. Urea values are in the normal range. There is a significant difference in 12 weeks among the groups ($p < 0.05$).

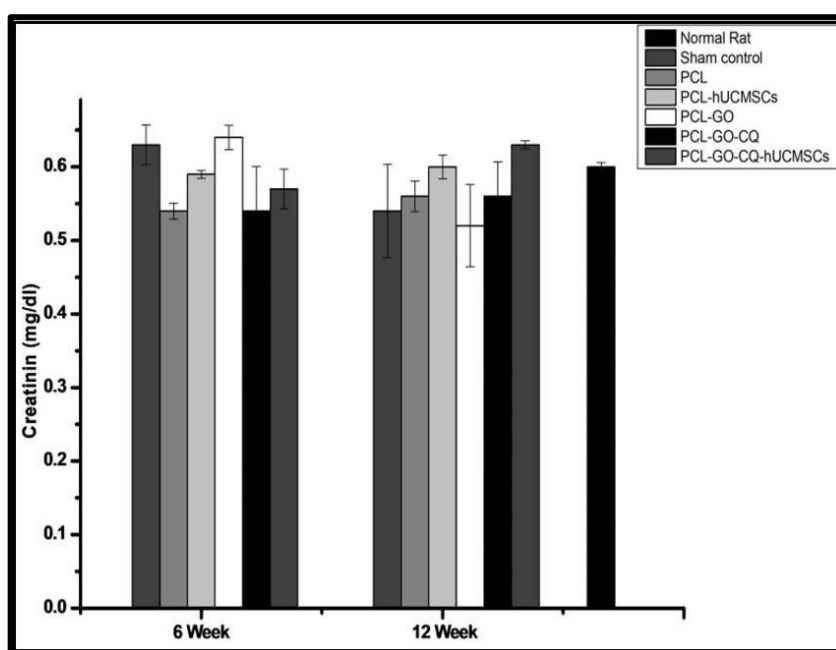


Figure 7.12: Creatinin values described for 6 weeks and 12 weeks. Creatinine values are in the normal range. There is a significant difference among the 6 weeks and 12 weeks group ($p < 0.05$).

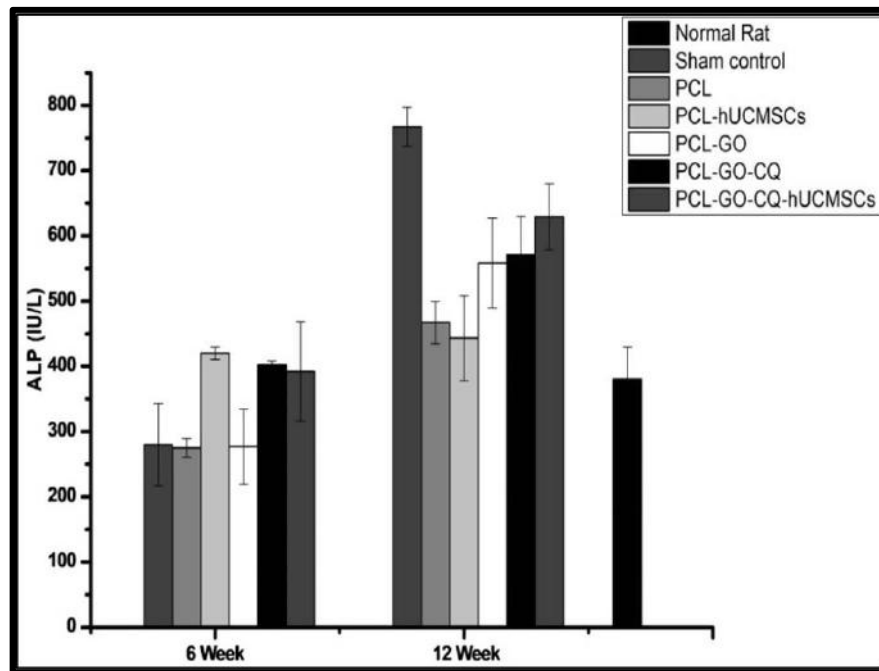


Figure 7.13: ALP values described for 6 weeks and 12 weeks. ALP values are in the normal range. There is no significant difference among the groups ($p > 0.05$).

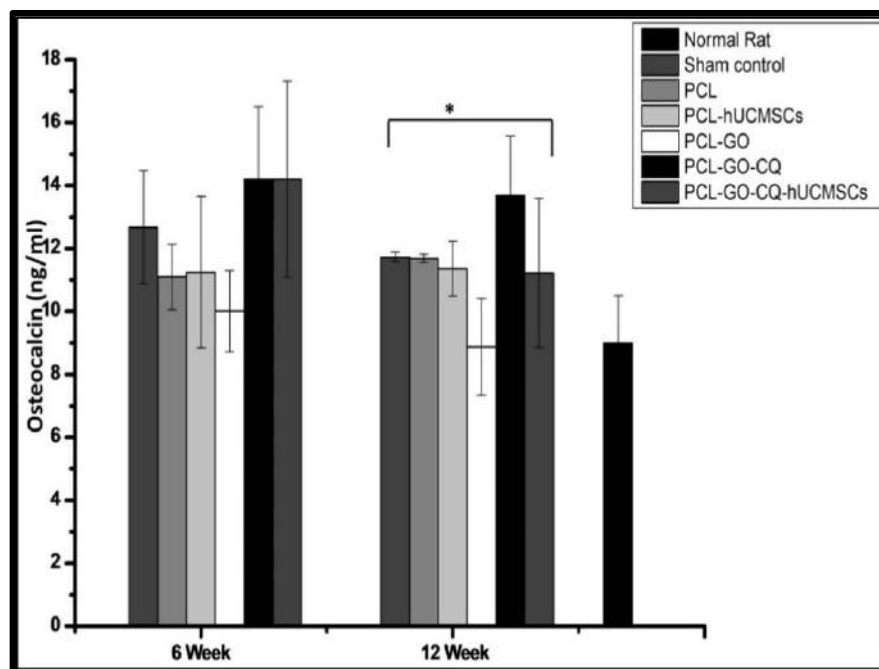


Figure 7.14: Osteocalcin (OCN) values described for 6 weeks and 12 weeks. OCN values are in the normal range. There is a significant difference among the 12-week groups ($p > 0.05$).

The biochemical parameters are examined to check the efficacy of essential organs of the animal body such as liver and kidney. In serum biochemistry liver enzymes SGPT (Figure. 7.9) and SGOT (Figure. 7.10) are found to be in the normal range. This signifies the proper working of the liver. Serum urea (Figure 7.11) and creatinin (Figure 7.12) levels among all the groups are within the normal range. This signifies the healthy state of the renal system. The similar results are observed when poly (L-lactic acid)-hydroxyapatite- gelatin and poly (L-lactic acid)-hydroxyapatite scaffolds are implanted in critical size calvarial bone defects for 6 weeks and 10 weeks²⁰. Also, a similar range of urea and creatinine levels are mentioned elsewhere^{18,19}. All the scaffolds are biocompatible and biodegradable. Therefore, there is no infection and inflammatory reactions are observed.

The ALP concentration is lower at 6-week time point among all the scaffold groups as compared to 12 weeks (Figure 7.13). At the 12 weeks, the Sham group show the highest concentrations of ALP compared to other groups. ALP is the marker of wound healing, tissue repair and angiogenesis. Osteocalcin (OCN) (Figure 7.14) levels are higher at 6 weeks and 12 weeks in all the groups than control normal rat. OCN concentrations are indicators of active osteoblasts that help to form new bone. The bone forming cells osteoblasts are active at 6 weeks and 12 weeks in all the groups. OCN concentrations are slightly lower in 12 weeks than in 6 weeks for PCL-GO-CQ and PCL-GO-CQ-hUCMSCs groups. The similar fluctuations and lower concentrations of OCN are found in bone fracture healing patients after 10 weeks of healing^{22,23}.

7.4.3 X-ray and Micro-CT analysis:

The digital X-ray images of rat calvaria of implanted groups after 6 weeks and 12 weeks are shown in Figure 7.15. No bone regeneration is observed in the defects of the Sham group as well as to defect implanted with PCL, PCL-hUCMSCs, PCL-GO, PCL-GO-CQ except PCL-GO-CQ-hUCMSCs groups after 6 weeks and even 12 weeks.

This could be due to the critical size of bone defect of 8mm, and there is no support for bone healing. However, after 12 weeks implantation, the PCL-GO-CQ-hUCMSCs group is showing the maximum amount of radiolucent bone formation in the calvarial

defect site. There is no significant bone growth in other groups even after 12 weeks of implantation.

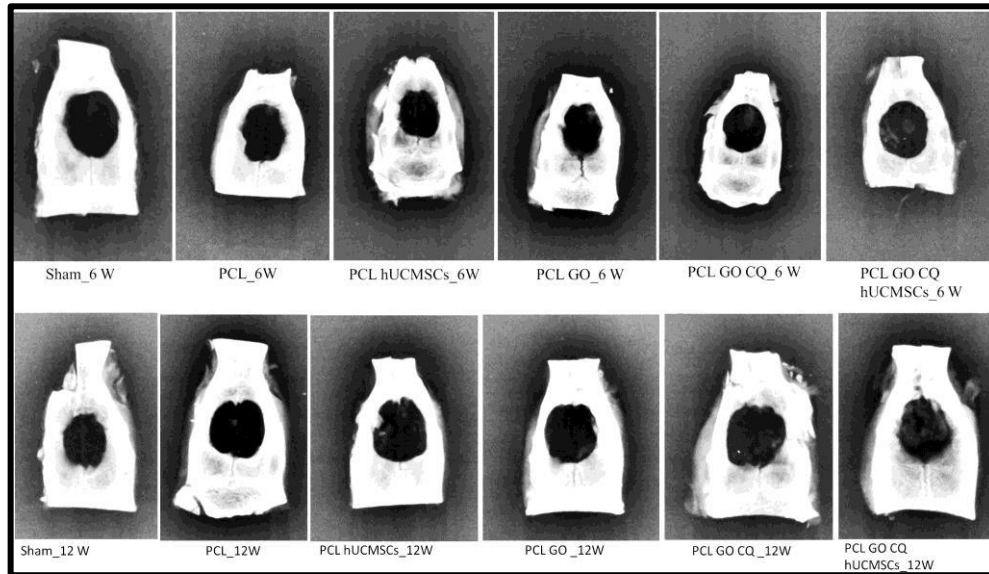


Figure 7.15: Digital X-ray of rat calvaria implanted with composite scaffolds after 6 weeks and 12 weeks of implantation. The highest bone regeneration is observed in PCL GO CQ hUCMSCs scaffolds after 12 weeks of implantation.

The 3D reconstructed images of bone calvaria from all the groups after 6 weeks and 12 weeks of implantation are shown in Figure 7.16. It is observed that Sham control group has the least bone healing after 6 weeks and 12 weeks of the study period as the defect is left untreated. The other groups PCL, PCL-hUCMSCs, PCL-GO are showing slightly higher bone growth after 12 weeks than 6 weeks of transplantation. The PCL-GO-CQ group shows slightly higher bone growth as compared to these groups. The highest amount of bone growth is observed in the PCL-GO-CQ-hUCMSCs group after 6 weeks and 12 weeks of transplantation. There is an almost complete closure of calvarial bone defect after 12 weeks. It could be due to hUCMSCs seeded into the PCL-GO-CQ scaffolds adhere well, proliferated and differentiated into osteoblasts that could boost new bone formation. While in PCL-hUCMSCs, the cells could have adhered but not differentiated into osteoblasts as like in PCL-GO-CQ-hUCMSCs group due to the synergistic effect of GO and CQ which probably have created a niche for MSCs.

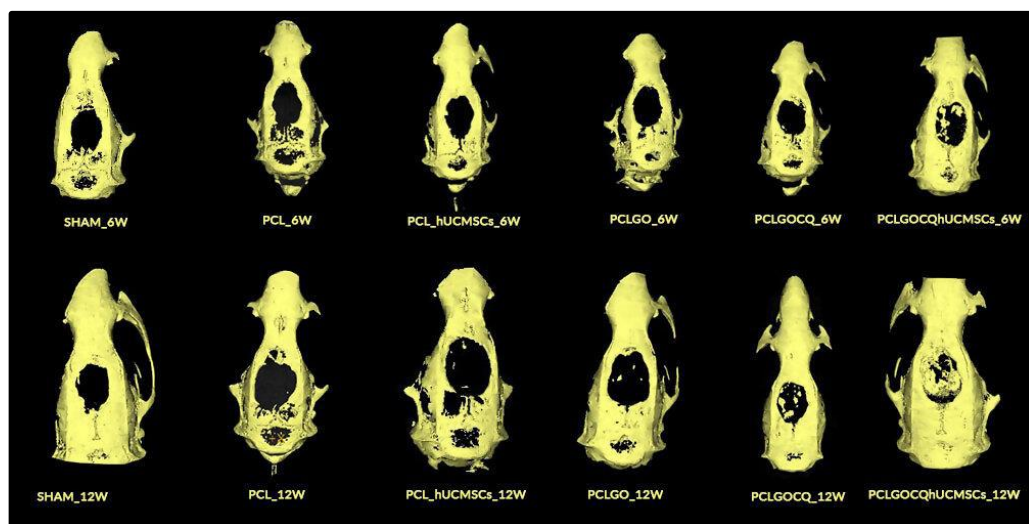


Figure 7.16: Reconstructed 3D micro –CT images of rat calvaria implanted with scaffolds after 12 weeks. The highest bone regeneration is in the PCL GO CQ hUCMSCs scaffolds after 6 Week and 12 weeks of transplantation.

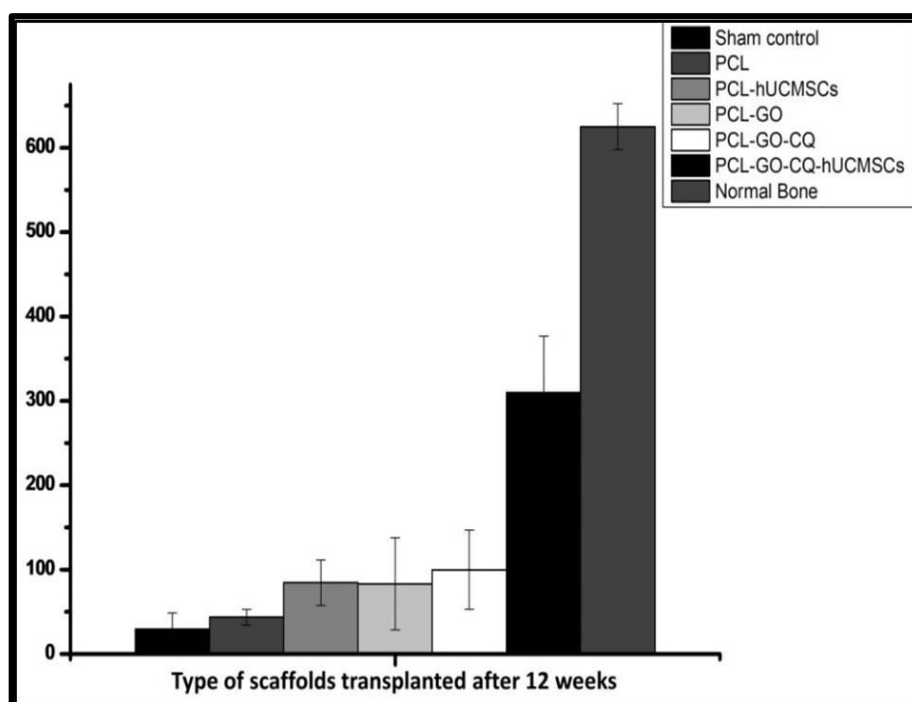


Figure 7.17 Bone mineral densities of Scaffolds after 12 weeks of implantation into rat calvaria. No significant difference ($p > 0.05$) observed among groups at 12 weeks of implantation.

Bone mineral density (BMD) is the indicator of new bone formation. It is calculated at the defect site after implantation and is analysed by MicroView. Figure 7.17 show the BMD values after implantation of 12 weeks. The lowest BMD values are of Sham control indicating minimum bone formation. The highest BMD values are of PCL-GO-CQ-hUCMSCs group as compared to PCL, PCL-hUCMSCs, PCL-GO, PCL-GO-CQ groups after 12 weeks of implantation. The normal bone BMD is highest as compared to all the implanted groups. These results are comparable to digital X-ray and micro-CT images. The similar results are observed when poly (L-lactic acid)-hydroxyapatite- gelatin and poly (L-lactic acid)-hydroxyapatite scaffolds are implanted in critical size calvarial bone defects for 6 weeks and 10 weeks²⁰ and PCL- hydroxyapatite and PCL-hardystonite scaffolds are implanted for 6 weeks and 12 weeks in rat calvarial defects ²¹.

7.4.4 Histological Analysis:

Our histology results (Figure 7.18 and 7.19) are in resemblance with micro CT and radiology results. There is minimal new bone tissue formation, low density of osteoblasts in Sham and PCL group after 6 weeks of transplantation. There is medium new bone tissue formation, the medium density of osteoblasts in PCL-hUCMSCs and PCL-GO group after 6 weeks of transplantation. There is high new bone tissue formation, high density of osteoblasts in PCL-GO-CQ group after 6 weeks of transplantation. There is higher new bone tissue formation, a higher density of osteoblasts in PCL-GO-CQ-hUCMSCs group after 6 weeks of transplantation.

There is minimal new bone tissue formation, low density of osteoblasts and osteocytes in Sham and PCL group after 12 weeks of transplantation. There is medium new bone tissue formation, the medium density of osteoblasts and osteocytes in PCL-hUCMSCs and PCL-GO group after 12 weeks of transplantation. There is high new bone tissue formation, high density of osteoblasts and osteocytes in PCL-GO-CQ group after 12 weeks of transplantation. There is the highest new bone tissue formation, a higher density of osteoblasts and osteocytes in PCL-GO-CQ-hUCMSCs group after 12 weeks of transplantation. Also there is presence of osteoclasts and matrix mineralization.

There is no abnormal development in bone tissues, inflammatory changes or necrosis after 6 weeks of transplantation or 12 weeks of transplantation. Inflammatory

cells are the primary source of the signals during the initial phase of bone healing. However, derivatives of MSC lineage including osteoblasts and osteoclasts are also responsible for the secretion of inflammatory cytokines within 3-7 days of injury and subsequent phases of healing^{24,25}. Also several *in vivo* studies have revealed that neutrophils, macrophages and lymphocytes are not always necessary for tissue repair. Their absence may even accelerate healing^{26,27}.

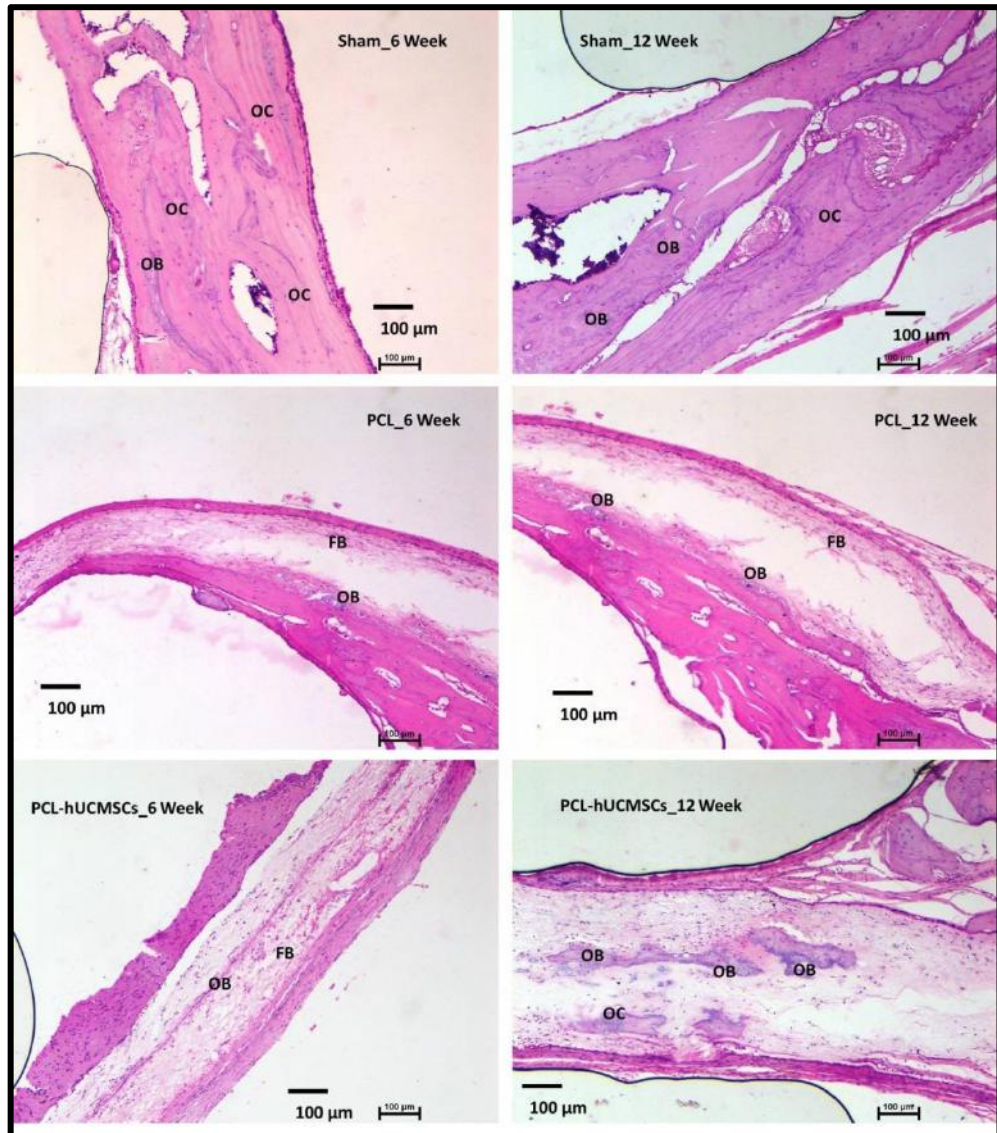


Figure 7.18: Histological analyses of calvaria after 6 weeks and 12 weeks of transplantation. (FB: Fibroblasts; OB: Osteoblasts; OC: Osteocytes, OCL: Osteoclasts; elliptical areas: matrix mineralization), Scale bar 100 μm

Similar kinds of results are mentioned elsewhere. There is increased new bone formation and density of bone forming cells in rat calvarial defects when BMSCs seeded Chitosan-alginate-hydroxyapatite loaded with BMP-2 scaffolds as compared to Chitosan-alginate-hydroxyapatite 12 week of transplantation²⁸. When polymethylmethacrylate (PMMA) and platelet gel (PG) are transplanted in radial bone defect of rats for 8 weeks there is an increased activity of osteoblasts, osteoclasts and new bone formation²⁹.

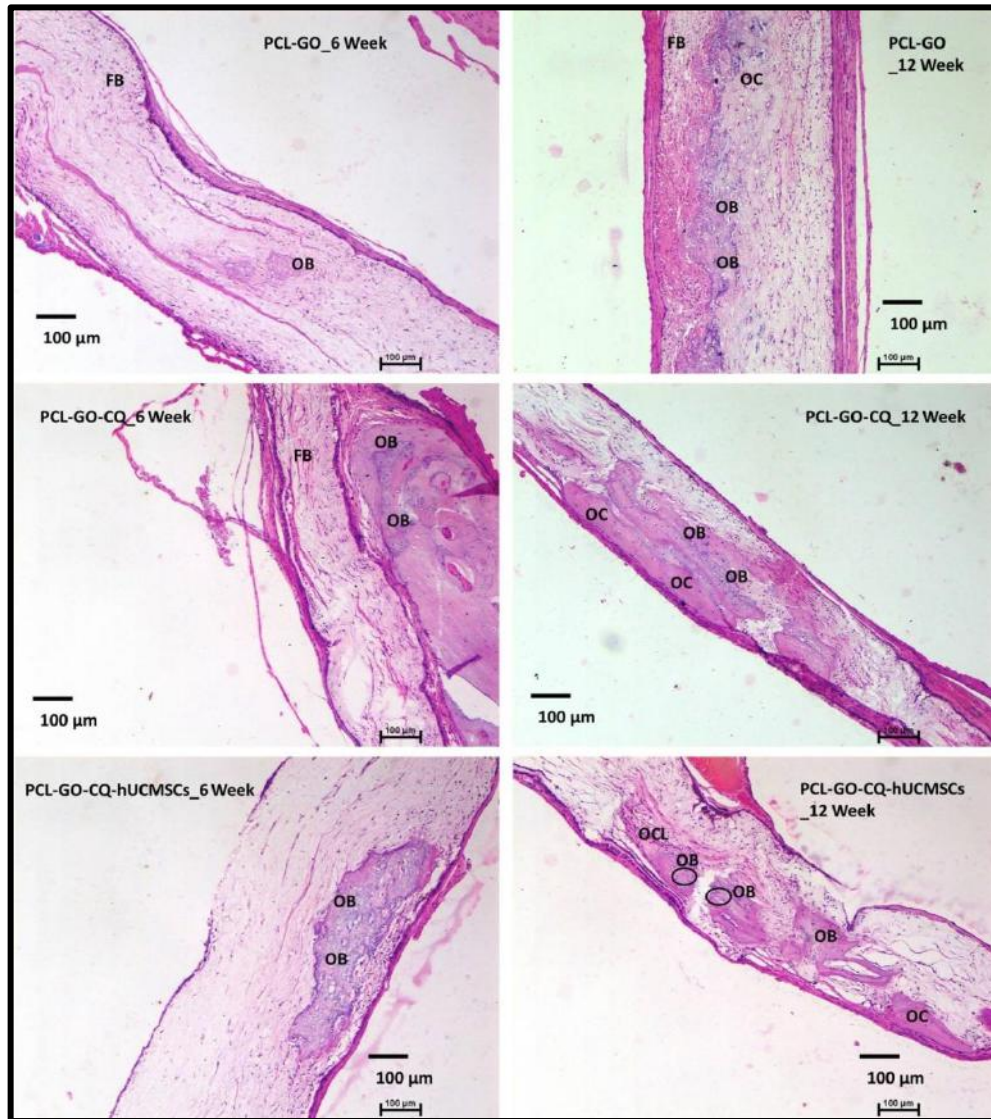


Figure 7.19: Histological analyses of calvaria after 6 weeks and 12 weeks of transplantation. (FB: Fibroblasts; OB: Osteoblasts; OC: Osteocytes, OCL: Osteoclasts; elliptical areas: matrix mineralization), Scale bar 100 μm

Histology have showed there are osteoblastic proliferation, osteoid matrix, with the presence of osteoclasts when poly (L-lactic acid)-hydroxyapatite-gelatin and poly (L-lactic acid)-hydroxyapatite scaffolds are implanted in critical size calvarial bone defects for 6 weeks and 10 weeks²⁰. Also when PCL- hydroxyapatite and PCL-hardystonite scaffolds are implanted for 6 weeks and 12 weeks in rat calvarial defects, histology revealed there is higher cell activity with the presence of inflammatory cells²¹.

The overall new bone tissue formation is higher in 12 weeks of transplantation compared to 6week of transplantation. There is increased new bone tissue formation in hUCMSCs scaffolds as compared to no hUCMSCs scaffolds. The bone formation process in the flat bone like skull occurs via intramembranous direct ossification. There is a slow process of bone formation due to the limited supply of MSCs in flat bones³⁰. This could be the main reason, as there is minimal new bone formation in the defect area in all the scaffolds groups except PCL-GO-CQ-hUCMSCs group. In PCL-GO-CQ-hUCMSCs group, the roughness, porosity of PCL-GO-CQ scaffold allowed hUCMSCs to adhere, grow and proliferate. However, osteoconductive and osteoinductive properties of GO and CQ eventually differentiated hUCMSCs to osteoblasts and fill the bone defect with new bone formation. In PCL- hUCMSCs group, however, the PCL alone could not able to proliferate and differentiate hUCMSCs into osteoblasts to regenerate the bone tissues.

7.5. Conclusions:

The aim of this study is to prepare a novel scaffold and to evaluate its potential for bone tissue engineering. PCL, PCL-hUCMSCs, PCL-GO, PCL-GO-CQ, PCL-GO-CQ-hUCMSCs are evaluated to heal critical size calvarial bone defects in the rat model. All the scaffolds are implanted into rat calvarial defects of 8mm size and bone healing are evaluated by digital X-ray, micro-CT and histology. These scaffolds are biocompatible and there is no adverse immune reaction. Results indicate that PCL-GO-CQ-hUCMSCs scaffolds i.e. PCL-GO-CQ seeded with hUCMSCs shows a higher amount of bone regeneration at 6 weeks and 12 weeks of time point compared to PCL, PCL- hUCMSCs, PCL-GO, PCL-GO-CQ. It almost closed critical size defect at 12 weeks of transplantation. There is a synergistic effect of GO and CQ in the PCL-GO-CQ scaffold for adhesion, proliferation and differentiation of seeded hUCMSCs. Therefore, it could be able to regenerate new bone effectively in the defect site. The PCL-GO-CQ-hUCMSCs

scaffolds have paved the way for clinical trials and could be a game changer in the bone tissue engineering applications.

References:

- 1 W. Wang and K. W. K. Yeung, *Bioact. Mater.*, 2017, **2**, 224–247.
- 2 S. Stewart, S. J. Bryant, J. Ahn and K. D. Hankenson, in *Translational Regenerative Medicine. Academic Press, Elsevier Inc.*, 2015, pp. 313–333.
- 3 S. Kashte, A. K. Jaiswal and S. Kadam, *Tissue Eng. Regen. Med.*, 2017, **14**, 1–14.
- 4 A. Alves, A. R. C. Duarte, J. F. Mano, R. A. Sousa and R. L. Reis, *J. Supercrit. Fluids*, 2012, **65**, 32–38.
- 5 I. Rajzer, E. Menaszek, R. Kwiatkowski and W. Chrzanowski, *J. Mater. Sci. Mater. Med.*, 2014, **25**, 1239–1247.
- 6 X. Liu and P. Ma, *Ann. Biomed. Eng.*, 2004, **32**, 477–486.
- 7 J. Qian, W. Xu, X. Yong, X. Jin and W. Zhang, *Mater. Sci. Eng. C. Mater. Biol. Appl.*, 2014, **36**, 95–101.
- 8 B. Chuenjitkuntaworn, T. Osathanon, N. Nowwarote, P. Supaphol and P. Pavasant, *J Biomed Mater Res Part A*, 2015, **104**, 264–271.
- 9 K. Ren, Y. Wang, T. Sun, W. Yue and H. Zhang, *Mater. Sci. Eng. C*, 2017, **78**, 324–332.
- 10 V. Y. Chakrapani, T. S. S. Kumar, D. K. Raj and T. V Kumary, *J. Nanosci. Nanotechnol.*, 2017, **17**, 2320–2328.
- 11 G. Mishra, S. Srivastava and B. P. Nagori, *Int. J. PharmTech Res.*, 2010, **2**, 1298–1310.
- 12 D. K. Deka, L. C. Lahon, A. Saikia and Mukit, *Indian J Pharmacol*, 1994, **26**, 44–45.
- 13 B. K. Potu, M. S. Rao, N. G. Kutty, K. M. R. Bhat, M. R. Chamallamudi and S. R. Nayak, *Clinics (Sao Paulo)*, 2008, **63**, 815–820.
- 14 S. Suganya, J. Venugopal, S. Ramakrishna, B. S. Lakshmi and V. R. Giri Dev, *J.*

- Appl. Polym. Sci.*, 2014, **131**, 1–11.
- 15 M. Shin, H. Yoshimoto and J. Vacanti, *Tissue Eng.*, 2004, **10**, 33–41.
 - 16 C. Wan, Q. He and G. Li, *J. Orthop. Res.*, 2006, **24**, 610–618.
 - 17 Y. Piao, Y. Liu and X. Xie, *J Toxicol Pathol*, 2013, **26**, 29–34.
 - 18 M. S. Baliga, G. C. Jagetia, J. N. Ulloor, M. P. Baliga, P. Venkatesh, R. Reddy, K. V. N. M. Rao, B. S. Baliga, S. Devi, S. K. Raju, V. Veeresh, T. K. Reddy and K. L. Bairy, *Toxicol. Lett.*, 2004, **151**, 317–326.
 - 19 Q. Liu, Z. Lei, Q. Wu, I. Awais and M. A. B. Shabbir, *Front. Pharmacol.*, 2018, **9**, 1–14.
 - 20 A. K. Jaiswal, R. V. Dhumal, S. Ghosh, P. Chaudhari, H. Nemani, V. P. Soni, G. R. Vanage and J. R. Bellare, *J. Biomed. Nanotechnol.*, 2013, **9**, 2073–2085.
 - 21 K. Khanna, A. Jaiswal, R. V. Dhumal, N. Selkar, P. Chaudhari, V. P. Soni, G. R. Vanage and J. Bellare, *RSC Adv.*, 2017, **7**, 37522–37533.
 - 22 T. Taniguchi, T. Matsumoto and H. Shindo, *Injury*, 2003, **34**, 477–479.
 - 23 S. A. Bowles, N. Kurdy, A. M. Davis, M. W. France and D. R. Marsh, *Ann. Clin. Biochem.*, 1996, **33**, 196–200.
 - 24 P. Kolar, K. Schmidt-Bleek, H. Schell, T. Gaber, D. Toben, G. Schmidmaier, C. Perka, F. Buttgerit and G. N. Duda, *Tissue Eng. Part B Rev.*, 2010, **16**, 427–434.
 - 25 T. Kon, T.-J. Cho, T. Aizawa, M. Yamazaki, N. Nooh, D. Graves, L. C. Gerstenfeld and T. A. Einhorn, *J. Bone Miner. Res.*, 2001, **16**, 1004–1014.
 - 26 P. Martin, D. D'Souza, J. Martin, R. Grose, L. Cooper, R. Maki and S. R. McKercher, *Curr. Biol.*, 2003, **13**, 1122–1128.
 - 27 D. Toben, I. Schroeder, T. El Khassawna, M. Mehta, J.-E. Hoffmann, J.-T. Frisch, H. Schell, J. Lienau, A. Serra, A. Radbruch and G. N. Duda, *J. Bone Miner. Res.*, 2011, **26**, 113–126.

- 28 X. He, Y. Liu, X. Yuan and L. Lu, *PLoS One*, 2014, **9**, 1–9.
- 29 A. Oryan, S. Alidadi, A. Bigham-sadegh and A. Moshiri, *PLoS One*, 2018, **13**, 1–17.
- 30 A. K. Teotia, D. B. Raina, H. Isaksson, M. Tägil and L. Lidgren, *Multifunct. Mater.*, 2019, **2**, 1–11.

CHAPTER 8:

SUMMARY AND

CONCLUSIONS

8.1 Summary and Conclusions:

In this study, we have used poly ϵ -caprolactone (PCL), graphene oxide (GO) and graphene (GP), *Cissus quadrangularis* (CQ) for preparation of scaffolds. The solution/ink of GO, GP and CQ callus culture extract was prepared with their respective combinations. Porous PCL electrospun sheets were modified with GO or GP and CQ solution/ink by layer by layer method and paint method. The layer by layer method offers advantages as a surface modification technique for polymers. It is a simple, relatively fast, environmentally benign, and potentially economic process to prepare uniform multilayer films on substrates from solution. The paint method is very simple and easy to apply for modification of scaffolds as compared to plasma treatment, spin coating, etc. It is very similar to ordinary painting. These composite scaffolds were characterized and studied for bone tissue engineering.

We have successfully isolated hUCMSCs which were spontaneously differentiated into osteoblasts upon contact with prepared scaffold. Therefore, these scaffolds in combination with hUCMSCs could be used for bone fracture healing in animal models that could give us potential scaffolds for bone tissue engineering;

Among the all the prepared scaffolds using layer by layer method, PCL-GO-CQ scaffold are herbal, and biocompatible in nature with an osteoinductive potential. Their porous, rough, hydrophilic nature, thermally and mechanically stable character helped the hUCMSCs to adhere, spread, proliferates and differentiates into osteoblast-like cells. The synergistic effect of GO and CQ in the PCL-GO-CQ scaffold enhanced the roughness, thermal and mechanical properties and wettability of the scaffolds. Mainly GO and CQ callus extract provided osteoinductive properties to scaffold that helps hUCMSCs to spontaneously differentiate into osteoblast *in vitro* without any osteogenic media or growth factors or added external stimuli.

The layer by layer prepared PCL, PCL- hUCMSCs, PCL-GO, PCL-GO-CQ and PCL-GO-CQ-hUCMSCs scaffolds were implanted into rat calvarial defects of 8mm size and bone healing were evaluated by digital X-ray, micro-CT. These scaffolds are biocompatible and there was no adverse immune reaction. Results indicate that PCL-GO-CQ-hUCMSCs composite scaffolds i.e. PCL-GO-CQ seeded with hUCMSCs showed higher amount of bone regeneration at 12 weeks of time point compared to PCL, PCL- hUCMSCs, PCL-GO, PCL-

GO-CQ. It almost closed critical size defect at 12 weeks. There was a synergistic effect of GO and CQ in the PCL-GO-CQ scaffold for adhesion, proliferation and differentiation of seeded hUCMSCs. Therefore, it could be able to regenerate new bone effectively in the defect site.

We have used widely available materials and simple, yet cost effective methods to synthesis scaffolds. The evaluation of prepared scaffolds for bone tissue engineering indicates these scaffolds are with accelerated morphological, mechanical and biological properties along with promoting osteoconductive, osteogenic and osteoinductive properties. Therefore, we have prepared simple yet effective composite bone regenerating scaffold.

The layer by layer PCL-GO-CQ scaffolds show vast potential for further *in vivo* bone tissue engineering and pave the way for human clinical studies in bone tissue regeneration.

ANNEXURE: I

CERTIFICATES



AMITY INSTITUTE OF BIOTECHNOLOGY

AMITY UNIVERSITY MUMBAI

(Established vide Maharashtra Act No. 13 of 2014, of Government of Maharashtra, and recognized under Section 2(f) of UGC Act 1956.)

Date: 10-08-2016

Authentication letter

This is to authenticate that the plant brought by Mr. Shivaji Kashte, Center for Interdisciplinary Research, D. Y. Patil Education Society (Deemed to be University), Kolhapur, Maharashtra, India is identified as *Cissus quadrangularis* L. of the Family Vitaceae. The voucher specimens of the same have been deposited in our herbaria with accession number SK/100816-01.

Dr. Sandeep Pai



D. Y. PATIL MEDICAL COLLEGE, KOLHAPUR

Constituent College of D.Y. Patil Education Society Deemed University, Kolhapur

NAAC Accredited 'A' Grade

Dr. Rakesh Kumar Sharma
Dean & Professor (Obst. & Gyn.)

Padmshree Dr. D. Y. Patil
Founder President

Dr. Sanjay D. Patil
President

Outward No. DMCK/57/2016

Date: 24 NOV 2016

INSTITUTIONAL ETHICS COMMITTEE, D. Y. PATIL MEDICAL COLLEGE, KOLHAPUR.

This is to certify that the research project titled,

"Synthesis and evaluation of a novel combination scaffold and its application in bone tissue engineering."

Submitted by

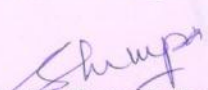
: **Mr. Shivaji Kashte**

Under the supervision of appointed Guide (if any): **Dr. Sachin Kadam**

Dr. Rakesh Sharma

Has been studied by the Institutional Ethics Committee (IEC) at its meeting held on **22/11/2016** and granted approval for the study with due effect with the following caveats:

1. If you desire any change in the protocol or standard recording document at any time, please submit the same to the IEC for information and approval before the change is implemented.
2. All serious and/or unexpected adverse events due to the drug/procedures tested in the study must be informed to the IEC within 24 hours and steps for appropriate treatment must be immediately instituted.
3. In case of injury/disability/death of any participant attributable to the drug/procedure under study, all compensation is to be made by the sponsor of the study.
4. The Chief investigator/Researcher must inform the IEC immediately if the study is terminated earlier than planned with the reasons for the same.
5. The final results of the study must be communicated to the IEC within 3 months of the completion of data collection.
6. The researcher must take all precautions to safeguard the rights, safety, dignity and wellbeing of the participants in the study.
7. The researcher must be up to date about all information regarding the risk/benefit ratio of any drug/procedure being used and any new information must be conveyed to the IEC immediately. The IEC reserves the right to change a decision on the project in the light of any new knowledge.
8. Before publishing the results of the study, the researcher must take permission from the Dean of the Institution.
9. Annual progress report should be submitted for all sponsored projects to the committee.
10. Unethical conduct of research in non-sponsored projects will result in withdrawal of the ethics approval and negation of all data collected till that date.


Dr. Mrs. Shrimpa R. Sharma
(Member Secretary, IEC)
Member Secretary,
Institutional Ethics Committee
D. Y. Patil Medical College,
Kolhapur - 416 008

869, 'E' Kasaba Bavada, Kolhapur-416 006 (MS) INDIA. Phone No. : (0231) 2601235-36, Fax : (0231) 2601238,
Web: dypatilmedicalkop.org. E-mail : dypatilmedicalcollege@gmail.com

ANNEXURE: II

PUBLICATIONS

PUBLICATIONS

- ✓ **Kashte S**, Arbade G, Sharma RK, Kadam S. Herbally Painted Biofunctional Scaffolds with Improved Osteoinductivity for Bone Tissue Engineering. J Biomimetics, Biomater Biomed Eng. 2019;41:49–68.
- ✓ **Kashte S**, Kadam S. Advances and Innovations and Impediments in Tissue Engineering and Regenerative Medicine. Innov Tissue Eng Regen Med. 2019;1(2):1–3.
- ✓ **Kashte S**, Jaiswal AK, Kadam S. Artificial Bone via Bone Tissue Engineering: Current Scenario and Challenges. Tissue Eng Regen Med [Internet]. Korean Tissue Engineering and Regenerative Medicine Society; 2017;14(1):1–14.
- ✓ **Kashte S**, Kadam S. Stem Cell Therapy : A Hope Business or a Magic Wand ? Br Biomed Bull. 2014;2(4):677–94.
- ✓ **Kashte S**, Anshuman Dwivedi, Shraddha Gautam, R.K. Sharma and Sachin Kadam, Treatment of Gingival Recession defect using mesenchymal stem cells cultured PCL based bone regenerating scaffold: a randomized controlled clinical study, Journal of Oral Biology and Craniofacial Research (First revision Submitted)
- ✓ **Kashte S**, R.K. Sharma and Sachin Kadam, Layer by layer decorated herbal biocompatible scaffolds for bone tissue engineering: A synergistic effect of graphene oxide and *Cissus quadrangularis*, Journal of Bioactive and Compatible Polymers (Under Review)
- ✓ **Kashte S**, Rohit Dhumal, Vikas Dighe, Pradip Chaudhary, R.K. Sharma, Sachin Kadam, Bone regeneration in critical size calvarial defect using functional biocompatible osteoinductive herbal scaffolds and human umbilical cord Wharton's Jelly-derived mesenchymal stem cells, Biomaterials (Submitted)

CONFERENCES

- ✓ International Conference on Nanotechnology: Ideas, Innovations, and Initiatives- 2017 (ICN: 31-2017) at IIT Roorkee, December 2017

- ✓ International conference on “Emerging Trends in Nanomaterial's and their Applications (IC-NACMBM 2017), D.Y. Patil University, Kolhapur, September 2017
- ✓ National conference on “Emerging Trends in Nanomaterials and their Applications (ETNA 2017), D.Y. Patil University, Kolhapur, June 2017
- ✓ Anveshan, at NIIMS University, Jaipur, March 2017
- ✓ National conference on Convergence of stem cells and Medical Nanotechnology, D.Y. Patil University, Kolhapur, June 2016
- ✓ National conference on Bioscience and Health Engineering: Current Scenario, Defence Institute of Advanced Technology, Pune January 2014